AD_____

GRANT NUMBER: DAMD17-93-J-3008

TITLE: Clinical Optimization of Current Digital Mammography Systems

PRINCIPAL INVESTIGATOR: Matthew Freedman, M.D.

CONTRACTING ORGANIZATION: Georgetown University
Washington, DC 20057

REPORT DATE: August 1996

TYPE OF REPORT: Final

PREPARED FOR: Commander
U.S. Army Medical Research and Materiel Command
Fort Detrick, Frederick, Maryland 21702-5012

REPORT DOCUMENTATION PAGE

Form Approved
OMB No. 0704-0188

1. AGENCY USE ONLY *(Leave blank)*	2. REPORT DATE	3. REPORT TYPE AND DATES COVERED
	August 1996	Final (15 Dec 92 - 14 Jul 96)

4. TITLE AND SUBTITLE
Clinical Optimization of Current Digital Mammography Systems

5. FUNDING NUMBERS
DAMD17-93-J-3008

6. AUTHOR(S)
Matthew Freedman, M.D.

7. PERFORMING ORGANIZATION NAME(S) AND ADDRESS(ES)
Georgetown University
Washington, DC 20057

8. PERFORMING ORGANIZATION REPORT NUMBER

9. SPONSORING/MONITORING AGENCY NAME(S) AND ADDRESS(ES)
Commander
U.S. Army Medical Research and Materiel Command
Fort Detrick, MD 21702-5012

10. SPONSORING/MONITORING AGENCY REPORT NUMBER

11. SUPPLEMENTARY NOTES

12a. DISTRIBUTION / AVAILABILITY STATEMENT
Approved for public release; distribution unlimited

12b. DISTRIBUTION CODE

13. ABSTRACT *(Maximum 200)*

The purpose of army grant DAMD17-93-J-3008 was to test existing methods for digital mammography. We discovered in this process that the methods current in 1992 were not sufficient for digital mammography. We have worked independently and with several manufacturers to develop a system for digital mammography that in our initial statistical study shows adequate quality for clinical implementation.

During this project we have investigated optimization of methods for image acquisition, image processing and image display. Each of these represented major challenges and it was only by the close working relationship established between the research team and our commercial suppliers that the goal of acceptable digital mammography was reached.

This project has, based on our findings and advice, we believe, guided manufacturers to develop the necessary tools for acceptable digital mammography. We believe that our presentations and publications have helped push the agenda for the development of still better digital mammography systems because our results were so promising.

Our tests and development work have shown that a Fuji FCR 9000 with image processing optimized by us, transferred through an Analogics Corporation Print Server to a 3M 969 laser printer provides adequate statistically documented quality sufficient for clinical diagnosis.

14. SUBJECT TERMS	15. NUMBER OF PAGES
Breast Cancer	200
	16. PRICE CODE

17. SECURITY CLASSIFICATION OF REPORT	18. SECURITY CLASSIFICATION OF THIS PAGE	19. SECURITY CLASSIFICATION OF ABSTRACT	20. LIMITATION OF ABSTRACT
Unclassified	Unclassified	Unclassified	Unlimited

NSN 7540-01-280-5500

Standard Form 298 (Rev. 2-89)
Prescribed by ANSI Std. Z39-18
298-102

FOREWORD

Opinions, interpretations, conclusions and recommendations are those of the author and are not necessarily endorsed by the US Army.

____ Where copyrighted material is quoted, permission has been obtained to use such material.

____ Where material from documents designated for limited distribution is quoted, permission has been obtained to use the material.

____ Citations of commercial organizations and trade names in this report do not constitute an official Department of Army endorsement or approval of the products or services of these organizations.

____ In conducting research using animals, the investigator(s) adhered to the "Guide for the Care and Use of Laboratory Animals," prepared by the Committee on Care and Use of Laboratory Animals of the Institute of Laboratory Resources, National Research Council (NIH Publication No. 86-23, Revised 1985).

____ For the protection of human subjects, the investigator(s) adhered to policies of applicable Federal Law 45 CFR 46.

____ In conducting research utilizing recombinant DNA technology, the investigator(s) adhered to current guidelines promulgated by the National Institutes of Health.

____ In the conduct of research utilizing recombinant DNA, the investigator(s) adhered to the NIH Guidelines for Research Involving Recombinant DNA Molecules.

____ In the conduct of research involving hazardous organisms, the investigator(s) adhered to the CDC-NIH Guide for Biosafety in Microbiological and Biomedical Laboratories.

PI - Signature Date

Table of Contents

Clinical Optimization of Current Digital Mammography Systems
Army Report 1996

Introduction

Army grant DAMD17-93-J-3008 was initiated in December 1992 for completion in December 1995. This was extended to a completion date of December 1996. This represents the final report for this project.

The original purpose of this project was to test existing methods for digital mammography. We discovered in this process that the methods current in 1992 were not sufficient for digital mammography and that we needed to encourage and cajole manufacturers into modifying and/or making the devices we needed. This resulted in delays in the progress of the project. In this process we have had to work directly with Fuji Photo Film Corporation in the US and with their development facilities in Japan, with DBA, Inc. in Florida, with Analogic Corporation in Peabody, MA, with 3M in St. Paul, MN, and with Polaroid in Newton, MA, as well as develop our own software. One of our outside suppliers was unable to meet equipment specifications for the film digitizer (this supplier was replaced). Another supplier delayed the delivery of equipment for six months and the software provided needed to be rewritten to eliminate bugs that resulted in equipment crashes (with a six month additional delay). We also found that a key component of printer server software that we needed did not exist in the commercial market. We have worked with our current suppliers over the last two years and now have a successful print server for acceptable quality mammographic images, but are continuing to encourage the development of a better hard copy display device as we believe that this will further enhance the image quality of these digital mammograms.

During this project we have investigated optimization of methods for image acquisition, image processing and image display. Each of these represented major challenges and it was only by the close working relationship established between the research team and our commercial suppliers that the goal of acceptable digital mammography was reached. We are currently engaged in the performance of an ROC study to validate our results. The results from the first reader have been calculated and indicate ROC areas of Az screen film = 0.7373Az digital = 0.7646 when tested for detection of cancer. When tested as a method of discrimination between cancer and benign lesions that were detected, the Az of screen film = 0.5743. The Az of the digital system = 0.7412 . We do not know how the other 6 readers will perform in the ROC study, but are encouraged by the results of this first reader.

The purpose of this project is to determine whether or not digital mammography is feasible with existing equipment either by using digitized film or by using direct digital acquisition using storage phosphor technology. The brief answer is that it was not feasible with the equipment available at the initiation of the grant. There has been substantial development over the past three years and we believe our data from the ROC analysis will show that digital mammography is feasible using direct acquisition, but not using digitized film. It is adequate using hard copy display, but not with soft copy display at this time. This project has, based on our findings and advice, we believe, guided manufacturers to develop the necessary tools for acceptable digital mammography. We believe that our presentations and publications have helped push the agenda for the development of still better digital mammography systems because our results were so promising.

Digitized Film Mammography

The evaluation of digitized film required a process of quality control of the digitization equipment and display equipment that has been completed and a preclinical trial of proven cases, the first phase of which has been completed. This first phase demonstrated that digitized film mammography at 100 micron pixel size was considered clearly inferior to the original films by each of the five radiologists who reviewed its display on a workstation and that this lower quality would decrease the detectability of breast cancer. Digitization of a small sample of two different film screen systems of different latitudes demonstrated that they both were of sufficient contrast that information close to the skin line and within the dense portions of the breast could not be adequately demonstrated with either system. The characteristic curves of these two screen film systems are shown in Appendix 1. Initial laser prints of 50 micron digitized film mammography in June 1993, were of poor quality because of the lack of an appropriate print server with correct image processing. We have been unable to produce adequate images based on digitizing conventional screen film mammograms either printed as hard copy or displayed soft copy. Both methods produced artifacts that could be easily confused with microcalcifications, and both methods obscured microcalcifications so that they could not be recognized. This is a problem we are continuing to work on as we believe that a solution to this would be most important both for further developments in digital mammography and that it may represent one of the problems limiting advances in the computer aided detection of microcalcifications.

A full report on the evaluation of digitized film mammography at 100 microns with soft copy interpretation compared to the original screen film mammogram is attached as Appendix 2. In this evaluation we used 25 cancer cases and 25 benign cases that had had biopsy for suspicion of cancer. In almost all cases the radiologists preferred the original mammogram to the soft copy 100 micron digitized mammogram for microcalcifications. The original mammogram also was preferred for most cases of masses, though there were a few more cases in which the two methods were considered equivalent.

Storage Phosphor Digital Mammography

The evaluation of direct digital mammography using storage phosphor technology required machine and software optimization. In order to accomplish this it was necessary to perform a long optimization procedure that has been detailed in the two prior annual summaries. Briefly, a multivariate analysis was performed using response surface experimental design methods to define the optimal exposure and image processing factors for digital mammography. The results of this, summarized below and in the attached paper (Appendix 3) demonstrated that storage phosphor digital mammography using a 100 micron pixel and proper exposure and image processing optimization could result in images of standard mammographic phantoms that showed objects equal in size or smaller than those shown in standard screen film mammography and that the resulting images were highly pleasing to viewers. Additionally, we found that digital mammography may prove to be especially useful for the detection of cancer in the radiodense breast. These findings are detailed below.

TABLE OF SMALLEST OBJECT SEEN

Test Object	Screen Film	100 micron phosphor	50 micron CCD
CDMAM	130micron 100 at 5x mag	100 at 1 micron thick	100 at 0.8 microns thick
CIRS Detail	240	160	160
RMI 156	240 (3/6)	240 (3/6))	240 (3/6)
Steel Fleck	100	50 (noisy, high contrast)	100
CIRS Half Round	160	160	160

This table demonstrates that in two of the test objects, the 100 micron storage phosphor allowed detection of smaller objects than screen film mammography and that in the other two standard geometric test objects, that it provided the same object visibility as screen film mammography. The steel fleck phantom is a home-made system and showed that if a 50 micron object were of sufficient radiodensity, it could be identified on a 100 micron system, though it would measure larger than its true size. (From Freedman, 1995 A)

A comparison of a 50 micron digital spot device based on CCD technology and a 100 micron whole breast system using storage phosphor technology was performed and reported in February 1995, and demonstrated that the 50 micron system provided higher contrast, but did not allow smaller objects to be detected, and that the 50 micron system needed 1.5 to 3 times the exposure of the 100 micron system. (Appendix 3) In the above table, the improved contrast from the 50 micron system is demonstrated for the CDMAM phantom for which a thinner object could be seen with the 50 as compared to the 100 micron system. Both were superior in resolution to screen film mammography. These results were specific to the devices tested and cannot be generalized however.

We have also reported on the classification of microcalcifications comparing screen film mammography with digital mammography (in a version earlier than the one used in our current ROC test). In this study, we selected 20 patients who had gone to biopsy. Half had benign calcifications and half had calcifications associated with malignancy. In each case, the region of the calcifications was outlined by Post-it Notes and the biopsy specimen radiograph was also provided as a measure of truth. The study showed that the four radiologists involved were split in their preferences for screen film vs. digital images both on individual cases and on the cases grouped together. In general, the radiologists preferred the conspicuity of the microcalcifications on the digital system. They were divided on preference between the digital and screen film systems for counting the number of microcalcifications and defining their shape. Whichever system the radiologists preferred, they were unable to use this information to make better decisions between benign and malignant calcifications on the two systems. Since that time we have improved the printing system for digital mammography and are using a better printing system in our ROC study. As previously stated, the first ROC reader in our multi-reader study was better at classifying benign vs. malignant on the digital compared to the conventional screen film system and the other results are not yet available. (Appendix 4)

Collaborative Relationship with Army Medical Centers

Our original intention of working with Madigan Army Medical Center (MAMC) and Brooke Army Medical Center (BAMC) has been modified so that we are now working with Col Robert Shah, MD at BAMC and Col Ted Raia's designee, (Major Morgan Williamson, MD) at Walter Reed Army Medical Center (WRAMC). We also consult with and obtain advice from by Major Donald Smith, MD at Madigan. Two WRAMC radiologists are participating in the ROC reading study. We have had discussions with radiologists at WRAMC, Bethesda Naval Medical Center, Mike Freckleton, MD at Wilford Hall AFMC, and Anna Chacko, MD at BAMC regarding our findings on digital mammography as well as discussions at special meetings with General Russ Zajtchuk, MD and his assistant Major Paul Zimnick, MD about the appropriate utilization of digital mammography.

Presentations for other Federal Agencies

Our material on digital mammography has been presented to Lillian Yin PhD, Director, Division of Reproductive, Abdominal, ENT and Radiological Devices at the FDA, and her

colleagues in a special meeting, Florence Houn, MD, MPH and her colleagues as an invited speaker at the Mammography Quality Standards Board meeting on Digital Mammography Quality Control July 10, 1996, to Faina Shtern, MD and her colleagues at their invitation at NIH. We have also presented material to Susan Blumenthal, MD, Deputy Assistant Secretary of Health for Women's Health, Health and Human Services (HHS) and have participated with exhibits at two meetings held for informing Congress of work in improving breast cancer detection and diagnosis.

Methods

Our work has involved system analysis, system development and clinical trials. We will briefly summarize our previous reports.

System Analysis

At the time of the initiation of this project, many parameters of requirements for digital analysis were incompletely understood. Work by our group and others has greatly extended knowledge in this field.

Required exposure: Digital radiography systems currently under development represent a different tradeoff in image quality than screen film images. In screen film images, one chooses a screen film combination based on three considerations: film granularity, system resolution, and image optical density. The choice of a desired exposure dictates which screen film system one uses. In general, one can consider that a decrease in dose requires a decrease in resolution. In digital radiography, exposure in any specific digital system is related to the resulting signal to noise ratio (SNR). In any specific system, dose does not dictate the resolution of the system. SNR however determines the visibility (conspicuity) of low contrast objects. Test objects of resolution are usually designed to measure high contrast resolution which can give a false representation of the likely value of different systems required for mammography. In mammography, the objects one wishes to detect are usually low contrast objects.

There are two components of exposure: energy distribution (usually measured as KVP) and exposure (often measured as mAs). In addition, it can be helpful to divide mAs into its components: exposure intensity and time. KVP affects the contrast of the resulting image, but higher KVP allows one to decrease the time of exposure limiting any motion that may occur. For any specific digital system, one needs to determine the best exposure range, both in terms of KVP and mAs. We did these measurements and reported our results in 1995 in a paper relating the visibility of objects in selected geometric test objects to both KVP and mAs. We showed, for the system we used, where the tradeoffs were. We showed that image processing could not recapture information on images obtained at 36 KVP because the use of image processing increased both the visibility of noise as well as the object contrast and that, in our tests, these two balanced out. If one used high contrast image processing to correct for the loss of contrast resulting from higher KVP, that one then had problems because of the varying thickness and composition of the breast. Certain regions became all black or all white as we applied corrective imaging processing. Between 22 and 28 KVP, no differences were encountered.

We also showed that there was a region of lesser exposure where the digital system still recorded information, while the screen film system resulted in a clear film. We have used this to develop experimental image processing for the radiodense breast. This is described below. We reported this in 1996. (Appendix 5)

Our experiments in exposure indicated that for the system we used, that standard mammographic exposures were sufficient to demonstrate the same sized objects as conventional mammography, but that decreases in exposure would likely result in some loss of information.

Image Processing Optimization: A large amount of our work was related to the optimization of image processing of digital mammography. Prior to the start of our work, published articles on digital mammography usually assumed that the best image processing for a digital mammogram would be a screen film look-alike image. Some work has suggested that edge enhancement using unsharp masking might improve the detection of microcalcifications, but this had not been fully explored. We began work by deciphering the meaning and image appearance effect of the image processing available on the digital imaging system available to us (the Fuji AC-1). Fuji was, at that time, not willing to make available to its customers detailed information of its system and was not and still is not our partner in the work we are doing in digital mammography. We therefore proceeded to test each of the image processing parameters in selected combinations using partial factorial design to gain understanding of the system. These results were published (Appendix 6) and since that time Fuji has begun to release increasing amounts of information about their system.

The effect of different image processing parameters on breast images and on breast geometric test objects had not been previously systematically explored. We tested selected combinations of the Fuji parameters on several geometric test objects and reported our results in 1994. (Appendix 7) We showed that there was a tradeoff (influenced by exposure) of the effect of image processing on the visibility of details in the test objects with kernel size and enhancement intensity and that the enhancement factors that best showed details could result in digital mammograms that were so distorted as to be uninterpretable for subtle signs of disease. As our concepts developed, we realized that any edge enhancement (using the available kernel sizes in the Fuji system) resulted in some loss of conspicuity of the smallest details in geometric test objects.

Histogram equalization: In 1994, Fuji selected the PI of this project to be one of two US research sites for a new method for histogram equalization to be used for digital chest radiographs. We attempted to apply this method for low resolution histogram equalization to digitally acquired mammograms. After a period of trials of different parameter settings, we arrived at a usable system. The use of this system presents problems because if the parameters are incorrectly selected, small masses in geometric test objects become of very low conspicuity and may not be seen. We have determined usable settings that we believe will prove useful in the imaging of microcalcifications in the radiodense breast. We have reported our findings (Appendix 5). This topic is discussed below in clinical trials.

New directions in image processing: We have been working to develop better look-up tables (LUTs) for digital mammography. These newer concepts are not yet fully developed and are only partially implemented. The goal is to create a contrast linearized look-up table optimized for the detection of microcalcifications and masses in the complex pattern and radiodense breast. In concept, one would expect low object (microcalcification and masses) contrast in areas of the breast containing fibroglandular tissue and high object contrast for microcalcifications and masses in fatty regions of the breast. One should therefore have a high contrast LUT in the low optical density regions and a low contrast LUT in the high optical density regions of the breast. We have partially implemented this and are looking toward further improvements of this method over the next 6 months. We reported on the conceptual basis for this in 1996 (Appendix 8).

Image display: The third major component we have been working with is image display. We have worked on both soft copy display and hard copy display. With soft copy display, we have encountered many problems and do not consider this to be currently adequate for clinical mammography. We have done progressive optimization of hard copy display and consider current systems adequate, but not optimal, and have been advising manufacturers on methods that could be used to improve the hard copy displays.

Soft copy display: At the current state of available technology, soft copy display of digital mammograms results in many problems. We have worked to define clinical scenarios of how soft copy display might be used and will discuss why soft copy display is not now suitable. Current soft copy displays have the following limitations: (1) Limited number of pixels: displays are limited to 2 K by 2.5 K. To have adequate demonstration of microcalcifications this resolution is required for each mammogram -- four mammograms in a study of each woman. In addition, comparison of old and new images is necessary to detect subtle changes. Thus one would need eight monitors for effective display. As a radiologist interpreting mammograms, I go back and forth between images: right-left, new-old, craniocaudal-mediolateral oblique (CC-MLO). The pattern varies with what I see on an image. Because of the limited number of pixels, displaying two breasts on one monitor works only if a woman has small breasts. (2) Display luminance: The limited luminance limits resolution in darker portions of the image. We have previously evaluated the ability of one high quality monitor to respond to changes in luminance and found that the characteristic curve was distorted in the blacker regions of the image. (Appendix 9) In effect the blacks are not black enough probably secondary to internal reflections in the CRT. Because of the wide variation of breast density that results in wide variations of exposure information, one needs the same range of output OD that one would have on a screen film or laser print image. (3) Bloom: In high brightness regions of an image, image bloom can occur decreasing the sharpness of small bright objects such as microcalcifications. In our study of digitized film we found that microcalcifications were less visible on monitors, which we believe is, at least in part, due to bloom effects. (Appendix 2) (4) Center-edge-corner variations in focus: All CRT displays vary in focus between the center and the edge and the corners of the monitor face. This is because of the radius of curvature of the CRT face is such that the distance from the CRT gun to the tube face varies. Because microcalcifications can occur anywhere in the breast, this may result in lesser degrees of detection.

Hard copy display: Quite early in our work we realized that the laser film printers available to us were not optimized for use in digital mammography. There are several reasons for this:

(1) Radiologists interpreting mammography usually use a magnifying lens to better see microcalcifications. Until quite recently, laser imagers were not designed with this need in mind and therefore, with magnification, the scan lines became visible. In the same way that grid lines interfere with the ability to see microcalcifications on screen film mammograms, scan lines decrease the visibility and degree of certainty of detection of microcalcifications. There are several potential solutions to this problem but each requires equipment modification and development. We have been monitoring this and believe that there are two current systems that are adequate (but not optimal), and a third that we will be testing in the near future. Improvements in the scanning mechanism of traditional laser printers to decrease the visibility of scan lines can occur in three ways: improved alignment control allowing a larger spot size without overlap, overlapping scanning, and increasing the number of pixels used for each pixel in the original image. We have found that the 3M 969 laser printer provides much less visible scan lines without affecting apparent conspicuity of microcalcifications. We have used this printer to print the images used in our ROC study. We are about to acquire a new Fuji laser printer that uses 4 pixels in the print for each pixel

at acquisition and will be testing this once it arrives. In addition, a newer method for producing a laser print: creating a digital representation of digital data, as is done in the Polaroid Helios printer, provides very high quality dry prints. We have tested this, but have not yet done a formal comparison study of it.

(2) Look-up table: The look-up tables available for laser printing of digital mammograms are not optimal. We have been working with Polaroid to develop new look-up tables to improve image quality for their printer. Look-up tables for digital mammography will probably have to be optimized to each individual laser printer.

(3) Display size: Digital mammograms are acquired at a specific pixel size. Laser printers print with a specific pixel size. Current digital mammography systems and current laser printers are not matched in pixel size. This results in images that are not life-size. Since minor enlargement of a mass may indicate that it is malignant, accurate measurement of the size of a mass is important. Correcting for differences in size is time consuming and can result in errors of interpretation.

(4) Electronic accuracy: Microcalcifications can result in quite subtle differences in optical density. Variations induced by scanning speed variations and ripples in the power system can result in visible variations in scan line optical density that can be confused with microcalcifications. The control requirements for this are higher than in laser imagers used for other purposes. Some laser images appear to have problems with the degree of scanning control needed.

Of the systems we have tested, we believe that the 3M 969 laser printer is appropriate for use and that the Polaroid Helios printer is probably appropriate for use. Better laser printers such improve the conspicuity of lesions on digital mammograms. These systems must be optimized for digital mammography prior to use.

Clinical Case Series

We have been collecting a set of cases in which we have in each case the original screen film mammogram, the storage phosphor 100 micron direct digital mammogram obtained on the latest update of equipment and software, and the biopsy specimen radiograph. We currently have over 130 cases containing more than 30 proven cancers. The data for the direct digital mammograms is stored electronically and each of the original screen film mammograms has been digitized and is available in 50 micron and 100 micron formats. As of November 1995, we have sufficient cases of adequate quality to perform an ROC study. Because of an important update in software that resulted in improved digital mammography acquisition, an earlier dataset was not used; the current dataset has been collected since March 1995. We delayed starting our ROC study because the laser imagers available to us were not considered adequate. We received our new 3M 969 laser and created with the aid of Analogic Corporation an adequate interface during the Summer of 1996 and are currently performing our ROC analysis.

We have also digitized 100 cases in which we can compare wider and narrower latitude films. The prior film system was the Dupont Mammography screen film system. The newer higher contrast system is the Fuji IM Fine mammographic system and has moderately higher contrast. We still do not have an adequate method of printing high quality images from this dataset.

Digitized Film Methodology

Our initial choice of film digitizer (DBA, Inc.) proved unstable and despite many attempts by the manufacturer to improve the product, remained unstable. Eventually we decided that the system would not be able to provide the quality we needed. In 1995, we switched to the Lumisys 50/100 micron system. We have digitized approximately 2000 mammogram films with this system. The system still shows intermittent instability, but is adequate for our experiments.

Digitized Film Mammography Display

We have developed display parameters for the soft copy display of digitized film mammograms on the Vicom display system. This Sun computer based system using Megascan monitors provides sufficient flexibility to allow us to test soft copy display. We have performed a reader comparison study in which 25 cancer images, 25 benign biopsy cases and 50 normal images were compared by 5 radiologists who evaluated the image preference looking at the visibility of microcalcifications, masses, and asymmetric densities on the original screen film mammogram and on the soft copy display. The full report of this is attached as Appendix 2. The radiologists were allowed to adjust the window level and width on the displayed images. All 5 radiologists expressed strong preference of the hard copy display for microcalcifications. In some cases the microcalcifications could not be seen on the soft copy display and in some cases dust and pick artifacts appeared on the soft copy display with an appearance that could not be distinguished from the appearance of microcalcifications, whereas on the hard copy display they could be easily determined to represent dust or pick artifacts.

So far we have assessed only 100 micron pixel digitized film images. We will evaluate a smaller sample of 50 micron digitized film images in the near future. We do not have a clinically usable method for the display of 50 micron digitized film images on soft copy displays since the pixel size exceeds that of available monitors. Thus one ends up looking at images in segments -- 1/4 of the image displayed at a time. This therefore would not be clinically practical. Our original concept was that one could assess the image with the pixels combined to produce 100 micron pixel size and zoom into the full dataset when a suspicious region was found. What we have found is that we cannot identify many of the regions containing suspect calcifications on the 2K matrix-100 micron pixel images and therefore would not know where to zoom the image. We consider zooming the entire image impractical for clinical use. We are unaware of any 4K display with sufficient luminance for clinical radiography.

Digitized Film Mammography: Hard Copy Display

Our first hard copy display of digitized film mammography was in June 1993. The initial system did not provide adequate control of contrast and unsharp masking. It was clear from this initial work that the image processing capabilities of our available print server system were not sufficient for adequate display of mammography. Over the past 15 months we have been working with a supplier of print servers (Analogic Corp.) to have them build into their system adequate capabilities for us to obtain proper control of the digitized film mammography printing to assure high quality images with our existing laser printers. We are still working towards an appropriate image print system with adequate image parameter control for digitized film images. We expect to have a working system in late October or November, 1996. At present, we do not consider the hard copy images of digitized film mammography adequate for clinical diagnosis. We do not know if this is caused by the digitization process or by the printing process, since we know that the printing process is still not optimal.

Direct Digital Method

Images are currently acquired using Fuji HR-V imaging plates and a Fuji 9000 Computed Radiography system. Based on problems we identified during beta testing of this system, it was modified and appears adequate for digital mammography. Images are automatically processed using Fuji's standard parameters and the unprocessed data is then stored on the Fuji 954 workstation. We reprocess the image data sets to meet our optimized image processing standards. The image data sets are then transferred for permanent storage to a Fuji optical disk drive to provide for long term optical disk storage. This image data can be transferred through an Analogic DASM to an Analogic experimental workstation which serves both as a print server and a method of transferring the images over our internal network. The Analogic print server can (as recently developed) mimic the Fuji print parameters (except for DRC) printing to a 3M laser printer. It can also send processed images for printing as TIFF files to other printers.

Image processing for the direct digital system can be performed using the standard Fuji parameter settings. We have also found it of value to use specially designed dynamic range control curves for printing digital mammography in the radiodense breast. Our previous Annual Reports to the Army documented the procedures used to optimize image appearance. (Appendix 10)

Direct Digital Images: Hard Copy Display

We have found that the standard Fuji laser printer supplied with the original Fuji 9000 was acceptable, but less than optimal. We have printed some of these images on a Polaroid Helios Printer and other images on a 3M 969 Laser Printer and have found the image quality of these prints superior to that of the Fuji laser printer. The main reason for this is that when the images are magnified with a hand lens, the scanning lines from the printer are sufficiently wide that they interfere with the detection of microcalcifications. We expect to receive an updated Fuji laser printer by December 1996 or January 1997 for testing. The other two printers have less apparent scan lines (3M) or inapparent scan lines (Polaroid) resulting in images that radiologists prefer. At this time, we believe that the Polaroid Helios Printer will prove to be optimal, but we do not currently have funds to purchase this printer and therefore must work through Polaroid's generosity and willingness to print these images for us in their research laboratory. Polaroid placed a Helios printer at Georgetown in October 1996 and we are currently developing the interface to this system for testing.

Direct Digital Images: Viewer Acceptance of Hard Copy Display

We have displayed comparison images from the Fuji computed radiography digital system and conventional screen film images in several meetings. The acceptability of these images has been considered high by many of those viewing the images at meetings. At the RSNA Annual Meeting, 1994, we demonstrated with a backlit display the original screen film images and CR digital images of the standard breast geometric test objects, three cancers (5, 6, and 15 mm) manifested by microcalcifications, one 8mm cancer manifested by spiculated mass, and two microcalcification cases that on biopsy showed benign findings. We provided magnifying glasses and asked those who wished to indicate which images they preferred. Ninety-four percent of those who responded preferred the digital images of the test objects, 83% preferred the clinical microcalcification cases, and 57% preferred the one mass case we showed. We have shown a similar exhibit at the American Roentgen Ray Meeting in May 1995, where the exhibit received a bronze medal. The direct digital images appear to be acceptable to many of those viewing them.

ROC Study of Direct Digital Images

This study was delayed because improvements of hardware and software that occurred in March 1995 were of sufficient magnitude that we decided not to use our prior data, but only the newest data. We have selected from our collected set of digitally acquired mammograms 24 biopsy proven cancer cases, 24 benign biopsy cases and 50 cases selected by radiologists as being normals for incorporation in our ROC study. In each case we have both conventional and digital mammograms. These cases have been randomized and radiologists are now providing interpretations of these comparing (in separate reading sessions one month apart or greater) interpretations of screen film and digital mammograms. The first radiologists results have been calculated and showed an Az screen film = 0.7373 and Az digital = 0.7646 when tested for detection of cancer. When tested as a method of discrimination between cancer and benign lesions that were detected, the Az of screen film = 0.5743. The Az of the digital system = 0.7412.

Direct Digital Mammography and the Radiodense Breast

In 1993, we determined that the wider exposure latitude of the storage phosphor plate system did indeed allow the recording of useful information in mammographic test objects over a wider range of exposures than did standard mammographic film screen systems. This information was included in our Annual Report to the U.S. Army in 1994. This was determined by our systematic response surface optimization experiments and was reported in 1995. (Appendix 11)

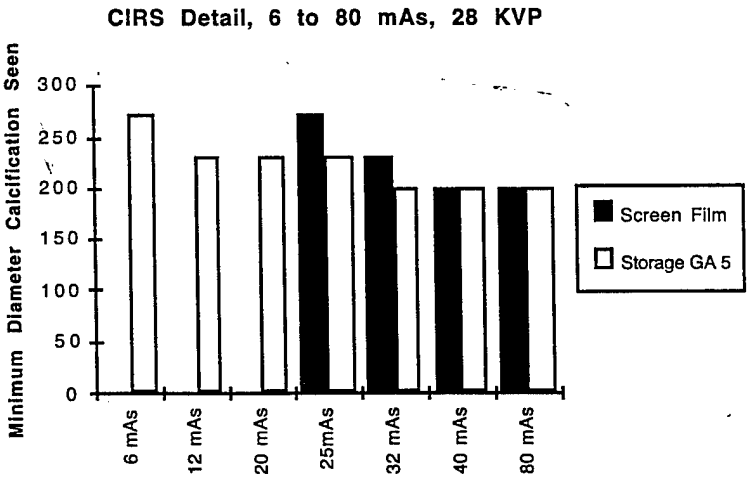

This chart demonstrates that at mAs less than 25, while the storage phosphor system could demonstrate objects, the screen film failed to demonstrate any of the objects. At 25 and 32 mAs, the storage phosphor demonstrated smaller objects than screen film. At 32, 40, and 80 mAs, the two systems performed equivalently. (Storage = Storage Phosphor Radiography. GA = gradient angle of the look up table.) These results indicate that there is information available that can be captured by the storage phosphor plate that correlates to those regions seen in mammograms as radiodense (clear or almost clear) regions of the image. (From Freedman, 1995 B)

Although we knew of this phenomenon in 1993, we did not have a clinically useful method of retrieving this information for display in a clinical setting. If we attempted to include the full range of information in a single image, the resulting image was of low contrast and not clinically useful. If we attempted to post-process the images so that one image reflected the high exposure image and another the low exposure image, the Fuji

PRIEF prevented it. In June 1994, I requested Fuji to modify their software so that I could test a system for bypassing the PRIEF effect using the Dynamic Range Control (DRC) system software with special DRC curves. These curves were provided in the Spring of 1995 but resulted in system crashes. The modified software became available in the Summer of 1995. The effect of DRC using these new curves was to provide images that contain both levels of exposure data in a single image.

Although the math is more complex, the easiest way to understand the effect of DRC in mammography is to consider it a complex form of image processing. In this image processing, the image is separated into two images: a low frequency mask and an original image. Histogram equalization is then performed on the low frequency mask and this mask is then subtracted from the original image. This final image shows a decreased range grayscale of pixel values that covers large regions of the image, but leaves intact the pixel values of high spatial frequency regions. Since the high frequency regions represent the microcalcifications and edges of most masses, the resulting image provides the ability to see the high frequency structures of the breast potentially from the skin line to the most dense regions of the breast (as shown in figure 1) while preserving the visibility of microcalcifications (as shown in figures 2 a and b).

Three types of modification of the look-up table are possible. These are explained in a paper presented at the SPIE Medical Imaging 1996 meeting (attached as Appendix 12).

The Fuji software still imposes limits so that we cannot produce the optimal image automatically and some cases show the effect better than others. Currently, we cannot reprocess images retrieved from the optical disk drive, but only those still stored as original data on the Fuji 254 workstation hard disk, but have requested a software modification from Fuji Japan to allow this. We have, however, been able to partially mimic this effect using wavelet transforms and are working to improve this. We are also working with Fuji to better define the applications of this algorithm. We believe that this will allow us to better image the radiodense breast allowing us to see microcalcifications and possibly masses better than on screen film mammography. If we are correct in our analysis, this new form of digital mammography may improve the sensitivity of mammography for the detection of breast cancer in women under the age of 50. Since 37% of the breast cancer new cases seen at Georgetown occur in this age group and the current sensitivity of mammography in this age group is 60-68% (compared to 90% in women over the age of 50), we consider this a most important development.

Digital Mammography and The Shape of Microcalcifications

Concern has been expressed that digital mammography at 100 micron pixel size will not allow sufficient information about the shape of microcalcifications to be seen. Based on this concern, we have recently performed an experiment in which we compared the original screen film mammogram, the 100 micron pixel storage phosphor mammogram and the biopsy specimen radiograph in 10 randomly selected cancer cases and 10 randomly selected benign biopsy proved cases. All cases contained microcalcifications. Four radiologists indicated their preferences between the screen film and digital images. This report is attached as Appendix 13. Briefly, the four radiologists expressed preference in the majority of cases for the digital s stem in microcalcification conspicuity. One of the four preferred the digital images for shape and number of microcalcifications, one considered each system preferable in an equal number of cases, and two preferred the screen film system. Whatever the radiologists' preferences, the radiologists were unable to distinguish benign and malignant cases on either the digital or conventional systems. Thus, although there may be a slight preference for evaluation of shape on the conventional system, this preference did

not appear to be of clinical importance since it did not help the radiologists to better classify the benign or malignant features associated with the calcifications.

The improved conspicuity of microcalcifications found by the radiologists with the digital systems suggests that these systems may prove to be better than screen film mammography in a screening setting. We are working to obtain funds for such a full scale screening test.

Current Recommendations for the Implementation of Digitized Film Mammography

We have been unable to define an adequate system for acquisition, image processing, and display for digitized film mammography that is diagnostically equivalent to conventional screen film mammography. We continue to work on this problem.

Current Recommendations for the Implementation of Direct Digital Mammography

Image Acquisition

Image acquisition with either the Fuji 9000 or Fuji AC-3 with the images printed on a 3M 969 laser printer appears adequate for diagnostic mammography. Our ROC study is expected to confirm this. This ROC study will, we expect, provide preliminary data supporting the use of this system for screening mammography. The Fuji AC-1 provides a lower quality image than the Fuji 9000 and the AC-3 and in our studies is not adequate. The lower signal to noise ratio of the AC-1 results in noisier images. It is possible that using higher exposures with the AC-1 could provide adequate images, but we have not tested that hypothesis since we would then have to exceed the standard dose used for conventional screen film mammography. The Fuji system is not FDA approved for mammography. The FDA published draft guidelines for those seeking approval of digital mammography systems. We submitted comments on their proposal. The final guidelines are still subject to comment. The guidelines resulted from a meeting the FDA held March 6, 1995. The PI of this project was one of the experts testifying at the FDA hearing.

The Fuji systems use a 100 micron pixel size which appears adequate. Tests of a commercially available 50 micron pixel small field system showed that that the 50 micron system required a higher radiation exposure and while it provided higher contrast, it did not allow the detection of smaller objects. We believe that the 50 micron system we tested can be improved upon and that the eventual 50 micron system may prove to be superior to the 100 micron system we currently use.

Image Processing

Fuji image processing modified to the following parameters appears to provide adequate display for hard copy direct digital mammography. An ROC study is in process to confirm this statistically. Application of special DRC methods appears potentially to provide improved imaging of the radiodense breast. Additional investigation of this new image processing method is underway.

GA=1.2, GT=G, GS=0.6, GC=0.3 RN=7, RT=R, RE=0.0

ABBREVIATIONS
GA, gradient angle; GC, gradient center; GS, gradient shift;
GT gradient type; RN, frequency number; RT, frequency type.

Image Display

Hard Copy Display: Display with the Fuji FL-IM3543 printer appears adequate, but not optimal. Display on the Polaroid Helios printer and 3M 969 printers result in better image appearance, but it is not yet shown that they affect diagnostic accuracy. The newest Fuji printer FL-IM D has not yet been tested by us, but in images of digital mammograms we have seen from other sites appears very promising. This system will be available for our testing late in 1996 or early 1997.

Soft Copy Display: We have not been able to produce images that we consider adequate on soft copy display systems.

Current Status of Items in Statement of Work

1. Recommended resolution size for digitized film mammography

Using existing technology, we have been unable to define a system configuration that will provide diagnostic information equivalent to conventional screen film mammography. We have more extensively tested 100 micron digitization and have shown it to be inferior to screen film in the display of microcalcifications. We have been unable to come up with a reasonable clinical scenario for the display of 50 micron digitized film.

2. Coordinating the testing of these parameters with the associate military sites

At various stages in the process of this project we have worked with Major Donald Smith MD, MAMC, Col Robert Shah, MD, BAMC, Col Ted Raia, MD, Major Robert Leckie, MD, and Major Morgan Williamson, all of WRAMC. We have also presented our results to Colonel Anna Chacko, MD of BAMC and General Russ Zajtchuk, MD, at MATMO. Two radiologists have participated in the ROC study of digital mammography; others were asked and declined. We are currently working with Major Michael Freckleton, MD, Wilford Hall AFMC on a related project.

3. Implementation document for direct digital mammography

We have defined the image acquisition parameters, image processing parameters and factors for display of direct digital mammography. Col Ted Raia, MD at WRAMC agreed prior to his retirement to have WRAMC serve as a test site for direct digital mammography to be managed by Major Morgan Williamson, MD. We are working with them towards a prospective clinical trial of direct digital mammography to be performed at WRAMC and Fort Belvoir, Virginia. The purpose of this trial will be to compile the data for FDA approval. We are currently awaiting the FDA response to comments on their draft recommendations on the performance of digital mammography clinical trials and for the FDA's final recommendations.

Conclusion

Work to optimize the appearance of digitized film mammography and digital mammography using storage phosphor technology is nearly complete. The attached report and its appendices indicate that digitized film mammography (digitized at 100 micron pixel size) is insufficient for clinical interpretation with soft copy display. Hard copy display is still insufficient. Digital mammography using storage phosphor methods has been optimized and an ROC analysis of this method using our current data set is underway. This ROC study compares matched conventional and digital images using six radiologists. Each of the

cancer and benign finding cases is pathologically proven. We are also exploring special image processing methods for the radiodense breast and these are discussed in this report. An analysis of the shape of microcalcifications comparing conventional and digital mammography using a 100 micron pixel size has been completed and shows that there is general preference for the conspicuity of microcalcifications on digital mammography. Analyses of shape and number of microcalcifications resulted in varying opinions from the four radiologists doing the comparisons. Whichever system the radiologists preferred, they were unable to differentiate benign from malignant in this series so any slight differences in shape visibility did not seem to affect classification.

Bibliography

Relevant Publications

1. Dawkins T, Freedman M, Lo S-C B, Mun S K: 35 Micron CCD Based Film Digitizer for Mammography. SPIE Poster. SPIE Medical Imaging paper 1897-53 (February 1993).

2. Freedman M, Pe E, Nelson M, Lo S-C B, Mun S K: Digital Mammography: Demonstration of a Method of Achieving Adequate Resolution on a Storage Phosphor System. CAR 93, 7th International Symposium Berlin (June 24-26, 1993); 783pp.

3. Fields F, Freedman M, Lo S-C B, Zuurbier R, Nelson M, Mun S K: Comparison of Conventional Film Screen Magnification Mammography and Electronic Magnification. Proc. SPIE: 2167, 682-689. Medical Imaging 1994: Image Processing Murray H. Loew, Ed.

4. Freedman M, Pe E, Zuurbier R, Katial R, Jafroudi H, Nelson M, Lo S-C B, Mun S K: Image Processing in Digital Mammography. SPIE: Medical Imaging, Vol. 2164 (1994); 537-554pp.

5. Freedman M, Steller D, Jafroudi H, Lo S-C B, Zuurbier R, Katial R, Hayes W, Wu Y C, Lin J-S J, Mun S K: Digital Mammography: Effects of Decreased Exposure. SPIE: Medical Imaging (1995). Paper 2432-49.

6. Freedman M, Steller D, Jafroudi H, Lo S-C B, Zuurbier R, Katial R, Hayes W, Wu Y C, Lin J-S J, Steinman R, Tohme W G, Mun S K: Digital Mammography: Tradeoffs Between 50- and 100-micron Pixel Size. Proc. SPIE: Medical Imaging 1995. Paper 2432-09. pp 114-125/ Physics of Medical Imaging, Richard L Van Metter; Jacob Beutel; eds.

7. Y. Chris Wu, Richard Patt, Matthew Freedman, Seong Ki Mun . Three dimensional image visualization and analysis in breast MR imaging for diagnosis of breast cancer. SPIE Medical Imaging 1996. In press.

8. S.-C. Benedict Lo, Huai Li, Matthew Freedman, BH Krasner, SK Mun Optimization of wavelet decomposition and feature-guided image compression for mammography.. SPIE Medical Imaging 1996. In press

9. Robert Jennings, FDA , Hamid Jafroudi, Georgetown; FDA: R Gagne; NIH: James Vucich. Georgetown: D. Artz, M. Freedman, SK Mun Storage phosphor-based digital mammography using a low dose x-ray system optimized for screen-film mammography system. SPIE Medical Imaging 1996. In press

10. Hamid Jafroudi, SCB Lo, MT Freedman, SK Mun. Dual Energy in mammography: feasibility study. SPIE Medical Imaging 1996. In press

11. Matthew Freedman, Dot Artz, H Jafroudi, J. Hogge, RA Zuurbier, R. Katial, SK Mun. Digital mammography in the radiodense and complex pattern breast. Proc. SPIE 2701, 783-793. Medical Imaging 1996. Image Processing, Murray H. Loew, Kenneth M Hanson eds.

12. O.Tsujii, YC Wu, MT Freedman, A Hasegawa, RA Zuurbier, SK Mun. Classification of microcalcifications in digital mammograms for the diagnosis of breast cancer. SPIE Medical Imaging 1996. In press

13. Matthew Freedman, Dot Artz, H Jafroudi, J. Hogge, RA Zuurbier, R. Katial, SK Mun Digital Mammography: an evaluation of the shape of microcalcifications. SPIE 2708, 626-632. Medical Imaging 1996. Physics of Medical Imaging. Richard L Van Metter and Jacob Beutel, eds.

14. Freedman MT, Artz DS, Mun SK: Image processing in digital mammography: the optimum image for each womans breasts. pp. 1/1-1/3. IEE Colloquium on Digital Mammography. 1996. The Institution of Electrical Engineers, London.

Relevant Exhibits

1. Dawkins T, Freedman M, Lo S-C B, Mun S K: 35 Micron CCD Based Film Digiter for Mammography. SPIE Poster. SPIE Medical Imaging Poster 1897-53 (February 1993).

2. Freedman M, Pe E, Nelson M, Lo S-C B, Mun S K: Digital Mammography: Demonstration of a Method of Achieving Adequate Resolution on a Storage Phosphor System. CAR 93, 7th International Symposium, Berlin, Germany (June 24-26, 1993); 783pp.

3. Fields F, Freedman M, Lo S-C B, Zuurbier R, Nelson M, Mun S K: Comparison of Conventional Film Screen Magnification Mammography and Electronic Magnification. SPIE: Medical Imaging (February 1994). Paper 2167-67.

4. Freedman M, Pe E, Zuurbier R, Katial R, Jafroudi H, Nelson M, Lo S-C B, Mun S K: Image Processing in Digital Mammography. SPIE: Medical Imaging, Vol. 2164 (1994); 537-554pp.

Relevant Abstracts

1. Freedman M, Zuurbier R, Pe E, Jafroudi H, Mun S K, Lo S-C B: Image Processing In Digital Mammography (abstract). Radiology (1993); 189P:408.

2. Freedman M T, Steller D E, Hasegawa A, Zuurbier R A, Wu Y C, Smith D V, et al: image Processing in Digital Mammography (abstract). Radiology (1994); 193(P):474.

3. Freedman M T, Steller D E, Zuurbier R A, Jafroudi H, Mun S K: Experimental Digital Mammography in the Detection of Microcalcifications 300 mm and smaller (abstract). Radiology (1994); 193(P):422.

Relevant Presentations

1. Dawkins T, Freedman M, Lo S-C B, Mun S K: 35 Micron CCD Based Film Digiter for Mammography. Poster. SPIE: Medical Imaging, Paper 1897-53 (February 1993).

2. Freedman M, Pe E, Zuurbier R, Katial R, Jafroudi H, Nelson M, Lo S-C B, Mun S K: Image Processing in Digital Mammography. SPIE: Medical Imaging, Vol. 2164 (1994); 537-554pp.

3. Freedman M T, Steller D E, Hasegawa A, Zuurbier R A, Wu Y C, Smith D V, et al: Image Processing in Digital Mammography (abstract). Radiology (1994); 193(P):474.

4. Freedman M T, Steller D E, Zuurbier R A, Jafroudi H, Mun S K: Experimental Digital Mammography in the Detection of Microcalcifications 300 mm and smaller (abstract). Radiology (1994); 193(P):422.

Appendices

LUT of conventional and New Mammography Films

Implementation and Testing of Digital Mammography for MDIS Environment

Digital Mammography: Tradeoffs between 50- and 100-Micron Pixel Size

Georgetown ROC Study of Digital Mammography: Results of first ROC reader

Digital Mammography in the Radiodense and Complex Pattern Breast

Image Optimization Procedures for the Fuji AC-1

Image Processing in Digital Mammography

Image Processing in Digital Mammography: The Optimum Image for Each Woman's Breasts

Display Characteristics and Tansformation in Film and CRT Monitor

First Year Annual Report to Army

Digital Mammograohy: The Effects of Decreased Exposure

Single-Image Hardcopy Display of Musculoskeletal Digital Radiographs

Digital Mammography: An Evaluation of the Shape of Microcalcification

Staff Supported on Contract # DAMD17-93-J-3008

Matthew Freedman, M.D.
Shih-Chung Benedict Lo, Ph.D.
Rebecca A. Zuurbier, M.D.
Akira Hasegawa, Ph.D.
Dorothy Stellar Artz, R.T.
Yue Wang, Ph.D.
Hamid Jafroudi, Ph.D.
Wendelyn Hayes, D.O.
Brian H Krasner, Ph.D.
Jyh-Shyan Lin, Ph.D.
Francine Fields
Walid Tohme, Ph.D.
Martha Nelson, M.D.
Hui Liu

STEP #	OD VALUE K&D	OD VALUE F&F
1	0.16	0.17
2	0.16	0.17
3	0.16	0.18
4	0.17	0.19
5	0.19	0.21
6	0.23	0.28
7	0.34	0.46
8	0.57	0.82
9	0.98	1.36
10	1.49	1.96
11	2.11	2.57
12	2.61	3.02
13	3.04	3.32
14	3.38	3.5
15	3.69	3.62
16	3.85	3.67
17	3.99	3.69
18	4.11	3.73
19	4.16	3.76
20	4.17	3.76
21	4.19	3.77

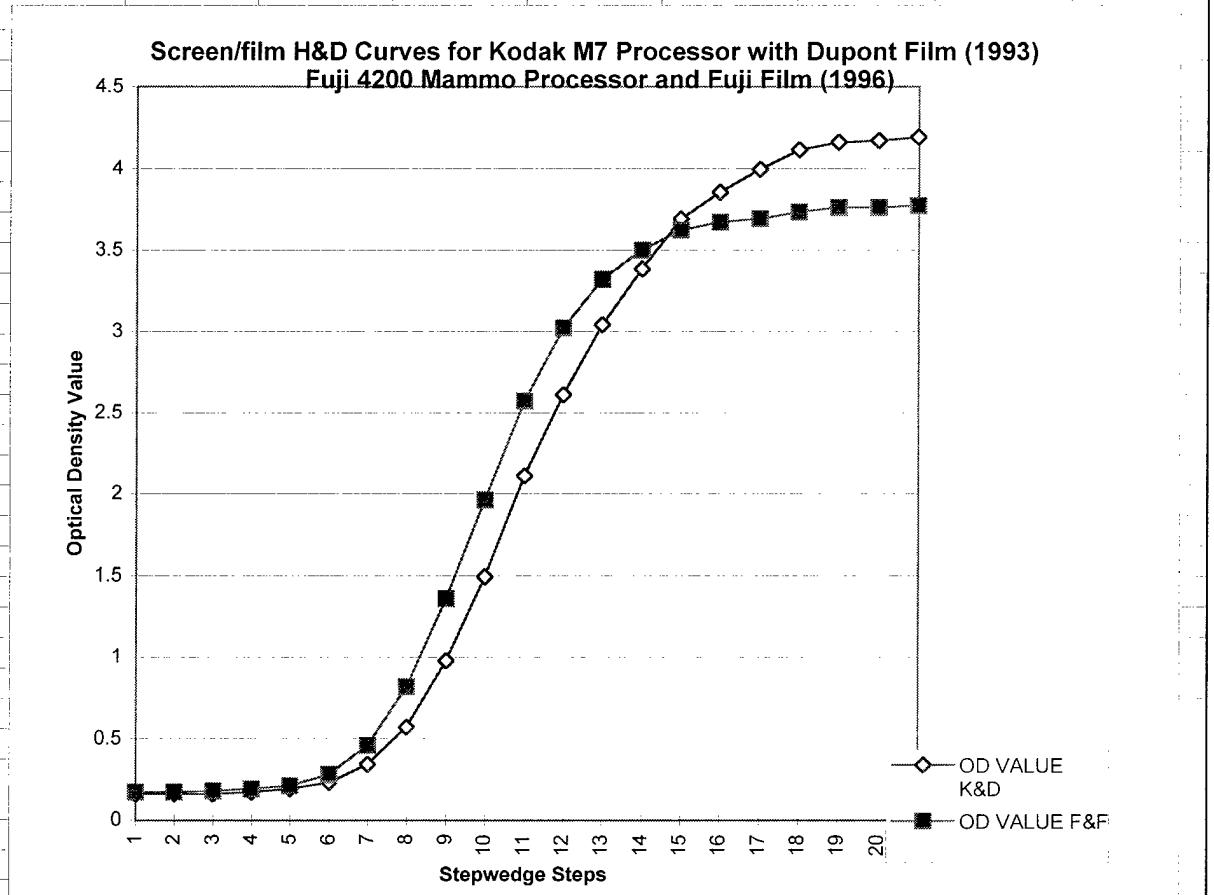

Implementation and Testing of Digital Mammography for MDIS Environment

December 31, 1995

Georgetown University Medical Center
Department of Radiology
Imaging Science and Information Systems (ISIS) Center
2115 Wisconsin Ave., NW, Suite 603
Washington, D.C. 20007

http://www.isis.imac.georgetown.edu

Project leaders

Seong K. Mun, Ph.D., Director of ISIS Center
Matthew Freedman, M.D., M.B.A., Clinical Director of ISIS Center

Principal Investigator

Jyh-Shyan Lin, Ph.D.
Research Associate
☎ 202/687-7953
Fax: 202/784-3479
E-mail: jslin@isis.imac.georgetown.edu

Table of Contents

List of Figures

List of Tables

1. INTRODUCTION

1.1. Objective

The objective of this project was to evaluate image quality of digital mammography based on computed radiography (CR) and high resolution film digitizer and develop a strategy to implement digital mammography into the military diagnostic imaging systems (MDIS) environment.

1.2. Project Schedule

Start Date: October 1, 1994
End Date: December 31, 1995
There are total 15 months which are divided into 5 quarters.

First Quarter (October 1, 1994 - December 31, 1994)
Budget request: 40%
Goals:
1. Set up of an experimental system.
2. Study of physics characterization of data acquisition modules.
3. Data collection and database management.

Second Quarter (January 1, 1995 - March 31, 1995)
Budget request: 20%
Goals:
1. Collection of 10 clinically relevant cases in all modalities.
2. Comparative reading of 10 cases in hard copy and soft copy.

Third Quarter (April 1, 1995 - June 30, 1995)
Budget request: 20%
Goals:
1. Collection of 10 clinically relevant cases in all modalities.
2. Comparative reading of 10 cases in hard copy and soft copy.
3. Technical evaluation of MDIS database to determine suitability for digital mammography.

Fourth Quarter (July 1, 1995 - September 31, 1995)
Budget request: 10%
Goals:
1. Collection of 20 clinically relevant cases in all modalities.
2. Comparative reading of 20 cases in hard copy and soft copy.
3. Determination of MDIS workstation functionality for digital mammography.

Fifth Quarter (October 1, 1995 - December 31, 1995)
Budget request: 10%
Goals:
1. Comparative reading of 10 cases in hard copy and soft copy.
2. Data analysis.
3. Final report.

1.3. Participants

- Case selection
  - Rebecca Zuurbier, M.D., Director of Breast Imaging, GUMC
  - Jaquelyn Hogge, M.D., Mammographer, GUMC
- Collection of Fuji CR9000 and screen film mammograms - Dot Artz, R.T., R.M.
- Digitization of screen film mammograms - Two part time students of Georgetown University
- Data management and image processing - Jyh-Shyan Lin, Ph.D., ISIS Center, GUMC
- Vicom display workstation - Akira Hasegawa, Ph.D., ISIS Center, GUMC.
- Comparative reading - Five board-certified radiologists of Radiology Department, GUMC
  1. Matthew T. Freedman, M.D., M.B.A. - Clinical Director of ISIS Center
  2. Rebecca Zuurbier, M.D. - Director of Breast Imaging
  3. Jaquelyn Hogge, M.D. - Mammographer
  4. Wendelin Hayes, D.O. - Associate Professor of Radiology
  5. Curtis Green, M.D. - Radiologist

2. EXPERIMENTAL SYSTEM CONFIGURATION

2.1. Set up of an Experimental System

The experimental system configuration is shown in Figure 1. The key components are: a Fuji CR9000 (FCR9000), a Lumisys film digitizer, a data acquisition and system management (DASM) host Sun workstation, a digitizer host Sun workstation, and a Vicom high resolution display workstation.

The Fuji Computed Radiography 9000 System

The DASM controls the data transfer from the FCR9000 to the host Sun workstation through the small computer system interface (SCSI) cable. Each CR image contains a 2048 bytes image header. The CR images were then processed and transferred to the Vicom display workstation. A second channel interface board (SCIB) was installed for the purpose of simultaneously interfacing with DASM and an optical disk device. Original CR images including biopsy specimen were backed up in the optical disks.

The Lumisys 150 High Resolution Laser Film Digitizer

Conventional screen films (SF) were digitized by a Lumisys high resolution film digitizer. Digitized SF images were transferred to the digitizer host Sun computer through the SCSI, processed, and then transferred to the Vicom display workstation.

- The Lumisys 150 meets the film digitizer requirements by MDIS which are variable spot size, different film sizes (from 8" × 10" up to 14" × 17"), minimum spot size of 210 microns, and 10 bits minimum dynamic range (i.e., 10 bits per pixel). The density resolution and precision is a linear function from 0 to 3.5 optical density (OD). The Lumisys 150 film digitizer can determine the film size automatically. It can convert films sized from 8" × 10" up to 14" × 17" into digital images of 2048 pixels × 2560 lines with 12 bits per pixel (10 Mbytes). The 8" × 10" films can also be digitized at 50 μm spot size which is equivalent to 4096 pixels × 5120 lines with 12 bits per pixel (= 40 Mbytes). The laser spot size can be auto-adjusted accordingly.
- The Lumisys 150 does not provide automatic sheet feeder. A more advanced Lumisys 200 digitizer will have the function of automatic sheet feeder which is able to hold and automatically feed at least 10 x-ray films of intermixed sizes. The digitizer generates two file formats: raw binary image and TIFF compressed images for image preview. The image previewing software is the x-window view (XV) software program run on the SUN digitizer host computer. The Lumisys 150 does not support the American College of Radiology (ACR)-National Electrical Manufacturers Association (NEMA) standard.
- Phantoms, such as CIRS, ACR, CDMAM, step wedge, and SMPTE, were digitized at 50 micron and 100 micron and displayed on the Vicom display workstation. The Lumisys digitized phantoms showed satisfactory quality.
- The Lumisys high resolution digitizer (Model: 150) is set up to digitize conventional SF at 100 μm resolution. Currently, the Lumisys digitizer is now located in the mammography reading room in Georgetown University Medical Center (GUMC) and is being used routinely to digitize clinical cases. Each clinical case consists of four recent and four previous mammograms with pathology reports.
- The Vicom display workstation is a Pixar-based system which has four high resolution MegaScan monitors. Each display monitor can display image data of 2048 × 2560 × 8 bits. The display workstation provided window-and-level function for adjustment of image brightness and contrast. Each monitor can be manipulated individually.

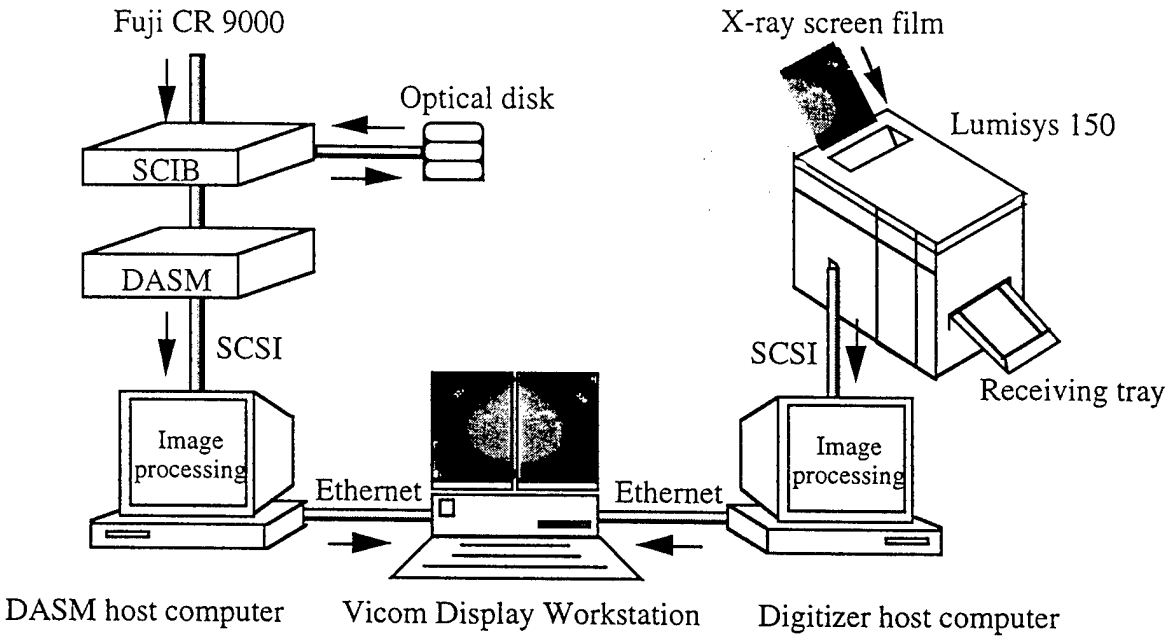

DASM: data acquisition and system management
SCSI: small computer system interface
SCIB: second channel interface board

Figure 1. Experimental System Configuration.

2.2. Study of Physics Characteristics of Data Acquisition Modules

• Quality control (QC) on a Fuji printer and a Fuji CR9000

• QC of 18 cm × 24 cm image plate (IP):

Every morning each 18 cm × 24 cm IP received secondary erasure through FCR 9000 to ensure that a properly erased IP was in each cassette before any images were obtained. This process reduces possible residual radiation in the plate and ensures the best possible image.

• QC of Fuji 9000 laser printer (LP):

Every morning a cleaning film was run through the LP, then the density and check density were adjusted. A step wedge was produced from both steps. After the step wedge pattern is obtained from the check density, the optical density values was displayed on the LP display. The values and graph similar to sensitometry graph for a film processor were recorded.

• QC of mammography film processor:

Normal sensitometry graphing, cassette cleaning, exposure monitoring were performed according to ACR standard.

The quality control for mammography film processor and Fuji LP was performed by in-house engineering.

• Lumisys Film Digitizer and the Vicom Display Monitors

• Lumisys film digitizer:

We have performed maintenance of the Lumisys scanner periodically. The maintenance includes dust removal of the reflection mirror, the pinch roller, and the aperture of the detector, and adjustment of the voltage of both the main and the reference detectors [1]. The digitizer is also calibrated based on a Lumisys test pattern. The maintenance is to assure the digitization quality and calibration of the digitizer.

• Vicom workstation:

The Vicom system has four 2k × 2.5k display monitors. Each monitor can display a full data set of a 8 × 10" mammogram digitized at 100 micron. The brightness is 60 foot-Lamberts and the gray level is 256 shades. Since there is no single set of window (i.e., contrast) and level (i.e., brightness) values for every image display, the look-up table of the system was preset to a set of window and level values visually determined by a physicist, a registered mammographer, and a scientist. The purpose is to adjust the two monitors such that they have similar intensity and contrast. The contrast and brightness can be adjusted by using a trackball during the study of comparative reading.

3. DATA COLLECTION AND MANAGEMENT

3.1. Case Selection and Data Collection Protocol

The database used in this study included 50 cancerous and non-cancerous cases. All the cases contained bilateral breast images, radiology reports, and related pathology reports. Biopsy was used as the standard proof of cancer or non-cancer. Each set of bilateral mammograms contained either left-right cranio caudal (CC) or left-right mediolateral oblique (MLO) views. We collected 50 CR soft copies, 50 CR hard copies, 50 SF hard copies, and 50 soft copies of digitized films. Table 1 lists the collected database of the 50 clinically relevant cases. The table shows fake patient identification numbers (ID) for patient confidentiality. A similar table with real patient name and ID is available and kept securely at GUMC. In the table, "BRST" represents breast, "BX" represents biopsy, "MAMMO" means mammogram, and "POS FOR CA" means positive for cancer. One half of the cases contained microcalcifications, one half of cases contained masses, and some cases of architecture distortions were included. Films were digitized in such a way that most patient demographic data were excluded.

3.2. Data Management

- The Lumisys model 150 film digitizer was set up at 100 micron scanning mode.
- Actual size of hard copy:
  - Hard copy SF: 8 inch × 10 inch.
  - Hard copy CR: 11 inch × 14 inch.
- Actual size of soft copy:
  - 100 micron/pixel for the CR soft copies.
  An image size is 8,404,136 bytes (including image header) per CR soft copy.
  - 100 micron/pixel for the soft copies of digitized SF.
  An image size is 10,485,760 bytes (including image header) per digitized SF.
- The soft copies of SF and CR both contain 2,048 bytes image header.
- Storage of soft copies: DEC optical disks (595 MB per optical disk).
  A set of two digitized films (left and right breasts) and two soft copies of CR (left and right breasts) has approximately 40 Mbytes, hence for 50 cases of processed and non-processed images we ned 50 cases × 40 Mbytes/set × 2 = 4 Gbytes = 8 DEC optical disks. For other ISIS research projects, such as the classification of benign and malignant microcalcifications, we have also digitized the mammograms at 50 μm resolution using the Lumisys film digitizer. Digitized image data were stored on optical disks as well as a Hewelett-Packard (HP) jukebox.

3.3. Image Processing Protocol

- Decode the image headers of Lumisys digitized images.
- Encode image data - rearrange display scanning lines.
- Attach Pixar II image header.
- Move images to the fast disks of Vicom workstation for display.

Table 1 Database of 50 Clinical Relevant Cases

ID #	DATE	DIGITAL VIEWS	BRST FOR BX	MAMMO FINDINGS	PATHOLOGY RESULTS	POS FOR CA
1	6/8/95	Bilat. CC	Left	Ca++	1mm ductal CA +DCIS	yes
2	9/29/95	Bilat. CC	Right	mass	fibroadenoma	no
3	12/12/94	Bilat. CC	Left	mass	fibrocystic changes	no
4	12/8/94	Bilat. CC	Right	spic. mass with Ca++	intraductal CA	yes
5	1/24/95	Bilat. CC	Right	Ca++	invasive intraductal CA	yes
6	7/13/95	Bilat. CC	Right A73	small mass	ductal hyper. Ca++	no
7	12/20/94	Bilat. CC	Right	spic. mass	ductal hyper. Ca++	no
8	3/3/95	Bilat. MLO	Right	mass	ductal hyperplasia	no
9	6/12/95	Bilat. CC	Left	mass with Ca++	fibrocystic changes	no
10	6/1/95	Bilat. CC	Left A111	mass with Ca++	small fibroadenoma	no
11	8/24/95	Bilat. CC	Bilat.	Ca++	intraductal CA	yes
12	7/24/95	Bilat. CC	Right A90	Ca++	intraductal CA	yes
13	6/19/95	Bilat. CC	Right A48	multiple masses	fibrocystic changes	no
14	6/2/95	Bilat. CC	Left	mass	8mm infiltrating ductal CA	yes
15	6/23/95	Bilat. CC	Right	micro Ca++	stromal fibrosis	no
16	6/12/95	Bilat. CC	Left	mass	small fibroadenoma	no
17	6/23/95	Bilat. CC	Left A58	Spic. mass with Ca++	1.radial scar 2. ID CA	yes
18	7/31/95	Bilat. CC	Right A113	Ca++	radial scar with ID CA	yes
19	7/11/95	Bilat. CC	Right A98	scattered Ca++	cystic change Ca++	no
20	3/10/95	Bilat. CC	Right A55	Ca++	normal	no
21	8/2/95	Bilat. CC	Right A113	posterior Ca++	intraductal CA	yes
22	4/24/95	Bilat. CC	Right A64	dense mass	3cm papil. ductal CA	yes
23	12/12/94	Bilat. CC	Right	Ca++ at prev. surg. site	intraductal CA	yes
24	2/3/95	Bilat. CC	Left	Ca++	fibrosis	no
25	3/6/95	Bilat. MLO	Left	Ca++	intraductal CA insitu atyphyper.	yes
26	12/29/94	Bilat. CC	Left	mass with ?Ca++	fibroadenoma	no
27	6/29/95	Bilat. CC	Right	mass/prev. CA	atypical intrduct. hyperp.	no/yes
28	7/20/95	Bilat. CC	Right A152	mass	invas.ductal CA with Ca++	yes
29	12/8/94	Bilat. CC	Right	spic. mass with Ca++	intraductal CA	yes
30	6/22/95	Bilat. CC	Right A70	Ca++	intraductal papill.	no
31	2/27/95	Bilat. CC	Right	subtle Ca++	ductal hyper. Ca++	no
32	12/8/94	Bilat. CC	Right	mass	ductal hyperplasia	no
33	10/9/95	Bilat. CC	Right+Left	masses	infiltrating ductal CA	yes
34	8/17/95	Bilat. CC	Left	SUBTLE microCa++	extensive ductal CA insitu	yes
35	12/16/94	Bilat. CC	Right	Ca++ dense tissue	intraductal CA	yes
36	6/6/95	Bilat. CC	Left	mass	infiltrating ductal CA	yes
37	6/12/95	Bilat. CC	Right	mass	fibroandenoma	no
38	12/5/94	Bilat. CC	Left	spic. mass with ?Ca++	intraductal CA	yes
39	12/27/94	Bilat. CC	Left	casting Ca++	fibrocystic changes	no
40	6/22/95	Bilat. CC	Right A108	2 masses	5mmand9mm invas.duct CA	yes
41	6/1/95	Bilat. MLO	Left A74	mass with Ca++	fibrocystic change	no
42	7/28/95	Bilat. CC	Left A116	Ca++	fibrocystic change Ca oxalate	no
42	3/6/95	Bilat. CC	Left	Ca++	hyperplasia	no
44	7/11/95	Bilat. MLO	Right A88	palpable mass not seen	no lesions indentified	no
45	7/13/95	Bilat. CC	Bilateral R A154	Ca++	R-early insitu L-fibrocyst.	yes-no
46	11/22/94	Bilat. CC	Right	spic. mass with Ca++	infiltrating CA	yes
47	1/13/95	Bilat. CC	Left	Ca++	ductal CA in situ	yes
48	8/17/95	Bilat. MLO	Left	hx nodular fascitis (benign)	mass excised no bx report	no
49	12/15/94	Bilat. CC	Left	nodule	fibrocystic changes	no
50	11/17/95	Bilat. CC	Right	subtle Ca++mid post.	intraductal CA comedo type	yes

4. COMPARATIVE READING

4.1. Preference Study of Hard Copy and Soft Copy of Screen Films

We performed a preference study to evaluate image quality of digital mammography derived from conventional screen films (i.e., hard copies) and a high resolution film digitizer (i.e., soft copies). We wanted to compare one view (either CC or MLO) of original mammograms with the digitized film at 100 micron spatial resolution. The SF hard copies were digitized and directly converted to Vicom format (see Section 3.3 Image Processing Protocol). Five board-certified radiologists, Dr. Wendelin Hayes (radiologist 1), Dr. Jaquelyn Hogge (radiologist 2), Dr. Matthew T. Freedman (radiologist 3), Dr. Curtis Green (radiologist 4), and Dr. Rebecca Zuurbier (radiologist 5), participated in this study of preference reading of soft and hard copies.

• **Set up of environment for human readers**

The reading environment for human readers was set up as follows:

- Low level ambient light.
- No time limit in the comparative reading of each case.
  - Radiologists can use trackball to control the window-and-level while viewing soft copies on the Vicom monitors. Note that, in this study, the window-and-level was controlled by the principal investigator while the radiologist requested the change of the intensity and contrast of the displayed images.
- Light box was used with emulsion side facing the reader.
- Human readers have to fill out the questionnaires (see Section 4.2) provided in this study
- Pairs of hard and soft copies of an SF will be displayed on the light box and two Vicom monitors, respectively (Figure 2). The human readers filled out the questionnaire.
- Hard copies and soft copies are both displayed in anatomically corrected views.
- Each hard copy was labeled as #1, #2, etc. The patients' demographic data on the screen films were covered up (on the dull side of the SF) by using black electrical tape.

• **Comparative reading and reading-order effects**

- Sample size (Table 1): 25 cases of proven biopsy cancer and 25 cases that appeared malignant but were proven by biopsy to be benign.
- In the first 25 cases, two of the human observers first read hard copies and then soft copies of the SF while the other three read the two modalities in the opposite order. In the second 25 cases, the two of the human observers read soft copies of the SF first and then hard copies while the other three read the two modalities in the opposite order. The purpose of this reading order arrangement was to reduce the *reading-order effects* [2]. The reading-order effects result in the biases that occur in a situation when two or more equivalent images of a particular patient are read in different order by the same observer. It is normally the case that the image read last will tend to be interpreted more accurately than the image read first if any relevant information is retained by the observer from a reading of one image of the patient to the next.
- During the comparative reading, the radiologist can always look back-and-forth to the two image modalities retrospectively and repeatedly.
- The questionnaire contained nine questions with check mark areas. If no lesions, such as microcalcifications (questions 1 and 2), masses (question 3 and 4), and asymmetric densities (questions 5 and 6), were found, the check mark areas were left blank. On the other hand, if both hard and soft copies of SF were equally well rated, both areas were marked.

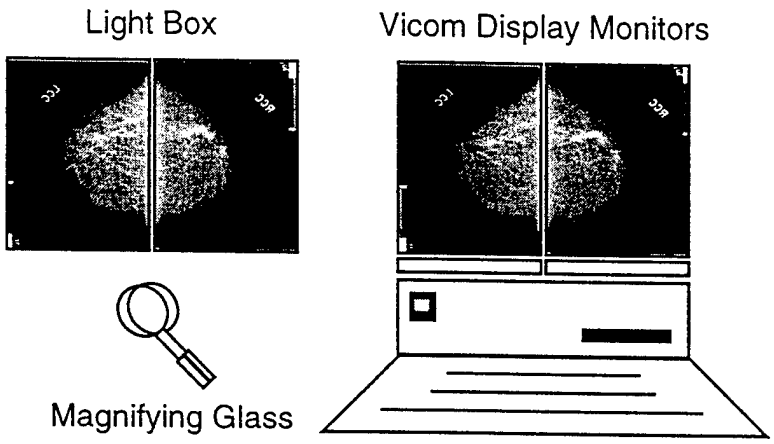

Fig. 2. Comparative Reading.

4.2. Questionnaire for Comparative Reading

Soft copy *vs.* Hard copy of SF

Viewer initial: _____ Date: _____

1. On which do you detect microcalcifications better?
   Hard copy _____ or soft copy _____.

2. Which one better characterized the microcalcifications as to malignant *vs.* benign?
   Hard copy _____ or soft copy _____.

3. On which do you detect masses better?
   Hard copy _____ or soft copy _____.

4. Which one better characterized the masses as to malignant *vs.* benign?
   Hard copy _____ or soft copy _____.

5. On which do you detect asymmetric density better?
   Hard copy _____ or soft copy _____.

6. Which one better characterized the asymmetric density?
   Hard copy _____ or soft copy _____.

7. Do you have a preference? Hard copy _____ or soft copy _____.

8. Do you see anything of clinical importance on the hard copy that you do not see on the soft copy? Yes _____ or No _____

If yes, what? _____

9. Do you see anything of clinical importance on the soft copy that you do not see on the hard copy? Yes _____ or No _____

If yes, what? _____

*Comment: _____

5. QUESTIONNAIRE RESPONSES AND DATA ANALYSIS

5.1. Questionnaire Responses

From the questionnaire (a pair of soft vs. hard copies of SF), we obtained histogram bars of the number of soft and hard copies of SF which better characterize microcalcifications, masses, and asymmetric density as to malignant *vs.* benign. Moreover, we will have the number of preferred soft and hard copies of the five human readers. The five radiologists' responses to the specific questions in the questionnaire are shown in Table 2.1 - Table 2.5 and Figure 3.1 - Figure 3.5. In each table, the columns of Q1 - Q9 represent answers for questions 1 through 9 for the 50 cases, H represents hard copy, S represents soft copy, Y means yes, and N means no. The answer "both" or "H/S" means that there was no preference, i.e., both hard and soft copies were equally well accepted. The blank and the answer "neither" mean that the question was not applicable, i.e., the disease patterns were not seen. In each Figure 3.1 - 3.5, R1 - R9 represent responses to Q1 - Q9, respectively, H means hard copy and S means soft copy.

For all the questions 1 - 7, Dr. Freedman prefers hard copy to soft copy in all cases.
For all the questions 1 - 6, Dr. Zuurbier prefers hard copy to soft copy in all cases.

Responses to question 1:
- On which do you detect microcalcifications better?
Dr. Green prefers hard copy to soft copy in 38 calcification cases and no preference in 12 cases.
Dr. Hayes prefers hard copy to soft copy in all calcification cases.
Dr. Hogge prefers hard copy to soft copy in 47 calcification cases and no preference in 3 cases.

Responses to question 2:
Which one better characterized the microcalcifications as to malignant *vs.* benign?:
Dr. Green prefers hard copy to soft copy in all 37 calcification cases and no preference in 13 cases.
Dr. Hayes prefers hard copy to soft copy in calcification cases.
Dr. Hogge prefers hard copy to soft copy in 48 calcification cases and no preference in two cases.

Responses to question 3:
- On which do you detect masses better?
Dr. Green prefers hard copy to soft copy in 6 mass cases and no preference in 26 cases.
Dr. Hayes prefers hard copy to soft copy in 23 mass cases and soft copy to hard copy in 6 cases.
Dr. Hogge prefers hard copy to soft copy in 5 mass cases, soft copy to hard copy in 10 cases, and no preference in 35 cases.

Responses to question 4:
- Which one better characterized the masses as to malignant *vs.* benign?
Dr. Green prefers hard copy to soft copy in 11 mass cases and no preference in 21 cases.
Dr. Hayes prefers hard copy to soft copy in 28 mass cases and soft copy to hard copy in one case.
Dr. Hogge prefers hard copy to soft copy in 4 mass cases, soft copy to hard copy in 8 cases, and no preference in 38 cases.

Responses to question 5:
- On which do you detect asymmetric density better?
Dr. Green prefers hard copy to soft copy in 3 asymmetric density cases and no preference in 18 cases.

Dr. Hayes prefers hard copy to soft copy in 6 asymmetric density cases and soft copy to hard copy in 2 cases.
Dr. Hogge prefers hard copy to soft copy in 5 asymmetric density cases, soft copy to hard copy in 14 cases, and no preference in 31 cases.

Responses to question 6:
- Which one better characterized the asymmetric density?
Dr. Green prefers hard copy to soft copy in 8 asymmetric density cases and no preference in 14 cases.
Dr. Hayes prefers hard copy to soft copy in all asymmetric density cases.
Dr. Hogge prefers hard copy to soft copy in 4 asymmetric density cases, soft copy to hard copy in 9 cases, and no preference in 37 cases.

Responses to question 7:
- Do you have a preference?
Dr. Green prefers hard copy to soft copy in all 50 cases.
Dr. Hayes prefers hard copy to soft copy in 48 cases, soft copy to hard copy in one case, and no preference (i.e., equally well accepted) in one case.
Dr. Zuurbier prefers hard copy to soft copy in 45 cases and no preference in 5 cases.
Dr. Hogge prefers hard copy to soft copy in 36 cases, soft copy to hard copy in 8 cases, and no preference in 6 cases.

Responses to question 8:
- Do you see anything of clinical importance on the hard copy that you do not see on the soft copy?
The five radiologists saw microcalcifications on the hard copy that they did not see on the hard copy. Sometimes dramatic window-and-level adjustment may enhance the subtle microcalcifications, however, the other breast will become either too dark or too bright. Though both masses and architecture distortion can be seen on the soft copies, they seem to increase the perception of normal soft tissue structures as abnormal .

Responses to question 9:
Do you see anything of clinical importance on the soft copy that you do not see on the hard copy?
The five radiologists saw microcalcification-like objects on the soft copy which are actually film defects on the hard copies. The five radiologists did not see anything else of clinical importance on the soft copy that they did not see on the hard copy.

Table 2.1 Questionnaire Responses of Radiologist 1

Radiologist 1	Q1	Q2	Q3	Q4	Q5	Q6	Q7	Q8	Q9
ID #	H/S	H/S	H/S	H/S	H/S	H/S	H/S	Y/N	Y/N
1	H	H					H	N	N
2	H	H	H	H			H	N	N
3	H	H	H	H			H	N	N
4			H	H			H	N	N
5	H	H	H	H	H	H	H	N	Y
6	H	H			H	H	H	N	N
7	H	H					H	Y	N
8	H	H					H	Y	N
9	H	H	H	H	H	H	H	Y	N
10	H	H					H	Y	N
11	H	H	H	H			H	Y	N
12			H	H			H	Y	N
13					H	H	H	N	N
14	H	H	S	H			H	Y	N
15	H	H	H	H			H	N	N
16			H	H			H	Y	N
17	H	H	H	H			H	Y	N
18	H	H	H	H			H	N	N
19					H	H	H	N	N
20	H	H					H	Y	N
21	H	H					H	Y	N
22	H	H	H	H			H	Y	N
23	H	H					H	Y	N
24			H	H			H	N	N
25	H	H	H	H			H	N	N
26			H	H			H	Y	N
27	H	H	H	H			H	Y	N
28			H	H			H	N	N
29			S	H			H	N	N
30			H	H			H	N	N
31	H	H	H	H	H	H	H	N	N
32			H	H			H	N	N
33			H	S			S	N	Y
34	H	H					H	N	N
35			S	H			H	N	N
36	H	H					H	N	N
37	H	H					H	Y	N
38	H	H	H	H			H	N	N
39					S	H	neither	N	N
40	H	H					H	N	N
41	H	H					H	N	N
42	H	H					H	N	N
43			S	H	H	H	H	N	N
44							H	N	N
45	H	H					H	N	N
46	H	H					H	N	N
47	H	H					H	N	N
48	H	H	S	H			H	N	N
49	H	H			S	H	H	N	N
50	H	H	S	H			H	Y	N

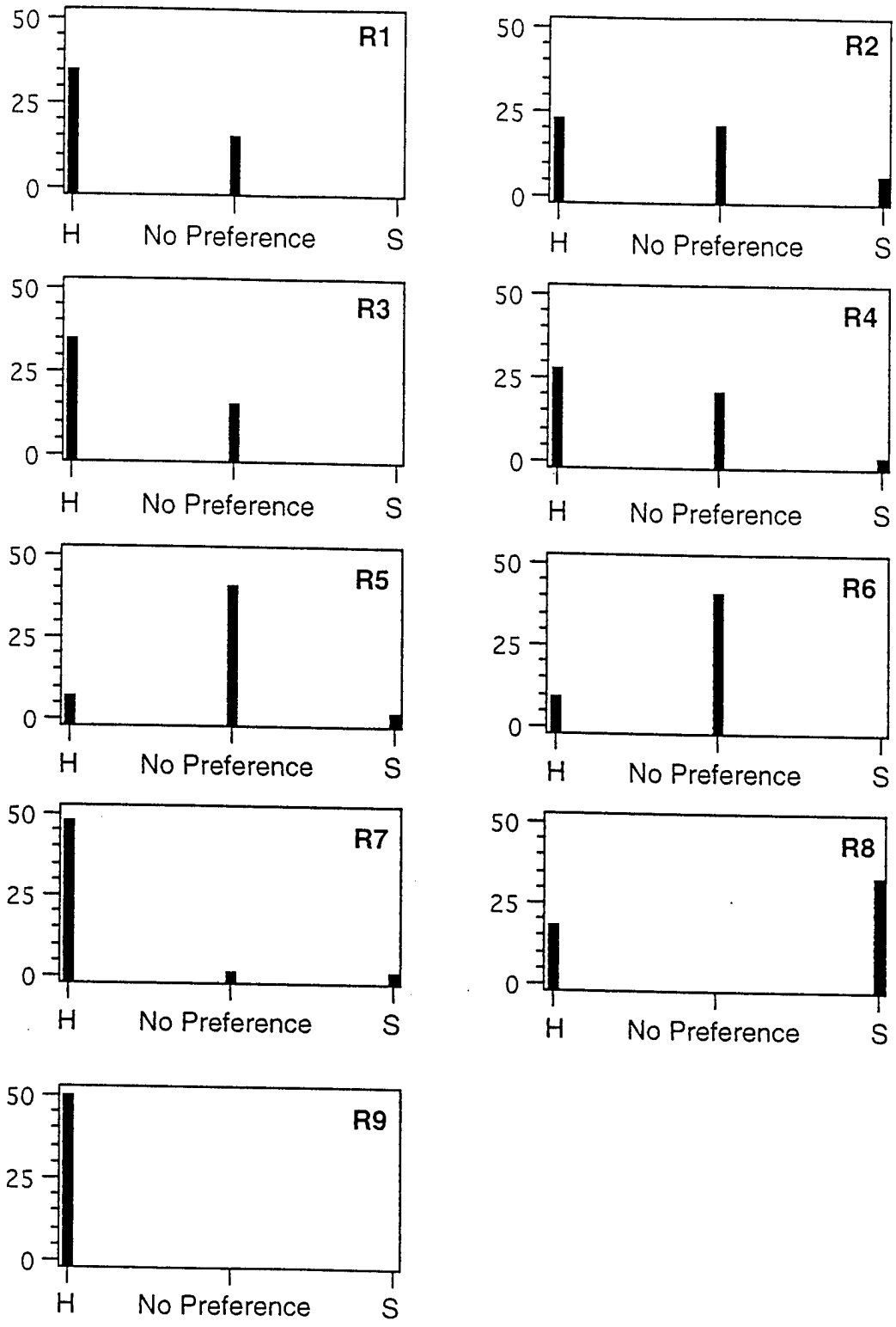

Figure 3.1 Questionnaire Response of Radiologist 1.

Table 2.2 Questionnaire Responses of Radiologist 1

Radiologist 2	Q1	Q2	Q3	Q4	Q5	Q6	Q7	Q8	Q9
ID #	H/S	H/S	H/S	H/S	H/S	H/S	H/S	Y/N	Y/N
1	H	H	H/S	H/S	H/S	H/S	H	Y	N
2	H	H	H/S	H/S	H/S	H/S	H	N	N
3	H	H	H/S	H/S	H/S	H/S	H	Y	N
4	H/S	H	H/S	neither	S	S	S	Y	N
5	H	H	S	S	S	S	S	N	N
6	H	H	H/S	neither	S	neither	neither	Y	N
7	H	H	H/S	neither	H/S	neither	H	Y	N
8	H	H	neither	neither	neither	neither	H	Y	N
9	H	H	S	neither	S	neither	H	Y	N
10	H	H	S	neither	neither	neither	H	Y	N
11	H	H	H/S	H/S	H/S	H/S	H	Y	N
12	H	H	H/S	neither	H/S	neither	neither	Y	N
13	H	H	S	S	S	S	S	Y	N
14	H	H	neither	neither	neither	neither	H	Y	N
15	H	H	H/S	neither	H/S	neither	H	Y	N
16	H	H	H	H	H	H	H	Y	N
17	H	H	H/S	neither	H/S	neither	H	Y	N
18	H	H	H/S	H/S	H/S	H/S	H	Y	N
19	H	H	neither	neither	S	neither	H	Y	N
20	H	H	neither	neither	neither	neither	H	Y	N
21	H	H	neither	neither	neither	neither	H	Y	N
22	H	H	H/S	neither	H/S	neither	H	Y	N
23	H	H	H/S	neither	S	neither	H	Y	N
24	neither	neither	H/S	neither	S	neither	H	N	N
25	H	H	H	neither	H	neither	H	Y	N
26	neither	neither	H/S	neither	H/S	neither	neither	N	N
27	H	H	H/S	neither	H/S	neither	H	Y	N
28	H	H	S	neither	S	neither	neither	Y	N
29	H	H	H/S	neither	H/S	neither	H	Y	N
30	H	H	H/S	H/S	H/S	H/S	H	Y	N
31	H	H	S	S	S	S	S	Y	N
32	H	H	H/S	neither	H/S	neither	H	Y	N
33	H	H	S	S	S	S	S	Y	N
34	H	H	S	neither	S	neither	no	Y	N
35	H	H	H/S	S	H/S	S	S	N	N
36	H	H	H	H	H	H	H	Y	N
37	H	H	neither	neither	neither	neither	H	Y	N
38	H	H	S	S	S	S	both	Y	N
39	H	H	H/S	neither	H/S	neither	H	Y	N
40	H	H	H/S	neither	H/S	neither	H	Y	N
41	H	H	H/S	S	H/S	S	S	Y	N
42	H	H	H	H	H	H	H	Y	N
43	H	H	H	H	H	H	H	Y	N
44	H	H	H/S	neither	H/S	neither	H	Y	N
45	H	H	H/S	neither	H/S	neither	H	Y	N
46	H	H	H/S	neither	H/S	neither	H	Y	N
47	H	H	neither	neither	neither	neither	H	Y	N
48	H	H	neither	neither	neither	neither	H	Y	N
49	H	H	S	S	S	S	S	Y	N
50	H	H	H/S	neither	H/S	neither	H	Y	N

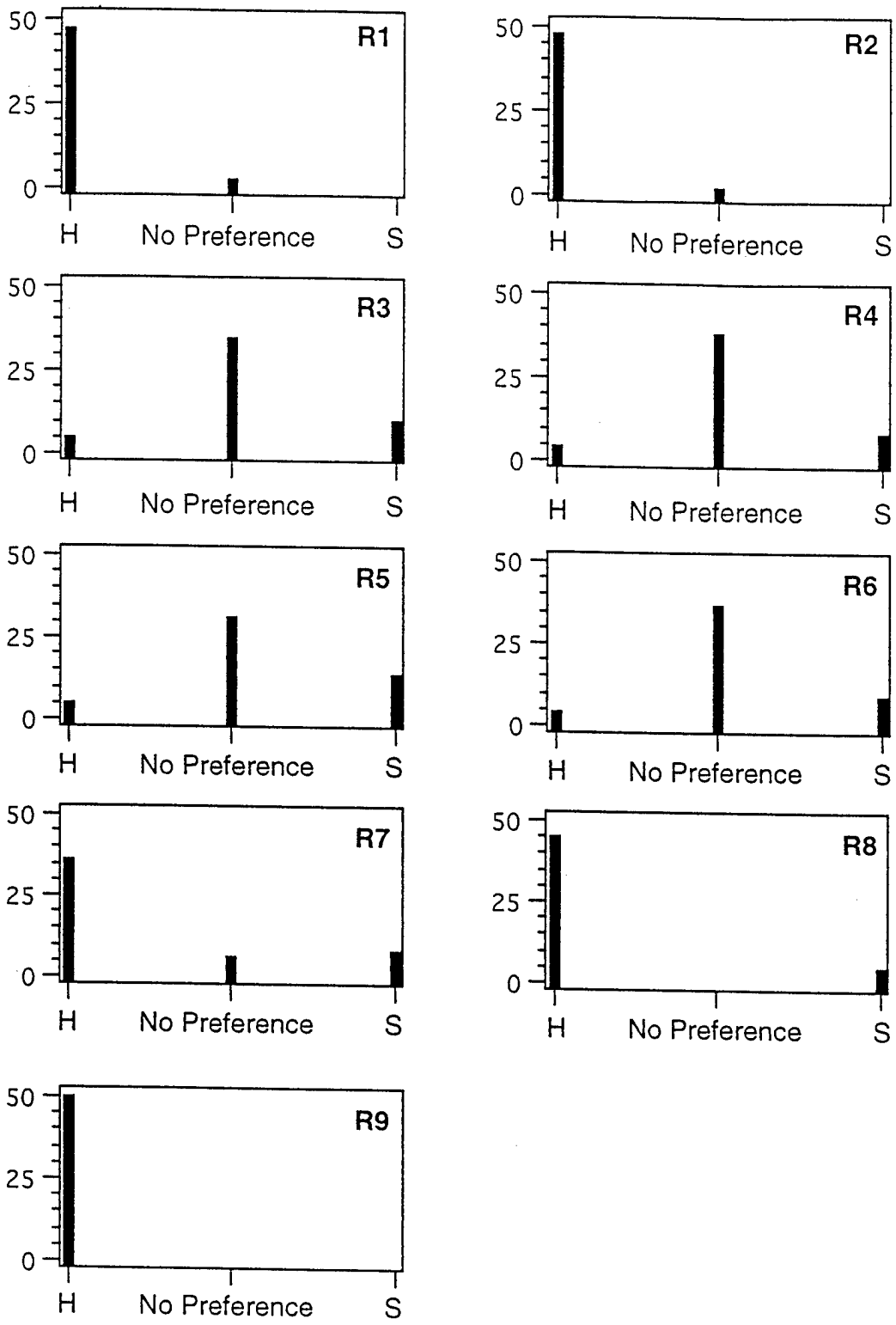

Figure 3.2 Questionnaire Response of Radiologist 2.

Table 2.3 Questionnaire Responses of Radiologist 3

Radiologist 3	Q1	Q2	Q3	Q4	Q5	Q6	Q7	Q8	Q9
ID #	H/S	H/S	H/S	H/S	H/S	H/S	H/S	Y/N	Y/N
1	H	H	H	H	H	H	H	Y	N
2	H	H	H	H	H	H	H	Y	N
3	H	H	H	H	H	H	H	N	N
4	H	H	H	H	H	H	H	Y	N
5	H	H	H	H	H	H	H	Y	N
6	H	H	H	H	H	H	H	N	N
7	H	H			H	H	H	Y	N
8	H	H			H	H	H	Y	N
9	H	H			H	H	H	Y	N
10	H	H	H	H			H	Y	N
11	H	H	H	H	H	H	H	Y	N
12			H	H	H	H	H	Y	N
13	H	H	H	H	H	H	H	Y	N
14	H	H	H	H	H	H	H	Y	N
15	H	H	H	H			H	Y	N
16	H	H			H	H	H	Y	N
17	H	H	H	H			H	Y	N
18	H	H	H	H	H	H	H	Y	N
19	H	H			H	H	H	Y	N
20	H	H			H	H	H	Y	N
21	H	H			H	H	H	Y	N
22	H	H			H	H	H	Y	N
23	H	H	H	H	H	H	H	Y	N
24	H	H	H	H			H	Y	N
25	H	H	H	H			H	N	N
26	H	H	H	H	H	H	H	N	N
27	H	H	H	H	H	H	H	N	N
28	H	H	H	H	H	H	H	Y	N
29			H	H			H	Y	N
30			H	H			H	N	N
31	H	H	H	H	H	H	H	Y	N
32	H	H	H	H			H	N	N
33	H	H	H	H	H	H	H	N	N
34	H	H					H	Y	N
35	H	H	H	H			H	N	N
36	H	H	H	H			H	Y	N
37	H	H			H	H	H	Y	N
38	H	H	H	H	H	H	H	Y	N
39	H	H			H	H	H	N	N
40	H	H	H	H			H	Y	N
41	H	H	H	H	H	H	H	Y	N
42	H	H	H	H	H	H	H	N	N
43	H	H	H	H	H	H	H	Y	N
44					H	H	H	N	N
45	H	H	H	H	H	H	H	Y	N
46	H	H	H	H	H	H	H	Y	N
47	H	H					H	Y	N
48	H	H			H	H	H	Y	N
49	H	H	H	H			H	N	N
50	H	H			H	H	H	N	N

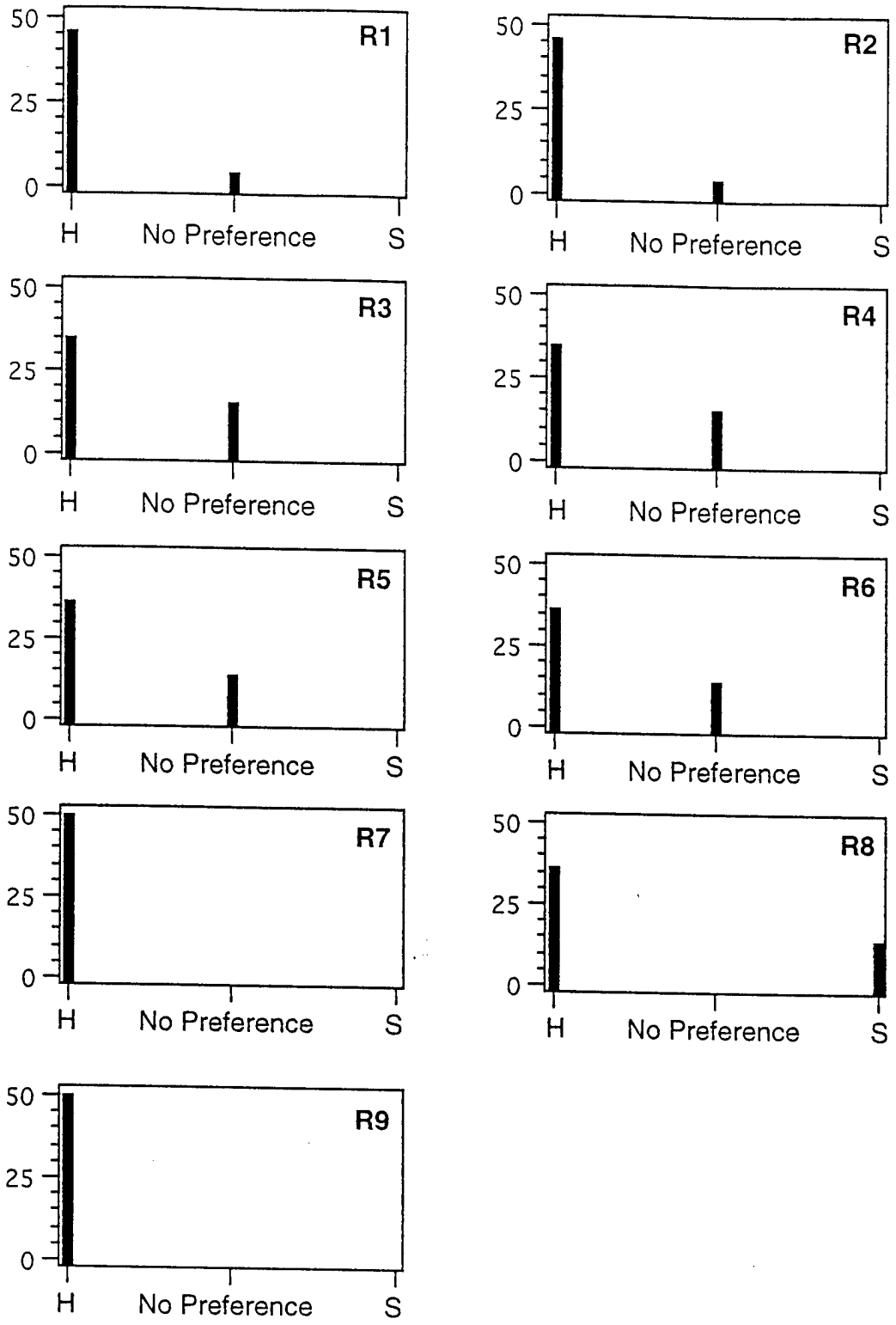

Figure 3.3 Questionnaire Response of Radiologist 3.

Table 2.4 Questionnaire Responses of Radiologist 4

Radiologist 4	Q1	Q2	Q3	Q4	Q5	Q6	Q7	Q8	Q9
ID #	H/S	H/S	H/S	H/S	H/S	H/S	H/S	Y/N	Y/N
1	H	H	H/S	H/S	H/S	H	H	Y	N
2	H	H	H	H	H/S	H/S	H	N	N
3	H/S	H/S	H/S	H			H	N	N
4	H	H	H/S	H/S			H	N	N
5	H/S	H/S	H/S	H/S			H	N	N
6	H/S	H/S			H/S	H/S	H	N	N
7	H/S	H/S			H/S	H/S	H	N	N
8	H/S	H/S			H/S	H/S	H	N	N
9	H	H	H	H	H	H	H	Y	N
10	H	H					H	N	N
11	H	H	H/S	H/S	H/S	H	H	Y	N
12	H	H	H	H			H	N	N
13			H/S	H			H	N	N
14	H	H	H/S	H			H	Y	N
15			H/S	H/S			H	N	N
16	H	H	H	H			H	Y	N
17	H	H					H	Y	N
18	H	H	H/S	H/S			H	Y	N
19	H	H			H/S	H	H	N	N
20	H/S	H					H	N	N
21	H	H			H/S	H/S	H	Y	N
22	H	H			H/S	H	H	Y	N
23	H	H					H	Y	N
24			H/S	H/S			H	N	N
25	H/S	H/S	H/S	H/S			H	N	N
26			H/S	H			H	Y	N
27	H	H	H/S	H			H	Y	N
28	H	H	H/S	H/S	H/S	H/S	H	Y	N
29			H/S	H/S			H	N	N
30	H	H	H/S	H/S			H	N	N
31	H/S	H/S	H/S	H/S	H/S	H/S	H	N	N
32			H/S	H/S			H	N	N
33			H	H			H	Y	N
34	H	H/S					H	N	N
35	H/S	H/S	H/S	H/S			H	N	N
36	H	H					H	N	N
37	H	H			H	H	H	Y	N
38	H/S	H/S	H/S	H/S	H/S	H/S	H	N	N
39	H	H			H	H	H	Y	N
40	H	H			H/S	H/S	H	Y	N
41	H	H	H/S	H	H/S	H	H	Y	N
42	H	H	H/S	H/S	H/S	H/S	H	Y	N
43	H	H/S	H/S	H/S	H/S	H/S	H	N	N
44							H	Y	N
45	H	H	H/S	H/S			H	Y	N
46	H/S	H/S	H/S	H/S			H	N	N
47	H/S	H/S					H	N	N
48	H	H	H	H	H/S	H/S	H	N	N
49	H	H			H/S	H/S	H	Y	N
50	H	H	H/S	H/S			H	Y	N

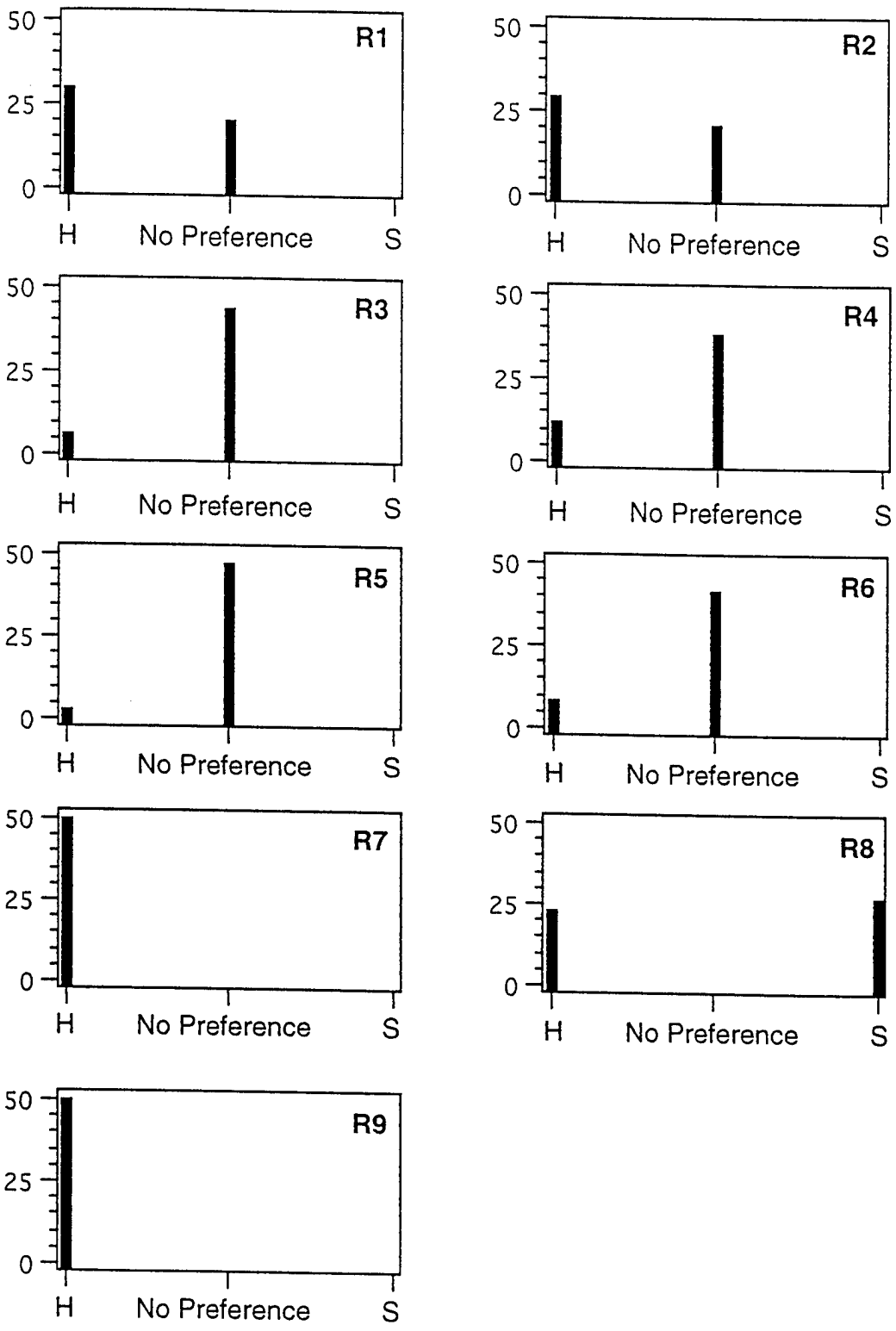

Figure 3.4 Questionnaire Response of Radiologist 4.

Table 2.5 Questionnaire Response of Radiologist 5

Radiologist 5	Q1	Q2	Q3	Q4	Q5	Q6	Q7	Q8	Q9
ID #	H/S	H/S	H/S	H/S	H/S	H/S	H/S	Y/N	Y/N
1	H	H	H	H	H	H	H	Y	N
2	H	H	H	H			H	N	N
3			H	H	H	H	H	N	N
4	H	H	H	H	H	H	H	N	N
5	H	H	H	H			H	N	N
6	H	H	H	H			H	N	N
7	H	H	H	H	H	H	H	Y	N
8	H	H					H	Y	N
9					H	H	H	N	N
10	H	H	H	H			H	N	N
11	H	H	H	H	H	H	H	N	N
12							H	N	N
13							H	N	N
14	H	H	H	H	H	H	H	Y	N
15	H	H					H	N	N
16	H	H	H	H			H	Y	N
17	H	H	H	H			H	N	N
18	H	H					H	Y	N
19	H	H					H	N	N
20	H	H	H	H	H	H	H	N	N
21	H	H	H	H	H	H	H	Y	N
22	H	H	H	H	H	H	H	Y	N
23	H	H	H	H	H	H	H	Y	N
24							H	N	N
25			H	H	H	H	H	N	N
26			H	H	H	H	H	N	N
27	H	H					H	Y	N
28	H	H					H	Y	N
29							neither	N	N
30							neither	N	N
31			H	H			H	Y	N
32			H	H			H	N	N
33							neither	N	N
34	H	H					H	N	N
35	H	H					H	Y	N
36	H	H					H	Y	N
37	H	H			H	H	H	Y	N
38	H	H	H	H			H	Y	N
39							neither	N	N
40	H	H					H	Y	N
41	H	H	H	H			H	N	N
42	H	H					H	Y	N
43							neither	N	N
44			H	H	H	H	H	N	N
45	H	H	H	H	H	H	H	N	N
46	H	H					H	N	N
47							H	N	N
48	H	H					H	Y	N
49	H	H	H	H			H	N	N
50	H	H					H	Y	N

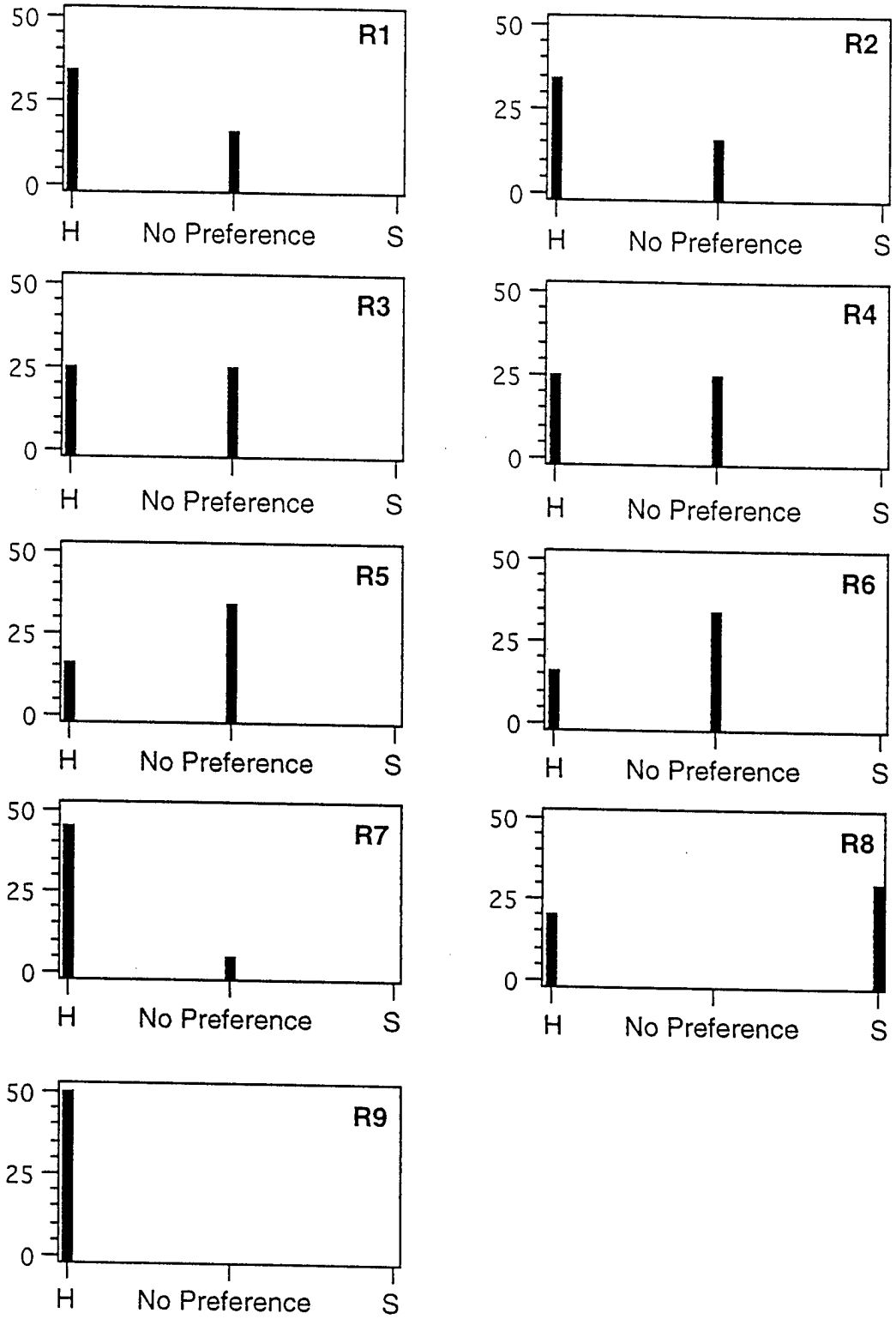

Figure 3.5 Questionnaire Response of Radiologist 5.

5.2. Comments of the Five Radiologists

Dr. Hayes's Comments:
- Prefer the hard copy to soft copy.
- Microcalcifications were difficult to see on soft copies unless the contrast was increased considerably, however, at that time the remainder of the breast is too dark.
- Microcalcifications can not only be identified more easily on hard copy (10 line pairs), they can also be better defined on hard copy as to benign vs. malignant.
- Due to the magnification with soft copies, masses sometimes are more easily detected and better characterized with soft copies.
- On soft copies it was difficult to evaluate the skin without changes in density.
- By changing density on soft copy skin retraction can be better detected than on hard copy without "hot light".
- Can better define number and sizes of calcifications and detect more scattered microcalcifications on hard copy.
- Can not determine adequate number of microcalcifications on soft copy. Microcalcifications are better delineated on hard copy. However, because of the lower resolution on soft copy, some microcalcifications are smudged and can not be seen on soft copy.
- Some easily identified artifacts on the hard copy almost look like microcalcifications on the soft copy. Artifacts are more clearly defined on hard copy.

Dr. Hogge's Comments:
- Calcifications are lost on soft copies in areas of dense tissue - this is a serious limitation.
- Masses are better depicted on soft copies in parts with fatty breasts, but not in dense breasts.

Dr. Freedman's Comments:
- Soft copy naturally makes it harder to see microcalcifications and sometimes they can not be seen at all.
- Masses and asymmetry density are lower central on soft copies and therefore harder to search.

Dr. Green's Comments:
- Manipulation of the window-and-level took time and diverted vision and attention away from the image being diagnosed.
- Some images, especially those containing dense tissues, needed to be enhanced dramatically in the contrast, however, the information in other breast areas is lost.

Dr. Zuurbier's Comments:
- In general, the soft copy images have a "gauze-y" veil-like effect (and resolution).
- Soft copy seems to increase the perception of normal soft tissue structures as abnormal.
- Soft copy loses faint but important microcalcifications in dense tissue.
- Hard copy provides better sense of the contrast of whole image, normal and abnormal soft tissues.
- See detail of dense soft tissue better on hard copy.

6. CONCLUSIONS

• **Image Spatial Resolution** - Our study results showed that, in general, the five radiologists preferred hard copy to soft copy screen films. It also showed that the disease patterns are better characterized on hard copy than on soft copy SF. Because of the spatial resolution of the soft copy, some subtle microcalcifications in the dense tissue area are not well characterized and become difficult to detect. Furthermore, some obvious film defects on the films become microcalcification-like on the soft copy where spatial resolution and contrast become lower than those on the hard copy. Specifically, the screen film hard copy has a spatial resolution of approximately 10 line pairs per millimeter while the digitized 100 μm SF (i.e., soft copy) has only about 5 line pairs per millimeter. The results indicate that high spatial resolution is important in the identification of some subtle and faint microcalcifications in the dense breast area. Direction digitization of screen film at 100 μm and without other image enhancement is not adequate to retain the important clinical information of the microcalcifications, especially those are small and subtle microcalcifications which lie in the dense breast areas. The radiologists experience and training in reading soft copy may have some effects on the study results.

• **Classification of Benign and Malignant Diseases** - The classification of benign and malignant disease patterns, such as microcalcifications and masses, presented a very challenging task for the radiologists. Our study results showed that the five radiologists achieved average 50% accuracy in the classification of benign and malignant disease patterns. The five radiologists found single or multiple disease patterns in all 50 cases (see also the "MAMMO FINDINGS" in Table 1), however, only 25 cases were biopsy proven cases. The 50% accuracy on cancer case was measured no matter what the disease - microcalcification, mass, or architecture distortion. The study of using artificial neural network (ANN) and computer-aided diagnosis (CADx) to classify benign and malignant microcalcifications is currently under intensive investigation at ISIS Center.

• **Display Workstation** - The Vicom display workstation which provides 8 bit (256 gray levels) display is not sufficient to the contrast information on the films as perceived by the radiologists. The contrast and intensity of the abnormal soft tissues as opposed to that of normal soft tissues are better perceived on the hard copy; the abnormal and normal soft tissues of the soft copy have similar contrast and intensity when displayed on the monitors. In some cases, masses and architecture asymmetry were easier to detect on the soft copy partly because of the magnification when displayed on the display monitors. However, the high contrast on the hard copy make the masses better characterized than on soft copy.

• **Periodic Maintenance and Quality Control** - Periodic maintenance of film digitizer and QC on Fuji CR9000 and display monitors are necessary in digital mammography of the MDIS environment. We are in the process of acquiring a multi-format pattern generator and a comprehensive display evaluation system for QC on high resolution display monitors.

• **On-going Researches** - The results of this study indicate that, based on our current experimental setting, soft copy display is not good enough to be clinically useful. However,

improvement and optimization of display equipment and advanced image processing, such as the unsharp masking technique provided by Fuji CR systems, may make soft copy display more clinically useful. Two possible research directions: one is to apply image processing to enhance microcalcifications especially in the dense breast areas of 100 micron images, the other is to use 50 mm images and a higher gray level (10 or 12 bit) instead of an 8 bit display monitor.

- The dispay of the full image dat of a mammogram digitized at 50 micron resolution (4096 pixels × 5120 lines × 12 bits) may require roaming of the image on the 2048 pixels × 2560 lines display monitor. The potential effects, such as the diversion of vision and attention away from the region-of-interest being viewed, caused by roaming and other image manipulations need to be further investigated.
- We have developed a region-based image processing technique to enhance the visibility of subtle microcalcifications in the dense tissues. The comparative study of SF and the processed 100 micron SF images is currently under development.

7. ADDENDA

7.1. Acronym / Symbol Definition

ACR -	American College of Radiology
ACR-NEMA -	ACR-National Electrical Manufacturers Association
CDMAM -	Contrast detail mammogram-phanton
CIRS -	Computerized Imaging Reference Systems
CR -	Computed radiography
DASM -	Data acquisition and system management
GUMC -	Georgetown University Medical Center
LCC -	Left cranio caudal
LMLO -	Left mediolateral oblique
MDIS -	Military diagnostic imaging systems
QC -	Quality control
RCC -	Right cranio caudal
RMLO -	Right mediolateral oblique
SCIB -	Second channel interface board
SCSI -	Small computer system interface
SF -	Screen film
SMPTE -	Society of motion picture and television engineers

7.2. References

[1] Lumisys, *Lumiscan Service Manual: Model 100/150/200*. Sunnyvale, CA 94086, 1994.

[2] C. E. Metz, "Some practical issues of experimental design and data analysis in radiological ROC studies," *Investigative Radiology*, vol. 24, pp. 234-245, 1989.

Preprint SPIE
Medical Imaging 95

Digital mammography: Tradeoffs between 50 and 100 micron pixel size

Matthew Freedman MD MBA, Dot Steller RT(R), Hamid Jafroudi PhD, S.-C. Benedict Lo PhD,
Rebecca A. Zuurbier MD, Raj Katial RT(R), Wendeli n Hayes DO, Y. Chris Wu PhD,
Jyh Shien Lin MS, Richard Steinman MD,Walid Tohme PhD, Seong Ki Mun PhD

Division of Imaging Science and Information Systems and Division of Breast Imaging, Georgetown University School of Medicine, 3800 Reservoir Road NW, Washington, DC 20007, USA

ABSTRACT

Improvements in mammography equipment related to a decrease in pixel size of digital mammography detectors raise questions of the possible effects of these new detectors. Mathematical modeling suggested that the benefits of moving from 100 to 50 micron detectors were slight and might not justify the cost of these new units. Experiments comparing screen film mammography, a storage phosphor 100 micron digital detector, a 50 micron digital breast spot device, 100 micron film digitization and 50 micron film digitization suggests that object conspicuity should be better for digital compared to conventional systems, but that there seemed to be minimal advantage to going from 100 to 50 microns. The 50 micron pixel system appears to provide a slight advantage in object contrast and perhaps in shape definition, but did not allow smaller objects to be detected.

INTRODUCTION

Several sites are working to develop 50 micron digital systems for whole breast digital mammography. There currently exists a 100 micron pixel storage phosphor whole breast digital mammography system. 50 micron digital spot devices also exist that are used for limited views of the breast. 50 and 100 micron film digitization devices are available. Moving from a 100 micron system to a 50 micron system involves costs and benefits. This paper will explore the tradeoffs involved and attempt to model the potential benefits that such a system might have. The potential costs, benefits, and examples of what can currently be seen with 100 and 50 micron pixel systems will be presented.

THE COSTS

The costs of using a 50 micron instead of a 100 micron system include the costs of increased Radiation, Data Volume which will affect the costs of Data processing, Transmission, Storage and Display. Design and manufacturing costs for the new equipment are also important cost considerations.

Increase Radiation

The change from 100 to 50 micron pixels results in four times as many pixels to include the entire breast. X-ray images can be considered to be quantum limited (i.e. everything that can be done to work at minimal patient absorbed dose has been done). If one has two detectors with the same detector quantum efficiency and covering the same area of the breast, the one with four times as many pixels will need four times as much exposure to maintain the same signal to noise ratio and presumably 4 times the patient absorbed dose. Several strategies can be used to decrease the patient dose: One can use a detector with higher quantum efficiency, one can modify or remove the grid from the system (our mammography grid requires us to use 2.2 to 2.5 times the exposure depending on the KVP), one can use a higher KVP (which results in a lower patient absorbed dose at the cost of lower contrast).

Data Volume

If one has four times the number of pixels, one has four times the data volume increasing the costs of data processing, storage and transmission. This increased data must also be displayed. Soft copy displays suitable in luminance for clinical radiology are currently limited to 2 x 2.5 K. Commercially available laser cameras for printing the images have a minimal spot size of 80 microns although 50 micron systems are under development. With an 80 micron laser camera, the breast will be displayed enlarged.

Design and Manufacturing Costs

The development of new devices results in major costs. These must be offset by benefits that most likely have to include the detection of breast cancer at an earlier stage with, therefore, an improved prognosis.

BENEFITS

There are three potential benefits that could occur in digital mammography from the use of a smaller pixel size: the detection of smaller objects, better definition of the shape of objects and a more accurate count of the number of objects present.

Detection of smaller objects:

The detection of smaller objects within the breast should allow the identification of smaller breast cancers. A 50 micron system might show smaller objects than a 100 micron system. Detection of objects depends on their ability to absorb x-ray photons. As objects become smaller they will usually also become thinner. If one has a 100 micron object and a 50 micron object, the absorption of the 50 micron object will be 1/8 that of the 100 micron object. In order to detect a 50 micron object, one would need to be able to use a high contrast look up table and have a relatively noise free background. The use of smaller pixels is likely to increase the noise level. It is therefore unlikely that a 50 micron system will be able to detect smaller objects than a 100 micron system given similar image processing capabilities.

V=4/3Pi r^3

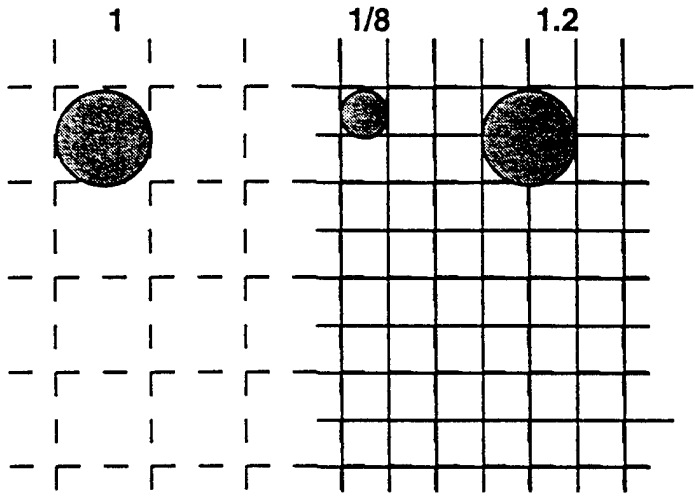

In our experiments, both the 100 and 50 micron systems allowed us to see objects of the same size.

TABLE OF SMALLEST OBJECT SEEN

Test Object	Screen Film	100 micron phosphor	50 micron CCD
CDMAM	130. 100 at 5x mag	100 at 1 micron thick	100 at 0.8 microns thick
CIRS Detail	240	160	160
RMI 156	240 (3/6)	240 (3/6))	240 (3/6)
Steel Fleck	100	50 (noisy, high contrast)	100
CIRS Half Round	160	160	160

Contrast

The contrast of the objects with the 50 micron system was slightly higher as demonstrated in the pictures of the CDMAM phantom shown below.

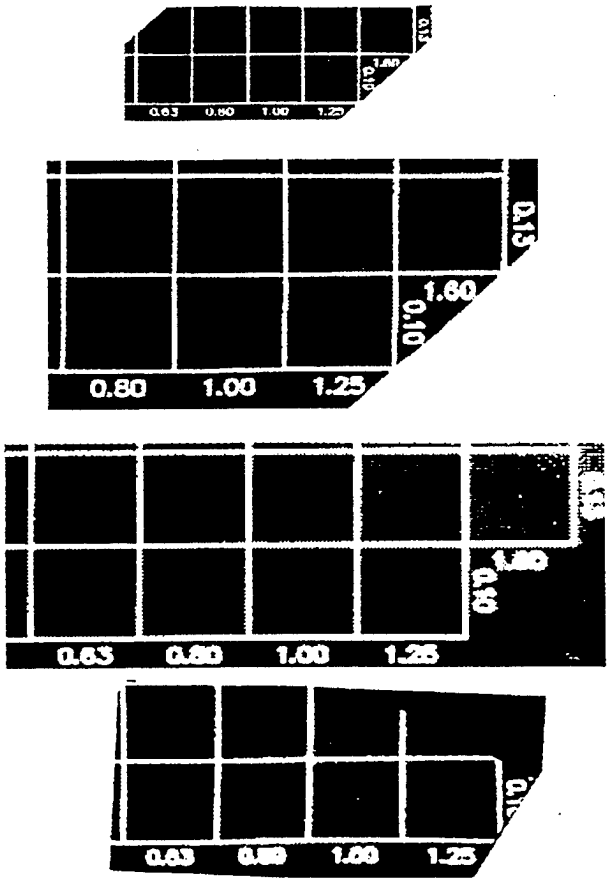

Nuclear Associates CDMAM Phantom: Screen film digitized at 100 microns and 50 micron pixel, 100 micron storage phosphor image, 50 micron digital spot device. The screen film image can show the 130 micron objects. The 100 micron system shows 100 micron objects at the 1.25 and 1.00 micron thicknesses. The 50 micron digital spot device shows the 100 micron object at 0.80 microns of thickness.

Penumbra

The penumbra around an object caused by the finite size of the focal spot results in a projection of the object that is less distinct at its edges than the true object (i.e. it has a lower contrast definition at its edges. Small faint objects would tend to be less distinct than larger or higher contrast objects. If one is using a 300 micron focal spot, a 65 cm focal spot detector distance and a 3 cm object detector distance, the penumbra is approximately 15 microns on each size.

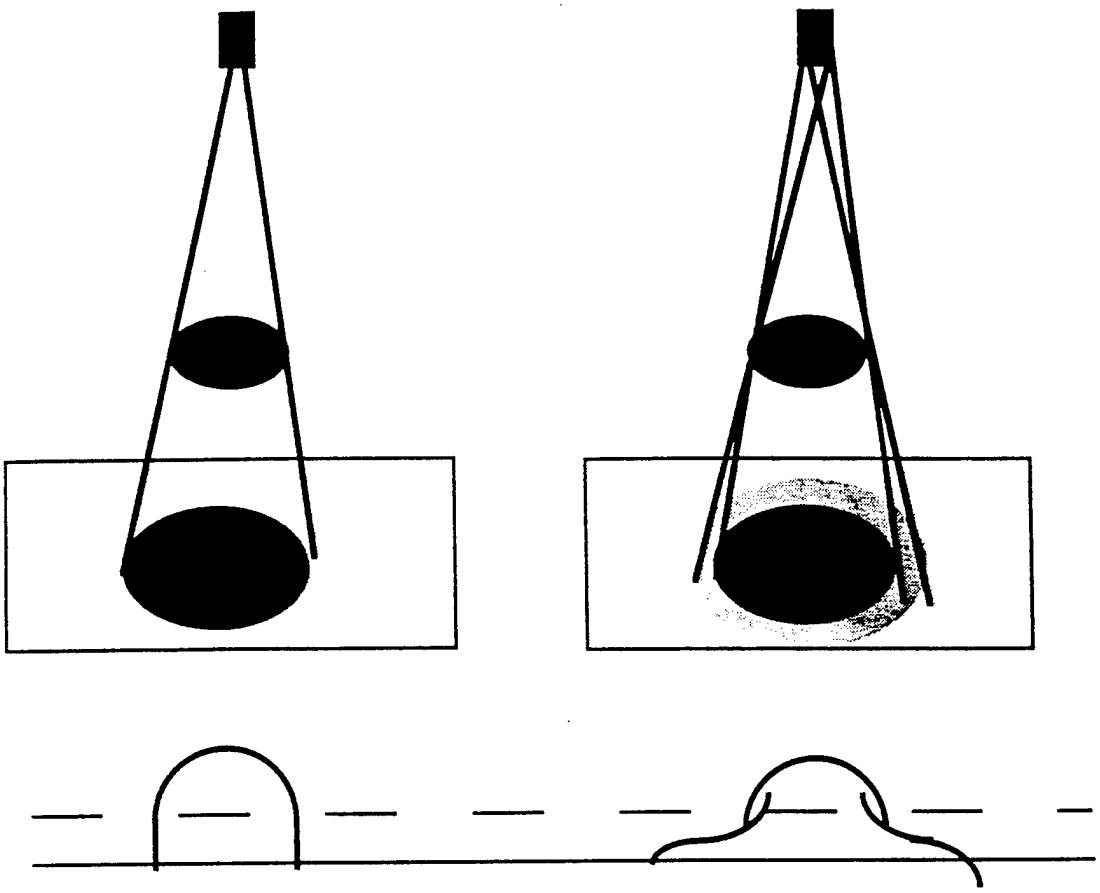

Better definition of object shape

Object shape evaluation depends on the number of pixels that an object is superimposed on. A 50 micron system could result in improved visualization of shape. Many writers have commented that shape is an important criteria in determining the potential for malignancy in microcalcification. Since screen film system can detect in the intact breast objects with a minimum object size of 250-300 microns, one would have to demonstrate that the difference in shape definition between an object projected on 9 pixels and 36 pixels is clinically important. The penumbra resulting from the measurable size of the focal spot will decrease the sharpness of the image and therefore the ability to determine shape.

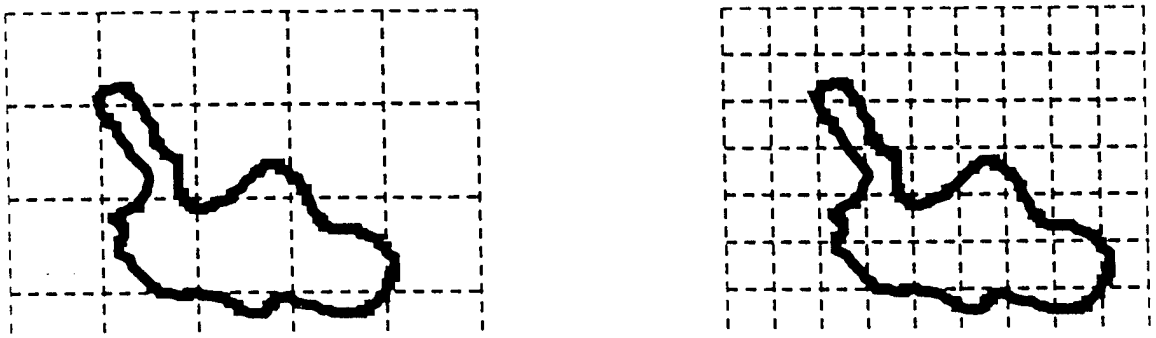

These images from the CIRS phantom demonstrate that the definition of shape of the microcalcifications measuring 240 microns is slightly better with the 50 micron system than with the 100 micron and screen film systems. With increasing enlargement, the effect becomes slightly easier to identify.

THE GOAL OF DIGITAL MAMMOGRAPHY: FINDING SMALLER BREAST CANCERS

The goals of digital mammography are (1) to allow the detection of smaller breast cancers and (2) to improve the differentiation of benign and malignant lesions. One or both of these should occur to justify the expenses in the use of digital mammography. While there may be a few instances where digital storage or transmission might be necessary, in general, that would not result in a sufficient volume of demand for machines to justify their cost of development.

What is the possible benefit and what is the possible risk from detecting smaller objects?

To demonstrate a true benefit from the detection of smaller objects that could be related to cancer, one would have to show that this earlier detection affects the long term outcome patient disease free survival. One can use a surrogate for this by showing that in historic data smaller cancers indeed do have a better prognosis. One can, using the data from Bedwani demonstrate that detecting cancer when it is 0.5 cm or less in size does afford a better prognosis than detecting it 0.6-1.0 cm in size.

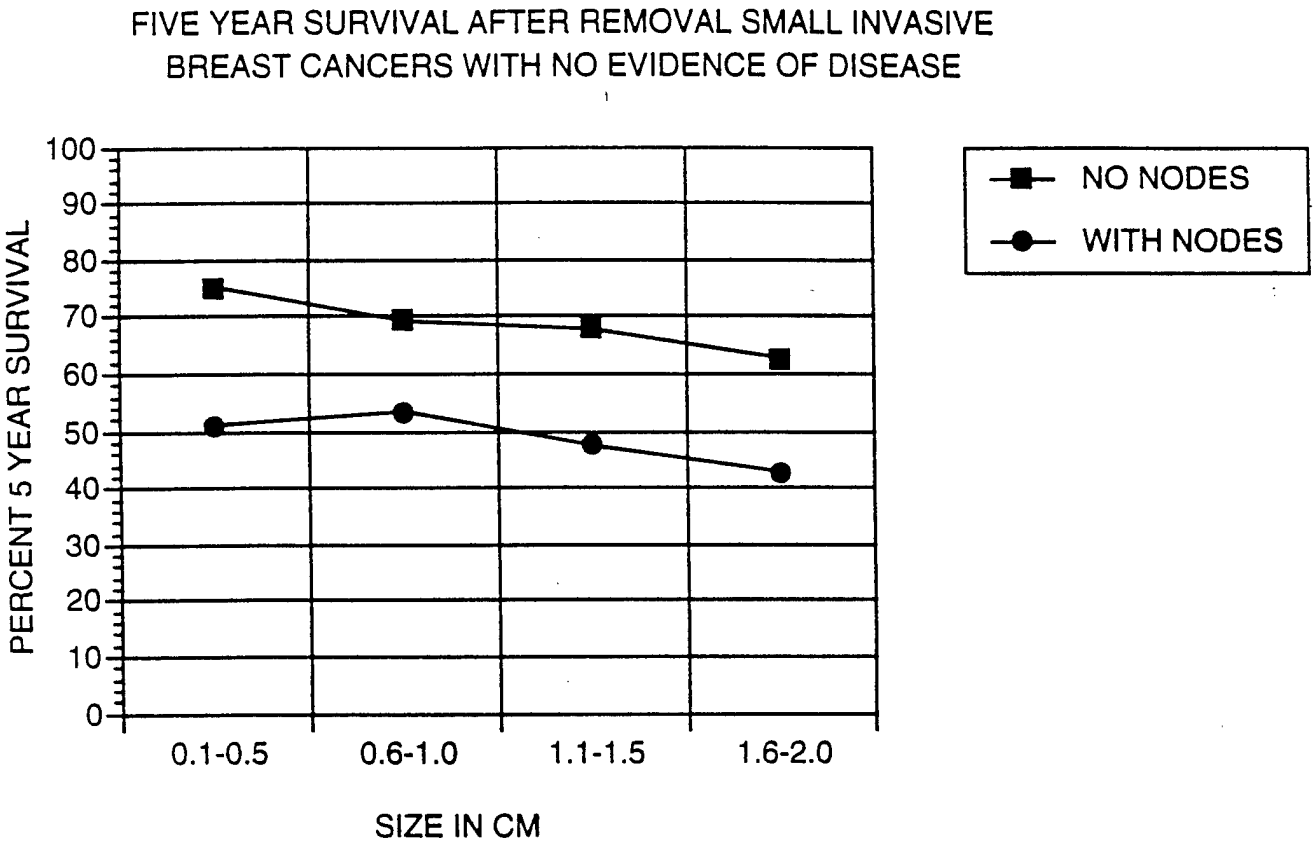

Bedwani et al. Cancer 47:2769-2778, 1981

Cancer with calcifications to small to be seen with conventional mammography

Cancer can containcalcifications too small to see with conventional screen film mammography. Egan found that in specimen radiographs that microcalcifications in 28 percent of patients were limited to those between 50 - 100 microns in size. This is usually considered too small a size to be seen by conventional screen film mammography.

SIZES IN MICRONS OF MICROCALCIFICATIONS IN 115 BREAST CANCERS
WITH MICROCALCIFICATIONS AS ONLY SIGN OF CANCER

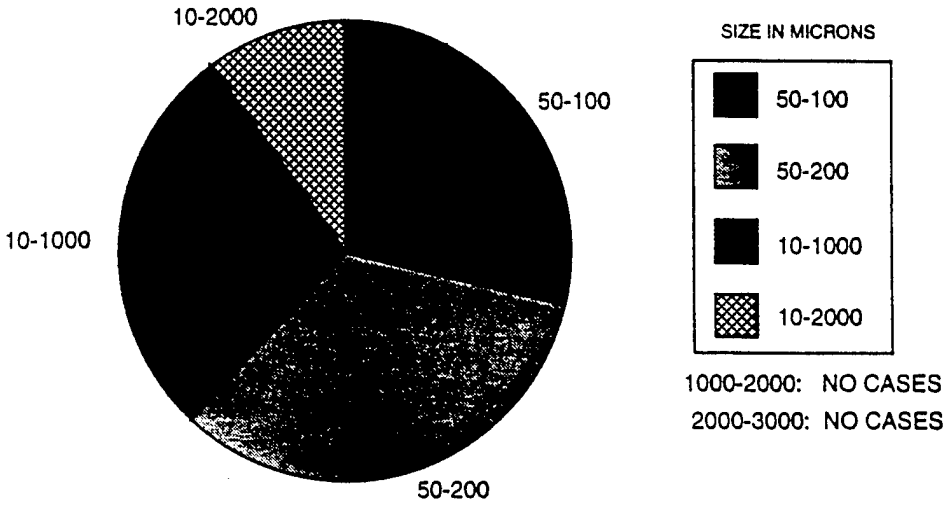

RL Egan. Radiology 137:1-7, 1980

The work of Millis also supports this conclusion.

RADIOLOGY PATHOLOGY CORRELATIONS
OF MICROCALCIFICATIONS IN BREAST CANCER

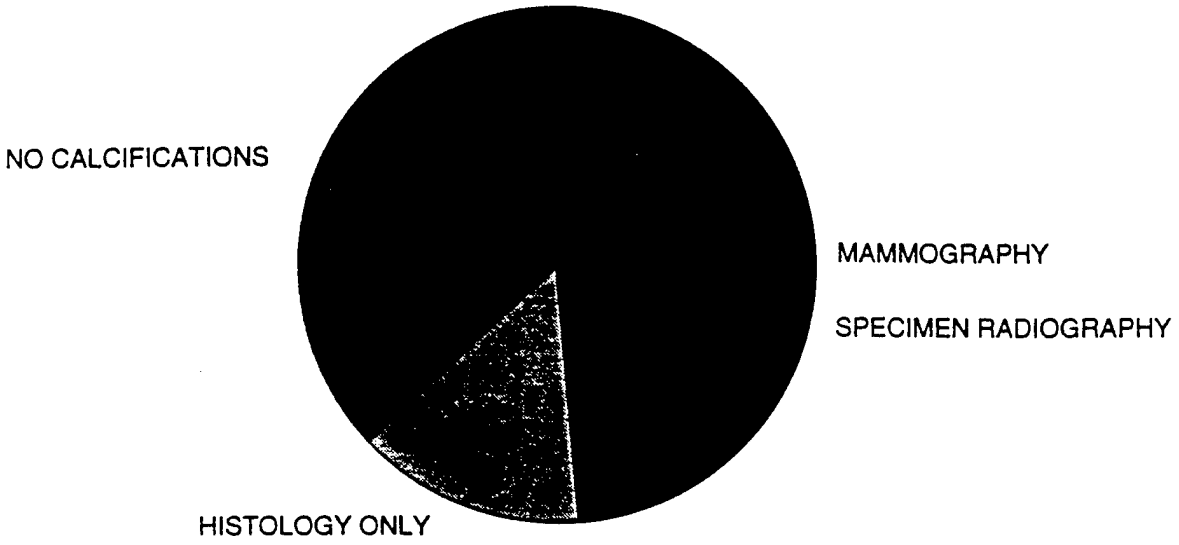

MILLIS, BRITISH J OF RADIOLOGY. 1976. 49:12-26

Number of microcalcifications

Improved resolution should allow an improved count of the number of microcalcifications present. This number appears to correlate with the likely presence of cancer.

NUMBER OF MICROCALCIFICATIONS IN BENIGN AND MALIGNANT CASES

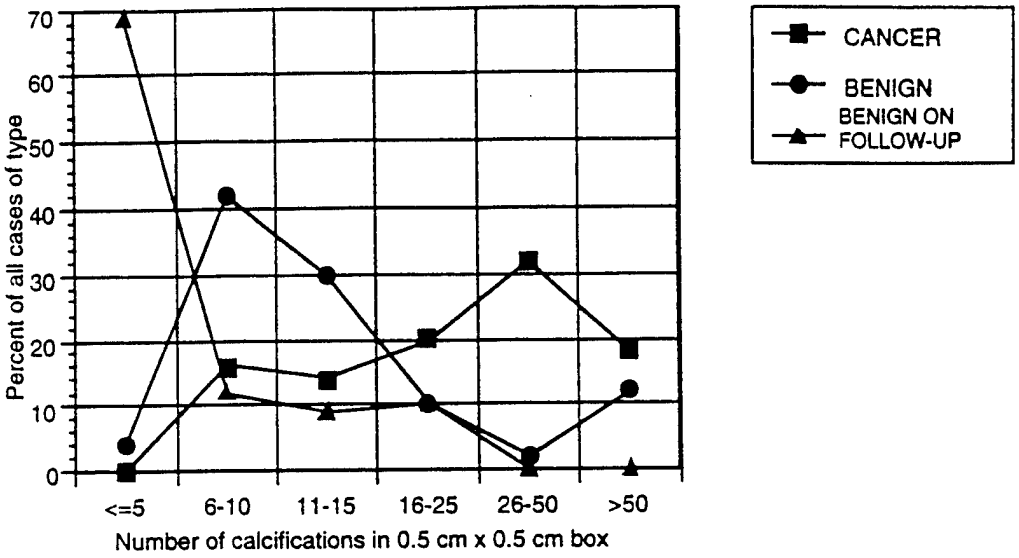

Egan, Radiology 137:1-7, 1980

The risk of detecting smaller signs of possible cancer is related to the concern that finding smaller objects might change the ratio between malignant and benign biopsies. Currently, we do approximately three biopsies for each cancer detected. In other centers it can be 1 in 5. In one series, only 17 % of biopsies done for microcalcifications showed cancer. If one finds smaller microcalcifications and smaller masses, one might find that the frequency of biopsies demonstrating cancer had increased or decreased. I am aware of no data on this issue. The data of Powell shows that from 1972 to 1983, the number ratio of cancers to benign disease detected decreased in patients biopsied for microcalcifications. A recent unpublished series (Smith) shows a 17 percent ratio of cancer in stereotactic biopsy, the same as in Powell's series from 1983.

BIOPSIES FOR MICROCALCIFICATIONS AS ONLY ABNORMALITY ON MAMMOGRAM

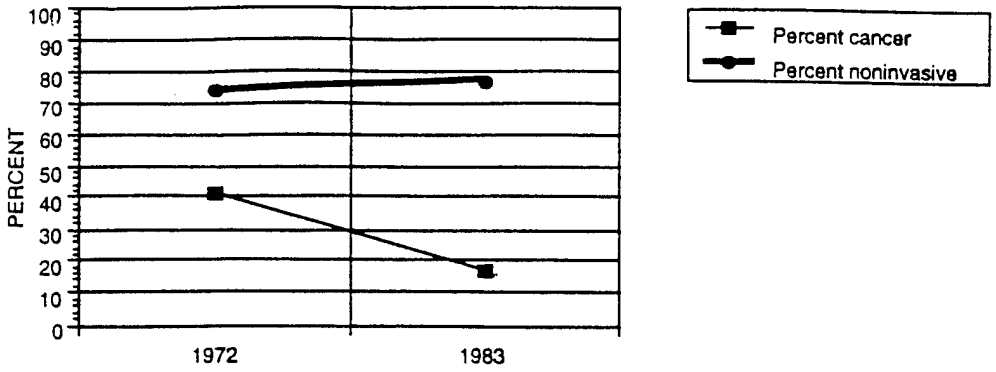

Powell et al. Annals of Surgery 197: 555-559, 1983

As shown in this drawing, there are several potential outcomes should new technology allow the detection of smaller lesions.

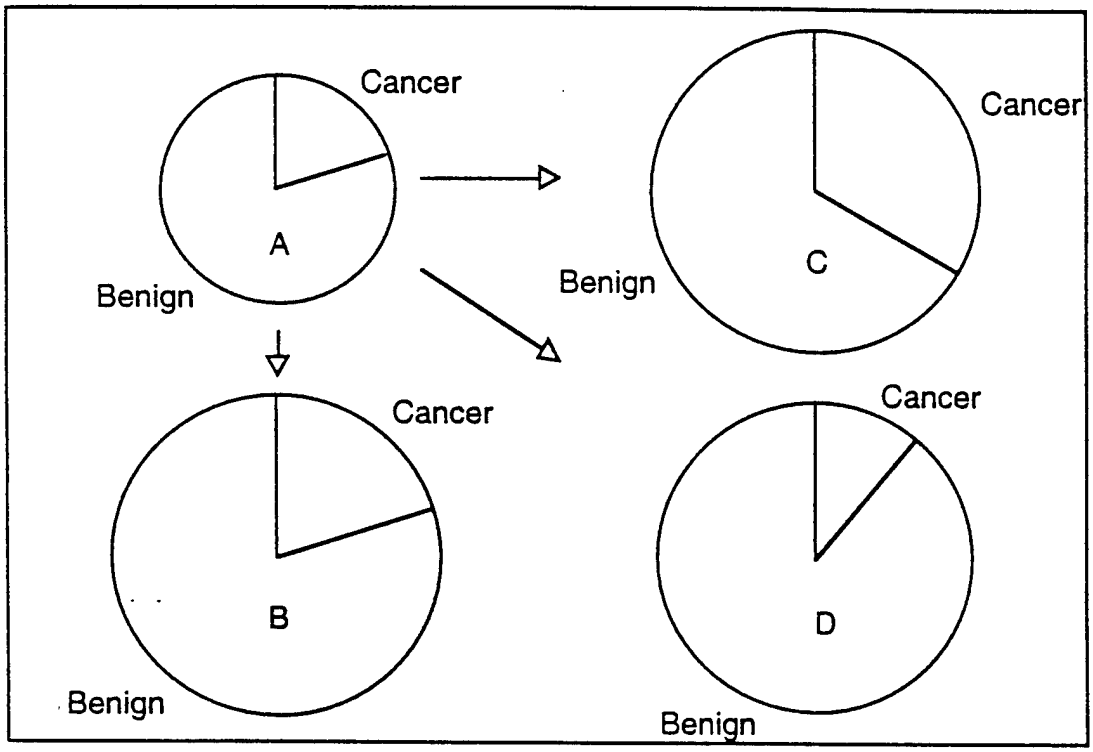

In this drawing, let A represent the current detection of microcalcifications and small masses. If we increase the detection rate as shown in B, then the percentage cancers remain the same and we have not altered the expected cost of detecting cancer. Ideally, as shown in C, we would hope that the better definition of detail would allow us to improve the proportion of cancers detected. But, as shown in D, the proportion of cancers might decrease resulting in an increased number of breast biopsies with little or no improvement in the detection of breast cancer. Which of these scenarios will occur is unknown.

OBJECT VISIBILITY: WHAT CAN BE SEEN

Detection vs. Resolution

Detection and resolution are different. One can detect an object smaller than the pixel size if it is of sufficient contrast because its effect on the pixel will be averaged over the pixel.

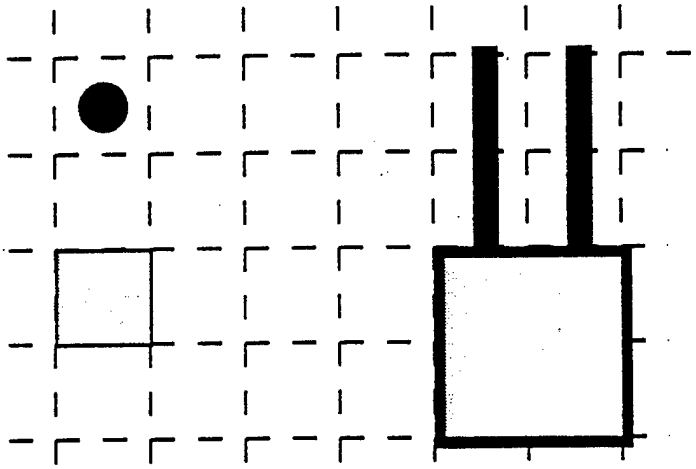

Detection is related to object contrast, pixel size and background noise. A high contrast object can be seen even if it is smaller than the pixel as shown in this home made test object. 50 micron steel flecks can be seen with a 100 micron pixel (in a visibly noisy background), but cannot be detected with the 50 micron digital spot device.

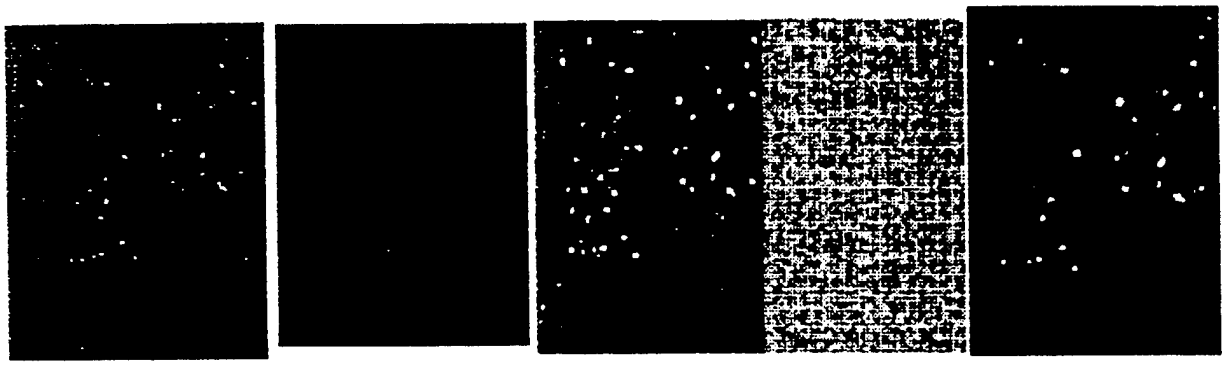

Homemade test object with steel flecks 50 microns and larger. A. Direct film exposure. On the original 50 micron objects can be seen and measured with magnifier. B. Screen film mammogram. 50 micron flecks seen with difficulty. C. Storage phosphor 100 micron pixel system 50 micron flecks (arrows) can be easily seen. D. Subtraction image done with two different exposures and storage phosphor imaging plates documents that 50 micron objects are not noise. E. 50 micron CCD image. With the image processing used, the 50 micron flecks cannot be seen.

BIBLIOGRAPHY

Bedwani R, Vana J, Rosner D, et al. Management and survival of female patients with "minimal" breast cancer. Cancer 47:2769-2778, 1981

Egan RL, McSweeeney MB, Sewell CW. Intramammary calcifications without an associated mass in benign and malignant diseases. Radiology, 1980. 137:1-7.

Millis rm, Davis R, Stacey AJ. The detection and significance of calcifications int he breast: a radiological and pathological study. British J of Radiology, 1976. 49:12-26

Powell RW, McSweeney MB, Wilson CE. X-ray calcifications as the only basis for breast biopsy. Annals Surgery 1983. 197:555-559.

Smith D. Personal communication regarding stereotactic biopsy results. August, 1994.

Freedman M, Pe E, Nelson M, Lo S-C B, Mun S K: Digital Mammography: Demonstration of a Method of Achieving Adequate Resolution on a Storage Phosphor System. CAR 93, 7th International Symposium, Berlin, Germany (June 24-26, 1993); 783pp.

Freedman M, Pe E, Zuurbier R, Katial R, Jafroudi H, Nelson M, Lo S-C B, Mun S K: Image Processing in Digital Mammography. SPIE: Medical Imaging, Vol. 2164 (1994); 537-554pp.

ACKNOWLEDGMENT

Supported in part by U.S. Army Medical Research Grant DAMD 17-93-J-3008. The content of this report does not necessarily reflect the position or policy of the U.S. Government and no official endorsement should be inferred.

Georgetown
ROC Study
of Digital Mammography

First reader

Georgetown employee at outpatient center three miles away, not involved in research projects. Does not interpret mammograms in Hospital

Test of detection of cancer

(Cancer cases vs. normal and biopsy benign cases)

Screen film Az= 0.7373 (SD = 0.0561)

Digital Az= 0.7646 (SD = 0.0515)

Test of diagnosis of biopsy proven cases

(Cancer cases vs. biopsy proven benign cases)

PPV of radiologists recommending biopsy=0.27 to 0.32

Screen film Az= 0.5743 (SD = 0.0985)

Digital Az= 0.7412 (SD = 0.0739)

Improved contrast allows better classification despite poorer resolution

(Freedman Digital Mammography and evaluation of the shape of microcalcifications. SPIE Medical Imaging, 1996)

Digital Mammography in the Radiodense and Complex Pattern Breast

Matthew Freedman, Dorothy Steller Artz, Hamid Jafroudi, Jacqueline Hogge, Rebecca A. Zuurbier, Jyh Shien Lin, Raj Katial, Seong Ki Mun.
Division of Imaging Science and Information Systems, Department of Radiology, Georgetown University Medical Center, 3800 Reservoir Road, NW, Washington, DC 20007

Abstract

The sensitivity of mammography for the detection of breast cancer is decreased in the radiodense breast. Storage phosphor digital radiographic systems have a wider latitude of exposure than conventional mammographic screen film systems. By using low resolution histogram equalization one can produce a mammographic image of the breast that retains the high frequency information that defines the edges of microcalcifications, architectural distortion and some masses but which, at the same time, allows one to look through into regions of increased breast radiodensity and identify microcalcifications within them. This paper demonstrates the effect of this special form of image processing.

Key Words: Breast Cancer Digital Mammography radiodense young women histogram equalization image processing.

Introduction

Conventional screen film mammography has a high sensitivity (88%) for the detection of breast cancer. In younger women, the sensitivity is substantially below that (60-68%) (Tabar). If one looks at reports summarizing the image characteristics of cancers missed on screening mammography, many of them occur in regions of increased breast radiodensity (Farria, Bird, Harvey, Silverstein). Our previous reports to SPIE Medical Imaging (Freedman, 1994 and 1995) reported that digital mammography had a wider range of effective exposures than did screen film mammography, as summarized in the following chart:

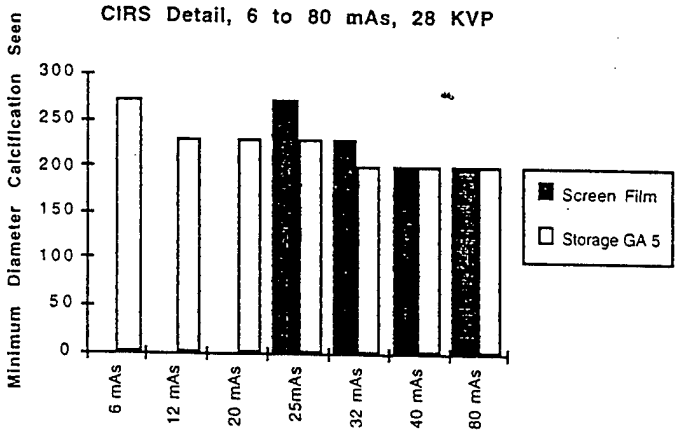

Chart 1: This chart demonstrates the smallest sized test details visible on the CIRS Detail Phantom as exposure is varied, comparing two systems: conventional screen film mammography and Fuji Digital Storage Phosphor radiography, processed in Sensitivity Mode. At low exposure levels, the digital system allows the detection of simulated microcalcifications that cannot be seen in the conventional system. This is analogous to detecting microcalcifications in radiodense regions of the breast. (From Freedman, 1995)

If one attempts to demonstrate this broad range of exposures, however, one ends up with an overall low contrast image--similar to the effect that would occur if one used a low contrast screen film system for mammography. The method for displaying this range of information without compromising local contrast of microcalcifications, breast fibers and masses is the subject of this report.

At SPIE Medical Imaging 95, we reported on the use of Dynamic Range Control (DRC) in images of the feet and wrists (Legendre). This report showed that if one used this process that one could have dramatic impact on the regional optical density of an image while preserving the contrast in fine detailed structures. The formulas for DRC processing were discussed at that time. It is easiest to think of the process we will be describing as the creation of a low resolution mask to which we apply histogram equalization which is then combined with the original image. The result is an image in which high frequency data is preserved, but regional gray scale information is compressed. The effect in mammograms, as will be shown, is to preserve the visibility of microcalcifications, breast fibers and the edges of well defined masses, while bringing the total image into a grayscale range so that one can display, potentially, from the skin line to the depths of the densest part of the breast in one image. DRC allows one to decrease high pixel value regions, increase low pixel value regions, or simultaneously compress the low and high pixel value regions. Because it is active only at low spatial frequencies, it preserves most of the structural information of high frequency structures such as microcalcifications. By appropriately adjusting the kernel size used in this process, one can, as shown below in Case One, "simplify" the complex pattern of many small focal radiodensities seen in some women with radiodense breasts.

Chart 2. These charts demonstrates the effects of DRC.

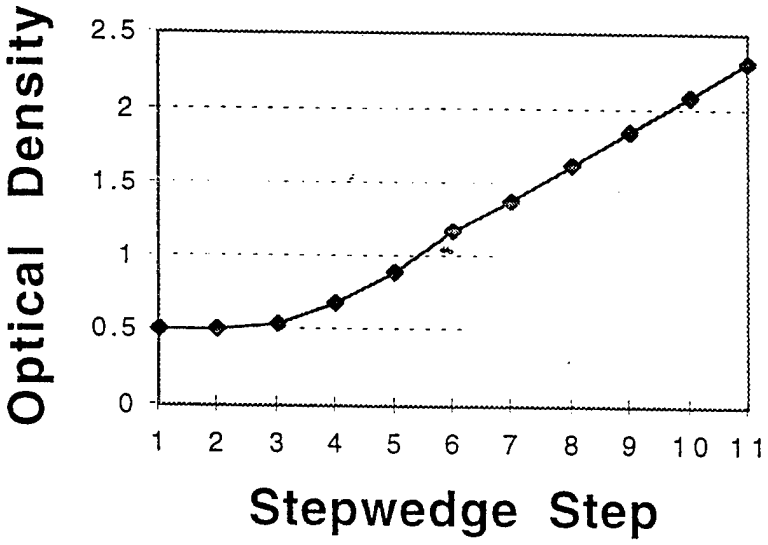

2A: The standard look up table. This is the approximate look up table for the high frequency components of the image.

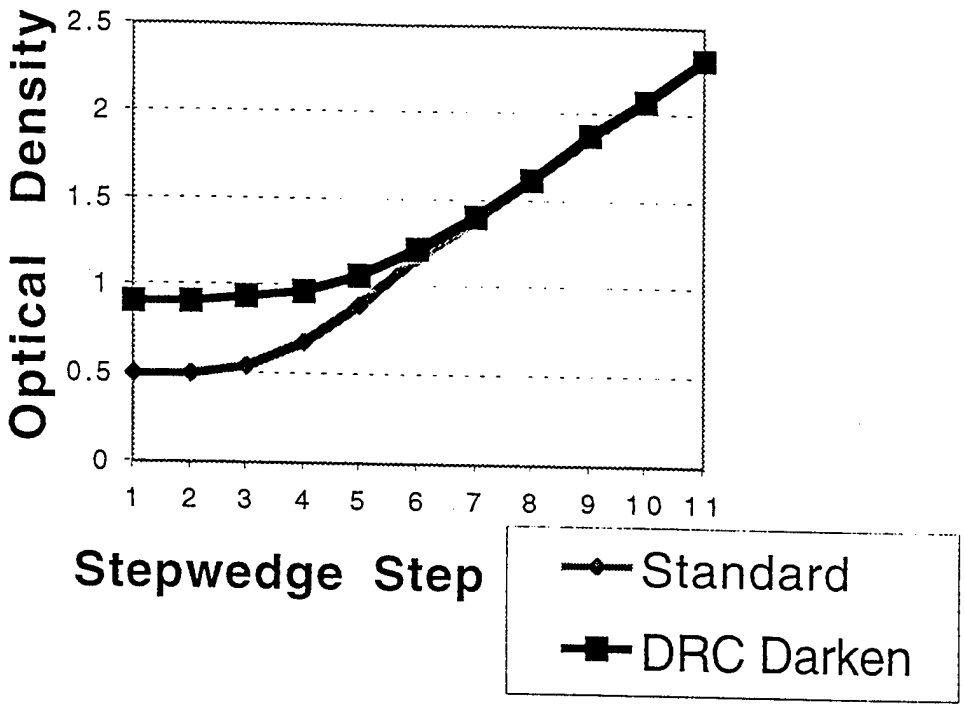

2B: DRC effect of increasing the low optical density regions of the image.

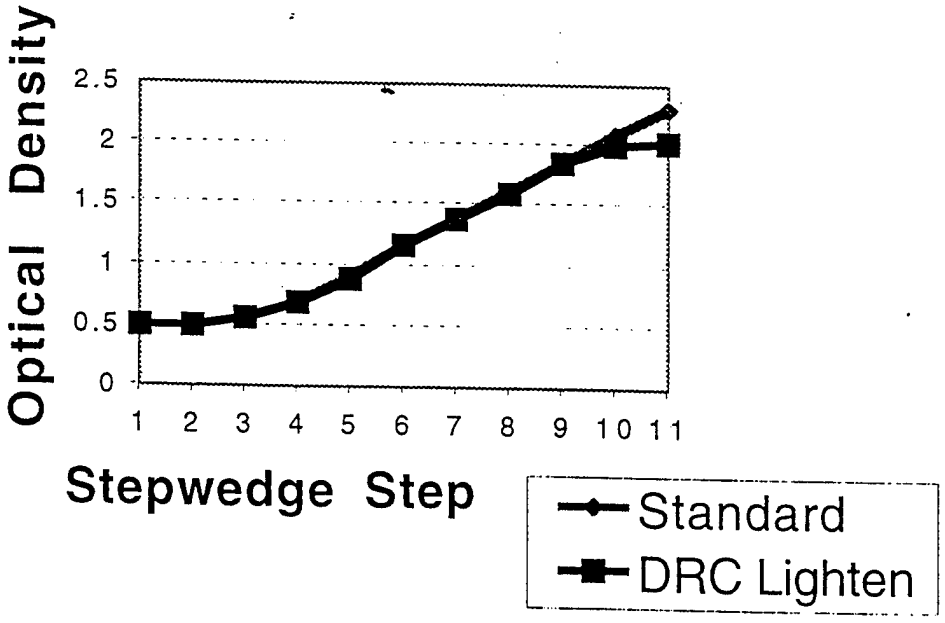

2C: DRC effect of decreasing the high optical density regions of the image.

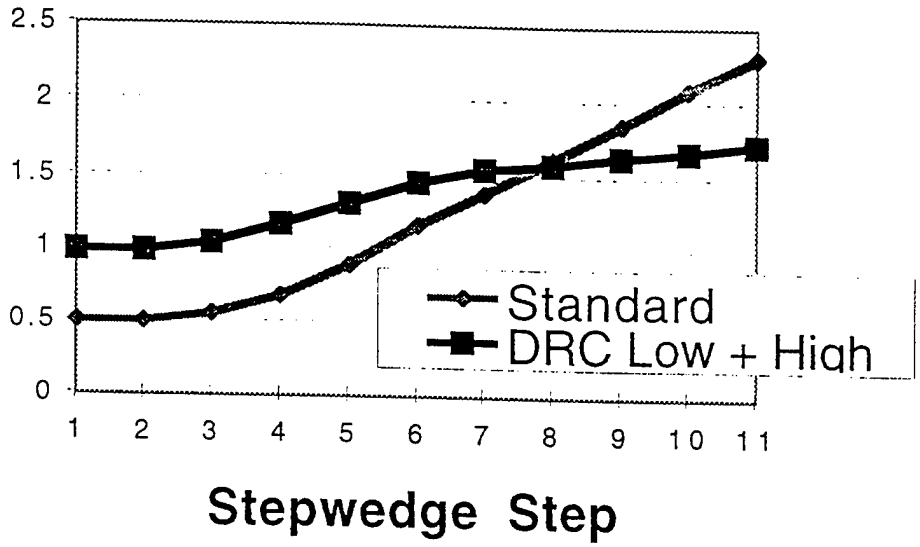

2D: DRC effect of decreasing the high optical density regions and increasing the low optical density regions of the image.

Methods: Digital mammograms are obtained with the standard exposure used for screen film mammography in women coming for breast biopsy using HR-V imaging plates and a Fuji 9000 Computed Radiography Plate Reader. Image processing includes the use of Fuji Dynamic Range Control with special equalization curves requested and designed by us. Each image is individually manually optimized for its complexity of pattern. More than 130 digital mammogram/screen film mammogram/specimen radiograph sets including more than 30 cancers have been assembled. ROC reading is pending.

Case 1. There are various methods of image processing available for enhancing the visibility of findings in t breast in digital mammography. The following demonstrate processing for emphasizing small details (microcalcifica in a complex pattern breast.

ORIGINAL SCREEN/FILM Image 1

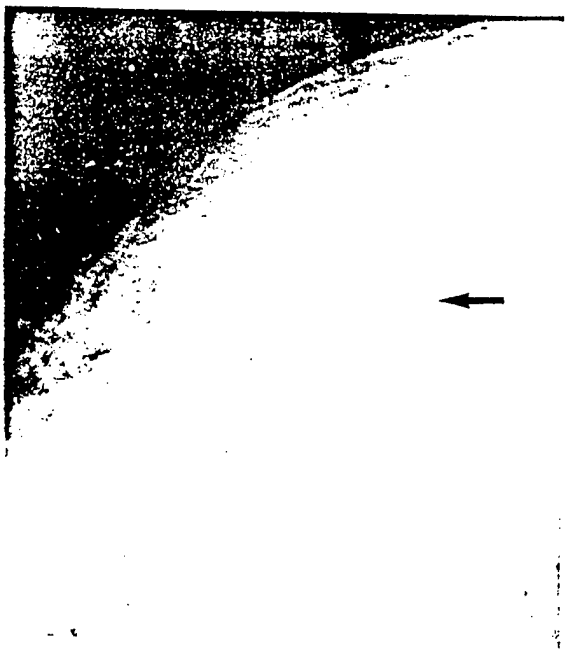

DIGITAL AT SAME EXPOSURE Image 2

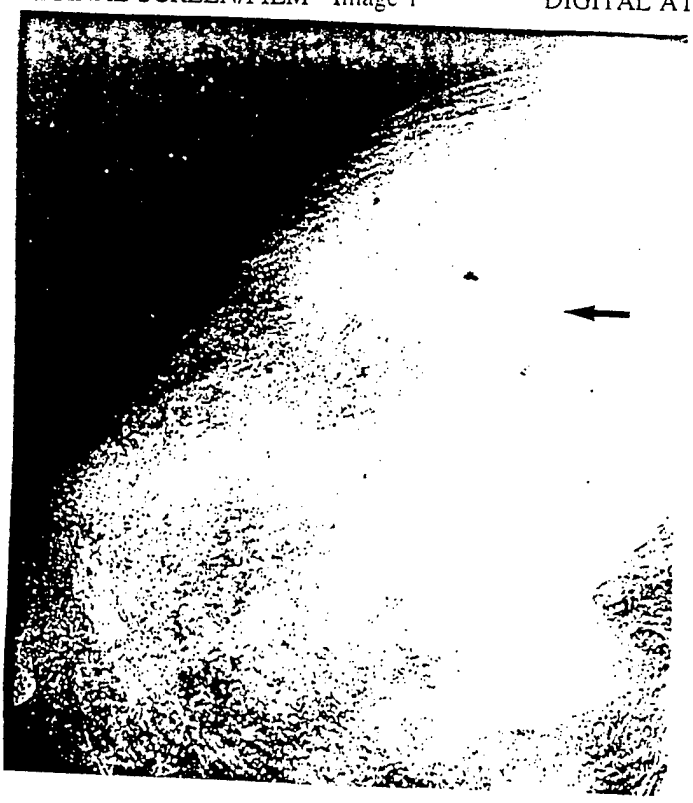

IMAGE PROCESSING FOR DETAIL *Image 3* The microcalcifications are enhanced, but the complex pattern is also enhanced. Noise is also enhanced.

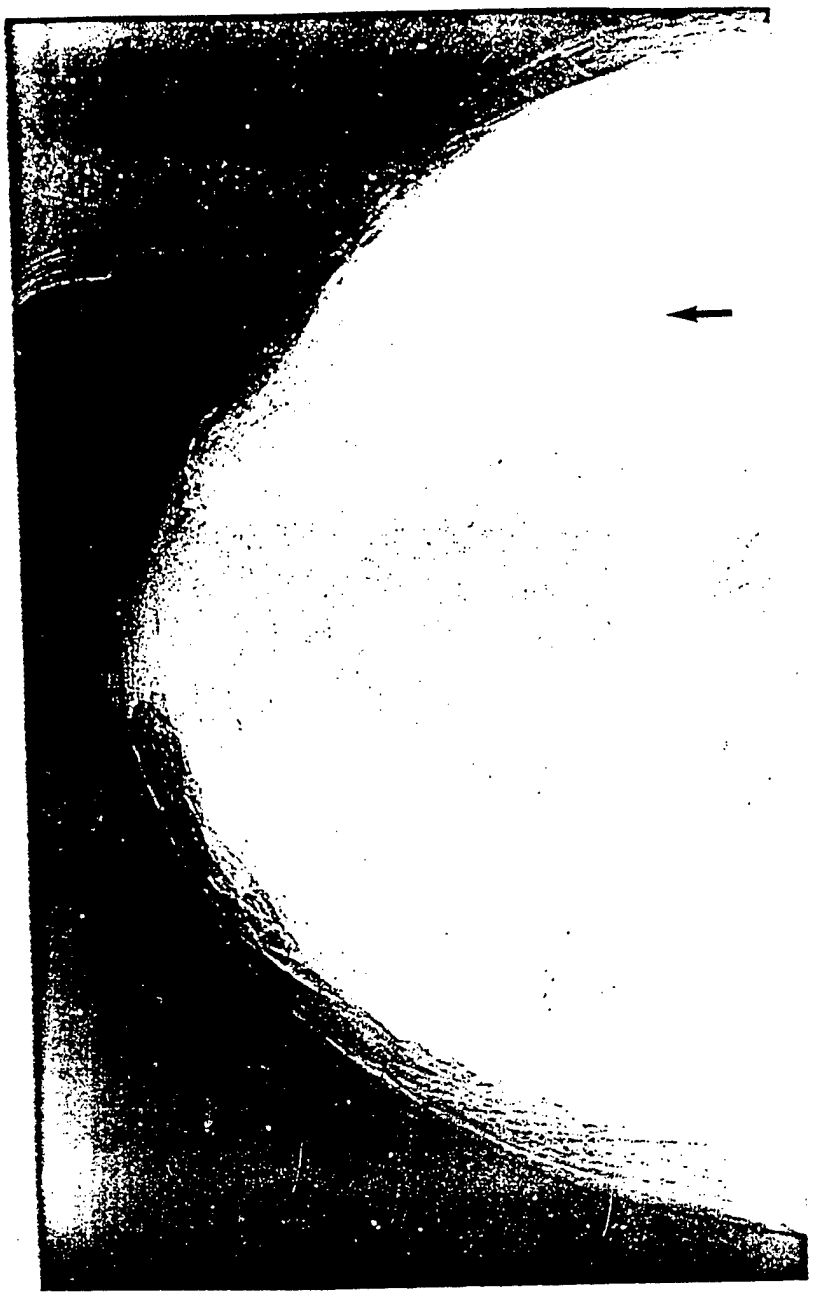

ADDITIONAL PROCESSING TO SIMPLIFY THE COMPLEX PATTERN OF THE BREAST IMPROVING THE CONSPICUITY OF MICROCALCIFICATIONS. *Image 4* The microcalcifications have increased conspicuity because the background pattern of the breast has been suppressed.

CASE 2

This case demonstrates the functionality of image processing to change the optical density of large regions of increased radiodensity, improving the visibility of microcalcifications.

FINDINGS: Asymmetric density with microcalcifications

PATHOLOGY: 3 cm ductal carcinoma with microinvasion

IMAGE PROCESSING: Frequency enhancement for microcalcifications and optical density shift specific to the tissue density

A. Conventional original RCC film *Image 5*

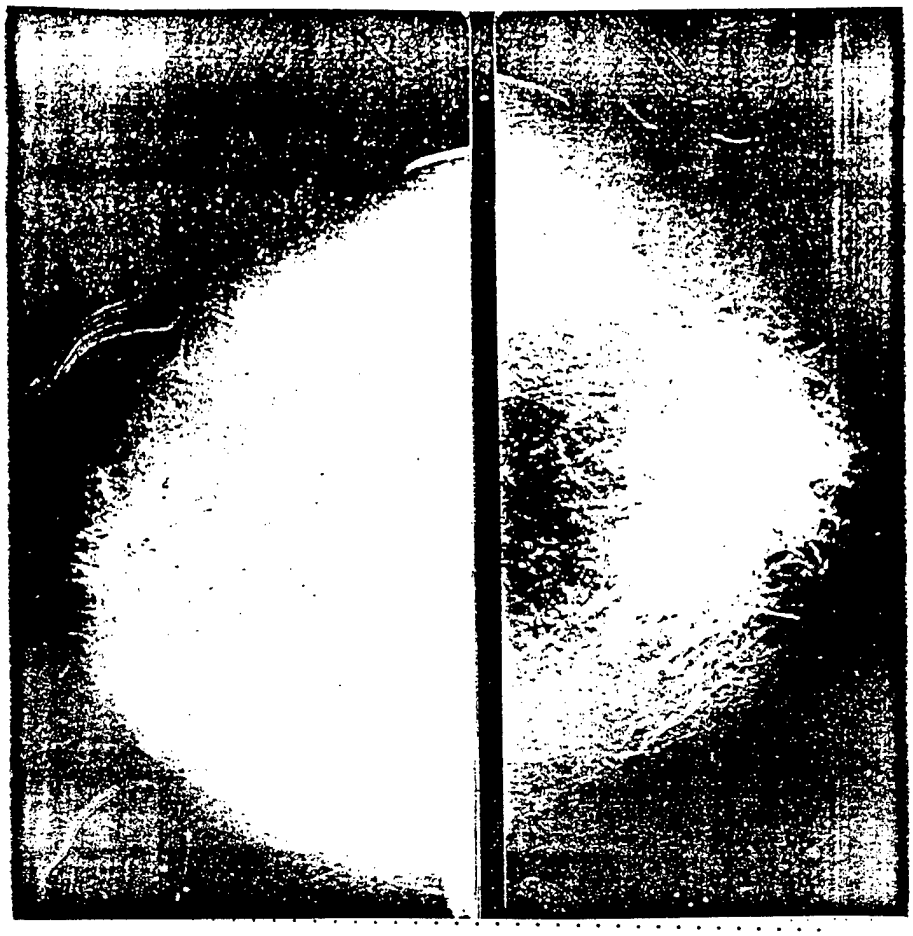

B. Digital at same exposure of LCC and RCC twin-format image *Image 6*

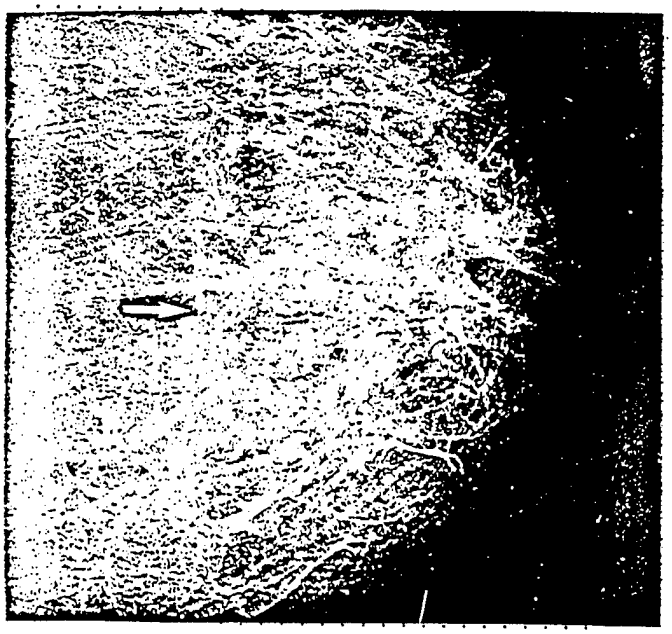

C. Processed digital image: *Image 7.* Low spatial frequency equalization of optical densities

On this image, the groups of microcalcifications (arrow) are easier to see than on either the screen film or film look alike digital images. The image processing has allowed us to look through the asymmetric breast density and see the microcalcifications within it.

CASE 3
FINDINGS: Microcalcifications within focal tissue density
PATHOLOGY: Fibrocystic changes with calcifications and ductal hyperplasia
IMAGE PROCESSING: High frequency enhancement with high and low spatial frequency equalization

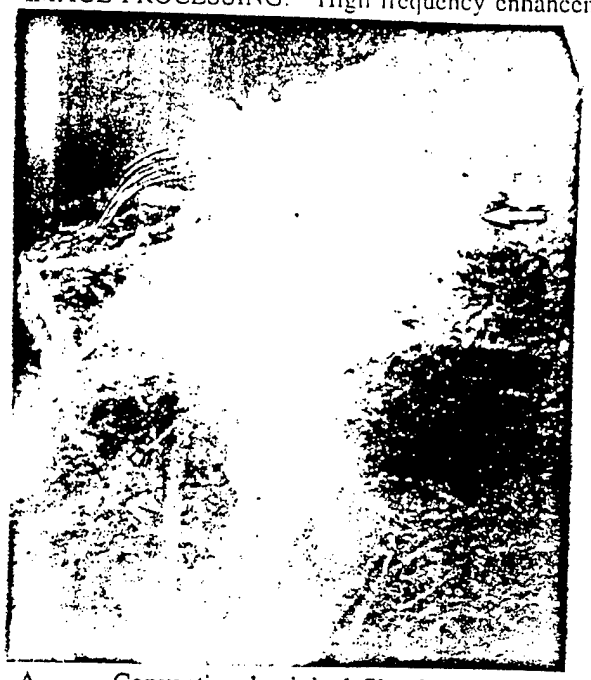

A. Conventional original film *Image 8*

B. Digital at same exposure *Image 9*

C. Processed digital image: *Image 10*
High frequency enhancement with low optical density equalization

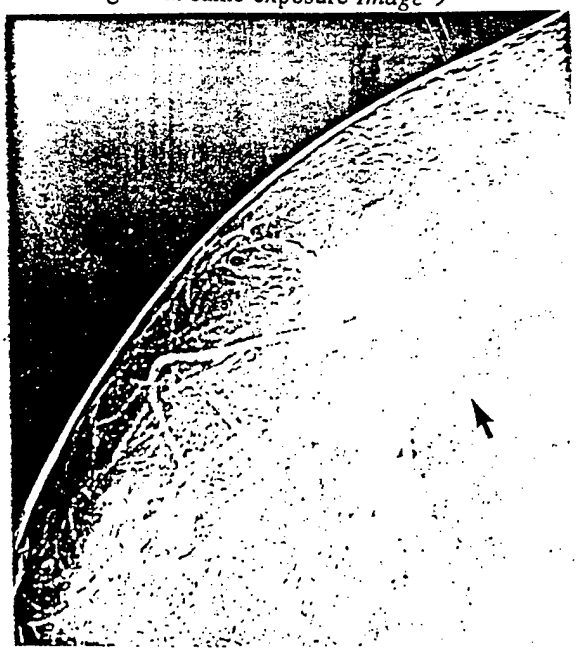

D. Processed digital image: *Image 11* High frequency enhancement with high and low optical density equalization. The visualization of the skin line is improved. One can still see the microcalcifications and mass. The architectural distortion is clearer.

CASE 4
FINDINGS: Mass upper outer quadrant left breast
PATHOLOGY: Benign recurrent fasciitis

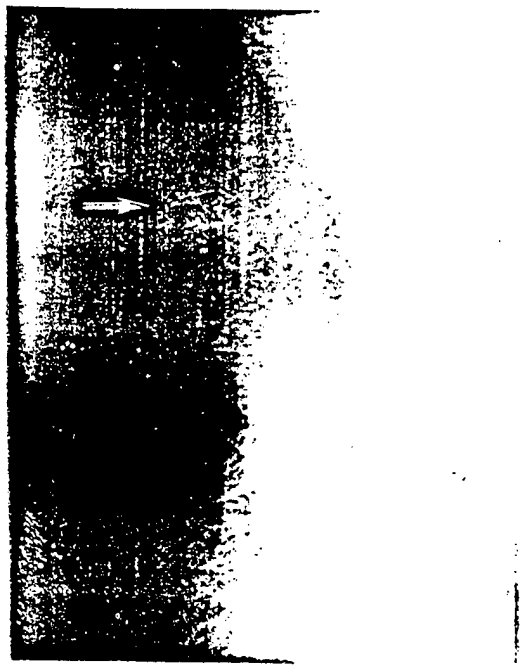

A. Conventional original film *Image 12.* The focal region of abnormal tissue close to the skin line is almost hidden.

B. Digital at same exposure *Image 13*

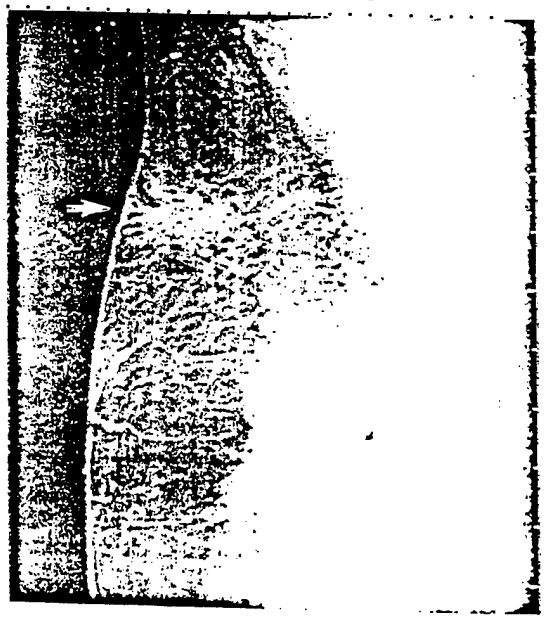

C. Processed digital image: *Image 14*
Low frequency enhancement with high optical density equalization. The focal tissue density lying close to the skin, high in the breast is much easier to identify., but the overall tissue appearance is distorted.

D. Processed digital image: *Image 15*
High frequency enhancement with high and low optical density equalization. The skin line is easily seen as is the tissue area of interest. The microcalcification is seen with slightly less contrast than on the other images.

Discussion

Low resolution histogram equalization appears to provide improved conspicuity of abnormalities within the radiodense breast by balancing the wide range of object radiodensities within the breast. This image processing approach can be reached by several methods and we are currently working to optimize a system based on wavelet decomposition as well. Digital acquisition appears optimal for this system since it can allow the recording of a wider range of exposure information than conventional screen film mammography. It is possible that this processing could also prove effective if a wide latitude film were used for mammographic image capture for secondary digitization, but this effect does not occur with standard screen film images with secondary digitization.

Inspection of these images should reveal problems occurring from noise in regions of increased breast radiodensity processed with this algorithm. On conventional mammograms, these regions would be clear or nearly clear. Because of the noise secondary to under-exposure, these "recaptured" regions have decreased conspicuity of the smallest calcifications compared to fully exposed regions of the imaging plate as reflected in the Chart 1 printed above.

Summary

Low resolution histogram equalization appears to offer advantages in the display of mammograms in the radiodense and complex pattern breast. The range of tissue densities that can be evaluated on these new images is greater than those normally visualized in the radiodense breast. The system still requires individual optimization of image appearance, but we expect that patterns will emerge that will eventually allow several standard forms of this image processing to be applied routinely. We are about to start our ROC reading to determine whether this new method of image processing does indeed enhance the detectability of breast cancer in the radiodense breast.

Bibliography

Bird RE, Wallace TW, Yankaskas BC. Analysis of cancers missed at screening mammography. Radiology 1992; 184:613-617.

Farria DM, Mund DF, Bassett LW. Evaluation of mised cancers using screening mammography. (Abstract) AJR 1995; 164S:126

Freedman M, Pe E, Zuurbier R, Katial R, Jafroudi H, Nelson M, Lo S-C B, Mun S K: Image Processing in Digital Mammography. SPIE: Medical Imaging, Vol. 2164 (1994); 537-554pp.

Freedman MT, Steller D, Jafroudi H, Lo SCB, Zuurbier RA,Katial R, Hayes W, Wu YC, Lin JS, Steinman R, Tohme WG, Mun SK. Digital Mammography: effects of decreased exposure. SPIE Medical Imaging 1995. Paper 2432-49. (1995)

Legendre K, Steller D, Freedman M, Mun S K: Single-image Hardcopy Display of Musculoskeletal Digital Radiographs. SPIE: Medical Imaging (1995). Paper 2436-19.

Harvey JA, Fajardo LL, Innis CA. Previous mammograms in patients with impalpable breast carcinoma: Retrospective vs blinded interpretation. AJR 1993; 161:1167-72.

Silverstein MJ, Gamagami P, Colburn WJ, et al. Nonpalpable breast leasions: Diagnosis with slightly over-penetrated screen-film mammography and hook wire directed biopsy in 1014 cases. Radiology 1989; 171:633-638.

Tabar L, Fagerberg G, Duffy SW et al. Update of the Swedish two-county program of mammographic screening for breast cancer. Radiologic Clinics of North America 1992; 30:187-210.

Acknowledgment

Supported in part by U.S. Army Medical Research Grant DAMD 17-93-J-3008. The content of this report does not necessarily reflect the position or policy of the U.S. Government and no official endorsement should be inferred.

Image optimization procedures for the Fuji AC-1

Matthew Freedman M.D., M.B.A.
S.K. Mun, Ph.D.
Einar Pe, R.T.R.
S.C.B. Lo, Ph.D.
Martha Nelson, M.D.

Department of Radiology
Georgetown University Medical Center
3800 Reservoir Road, N.W.
Washington, D.C. 20007-2197

1. INTRODUCTION

The Fuji AC-1 is a popular system for digital radiography with great potential, but for many the initial implementation of the system in a radiology service is a frustrating experience for lack of effective support and a clear operational manual. Adjusting the image processing settings for site specific image optimization has been, for most users, difficult and confusing[1, 2]. The effect of each of the image processing parameters available on the Fuji AC-1 is not easily understood by users of the machine. The application manual[3] that comes with the machine briefly defines the parameters and gives recommended settings for different types of examinations, but the manual does not provide the user with adequate information or a suggested method to allow the user to easily optimize the image for that user's site. This paper defines in more precise terms the meaning of the various parameters and suggests a method of procedure to optimize the parameters to each radiologists preference. The results are based on experiments and measurements we performed with a Fuji AC-1 +.

This information should assist the radiologist to use a more systematic method of image quality improvement rather than the somewhat random trial and error process that current users (1, 2) have described.

2. METHODS

The information reported here is based on experiments done with a step wedge phantom in which each of the parameters was varied individually. Selected combinations of parameters were also tested. Based on these tests with a step wedge, tests of the optimization method were done on images of phantoms (bones of the foot and hip imbedded in plastic) and on clinical images of the chest and abdomen.

2.1 Organization of the discussion

This paper discusses the meaning of the individual parameters and gives recommendations on methods for modifying them to be closer to the users' preference. These two themes are intertwined in the paper. The parameters are discussed in the

0-8194-1129-9/93/$6.00

sequence that we recommend for setting their values for an individual body part and type of exam. It does not follow the sequence given in the Fuji application manual.

2.2 Basic types of Fuji image processing

There are two fundamental groups of image processing (Fuji calls it image enhancement) that can be performed. The first relates to changes in image optical density and contrast. The second relates to filtering and the selective amplification of certain spatial frequencies within the image. Those parameters affecting image optical density and contrast will be discussed first.

2.3 Selecting the initial parameters settings that are to be modified

It is recommended that one start with the settings for each parameter recommended by Fuji for the specific type of exam being done. Clearly, much work has gone into selecting these parameters and they are likely to be close to the final parameters wanted. Use the exposure recommended by Fuji if that exposure level is acceptable; if not, use the exposure settings preferred. An exposure of less than a 400 speed equivalent will not provide full diagnostic information.

3. PARAMETERS AFFECTING IMAGE OPTICAL DENSITY AND CONTRAST

Those parameters affecting image optical density and contrast should be adjusted first. The Fuji names for these parameters are "GT", "GS", "GC" and "GA". The "G" refers to the gradient and shape of the characteristic contrast curve and describes features of a curve equivalent to the characteristic curve (H and D curve) of film screen systems. Because the gradient is electronic rather than fixed in the film chemistry, there are many more potential curve shapes and positions possible with the Fuji system than can be seen with film.

We have chosen to use the term contrast curve for the electronic curve equivalent to the characteristic curve of a film.

The graphs of image optical density used in this paper have image optical density on the Y-scale and the log of the relative exposure on the x axis. These are the same axes usually used for the display of film characteristic curves.

3.1 The GS parameter - gradient shift

The predominant effect of the GS parameter is to shift the contrast curve up or down (Graph 1). This has no direct analogy to film screen imaging. The units of the GS parameters are approximately equivalent to O.D. units. This parameter has little effect on the shape of the contrast curve. It makes the image lighter or darker, but does not affect the contrast characteristics. If one starts with a GS parameter of 0, a shift of the GS parameter to a positive value, such as + 0.40, increases the optical density of the final image overall by approximately 0.40 optical density units in all areas of the image. This is represented on the graph as a shift of the contrast curve superiorly. A negative value, such a -0.40 makes the overall image lighter and shifts the curve approximately 0.40 OD units downward.

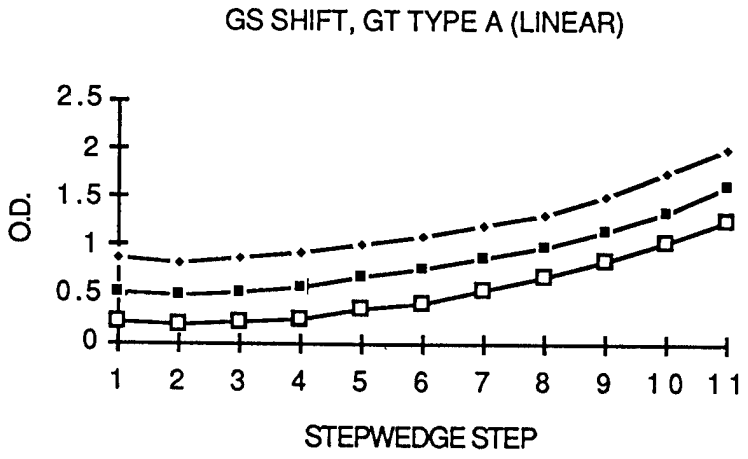

The graph of the step wedge optical density values shown in Graph 2 shows that in this experiment, the GS effect is slightly non linear; at low density levels, the actual shift is slightly less than 0.40 OD units, at mid densities it is slightly greater that 0.40 OD units and at high densities it would be again less than 0.40 OD units. This occurs with most of the Fuji contrast curves because most are S-shaped and non-linear. If one does the GS shift with linear curves (Fuji GT type A)(Graph 1), then the distance between the curves is almost constant.

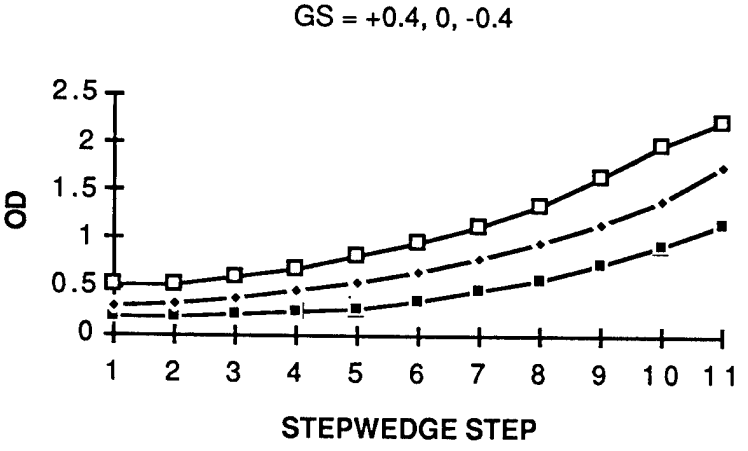

3.11 Clinical application of the GS curve: Changing the image overall degree of blackness

It is suggested that the following procedure be used to optimize the overall image optical density.

GS Step 1. Select a person with an average height, weight and body shape for the types of patients to be imaged. Take an optimally exposed screen-film image (SF) of the

anatomic area of interest Take a Fuji storage phosphor image (SR) of the same area and process the image using the Fuji recommended technique. For the Fuji image use the exposure setting planned for use for Fuji images of that part of the body (either the Fuji recommended exposure or the parameters preferred at your site.)

GS Step 2. Select two key areas of the SF image that have different optical densities. The key areas selected should be those that should be demonstrated optimally: i.e. the lungs and the area behind the heart on a chest radiograph; renal shadow and lumbar spine. on an abdominal image; maxillary sinuses and frontal sinuses on a Waters view of the sinuses. For use in this article, consider these to be key area 1 and key area 2.

GS Step 3. Measure the optical density at one of these two key areas on the screen-film image.

GS Step 4. Measure the optical density at the same point on the Fuji AC-1 image.

GS Step 5. If the optical density of the SF and SR images are different, subtract the OD of the SR image from that of the SF image.

GS Step 6. Enter the difference of the OD parameters of SF less SR as the GS parameter setting. If the SF image OD is greater than the SR OD, the parameter setting should be a positive (+) number. If the OD of the SF image is less than the SR image, the GS parameter setting should be a negative (-) number.

GS Step 7. Print an SR image with the new settings and check that the OD of the SF and SR images in the selected first key site are approximately the same. If they are the GT parameter has been correctly adjusted.

Optional GS Step 8.If the optical density of key point 1 on the SF image is not exactly as desired, one can, at this point, chose a better optical density than is seen on the SF image--using that selected OD as the desired optimal OD.

3.2 Parameter Two: The Rotation Center (GC) (gradient curve center)

The rotation center is a point on the contrast curve that is to remain fixed in position during subsequent manipulations of the gray scale. The contrast curve will rotate around this center point, thus preserving the first optimized point in the SR image. As shown in graph 3, if one changes the GC without changing the GA, the change in GC will have no effect on the contrast curve.

GC 0.3, GC 0.6, same GA & GT

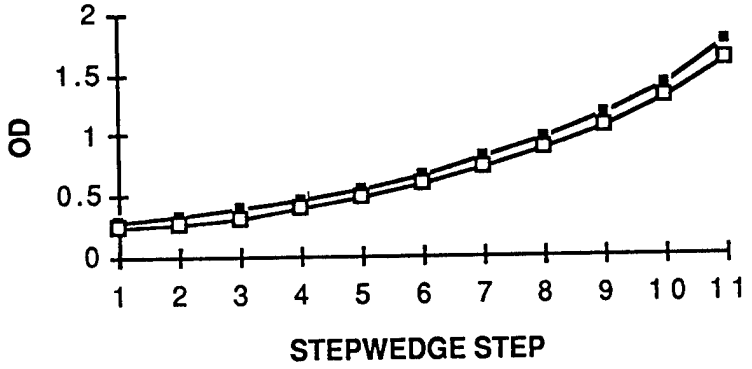

Graphs 4 and 5 indicate that the number chosen as the rotation center is the optical density of the point around which the curve will be rotated. Thus in graph 4, the rotation point selected is GC = 0.3. In Graph 5, the rotation point selected is GC = 0.6. In each we have increased the GA from 0.7 to 1.3. The graphs demonstrate that these are the points around which the graphed contrast curves have rotated.

GC 0.3, GA 0.7 and 2.3

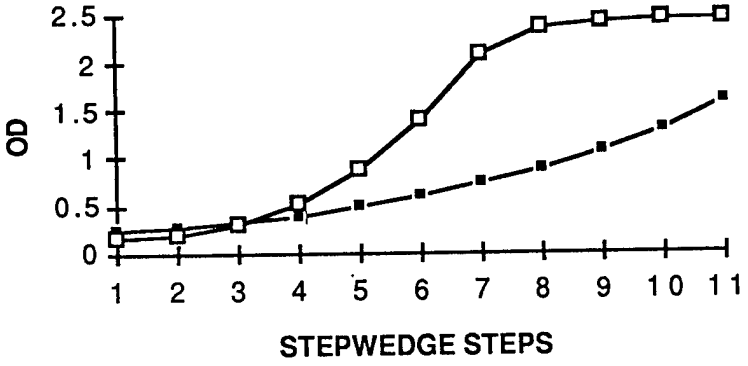

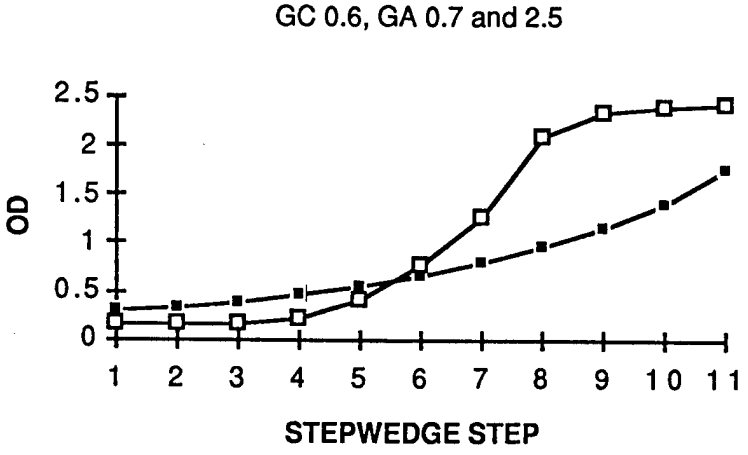

3.21 Use of the GC in image optimization

If one is following the optimization procedure given for the GS parameter given above, one should now set the GC parameter to be the optical density of key point #1 used above. In this way the first optimized OD key point will not be changed by subsequent changes in the settings of the other parameters.

Once this GC point has been set, then changes in the slope of the contrast curve can be performed. The contrast curve will rotate around the point previously selected.

3.3 Parameter Three: Rotation Amount: GA parameter (gradient slope)

The rotation parameter changes the slope of the contrast curve. The higher the number of the parameter setting the steeper the contrast curve and the higher the contrast present so that a GA of 0.8 represents a relatively wide contrast range (wide latitude, gentle slope) and a GA parameter setting of 2.3 represents a relatively contrasty image with a narrow range of contrasts (narrow latitude, steep slope).(Graph 4). The GA number is the maximal slope of the contrast curve when specific values are used to indicate the scale of the log relative exposure amounts along the y axis. The higher the number, the steeper the slope at the maximal slope portion of the contrast curve.

3.31 Selecting a GA parameter

The method described below is a stepwise method for selecting a new value for the GA parameter. It is based on the concept of having a fixed point (the GC parameter setting) and rotating the curve around this point. The purpose is to find a new second key point (see GS Step 2) that has the optical density desired. This is done by plotting the new second point at the place where the relative exposure to the imaging plate is the same as the original second key point, but the optical density is different. This means that one must first identify the relative exposure to the phosphor plate at the initial second key point (as identified in GS Step 2) and then locate where that new second key point would have that same exposure but have the new preferred optical density.

Given this information, how does one select a value for the GA parameter. One determines an approximate value as follows using linear graph paper. (The method is approximate because most GT curves are non-linear.)

GA Step 1: Draw a graph with the y axis representing OD units and the x-axis representing relative exposure units. Label the y axis with OD units from 0.5 to 3 at a scale of 0.1 units (i.e. 26 divisions). Label the x-axis with log relative exposure units from 0.5 to 3 at a scale of 0.1 units (i.e. 26 divisions). (Graph 6) (because these are log relative exposure units, the precise exposure values are unimportant, only the relative values are important)

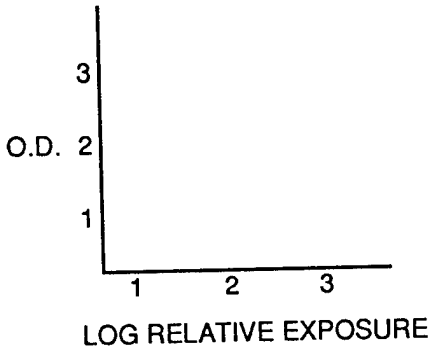

GA Step 2: Plot the GC number so that on the y-axis it is at the location of the actual number. For simplicity use the same number on the x-axis to represent the relative exposure level. (Graph 7)

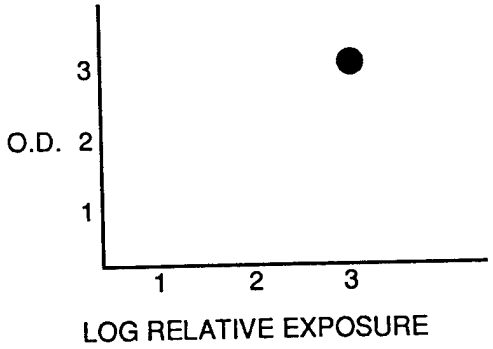

GA Step 3: Through the GC point plotted above, draw a line with the slope equal to the GA value on the SR image obtained after the GS number has been set (as described under the section for the GS value). (Graph 8)

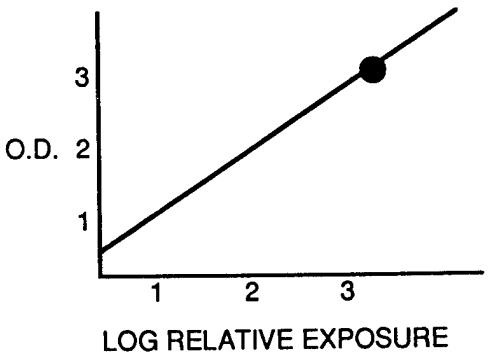

GA Step 4: Measure the optical density of the second key region (from GS Step 2) of SR image after the GS has been set. (from GS Step 7)

GA Step 5: Plot this point along the line drawn in GA Step 3. (Graph 9) (The x-value has the measured OD. By plotting it along the GA line, it is possible to project that point to the Y axis to determine the log relative exposure that resulted in that OD on the original image.)

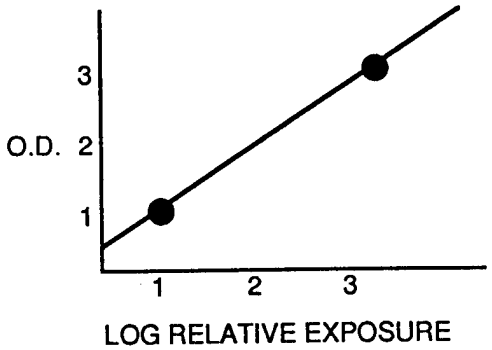

GA Step 6: Plot a point which has as its y coordinate, the same y coordinate as the point plotted in GA Step 5 (that is, it has the same relative exposure value as the previous point), and has as its x-coordinate the optical density desired for the final image at the second selected area of interest (from GS Step 1, the optimally exposed conventional film). (Graph 10)

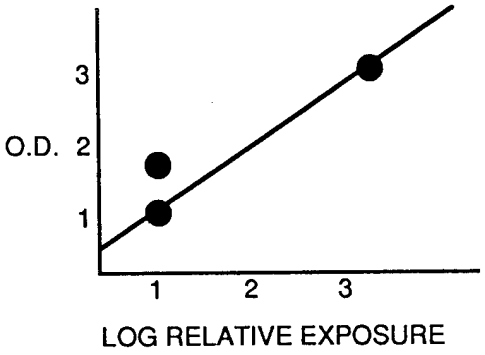

GA Step 7: Draw a line connecting the point in GA Step 6 and the GC. (Graph 11)

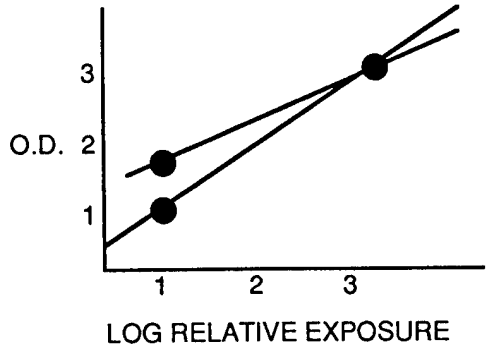

GA Step 8: Measure the slope of this line and use this slope as the GA parameter setting.

Now reprocess the SR image using the GS, GC and GA parameter settings selected above. The image optical density at the sites selected as the 2 key sites should be close to the values chosen based on the original properly exposed conventional film.

3.4 Combined changes of GC and GA parameter values

Combined changes in the GC-GA settings have a different effect than is shown in Graphs 4 and 5: If one changes both the GC and GA parameter settings (using two different GC settings and then increasing the GA value), the contrast curves that result have an important new relationship to each other. (Graph 12) The change is analogous to the change that occurs with a change in the sensitivity of a film screen system. It is in effect a shift of the gradient curve in its entirety to the right or left. Thus a selection of different GC values combined with a change in the GA value will, in addition to fixing a single point for rotation of the gradient curve, also results in a shift of the entire curve; thus this makes the overall image lighter or darker, and thereby overlaps the effect of the GS parameter.

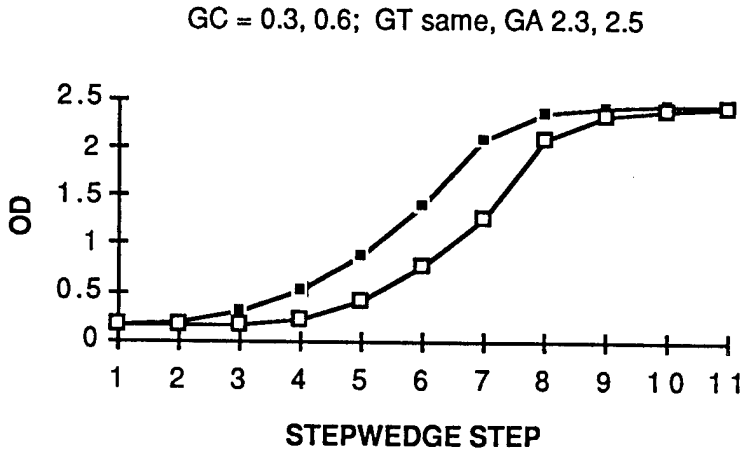

There is a difference between the type of shift occurring with the GS shift and the combined GC selection and GA shift. The difference between changes in the GC-GA combined change and GS value changes are easiest to understand if one considers the toe or shoulder of the curve. If one makes the final image darker by using the GS shift, the entire curve shifts upward. The shape of the curve is unchanged: thus the relative contrast within the toe and shoulder of the curve is unchanged. If one increases the optical density of the image by using different GC-GA settings, then one can shift the region of exposure that falls in the toe or shoulder of the curve (with its gentle slope) into a region of the curve that is more towards the middle, thus giving higher contrast. The GS shift by in large does not affect the contrast in an area, only its optical density.(footnote: if the GS shift moves the image into an area of the recording medium that has a steeper contrast curve, the contrast will increase, but this is due to the contrast response of the recording medium, not directly from the effect of the GS shift.) The GC-GA combined setting changes the contrast as well as the density if the region of interest is in the toe of the curve (for images made darker) or in the shoulder of the curve (for images made lighter).

One can determine the direction (right or left) that the contrast curve will shift and estimate the magnitude of the shift as follows. Identify the mid portion of the contrast curve. If one chooses a GC point below the mid portion of the curve and increases the GA, the total curve will shift to the left. If one chooses a GC point below the mid portion and decreases the GA, the curve will shift to the right. If one chooses a GC above the mid point and increases GA, the curve will shift to the right. If one chooses a GC above the mid point and decreases the GA, the curve will shift to the left. The further the GC is from the center point, the greater the shift. The greater the change in GA, the greater the shift. The amount of the right-left shift can be estimated graphically and its effect on the OD and contrast of any particular part of the image thus evaluated.

3.5 Alternative method for selecting GS, GC and GA parameters

The method described above is based on the assumption that there is a properly exposed image that can be used as a guide to the selection of the optical density parameter settings. The same technique can also be used based on a conceptual, rather than a physical ideal image. One can substitute for the measured OD from the ideal SF film, the radiologist's idea of the optical density desired at two particular sites on an SR image and

use the same step-wise procedure to arrive at this point. If a matched set of SF and SR images is not used, be very careful that the image used as the master SR image is not under or overexposed as this will affect the settings for several of the parameters. A quick check for proper exposure (if the machine has been properly calibrated) is to check that the "S" number on the image is between 100 and 500. This is discussed below under possible complicating factors.

3.6 Parameter Four: Contrast Type (GT, gradient type)

The contrast types are H and D curve equivalents. Fuji provides in their application manual sketches of the contrast curves that are provided within the system. Most of these resemble typical H and D curves (characteristic curves) of film. Because these curves are copyrighted, they are not reproduced here. Most of these curves are fairly similar to each other and represent typical varieties of S-shaped curves seen with film. There is also a direct linear curve (type A) and a reverse linear curve that gives black white inversion (curve M). Curves L and K have the steepest vertical portion of the curve. The curves are each drawn so that almost all of them have approximately the same maximal slope (gradient) until they are rotated using the GA parameter. They differ primarily in the shape of the curve in the low exposure and high exposure regions (the toe and shoulder). The GA parameter changes them by changing their maximal slope thus changing the latitude (contrast) of the mid portion of the contrast range.

These contrast curves can be used to fine tune the appearance of the SR image based on the GS, GC, and GA parameter settings selected above. They are used primarily to affect the contrast curve shape at the least optically dense (toe) and most optically dense portions of the image (shoulder). The best shape for the toe and shoulder of the contrast curve will be determined by the body area radiographed and the key areas selected in setting the optical density (GS) and contrast curve angle (GC with GA) using the above methods. It is suggested that one proceed as follows.

GT step 1: Start with the Fuji recommended GT for the body part being radiographed. Complete the density and contrast correction steps for the GS, GC and GA parameter settings as described above.

GT step 2: If the image is not satisfactory in the toe or shoulder regions of the curve, decide whether the region has too little or too much contrast. If there is too much contrast, use the Fuji curve drawings to compare the GT curve used to the other curves to find one with a less steep curve in the optical density region of interest (toe or shoulder). If more contrast is wanted, look for a curve that has a steeper curve (in the toe or shoulder) than the one currently used.

GT step 3: Process the image with this new GT curve and evaluate the image.

3.7 Patient variation and its effect on the selection of GA and GT curves

If the curves have been properly selected as described above based on a single optimized screen-film image, the main need for further adjusting the toe and shoulder of the curve (the GT type) or of adjusting the slope (GA) of the contrast curve would be either to capture information in portions of the image of lesser importance than the two key sites selected in GS Step 2 or to adjust for patients with different body builds.

The use of changes in the contrast curve to accommodate differences in body build is based on the following: The computer in the imaging system does not know the area of

the chest or bone image that is of greatest importance; it bases its image processing on the relative exposure of different parts of the image. Thus, in the above system, if one decided to use the cortex of the femur as the first key region, what the computer algorithm does is to assign any future image processed with the same parameter settings and with the same relative exposure, the same relative radiodensities. The computer looks at the total exposure of the imaging plate and assigns in each area a corrected exposure value that represents the relative exposure of the imaging plate in that location. This means that an overall increase or decrease in the exposure does not affect the relative exposure at any point on the imaging plate or affect the final radiodensity on the final image corresponding to that site.

Fuji has not explained precisely how its algorithm works, but one way in which it could work is as follows: the machine that reads the exposure of the imaging plate divides up the plate into approximately 50 million picture elements called pixels. Each pixel has received a certain amount of exposure. The machine calculates the overall exposure of the IP and divides that by 50 million to determine the average exposure of the plate. This average exposure is then is used to determine the amount of IP exposure that should correspond to the average optical density of the final image when laser printed on film. If one exposes the entire IP to an average exposure of 100 units and has determined by the values selected for each of the image processing parameters that an area that has half the average exposure should correspond to an image OD of 0.5, then each area that has half of the average exposure (in this case 50 exposure units) will be assigned a final image OD of 0.5. If the IP had received a higher exposure averaging 150 exposure units, then 1/2 of this (75 exposure units) will correspond in the final image to an OD of 0.5. By adjusting the G parameter settings, the computer has been set to make that adjustment.

When the patient has a different physical size or shape, the correspondence between the average IP exposure and the selected desired optical density may or may not be different. If the patient is symmetrically increased in size so that the relative exposure of different parts of the IP remain the same, then the final OD of different parts of the final image will maintain the same relative ODs that were previously selected. If the increase in size is asymmetric, then that asymmetry will be reflected in the average radiodensity of the final image. If the patient is asymmetrically thicker in one region, then that region will be relatively lighter than it was on the optimized image. For example, a patient with cardiac enlargement will have a heart that is printed with a lower optical density than a patient with a normal size heart. A patient with a unilateral pleural effusion that opacifies the hemithorax will cause the normal opposite hemithorax to appear blacker than the usual setting. Because a patient with a different size or shape may have a different balance of exposures across the IP, one must accommodate that variation in the selection of values for the algorithm.

Although no absolute method can be given for accommodating variations in patient size and shape, in general this is done in the same fashion as with SF images: one selects a contrast curve (a gamma in SF images or a GA in SR) that is not as steep as one might otherwise choose. Once one has set the GS, GC, GA and GT settings, one needs to look at a large number of images to determine whether any fine adjustments needs to be made in the slope (GA) or to the shape of the toe and shoulder of the contrast curve (GT) because of differences among patients.

Summarizing the approach to those factors affecting OD and contrast, it is suggested that the choice of parameter settings affecting image optical density and contrast be performed in the following sequence:

1. Make an exposure of an area of the body in question using the same exposure factors for SF and SR. The SF image should be of good quality.

2. Select the desired density wanted in some portion of the image.

3. Adjust the value of the GS parameter so that optical density in this desired region is at the density desired.

4. Set this point as the point for the center of rotation.

5. Choose a second point. Measure its current OD and decide on its desired OD. Graph the curves.

6. Enter the slope of the new (desired) curve as the GA value.

7. If one desires to improve the optical density response in the region of the lightly expose portion of the image or the darkly exposed portion of the image choose a contrast curve based on the chart provided by Fuji.

This should provide a reasonably efficient method of selecting the optical density for the image.

4. SECOND SET OF PARAMETERS: THOSE RELATED TO SPATIAL FILTERING AND EDGE ENHANCEMENT

There are three parameters related to filtering and the preferential emphasis of certain frequencies in the image: the RN, RT, and RE parameters. The RN parameter affects the spatial frequencies of the entire range of OD in the image. The RT parameter affects the spatial frequencies of only the more lightly exposed regions of the image. The RE parameter relates to the degree of emphasis of those frequencies that are accentuated.

In order to understand the filtering, it is important to have some understanding of the frequencies of objects with edges of different degrees of sharpness. Using Fourier analysis it is possible to describe any shape as a combination of sine waves of different frequencies and amplitudes. Sharp edges contain higher frequency sine waves than do unsharp edges. If one selectively filters out the lower frequency sine waves or selectively amplifies the high frequency sine waves, the high frequency sine waves are emphasized, thus the edge of a sharply defined object is enhanced. If the high frequency sine waves are filtered out, leaving only the mid and lower frequency sine waves, then edges will appear smoother and therefore will be less distinct.

4.1 The types of frequency filtering

There are two different methods that can be used to enhance selected spatial frequencies. These are (1) unsharp masking with different kernal sizes and (2) the filtering or amplification of certain spatial frequencies following a Fourier transform of the spatial frequency data. A discussion of these two methods is beyond the scope of this paper.

4.11 The advantage of emphasizing high frequency sine waves

Amplifying high frequency waves enhances the detectability of sharp edges and small objects on the image. This has advantages in detecting the margins of tubes and line on a chest image and of the cortical and trabecular margins on bone images.

4.12 The disadvantages of emphasizing high frequency sine waves

Noise tends to contain high frequency edges and thus filtering to emphasize high frequency sine waves will also amplify the noise in an image. This noise is thought to make it more difficult to detect the margins of low contrast objects.

Most structures contain many edges that can be emphasized by filtering. The most common of these are the margins of the blood vessels in lungs. Images of lungs with marked edge enhancement are not what radiologists are used to looking at and can be confusing. The overemphasis of normal structures can be confusing to the radiologist and could result in misdiagnoses. (FIGURE 1 A, B)

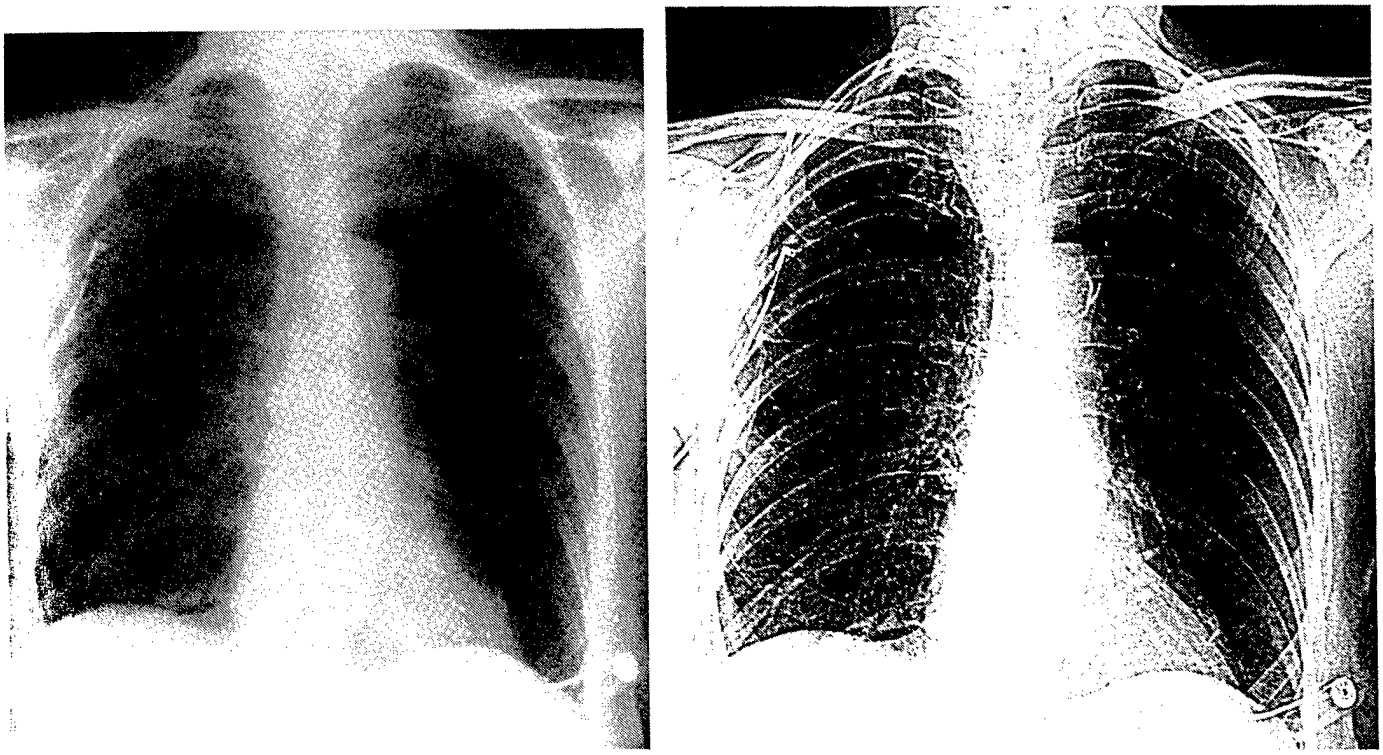

Figure 1. *Normal chest radiograph processed with RE = 0 and RE = 10. The degree of edge enhancement distorts the appearance of lung and bone structures. (Fuji algorithm settings: G0.9D#1.6-0.1R5F0.0, G0.9D#1.6-0.1R5F10)*

4.2 Using the edge enhancement functions

Because frequency filtering and amplification are relatively new concepts to radiologists, it is more difficult to define how much and what type of filtering and frequency amplification parameters will improve disease detectability and image

appearance. Thus, at present, the settings for these parameters are a matter of individual preference.

4.3 The RN parameter (frequency rank)

The RN parameter represents a series of filters of the sine waves that make up the images. Low number RN (0-3) emphasize low frequencies. These tend to minimize the visibility of noise and thereby enhance the ability to see low contrast, larger, less well defined structures such as the margins of the abdominal organs. (Figure 2)

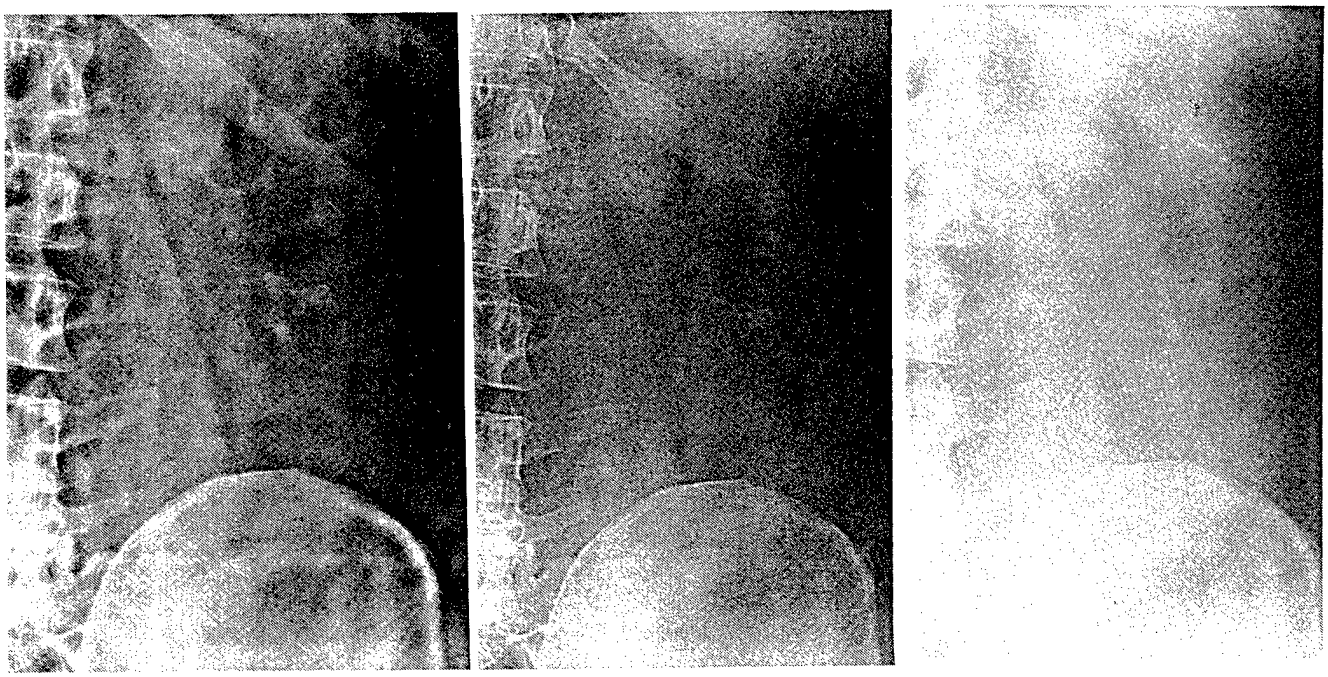

Figure 2: *Portion of abdominal radiograph demonstrating a staghorn type renal calculus. A: RN = 1. The outlines of bowel loops and of the stome are emphasized. B: RN = 5. Bowel markings and margins of calculus are less distinct. Quantum noise is emphasized. C: RN = 9. Fine edge of calculus and edge of psoas muscle are emphasized. Bowel pattern has almost disappeared. Bone structures are shown in best detail. (Fuji algorithm settings: G0.9D1.5+0.22R0T5.0, G0.9D1.5+0.22R4T5.0, G0.9D1.5+0.22R9T5.0)*

RN parameter settings 4 and 5 represent emphasis of medium spatial frequency sine waves thereby providing more enhancement of well defined structures, but still limiting the appearance of noise. Fuji recommends them for lung vessels, bone contours and contrast filled Gastrointestinal organs. (Figure 3)

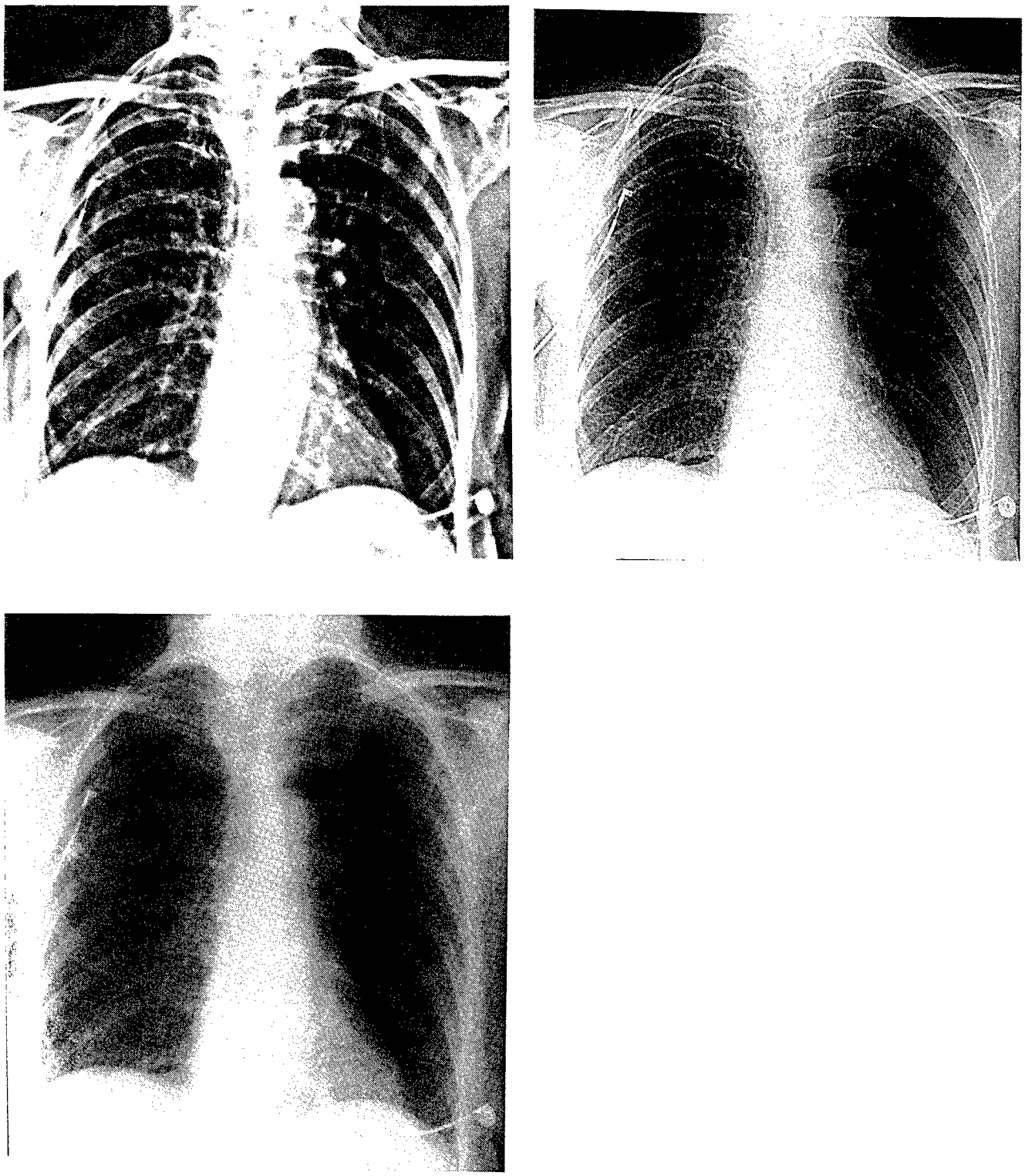

Figure 3. Normal chest radiograph. A. RN = 1. The rib structures and margins of the diaphragm and mediastinum are emphasized. B: RN = 5. Lung markings are emphasized. C: RN = 9. The fine edge of bone and lung markings are emphasized. (Fuji algorithm settings: G0.9D#1.6-0.10ROF5.0, G0.9D#1.6-0.10R5F5.0, G0.9D#1.6-0.10R9F5.0)

RN parameter settings 6-9 emphasize high spatial frequencies, thereby emphasizing sharp edges, but also emphasizing noise. Fuji recommends high spatial frequencies for bone trabeculae and for the gastric mucosa in air-barium double contrast exams. (Figure 4 A, B, C)

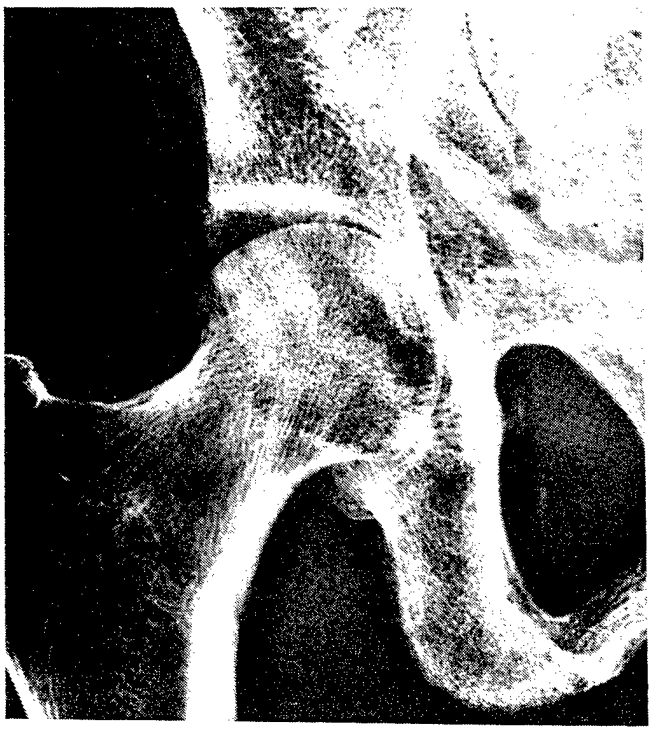

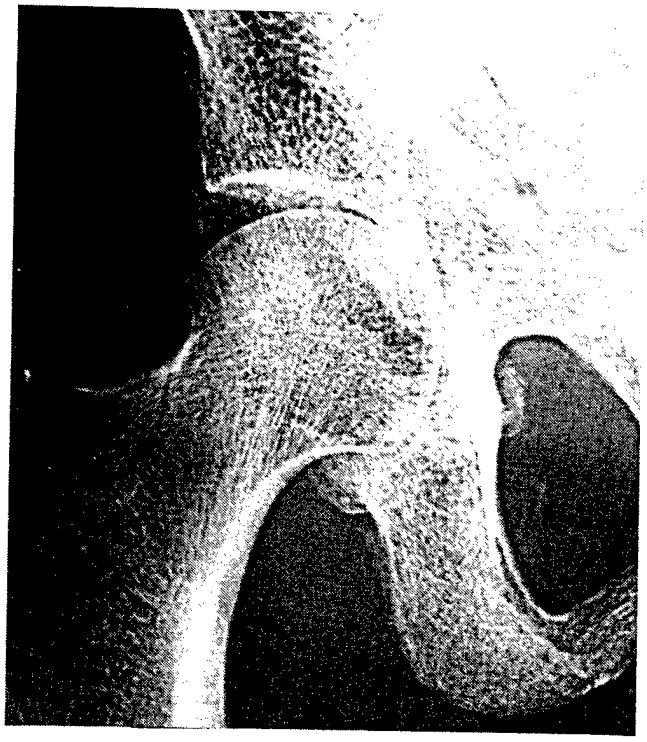

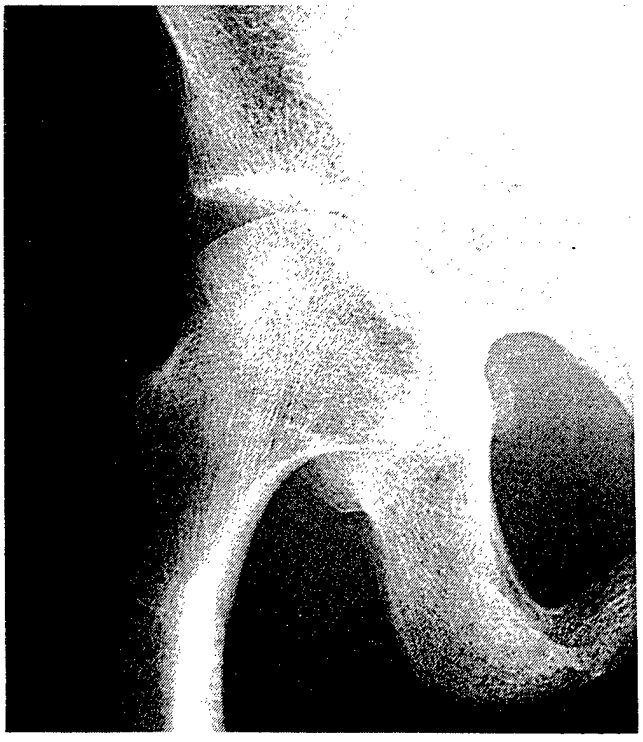

Figure 4. Hip joint in plastic phantom containing real bone. A: RN = 1. Larger structures of bone are emphasized. The lack of trabecular detail might suggest that osteoporosis is present. B: RN = 5. Mid sized trabeculae are emphasized. Osteoporosis could be misdiagnosed. C: RN = 9. Fine trabeculae are emphasized indicating that osteoporosis is not present. (Fuji algorithm settings: G1.1D#1.6+0.40R0R5.0, G1.1D#1.6+0.40R5R5.0, G1.1D#1.6+0.40R9R5.0)

4.4 Parameter Two: RT

RT is a parameter that filters the sine waves in the image in regions of low optical density. Thus it is the parameter that should mainly influence the ability to see structures within the mediastinum, of bone, and of other lightly exposed regions. Figures 5 A and B demonstrate the influence of some of these parameter settings in an underexposed (to make it noisy) image of a step wedge. As one can see in 5A, the low density region shows increasing emphasis of high frequency sine waves (noise), while the darker region of the images is unaffected.

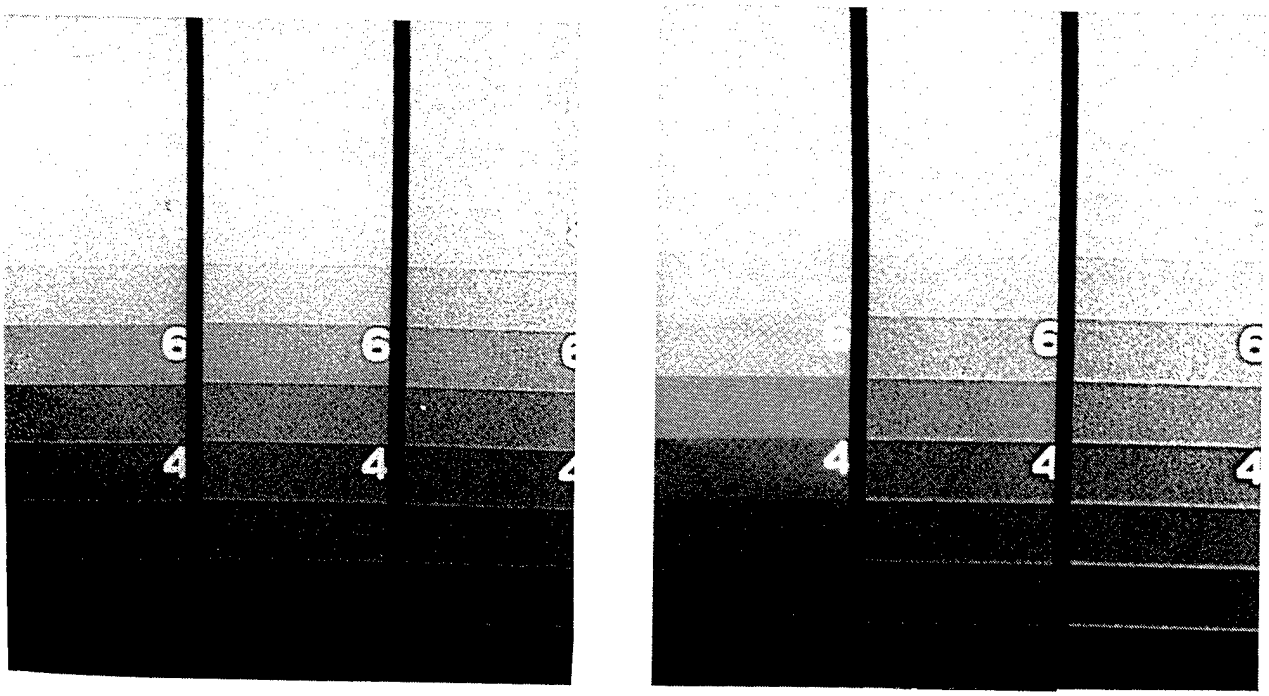

Figure 5: Radiographs of stepwedge. A: RT factors S, T, and F. This demonstrates that the RT factor affects the filtering only in the lower optical density region of the image. (Fuji algorithm settings: G0.8N#0.6+0.0R5S,T AND F5.0°. Compare this to B with RT factors of T and with RE of 0, 5, and 9. This demonstrates that the T settings affects all optical density regions.

Parameter setting U, T, P, and F (the parameter setting U was tested below) emphasize sharp edges. Conversely the parameter setting Q, R and S (Q parameter setting tested below) result in an image with low visible noise in the low density portion of the film. Thus this parameter setting should be adjusted to improve the visualization of catheters, nodules and infiltrates projected through the heart and behind the diaphragm. One would likely choose to test Q, R, and S parameter settings to better view the light areas on a chest image by minimizing the visualization of noise (Figure 6 A and B)

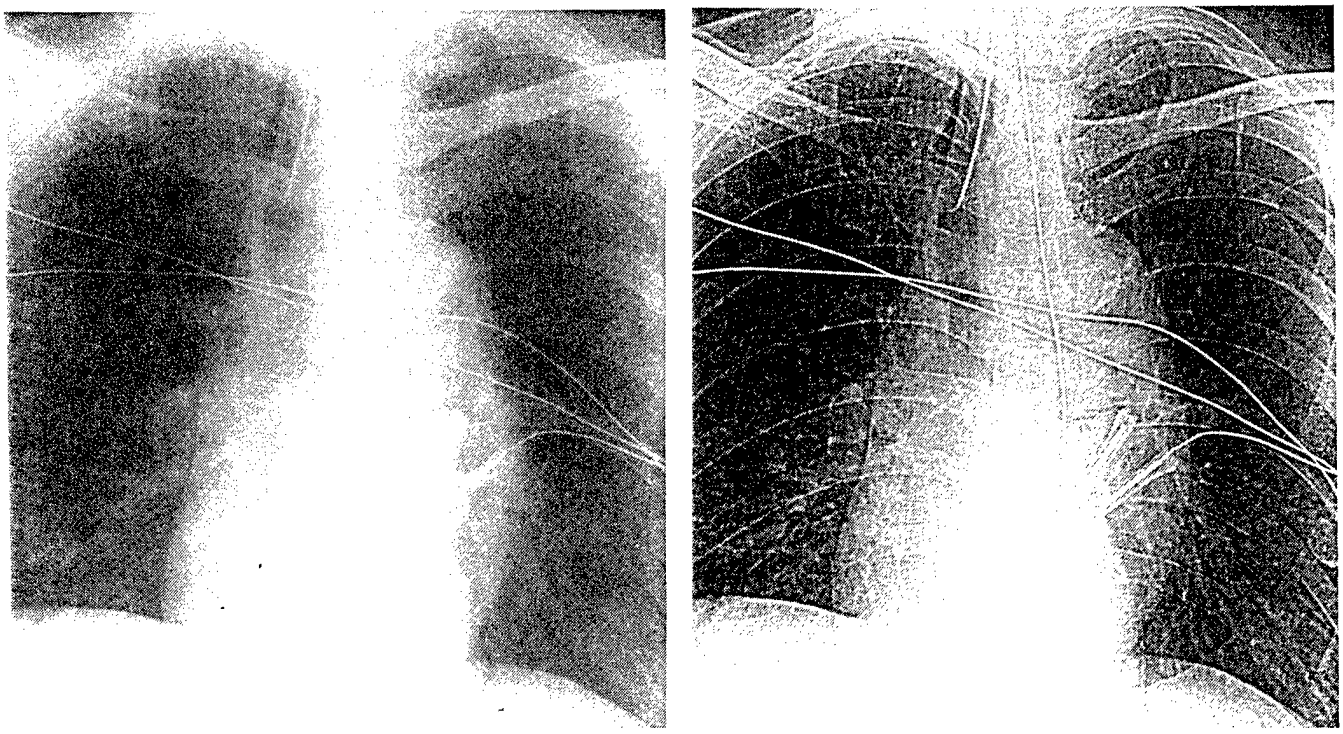

Figure 6: View of central area of portable chest radiograph. A: Processed with limited edge enhancement (Fuji algorithm settings: G0.9D#1.6-0.10R5F0.6). The catheter is lost in the mediastinum. B: With the following factors changed: RN = 5, RE = 10, RT = F. The lung markings are emphasized, but there is increased visible noise in the mediastinum. (Fuji algorithm settings: G0.9D#1.6-0.10R5F10)

4.5 Combining RN and RT

One useful method of combining RN and RT is to select an RN (general frequency filtering) for edge enhancement effect for the lungs. This will increase the visibility of noise in the mediastinum. If one then selects low frequency emphasis from the RT group, such as "S" one can decrease the visibility of noise in the retrocardiac region. (Figure 6 C)

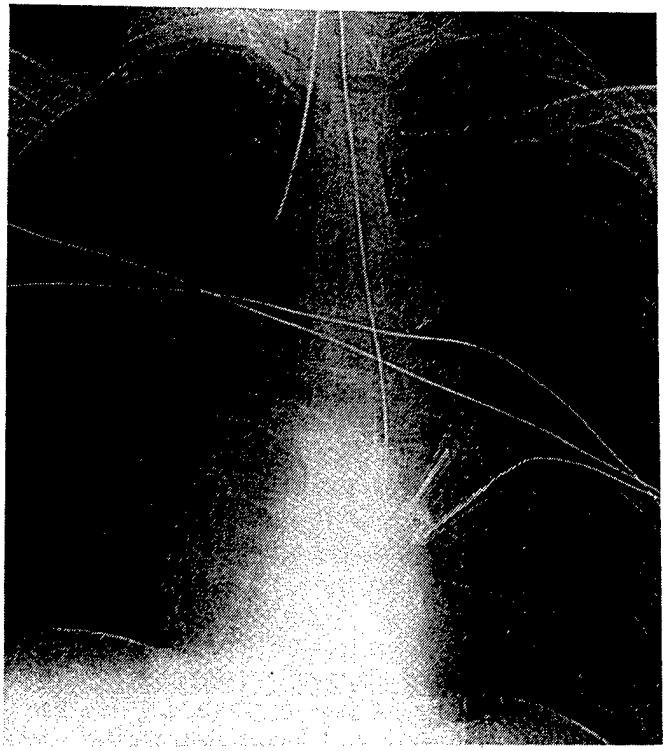

Figure 6: C. With RN = 5, RE = 5, RT = V. The noise in the mediastinum has disappeared, while the lung markings remain the same. (Fuji algorithm settings: G0.9D#1.6-0.10V10)

4.6 Parameter Three: Frequency Enhancement Degree (RE)

This parameter represents the degree of emphasis of the filtered image. It is not completely clear how it works. I believe it represents a percentage of the image that is filtered and then added back to the original image. Thus a setting of 1 may indicate that the original image is displayed at 90% intensity and that 10% of the image is the filtered image is added back to the original image; 2 that 80% is original and 20 % is added back and so on. It is clear that increasing numbers increase the amount of visible enhancement. (Figures 1 A, B and 6 A, B) (figures of image of lungs with low pass filter (RN 1) at RE settings 0 and 5 and with high pass filter(RN 9) at settings of 0 and 5. (RE settings range from 0 to 16)

The RE parameter can enhance (amplify) whichever type of filtering (RN or RT) has been performed.

4.7 The Selection of the Degree and Type of Edge Enhancement

Currently, there is only limited experimental data that filtered images result in more diagnostic accuracy than unfiltered images[4]. The best type of filtering to use is still uncertain, though clearly it shoujld be based on the size and edge characteristics of the object to be visualized[5]. While guidelines on the use of RT and RN can be given based on the size and edge characteristics of the medically important objects in the field, the degree of enhancement (RE) is currently based mainly on user preference.

Should the radiologist wish to use frequency filtering, one should proceed as follows:

R step 1: Set the RE parameter setting to 5 so that the frequency filtering will be visible.

R step 2: Select an SR image of a patient of average size, weight and shape that has been exposed with a typical exposure. Check the "S" number. For setting the amount of frequency filtering, it should be between 100 and 500.

R step 3: Starting from this base image, determine which area of the image one wishes to filter: Is it a lightly exposed or darkly exposed portion of the image or is it both the lightly and darkly exposed portion of the image? If it is desired to filter only the lightly exposed portions of the image, then the RT parameter should be used. If the desired change is to affect the entire image, select an RN value. If it is desired to affect mainly the darker portions of the image, use a combination of the RT and RN factors, by setting the RN factor first, followed by selection of an RT factor.

R Step 4: Determine if the filtering is to be used to enhance the visibility of sharp structure of high contrast and small size or unsharp larger structure of low contrast. Determine how distracting noise might be in regions of low exposure. Use the chest, abdomen and femur images shown in figures 2, 3, and 4 to help you determine the effect of different types of imaging on these different body parts.

R step 5: If the area of interest is of low optical density select from among the RT parameter settings. The parameter settings Q, R, and S are low frequency filters of differing types that should improve the ability to visualize less well defined low contrast objects. The U, T, P, and F parameter settings are high frequency parameter settings of differing types that should improve the visualization of sharply defined objects and high contrast structures.

R step 6: If the area of interest determined from R step 3, is either the entire image or the more darkly exposed portion of the image use the RN parameter settings. Low numbers (0-3) emphasize low contrast, less well defined objects and limit the visualization of image noise. Mid numbers (4-5) balance edge enhancement and noise enhancement. High numbers (6-9) emphasize sharp-edge enhancement and also enhance noise. Once a desired RN value has been selected, the lightly exposed regions of the image should be reevaluated. If the value selected for the RN parameter setting is above 5, there may now be too much noise emphasis in the lightly exposed regions of the image. In that case a combination of an RT parameter with an RN parameter may result in the desired degree of edge enhancement in the darker region of the image and less visible noise in the lightly exposed region.

R step 7: Once you are close to the type of frequency enhancement desired, either from use of the RN or RT parameters, minor adjustments of these parameter settings may be worthwhile. This is an iterative process that may take several steps.

R step 8: Once the initial selection of parameter settings in R step 5 or R step 6 has been made, then the degree of enhancement should be selected by setting the RE parameter. In this schema, we have started with an RE setting of 5. If more emphasis is wanted, use a high number (6 to 10). If less effect of the filtering is wanted, choose a low number (0.5 to 4.5). If no filtering is wanted, choose RE of 0. Once the RE has been set, it may be necessary to reset the RN or RT values to more closely adjust the final image

appearance. This is an iterative process, but this systematic approach should decrease the number of tests made.

5. FACTORS THAT MAY COMPLICATE THE SELECTION OF IMAGE PROCESSING PARAMETER SETTINGS

5.1 The importance of using a matched pair of SF and SR images obtained with the same exposure

If a matched pair of SR and SF images obtained with the same exposure is not used, there is a risk that the exposure settings for the SR image may be set too high or too low. Because noise is an important factor affecting the appearance of an image, the use of improper exposures will affect the amount of noise and therefore may affect the settings selected for filtering. Overexposures of sufficient magnitude also seem to interact with gradient settings in some cases. If there is no comparison image, the "S" number on the SR image should be checked. If it is below 100 or greater than 500, a different image should be used for selecting the parameter values.

5.2 Collimation and its effect on choice of parameter settings

Collimation affects the average exposure of the imaging plate and can under certain circumstances affect the imaging parameter settings. This is too complex to explore in this paper.

5.3 Multiple images on a single imaging plate and their effects on the choice of exposure factors

The system described above works best if the average exposure to the imaging plate is fairly uniform. If several images are placed on the same imaging plate, each image should be made with the same exposure settings.

6. SUMMARY

Each of the parameters used in image enhancement on the Fuji AC-1 has been discussed above. The recommended sequence for selection of an optimal combined setting of the parameters has been presented as well. It is suggested that the desired image optical density and contrast be selected first followed by a selection of the type and amplification of the filtering desired.

Initially, a SR image and a matched SF image should be obtained. The initial density adjustment should be done by changing the GS parameter setting. Next two key areas should be selected. The optical density of the first key area should be measured and used as the GC value. Following this, the optical density of the second key area on the SF and SR images should be measured and used to determine the slope for the GA parameter setting. Minor adjustments of the toe and shoulder of the contrast-density gradient curves should then be done by selection of an appropriate GT.

The selection of R parameter settings is based on the optical density of the region for which filtering is desired. RN parameters filter the frequencies in the entire range of image OD. RT parameters filter predominantly the lower optical density regions of the image. The selection of RN and RT parameter settings should be based on whether high

frequency sharp boundaries or lower frequency unsharp edges are to be emphasized. Starting with an RE parameter value of 5, the RN and RT parameter settings can be selected, based in part on the images included in this article. Once satisfactory RN and RT parameters are set, then the RE parameter should be adjusted to reflect the degree of filtering desired.

7. REFERENCES

1. Busch, HP, Georgi, M, Editors: Digital Radiography Workshop: Quality Assurance and Radiation Protection. Schnetztor-Verlag GmbH, Konstanz, 1992

2. MDIS Users' Meetings, Internal Documents.

3. Fuji Computed Radiography FCR AC-1 Application Manual. Edition of November 30, 1989. Fuji Photo Film Co., LTD. Japan.

4. Schaefer CM, Greene R, Hall DA et al. Mediastinal Abnormalities: Detection with Storage Phosphor Digital Radiography. Radiology 1991; 178:169-173.

5. Prokop M, Schaefer CM, Galanski M, Oestmann JW. Predictability of Effects of Image Processing on Digital Chest Radiographs. Abstract of paper 892, Radiological Society of North America, 78th Scientific Assembly and Annual Meeting. Chicago, 1992.

Reversible compression of medical images with adaptive context selection

Keshi Chen and Tenkasi V. Ramabadran

Department of Electrical Engineering and Computer Engineering
Iowa State University, Ames, Iowa 50011

ABSTRACT

An improved version of an efficient method [4] for the reversible compression of digitized medical images is described. The modifications made in this version are aimed at reducing some of the limitations imposed by the original method. As in the original method, the improved method uses the well-known linear prediction technique to decorrelate a given image. A statistical source model with multiple contexts is employed to model the sequence of decorrelated image pixels. The selection of contexts for the source model is based on the horizontal and vertical components of the gradient in the given image as well as the predicted gray-level value of a pixel. The selection procedure is however entirely adaptive in the improved method, whereas it is only partially adaptive in the original method. The source model statistics are also calculated adaptively. The decorrelated image pixels are encoded using the appropriate contextual statistics with the arithmetic coding technique. Experiments on three groups of medical images show that the compression performance of the improved method is comparable to or slightly better than that of the original method.

1. INTRODUCTION

Image compression is concerned with reducing the storage and/or transmission bandwidth requirements of digital images through efficient data representations. The techniques for such purpose are usually classified into two categories: *reversible* and *irreversible*. In reversible compression, the original images can be exactly reconstructed from the compressed data; whereas in irreversible compression the reconstructed images are distorted versions of the originals. The choice as to which class of techniques to use in a particular situation depends on the application. In general, irreversible compression methods can provide better and predictable compression, and therefore are more suitable to applications where some loss in image fidelity can be tolerated in order to more efficiently utilize a storage or transmission medium. On the other hand, reversible methods are preferred in situations where even a little amount of distortion cannot be tolerated and/or post-processing of images is involved. Recently, there has been a growing interest in reversible compression of medical images [2,8], motivated by the huge amount of image data involved coupled with the fact that no loss of fidelity can be tolerated in most medical applications. In this paper, we will be mainly concerned with reversible compression of medical images.

Motivated by and analogous to some well-known irreversible methods, conventional reversible image compression methods [8] are usually carried out in two consecutive steps, *viz.*, *decorrelation* and *coding*, although different methods combine these two steps in different ways. In the decorrelation step, the redundancy in the original image representation due to the correlation among image data is reduced or removed. The techniques available for this purpose consist of *predictive*, *transform*, and *multiresolution* decorrelation. In the coding step, the redundancy due to the nonuniform gray-level distribution of the decorrelated image pixels is further reduced. As a result, the gray-levels are transformed into another data sequence which is to be retained for transmission or storage. Typical coding techniques are, for example, *Huffman* coding and *arithmetic* coding.

An implicit assumption made in most conventional reversible compression methods is that the decorrelated pixels are independent and identically distributed or, in other words, they are emitted from a *memoryless* information source. By employing advanced statistical source modeling techniques [5,7,11] for the decorrelated pixels, *e.g.*, one with multiple *contexts* or *conditioning events*, and the powerful *arithmetic* coding technique [1,6,12], it is possible to achieve a better compression performance. Based on this idea, several improved methods have been proposed recently [3,4,5,10]. Out of these methods, the one proposed by the authors using predictive decorrelation and selecting contexts based on gradient estimates of image pixels [4] has succeeded in substantially improving the compression performance. In this paper, we present an improved version of the method, aimed at reducing some of the limitations imposed by

0-8194-1129-9/93/$6.00

the original version. A detailed description of the source model used in the original method as well as its revision used in the improved version is given in Section 2. The decorrelation and coding techniques used in both the original and the improved versions are also described briefly in the same section. Section 3 presents the experimental results comparing the compression performances of different methods on three groups of medical images. In Section 4, we summarize our conclusions.

2. SOURCE MODELING AND CODING

Most image compression algorithms rely on the basic statistical property of digital images that there is a high degree of interpixel dependency, especially interpixel correlation, among image data. In other words, most of the raw image data are redundant, and this redundancy makes compression possible. Therefore, the degree to which a given image may be compressed while preserving high reconstruction fidelity relies upon the dependency characteristics of the pixels in the image; and the performance of a specific compression algorithm for the given image relies upon how much the algorithm can capture and exploit these dependency characteristics.

The reversible compression of a data sequence such as the sequence of pixels of an image can be regarded as consisting of two distinct parts: *source modeling* and *coding*. Source modeling deals with how to view the data sequence based on some *a priori* knowledge and subsequently how to capture the intersymbol dependencies inherent in the data; whereas coding transforms the original sequence into another sequence called the *code sequence*. As a result, the *compressed sequence* is composed of two parts: 1) a set of *model parameters* that identifies the source model associated with the original sequence, and 2) the code sequence that identifies the original sequence among all the data sequences having the same source model. The objective of compression is then to minimize the length of this compressed sequence.

In general, a source model for a data sequence determines how a specific coding technique is to be applied to the sequence, and supplies parameters to the coding process as well. Therefore, source modeling has played a central role in the modern data compression paradigm and has attracted increasing research efforts. The fundamentals of statistical source modeling for data compression applications were put together by Rissanen and Langdon in their landmark paper [7]. Based on their theory, advances [5,11] have been made in building sophisticated source models that can describe a data sequence more accurately, *i.e.*, predict the sequence with higher probability, than trivial models and thereby lead to shorter code sequences. Typically, such sophisticated models employ a number of *contexts* or *conditioning events* to exploit the dependencies between symbols at different positions within a data sequence. Meanwhile, for image data sequences where most intersymbol dependencies appear in the form of interpixel correlation, *decorrelation* has proved to be a very powerful modeling method to achieve efficient compression performance.

2.1. Linear predictive decorrelation

As mentioned above, the length of code sequences can be reduced by employing multiple contexts in the source models for data sequences to be compressed. In building such a source model for a data sequence, one of the most straightforward approaches is to simply use the immediately preceding symbols of any given symbol within the sequence to form the contexts. However, even for a modest number of the preceding symbols and a symbol alphabet of modest size, the complexity of such a model is staggering. For example, suppose that we use the west, the northwest, and the north neighbors of any given pixel in an image to define contexts and that the gray-levels of the pixels range from 0 to 255, corresponding to 8-bit quantization. Then, the model will have a total number of $256^3 \approx 17 \times 10^6$ contexts. Clearly, this large number of contexts will result in a large model description part of the compressed sequence, which in turn substantially degrades the overall compression performance and makes the modeling algorithm unadvantageous.

In the case of image compression, by taking into account the fact that image data are highly correlated, the general strategy to alleviate the above problem is to apply some linear or nonlinear invertible transform operation to the original images such that the transformed values are less correlated or even uncorrelated and consequently can be modeled as outcomes of an information source with a smaller number of contexts. The invertible transformation is referred to as *decorrelation*. It can be accomplished in either the spatial or the frequency domain [8,9].

A well-known and important technique for spatial domain decorrelation is *linear prediction.* Suppose a digitized image is represented mathematically as an $M \times N$ matrix $[f(m,n)]$ where M and N denote the numbers of rows and columns, respectively, and $f(m,n)$ denotes the gray-level of the pixel at the m-th row and n-th column. In linear predictive decorrelation, the gray-level value of a pixel $f(m,n)$ is predicted as a linear combination of the values of the pixels in a suitable neighborhood Ω, *i.e.*, the predicted value is expressed as

$$\hat{f}(m,n) = \sum_{(k,l)\in\Omega} \alpha(k,l) f(m-k, n-l), \tag{1}$$

where $\alpha(k,l)$ are called the prediction coefficients. The prediction error is given by

$$e(m,n) = f(m,n) - \hat{f}(m,n). \tag{2}$$

In compression methods using linear predictive decorrelation, the prediction errors are encoded and then stored or transmitted. Usually, it is assumed that the image data are available as a sequence of pixels obtained by scanning the image from left to right and from top to bottom. Therefore, if the neighborhood Ω is chosen to be causal and appropriate boundary values are assumed, then the original image can be reconstructed from the prediction errors by means of the relationship

$$f(m,n) = \hat{f}(m,n) + e(m,n) \tag{3}$$

where the predicted value $\hat{f}(m,n)$ is calculated from that part of the image already reconstructed. In the original compression method [4] proposed by the authors as well as the improved version presented in this paper, the causal neighborhood Ω of a pixel $f(m,n)$ consisting of the west $(f(m,n-1))$, the northwest $(f(m-1,n-1))$, and the north $(f(m-1,n))$ neighbors is used. For this choice of Ω, the prediction equation (1) can be simplified as

$$\hat{f}(m,n) = \alpha_1 f(m,n-1) + \alpha_2 f(m-1,n-1) + \alpha_3 f(m-1,n). \tag{4}$$

Ideally, the prediction coefficients in (1) and (4) are chosen to minimize the mean squared value of the prediction errors, *i.e.*, $E[e^2(m,n)]$ where $E[\cdot]$ denotes the expectation operator. In such a case, the prediction coefficients are the solutions of a set of special linear equations referred to as the *Yule-Walker* equations [9] and can be shown to be functions of the autocorrelation values $R_{ff}(k,l) = E[f(m,n)f(m-k,n-l)]$ between the pixel $f(m,n)$ and its neighbors in Ω. Since the adjacent pixels of a typical image are in general highly correlated and the predicted value of a pixel is a linear combination of the neighboring pixel values based on the correlations between the pixel and the neighbors, it can be expected that the prediction errors will be small and less correlated than the original image pixels.

The prediction coefficients are in general real (noninteger) valued and consequently the predicted pixel values $\hat{f}(m,n)$ and the errors $e(m,n)$ are also real valued. In order to achieve reversible compression, the predicted values $\hat{f}(m,n)$ are usually rounded and limited so as to assume integer values in the same range as that of the original pixel values $f(m,n)$. As a result, the prediction errors $e(m,n)$ are also integer valued and can be coded by using a suitable coding technique, such as arithmetic coding, thereby preventing introduction of distortion in the decoding process.

2.2. Source modeling

Substantial amount of intersymbol dependencies may still remain in the sequences of decorrelated image pixels. It is therefore expected that the compression performance can be enhanced by using source models with multiple contexts for such data sequences. Notice that the decorrelation discussed earlier has made it possible to model the sequences using a relatively small number of contexts, instead of a large number.

2.2.1. Context selection

As far as the selection of contexts is concerned, it can be made in several ways [3,4,5,10,11]. In the original compression method proposed by the authors [4], the selection of contexts of the source model for a sequence of decorrelated image pixels $e(m,n)$ is based respectively on the horizontal and vertical *gradient* components, $d^h(m,n)$ and $d^v(m,n)$, of

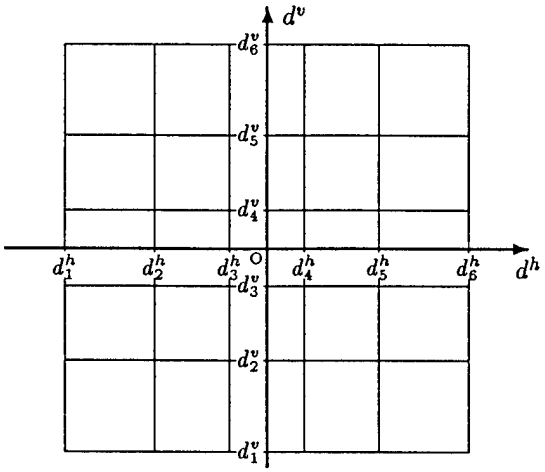

Figure 1: Partitioning the $d^h - d^v$ plane with each region defining an initial context.

the original image pixels $f(m,n)$ as well as the *predicted values* $\hat{f}(m,n)$. The gradient components of a pixel $f(m,n)$ are estimated respectively as

$$d^h(m,n) = f(m-1,n) - f(m-1,n-1) \qquad \text{and} \qquad d^v(m,n) = f(m,n-1) - f(m-1,n-1). \tag{5}$$

From these formulae, it is clear that range of values of $d^h(m,n)$ and $d^v(m,n)$ is nearly twice that of the original image pixels, *e.g.*, -255 to 255 for 8-bit quantization. With reference to the $d^h - d^v$ plane, the contexts of the source model are selected initially by partitioning the plane into several (K_i) regions, as shown in Figure 1, and treating each of the K_i regions as a context. The motivation for this approach of selecting contexts is that the different gradient regions correspond to different types of details presented in the original image, and therefore would provide some amount of mutual information about the distribution of the decorrelated image pixel values. For example, a region with large $|d^h|$ and small $|d^v|$ values can be identified with vertical lines in the original image. Similarly, regions corresponding to horizontal lines (small $|d^h|$ and large $|d^v|$), diagonal lines (large $|d^h|$ and large $|d^v|$), uniform sections (small $|d^h|$ and small $|d^v|$), and others in the original image can also be identified. It is reasonable to expect that the distributions of decorrelated pixel values corresponding to these different regions will be different. The exact partitioning of the $d^h - d^v$ plane, *i.e.*, the determination of d_i^h and d_j^v, is based a trial and error procedure. As a guideline to the determination of the partitioning, the resulting regions should have as fair numbers of gradients as possible. In other words, the partitioning of the gradient plane should ensure that each of the contexts so defined will occur a significant number of times.

Starting from the initial contexts selected as described above, additional contexts are created through a series of context splitting operations on the existing contexts. The selection of these additional contexts is based on the predicted values $\hat{f}(m,n)$ which have a range equal to that of $f(m,n)$ and is adaptive. The selection procedure continues until the total number of contexts of the source model reaches a predetermined value K_t. The criterion for a context γ to be split is that the number of times it has occurred exceeds a predetermined value F_a while the probability of occurrence of the most probable (decorrelated) pixel value under γ be lower than another predetermined value P_a. When this criterion is met, γ will be split into two new contexts γ_1 and γ_2 by dividing the value range of $\hat{f}(m,n)$ under γ into two halves, with one half corresponding to γ_1 and another to γ_2. Notice that the contexts so defined can be easily identified from a few most significant bits in the binary representation of the predicted value $\hat{f}(m,n)$. Besides ease of implementation, the rationale behind selecting the contexts in this manner once again is that they would provide some mutual information about the distribution of the decorrelated image pixel values. Also notice that the context at any position (m,n) in the image can be determined with only the knowledge of $f(m,n-1)$, $f(m-1,n-1)$, and $f(m-1,n)$.

From the above description, it can be seen that in the original compression method the initial contexts are selected non-adaptively based on the partitioning of the gradient plane. This partitioning requires *a priori* knowledge about

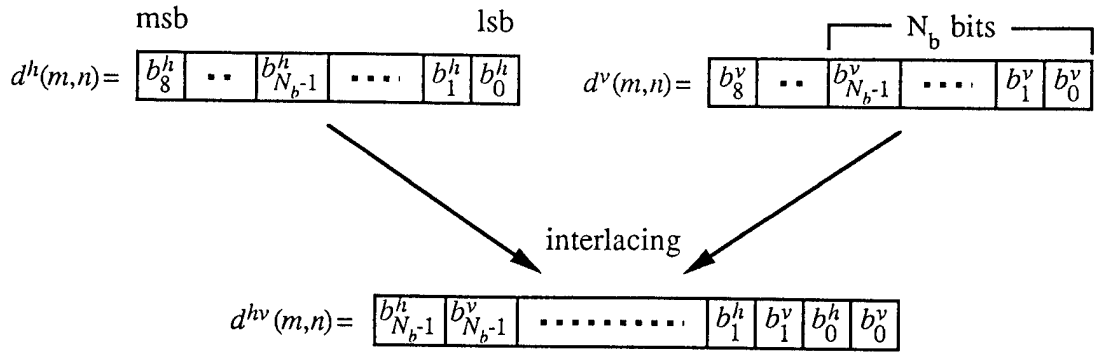

Figure 2: Interlacing the bit fields of $d^h(m,n)$ and $d^v(m,n)$ to form a new number $d^{hv}(m,n)$

the image to be compressed and is obtained through a trial and error procedure. In practice, it is impossible to go through this trial and error procedure for every image to be compressed. Instead, a typical partitioning configuration is used for a group of images of similar characteristics, and this partitioning may not define the best possible contexts for each individual image in the group. Also, since the partitioning of the $d^h - d^v$ plane is not closely under the guideline of capturing mutual information, the contexts defined by the partitioned regions do not necessarily provide significant amount of mutual information about the value distribution of the decorrelated pixels. In the following, a modified scheme for selecting the initial contexts that is used in the improved compression method is presented.

In the improved compression method, the estimated horizontal and vertical gradient values $d^h(m,n)$ and $d^v(m,n)$ are once again used to define initial contexts. Consider again the $d^h - d^v$ plane shown in Figure 1. Since $d^h(m,n)$ and $d^v(m,n)$ assume integer values from -255 to 255 and stored in most of today's computers in two's complement representation, they are represented by the 9 least significant bits in a word. Therefore, a gradient pair $(d^h(m,n), d^v(m,n))$ falling in the top-left quarter of the gradient plane must have the most significant bit of the 9-bit representations of $d^h(m,n)$ and $d^v(m,n)$ equal to 1 and 0, respectively. Similarly, if the two most significant bits of $d^h(m,n)$ and $d^v(m,n)$ are 10 and 00, respectively, then the pair $(d^h(m,n), d^v(m,n))$ must be located in the region of the $d^h - d^v$ plane specified by $-255 \leq d^h < -128$ and $0 \leq d^v < 128$. Clearly, we can use the bit fields in the two's complement representations of $d^h(m,n)$ and $d^v(m,n)$ to partition the gradient plane and correspondingly define contexts through an adaptive context splitting procedure similar to that used in the original compression method for selecting additional contexts. Starting from the most significant bit and in the order of decreasing significance, the more bits of $d^h(m,n)$ and $d^v(m,n)$ are used, the finer the partition will be and the more contexts will be created. For example, suppose we start from the entire gradient plane which corresponds to the single null context λ. When the criterion for splitting is satisfied, *i.e.*, λ has occurred more than F_i times and the probability of occurrence of the most probable decorrelated pixel value is lower than P_i, the null context λ will be split into two new contexts γ_1 and γ_2. In such case, the entire gradient plane will be divided into two halves, *e.g.*, along the d^v axis, with the right half corresponding to the new context γ_1 and the left half to γ_2. From this point on, whenever the most significant bit of a $d^h(m,n)$ is 0, the context γ_1 is considered to have occurred; otherwise, γ_2 is considered to have occurred. Next, supposing γ_2 meets the conditions for splitting, then it will be split into another two contexts γ_{21} and γ_{22}. In correspondence, the left half of the $d^h - d^v$ plane under γ_2 is partitioned into the top-left quarter and the bottom-left quarter under γ_{21} and γ_{22}, respectively. Clearly, the new context γ_{21} corresponds to the most significant bits of $d^h(m,n)$ and $d^v(m,n)$ being equal to 1 and 0, respectively; and γ_{22} corresponds to both the bits being equal to 1. Notice that since in general $d^h(m,n)$ and $d^v(m,n)$ are equally important in determining contexts, the successive partitioning of the $d^h - d^v$ plane should be made such that the bit fields of $d^h(m,n)$ and $d^v(m,n)$ are alternately used to identify contexts.

It can be seen that with the splitting procedure described above, the selection of contexts based on the gradient components $d^h(m,n)$ and $d^v(m,n)$ is entirely under the guidance that the new contexts selected from a splitting operation should provide additional information about the decorrelated pixel values. To implement this context selection algorithm and make the entire compression process systematic, in the improved method, the bit fields of the two gradient estimates $d^h(m,n)$ and $d^v(m,n)$ for each image pixel $f(m,n)$ are interlaced to form a new number

$d^{hv}(m,n)$ as shown in Figure 2. Then, this new number is used in the context selection procedure exactly in the same way that $\hat{f}(m,n)$ is used in the additional context selection procedure of the original method. Notice that since the adjacent pixels in an image are highly correlated, majority of the gradient estimates $d^h(m,n)$ and $d^v(m,n)$ assume small integer values. Therefore, most of these estimate values (including their polarity sign) are effectively represented by a few least significant bits in their two's complement representations. So, only the N_b least significant bits of $d^h(m,n)$ and $d^v(m,n)$ are used in the interlaced representation of $d^{hv}(m,n)$ (see Figure 2) in order to generate the best possible contexts. The adaptive context splitting (selection) procedure in the improved compression method based on the values $d^{hv}(m,n)$ proceeds until the total number of selected contexts for the source model of the decorrelated pixel sequence reaches a predetermined value K_i after which the splitting stops. Then, another adaptive splitting procedure for additional contexts based on the predicted values $\hat{f}(m,n)$ starts and continues until the total number of contexts (based on both $d^{hv}(m,n)$ and $\hat{f}(m,n)$) reaches the predetermined value K_t. As a summary, we can view the structure of the whole set of contexts as a variable-depth binary tree. This tree is constructed adaptively based on the bit strings $d^{hv}(m,n)$ and $\hat{f}(m,n)$, with the part of the tree close to the root corresponding to $d^{hv}(m,n)$ and others to $\hat{f}(m,n)$. Each terminal node of the tree, or more accurately, the bit string representing the path from the root node to the terminal node defines a context. The context splitting procedure begins with a null context represented by the root node. Existing contexts are split to form new contexts (thereby growing the tree) based on rules designed to maximize the mutual information that the new contexts provide about the decorrelated pixel values.

2.2.3. Model parameter estimation

After selection of contexts of the source model for a sequence of decorrelated image pixels, the statistical parameters of the model (*i.e.*, the conditional probability distribution of the decorrelated pixel values under each context) can be calculated either adaptively or nonadaptively. In the compression method reported in this paper, the adaptive approach is adopted in accordance with the adaptive context selection procedure. Specifically, the parameters are obtained using the *cumulative adaptive* technique [4,7]. That is, the model parameters are initially set to some values depending on our *a priori* knowledge about the pixel values, and then updated as the encoding proceeds. Every time a pixel is encoded, the model parameters are updated accordingly. The updated statistics are then used in the encoding of the next pixel as well as the context selection procedure, and so on. In this manner, both source modeling and encoding can be accomplished simultaneously such that a single scan of the decorrelated image is sufficient. Note that since the statistics used to encode each decorrelated pixel are determined before actually encoding the pixel, they can also be identically retrieved in the decoding process and, therefore, the pixel can be decoded accurately.

2.3. Coding

Given the probability distribution of the decorrelated pixel values, the pixels can be encoded by means of an *arithmetic* code [1,6,12]. Arithmetic coding has several advantages [12] over the traditional block coding techniques, *e.g.*, *Huffman* coding. Its efficiency is higher even when the entropy of the source model is low. It is computationally efficient in most cases and can easily accommodate source models with multiple contexts and adaptive statistics. These, in turn, encourage us to employ more sophisticated and accurate source models for data sequences to be encoded, such as decorrelated images. Therefore, arithmetic coding has been employed in our compression methods.

3. EXPERIMENTAL RESULTS

The compression performance of the improved compression method has been evaluated using three groups of digitized medical images and compared against that of the original method. The first group consists of 15 magnetic resonance (MR) images of sizes 512×696 and 480×648; the second consists of 5 ultrasound (UT) images of size 512; and the last consists of 4 X-ray images of size 4096×4096. All of the images are with the gray-level values ranging from 0 to 255 corresponding to 8-bit quantization.

In the experiments, the linear prediction equation

$$\hat{f}(m,n) = f(m,n-1) + f(m-1,n) - f(m-1,n-1)$$

Table 1: Parameters Used in the Original and the Improved Methods for the Three Groups of Images

Image	*Original Method*				*Improved Method*						
Group	K_i	K_t	F_a	P_a	K_i	K_t	N_b	F_i	P_i	F_a	P_a
MR	$7 \times 7 = 49$	350	30	0.8	150	250	6	50	0.8	100	0.9
UT	$7 \times 7 = 49$	150	30	0.8	70	100	6	5	1.0	5	1.0
X-ray	$7 \times 7 = 49$	200	50	0.7	100	200	7	20	0.9	50	0.7

Table 2: Compression Results in bits/pixel for MR Images

Image	*Conventional DPCM*	*Original Method*	*Improved Method*
MR01	1.75	1.34	1.32
MR02	2.24	1.83	1.83
MR03	2.21	1.81	1.81
MR04	1.93	1.48	1.47
MR05	1.96	1.51	1.50
MR06	2.04	1.61	1.61
MR07	2.53	2.04	2.03
MR08	2.52	2.04	2.02
MR09	2.51	2.03	2.03
MR10	3.54	2.43	2.44
MR11	3.45	2.37	2.38
MR12	3.44	2.36	2.38
MR13	2.61	2.09	2.08
MR14	4.39	3.21	3.18
MR15	2.55	2.05	2.04

Table 3: Compression Results in bits/pixel for UT Images

Image	*Conventional DPCM*	*Original Method*	*Improved Method*
UT01	2.55	1.42	1.40
UT02	2.33	1.29	1.27
UT03	1.37	0.81	0.82
UT04	3.21	1.83	1.80
UT05	3.20	1.81	1.77

Table 4: Compression Results in bits/pixel for X-ray Images

Image	*Conventional DPCM*	*Original Method*	*Improved Method*
XR01	3.84	3.09	3.00
XR02	3.30	2.57	2.50
XR03	3.60	2.80	2.72
XR04	3.34	2.57	2.51

is used for decorrelating the MR and UT images and

$$\hat{f}(m,n) = \frac{1}{3}f(m,n-1) + \frac{1}{3}f(m-1,n) + \frac{1}{3}f(m-1,n-1)$$

is used for the X-ray images, for both the original and the improved methods. All other parameters used in the two methods are listed in Table 1. The compression performances of the two methods as well as the traditional DPCM compression method, wherein only one context (the null context λ) is used in the source model of the decorrelated pixel sequences, for the three groups of images are given in Table 2, 3 and 4, respectively.

4. DISCUSSION AND CONCLUSION

From Tables 2 through 4 given in the last section, it can been seen that the improved compression method performs equally well or slightly better than the original method. In addition, the improved method offers the following advantages over the original method: 1) the contexts selected are image specific by taking into account the statistics of the image being compressed, 2) it requires less prior knowledge about the images to be compressed since the selection of the initial contexts is made adaptively instead of through a prephase trial and error procedure, 3) the same algorithm can be applied to different classes of images, and 4) it offers much more flexibility for further development.

It should be mentioned that during the course of this study, we have tried to use some other sets of quantities, *e.g.*, the pair $(e(m,n-1),\ e(m-1,n))$ and the triple $(e(m,n-1),\ e(m-1,n-1),\ e(m-1,n))$, in the selection of initial contexts, prompted by the fact that in several recently proposed reversible compression methods, one type or another of *differential* quantities have been used to define contexts. However, it was found from our experiments that the use of the gradient pair $(d^h(m,n),\ d^v(m,n))$ yields the best compression performance.

5. ACKNOWLEDGEMENTS

This research was supported in part by the National Science Foundation under Grant No. MIP-9010361. We would like to thank Dr. C. B. Chittineni, Imaging Systems Department, DuPont Company, and Dr. G. Seeley, Professor of Radiology, Arizona State University for providing us with digitized medical images used in the experiments.

6. REFERENCES

1. C. B. Jones, "An efficient coding system for long source sequences," *IEEE Trans. Inform. Theory*, Vol. IT-27, No. 3, pp. 280-291, May 1981.

2. G. R. Kuduvalli and R. M. Rangaraj, "Performance analysis of reversible image compression techniques for high-resolution digital teleradiology," *IEEE Trans. Med. Imaging*, Vol. MI-11, No. 3, pp. 430-445, September 1992.

3. G. G. Langdon, Jr. and J. Rissanen, "Compression of black-white images with arithmetic coding," *IEEE Trans. Commun.*, Vol. COM-29, No. 6, pp. 858-867, June 1981.

4. T. V. Ramabadran and K. Chen, "The use of contextual information in the reversible compression of medical images," *IEEE Trans. Med. Imaging*, Vol. MI-11, No. 2, pp. 185-195, June 1992.

5. T. V. Ramabadran and D. L. Cohn, "An adaptive algorithm for the compression of computer data," *IEEE Trans. Commun.*, Vol. COM-37, No. 4, pp. 317-324, April 1989.

6. J. J. Rissanen, "Arithmetic codings as number representations," *Acta Polytech. Scandinavica Math.*, Vol. 31, No. 6, pp. 45-51, December 1979.

7. J. J. Rissanen and G. G. Langdon, Jr., "Universal modeling and coding," *IEEE Trans. Inform. Theory*, Vol. IT-27, No. 1, pp. 12-23, January 1981.

8. P. Roos, M. A. Viergever, M. C. A. Van Duke, and J. H. Peters, "Reversible intraframe compression of medical images," *IEEE Trans. Med. Imaging*, Vol. 7, No. 4, pp. 328-336, December 1988.

9. A. Rosenfeld and A. C. Kak, *Digital Picture Processing*, Academic Press, New York, 1982.

10. S. Todd, G. G. Langdon, Jr., and J. Rissanen, "Parameter reduction and context selection for compression of gray-scale images," *IBM J. Res. Develop.*, Vol. 29, No. 2, pp. 189-193, March 1985.

11. R. N. Williams, *Adaptive Data Compression*, Kluwer Academic Publishers, Boston, 1991.

12. I. H. Witten, R. M. Neal, and J. G. Cleary, "Arithmetic coding for data compression," *Commun. ACM*, Vol. 30, No. 6, pp. 520-540, June 1987.

IMAGE PROCESSING IN DIGITAL MAMMOGRAPHY

M. Freedman, E. Pe, R. Zuurbier, R. Katial, H. Jafroudi, M. Nelson, S.-C. B. Lo, S. K. Mun

Georgetown University Medical Center
Washington, D.C., U.S.A.

OVERVIEW

INTRODUCTION

Digital mammography is likely to replace conventional mammography within a few years. In anticipation of this, our group has been exploring the implications of image processing in digital mammography. Some of our findings are reported here.

INITIAL STATUS

Initial investigations of a commercially available full breast digital mammography system demonstrated that, when evaluated on phantoms, the detection of small faint objects was less than with conventional screen film mammography (Chart 1).

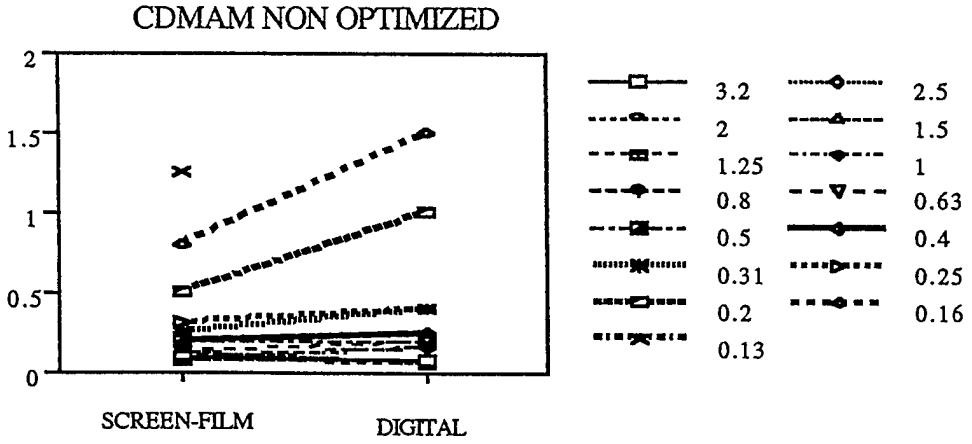

Chart 1: This chart reports a comparison between screen film (SF) mammography and storage phosphor (SR) digital mammography using the image processing settings provided by the manufacturer. For all smaller objects, the screen film system performed better. (The Y axis represents the minimal thickness at which an object could be identified, each line represents a small gold disk of decreasing diameter. A lower position on the chart indicates better performance.) (CDMAM Phantom, Nuclear Associates). Tests of the RMI #156 and CIRS phantom confirmed the initial inferior performance of the digital system.

0-8194-1459-X/94/$6.00

Figure 1: an image of the CDMAM Phantom.

Conversely, using experimental techniques, it is possible to demonstrate all objects of the phantom used for ACR accreditation. This experimental system can only image part of the breast and produces an image with obvious artifacts. (Figure 2)

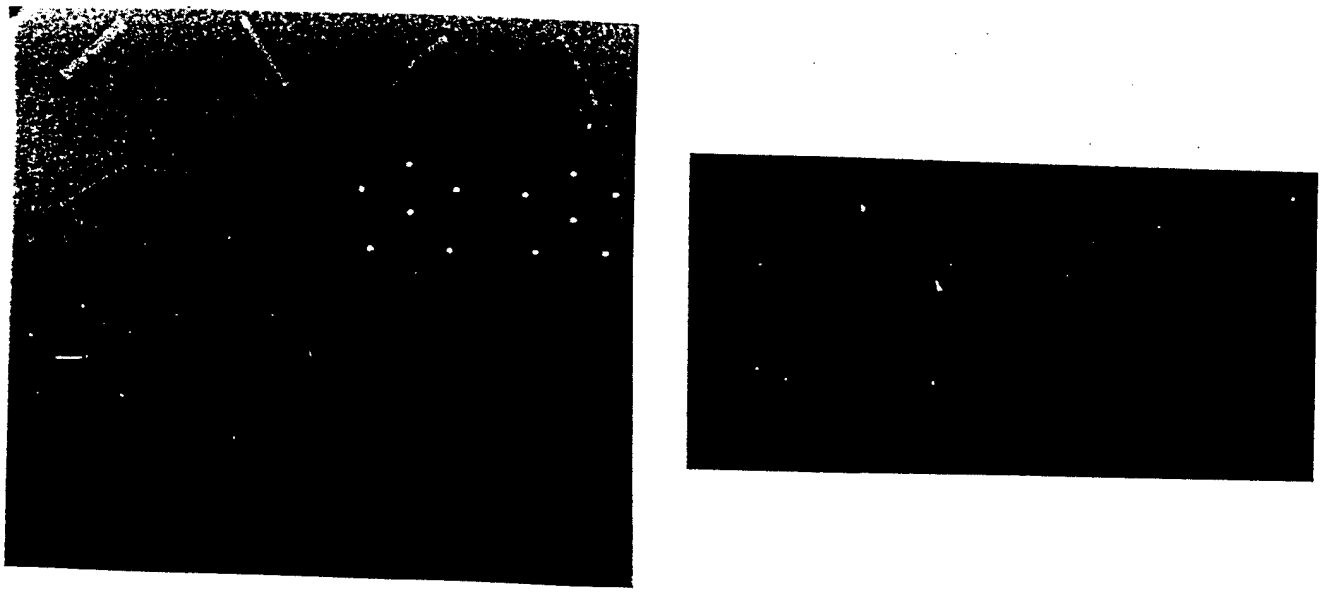

Figure 2: Digital radiograph of complete phantom (wax insert and plastic case) used for ACR accreditation (RMI #156). All objects on the phantom are visible. A magnified view of the same image shows the smallest two groups of "calcifications. This system can only image part of the breast.

IMAGE PROCESSING OPTIMIZATION PROCEDURE

A series of 3 dimensional response surfaces were obtained by processing images of the RMI, CDMAM, and CIRS phantoms. The following factors were considered: optical density, contrast, rotation center for contrast adjustment, spatial frequency filtering with different kernel sizes, spatial frequency emphasis, mAs, KVP, magnification, 2 types of phosphor plates, and focal spot size. These 10 different factors interact to varying degrees. Only selected pairs have been evaluated. In addition, the effects of 4 different effective pixel sizes were evaluated. Once improved images were found using these phantoms, the same settings were tested on several digitally acquired and electronically stored mammograms. Those image processing combined settings that resulted in unacceptably distorted images of the breast were rejected.

Optimization of a single factor was not sufficient to result in full potential information. Multiparameter, non-linear optimization was necessary and was roughly approximated by varying factors in pairs and substituting best settings of these factors in the optimization procedure of the other factors.

CURRENT STATUS

Based on the optimization procedure, a graph using the CDMAM phantom now demonstrates that using the commercially available full breast phosphor plate system, that for each object size, both systems detected or failed to detect objects of the same diameter and same minimal thickness. (Chart 2)

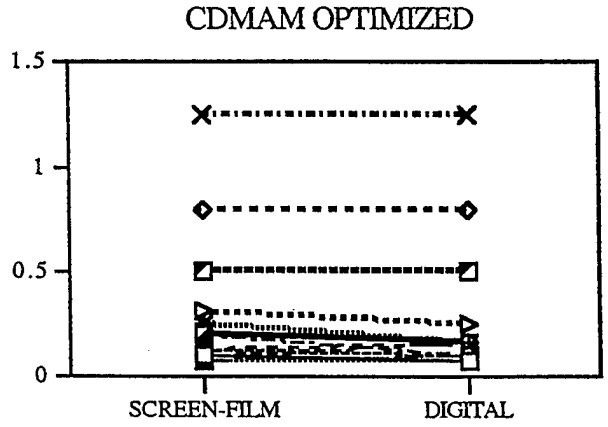

Chart 2: This chart demonstrates that for each diameter object, that the screen film and storage phosphor systems perform essentially the same as demonstrated by the lines being horizontal.

This can be achieved with a mammographic image that is different than conventional mammography, but is considered acceptable in appearance. (Figure 3)

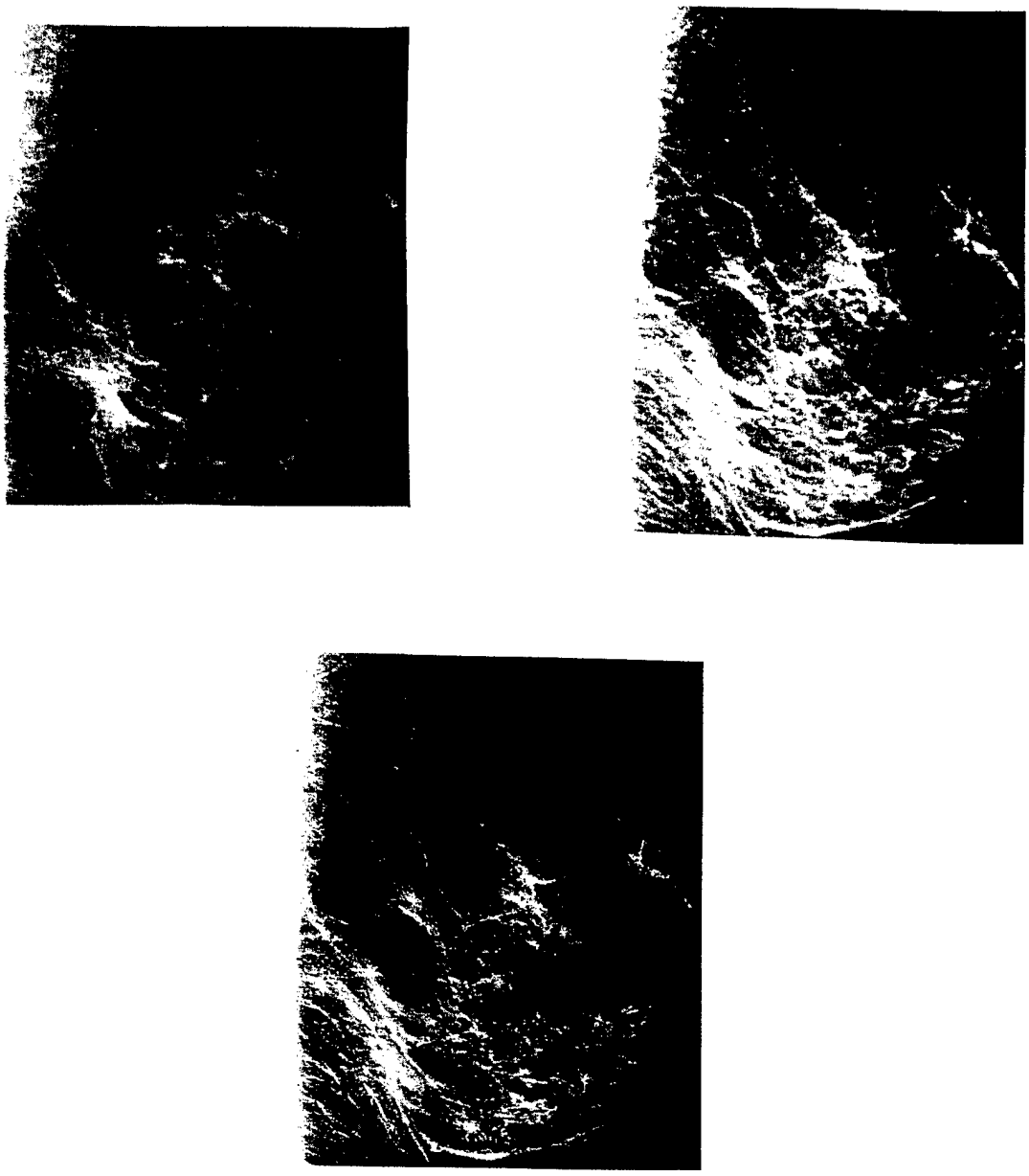

Figure 3: Mammogram of normal breast containing a few scattered microcalcifications. A. Conventional mammogram,
B. Digital mammogram. (GA=1.2, GT=G, GC=+0.3, RN=5, RT=P, RE=1). C. "Optimized" processed digital mammogram. (GA=1.9, GT=G, GC=+0.3, RN=9, RT=P, RE=5).

It was possible to devise algorithm settings that provided enhanced visualization of very small objects and of simulated masses when the digital image was compared to screen-film, but these processing settings resulting in human breast images that were considered unacceptably distorted. These distorted images might however prove to be clinically useful in selected problem cases when combined with other optimized images.

CONCLUSIONS

It is possible with a current digital mammography with proper image processing to equal the object detectability of a current screen-film mammography system, as measured on the RMI, CIRS and CDMAM phantoms and to produce a breast image that is likely to be acceptable to practicing radiologists.

BASIC CONCEPTS OF IMAGE PROCESSING:

This exhibit is intended to provide background information for understanding image processing in digital mammography.

RESOLUTION AND CONSPISCUITY:

The potential benefits from digital mammography would come from improved visualization of micro calcifications, thin linear structures and masses. The ability to detect objects depends on a combination of resolution and conspicuity. Resolution relates to the smallest sized object that can be seen. Conspiscuity refers to the detectabilty of an object as separate from its background by a human observer (how conspicuous it is) and is related to resolution, contrast, and viewing conditions.

THE USE OF PHANTOMS IN TESTS:

There are several mammography phantoms in use. These phantoms have different structures and their use reveals different aspects of image quality.

RESOLUTION:

Fundamental concepts:

REQUIRED PIXEL SIZE TO DETECT A SMALL OBJECT

A pixel is a picture element. Resolution and the pixel size necessary to detect a small object are not same. The maximal resolution of a picture divided into pixels, is the pixel size. The smallest detectable object is based on four factors: the size of the object, the size of the pixel, the position of the object in relation to the pixel and the relative radiodensity of the object compared to the background. Given adequate differences between the object and background density, the detection of a spherical calcium radiodensity object requires that the object and its penumbra be approximately $2\sqrt{2}$ times the size of the pixel. If the object is of greater radiodensity or is thicker, then smaller objects can be detected.

FILLING THE PIXEL:

If the pixel area is not filled, contrast is reduced.
The minimum detectable size is greater than the pixel size in most situations.

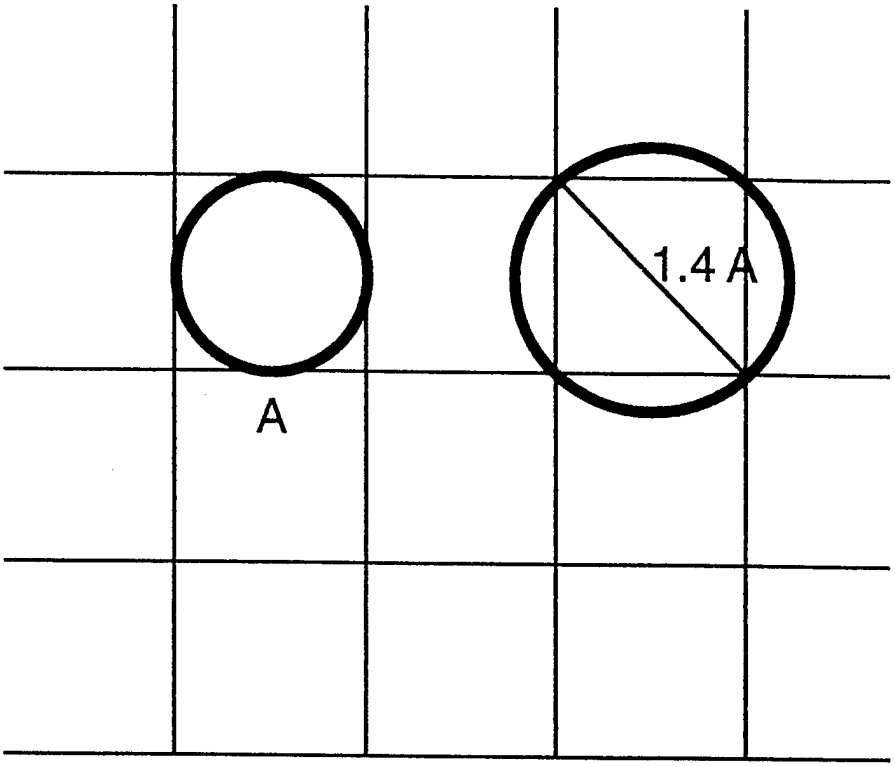

Figure 4: A sphere within a pixel has the same diameter as the pixel, but fills only 50% of a cubic voxel of the same size. Thus its radiodensity is only 1/2 of an object of similar thickness that completely fills the pixel. To fill a pixel of size A, need a sphere

If centered on pixel of size A
by Pythagorean Theorem: A $\sqrt{2}$.

EFFECT OF NOT FILLING PIXEL

Decreased contrast (similar to partial volume effect)

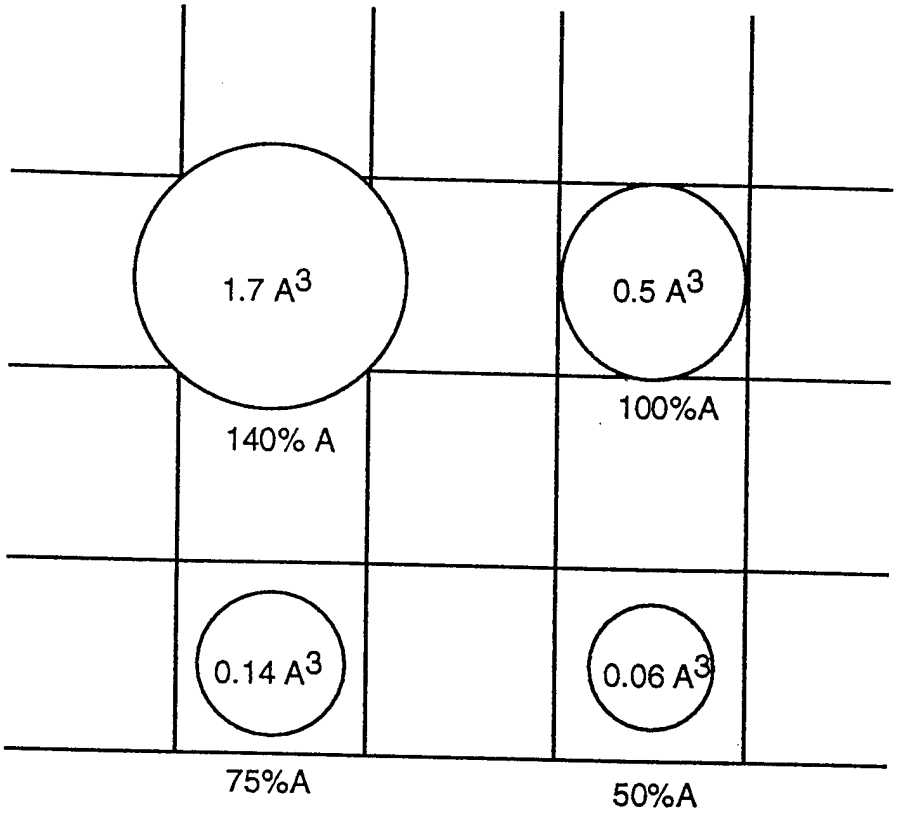

Figure 5: The volume of calcium projected in sphere of pixel size A with spheres of different sizes projected in center of pixel. (Based on solid geometry formulas.) The radiodensity projected on the pixel and averaged over the total area of the pixel rapidly decreases.

If an object is of increased radiodensity, then it can be smaller. Thus an object of 2 times the pixel size can be seen if it is twice as radiodense as an object seen when it is $2\sqrt{2}$ times the size of the pixel. This is demonstrable on the CDMAM phantom.

EFFECT IF OBJECT IS NOT CENTERED TO PIXEL

If calcium size is $\sqrt{2}$ A, minimum density will be 1/4 of that if the pixel is completely filled. (37% filled, but because of sphere only 1/4 of density). (Figure 6)

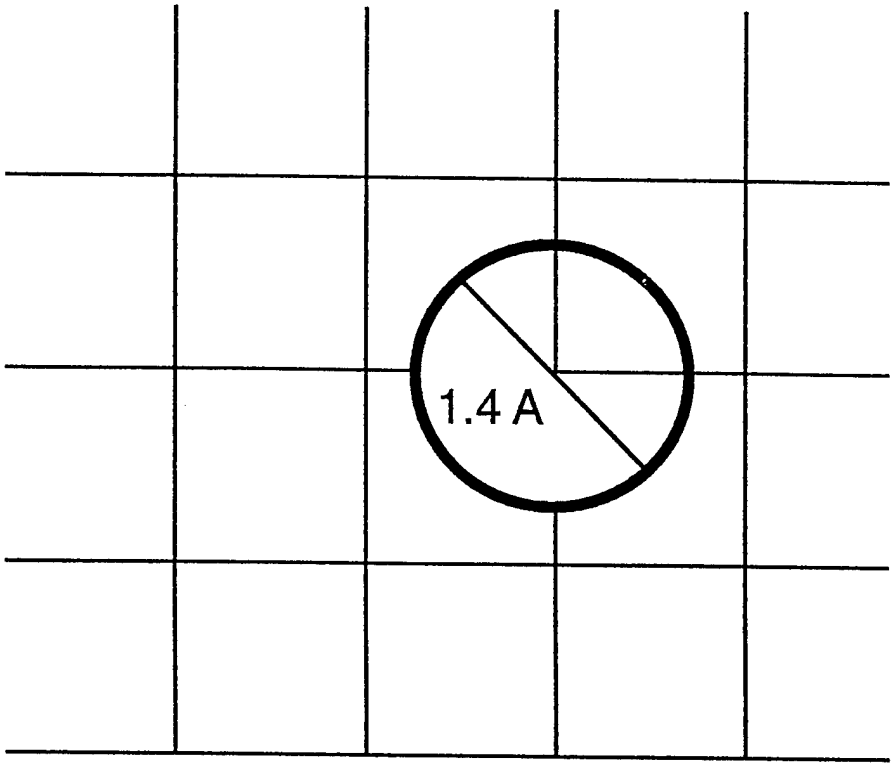

Figure 6: Drawing showing effect of maximal offset of $\sqrt{2}$ A sphere on area of pixel filled.

This is not of sufficient radiodensity to be detectable for spherical objects of calcium radiodensity.

If offset maximal amount (oblique) need 2A $\sqrt{2}$ to be certain that one pixel is completely filled.

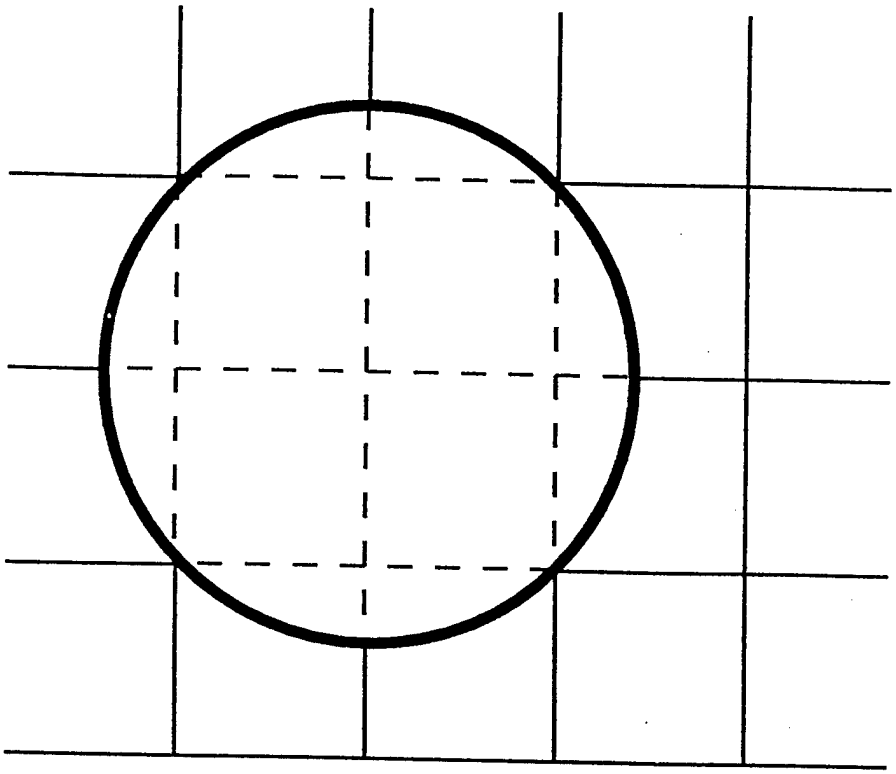

Figure 7: Drawing of sphere of diameter 2A $\sqrt{2}$ offset to corner of pixel.

Therefore, to consistently detect an object, one needs a 2A $\sqrt{2}$ sized object.

For a

320 micron object need 114 micron pixel
240 micron object need 85 micron pixel
160 micron object need 57 micron pixel

THE DIRECT HIT

Occasionally, a smaller object will be sufficiently superimposed on the center of a pixel so that it can be seen. This is a random, rather than a predictable occurrence.

FILLING THE PIXEL: EXPERIMENTAL EVIDENCE

We can just faintly see an object 160 microns plus penumbra with an 83 micron pixel. (from Figure 2). In that image, the object with penumbra is approximately 205 microns.

On the Fuji mammography system should be able to just see 290 micron object, but not the 200 micron object. In experiments, we can see 200 micron calcification in CIRS phantom. When actually measured on a screen film image, this 200 micron calcification actually measures 300 microns. Thus the value of 2 A $\sqrt{2}$ is a reasonable approximation. (Figure 8)

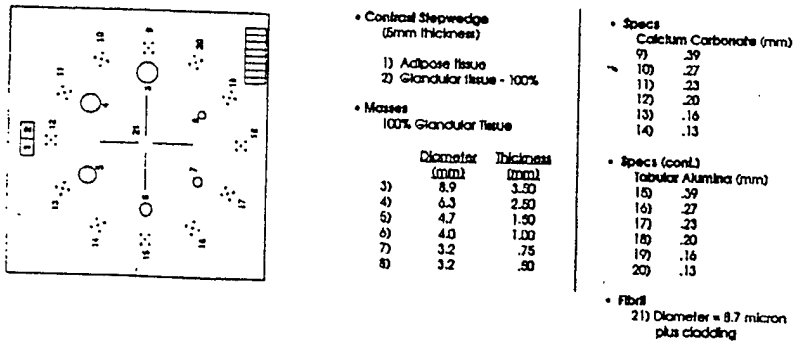

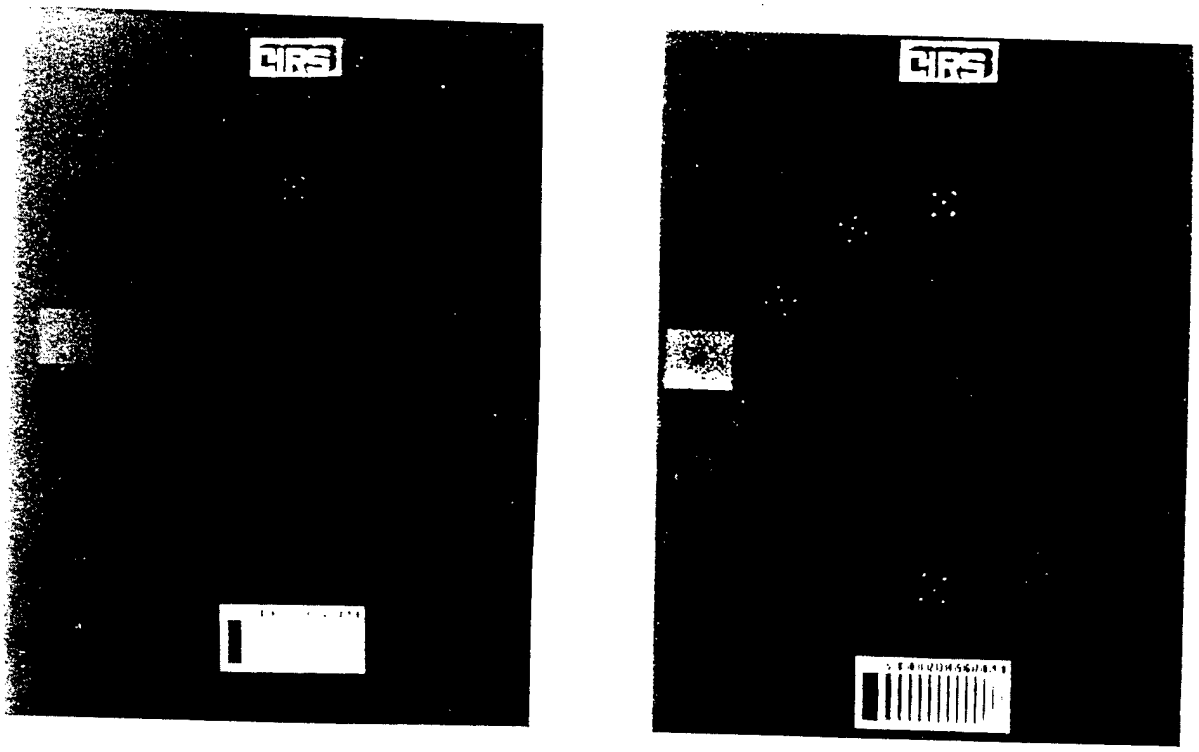

Figure 8: Storage phosphor image of CIRS phantom. Fuji HR-V plates. No magnification.

A: Drawing and measurements.

B: Screen-Film Radiograph.

C: Storage Phosphor Radiograph (Fuji high resolution system with HR V plates).

FACTORS AFFECTING OPTICAL DENSITY AND CONTRAST:

Image processing can be used to change the optical density and contrast of an image. The relation of this to improved images through digital mammography is discussed below.

EXPOSURE, NOISE, AND CONSPISCUITY:

In screen film systems, underexposure results in light images that limit the visibility of objects. In phosphor plate images, because one can correct the optical density of the image, the decreased exposure results in increased noise that limits the visibility of objects. At exposure levels necessary for full information, both systems performed equivalently. (Chart 3 A and B.)

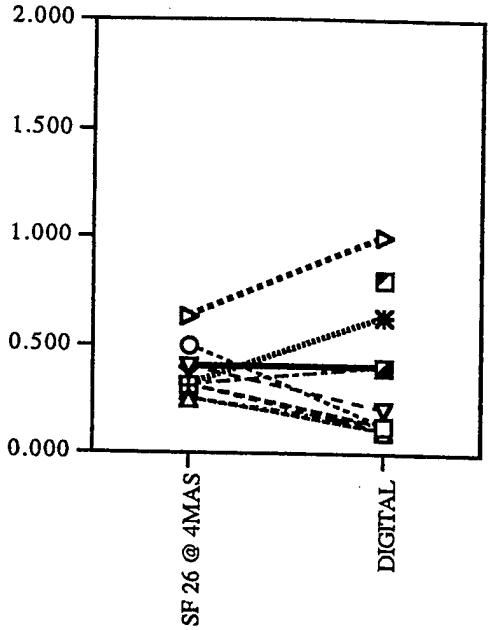

4

Chart 3A records a comparison at 4 mAs of screen film and digital CDMAM object. The screen film (SF) system performs better for some objects sizes and poorer for others when compared to the digital system The digital system system shows one object (0.2 mm) that is smaller than those seen with the screen film system.

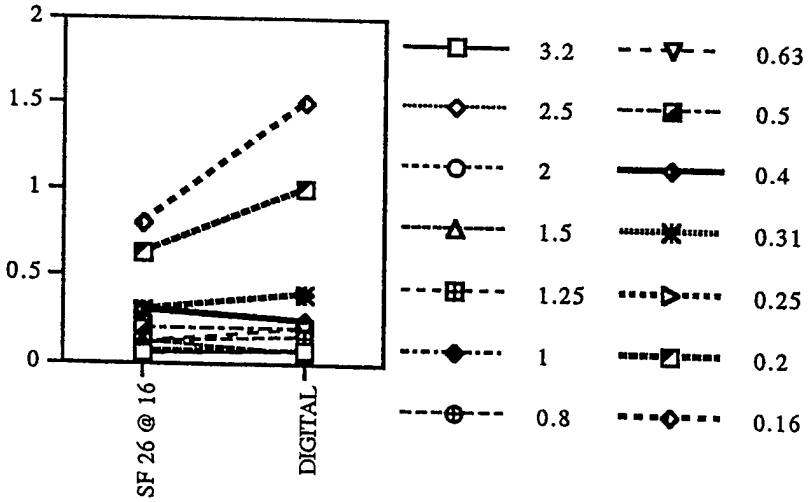

Chart 3 B demonstrates that at 16 mAs, the screen film system shows thinner objects for all object sizes than does the digital system. At 16 mAs, both systems showed the 0.16 mm diameter object. This object could not be seen with 4 or 6 mAs. The digital system was only partially optimized when this experiment was done.

Chart 4 This chart demonstrates the effect of increased exposure on detection of objects on the CDMAM phantom. A. Screen film. B. Storage phosphor

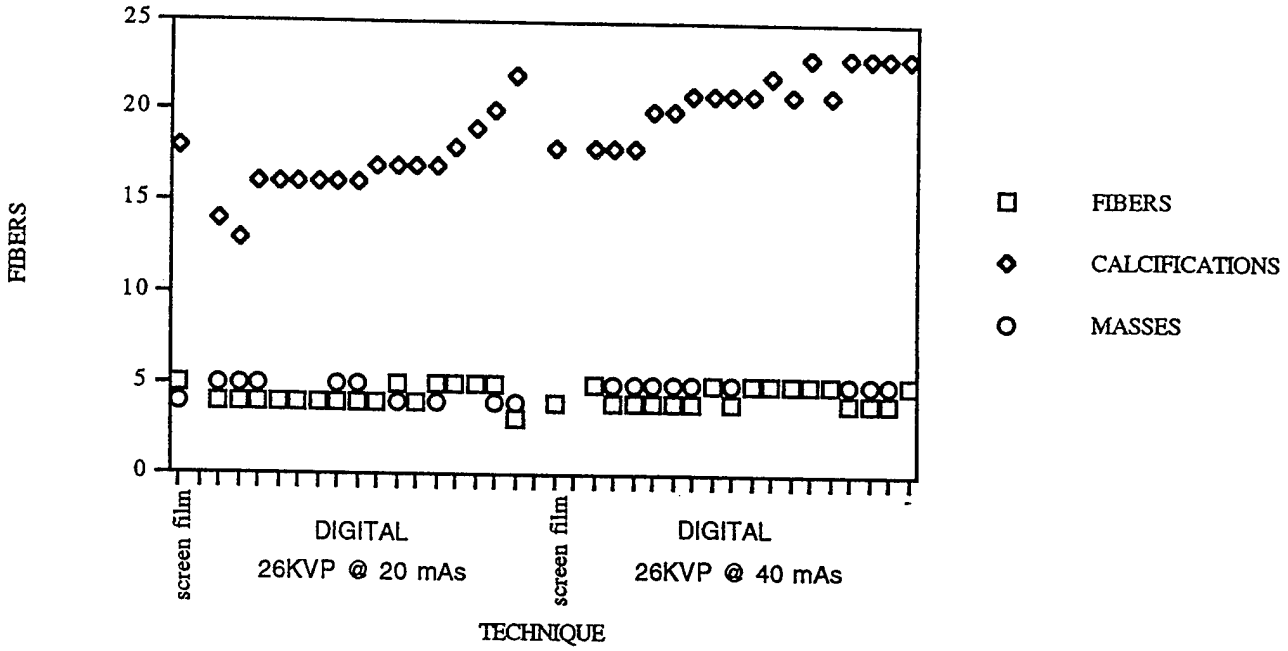

Chart 4. With the RMI phantom, increasing the exposure from 26 KVP at 20 mAs to 26 KVP at 40 mAs increases the detectability of calcifications in SR, but not with screen film. With the higher exposure, the SR system demonstrate more "calcifications" than the screen film system. Whether or not it is worthwhile to increase the exposure beyond that needed for SF mammography will depend on how useful finding these smaller calcifications proves to be.

OPTICAL DENSITY

Changing the optical density of an image can improve the visibility of objects that otherwise would fall in the toe or shoulder region of the image. Increasing the optical density in a region of calcifications by electronically shifting the calcifications to the steep portion of the contrast gradient can increase contrast and therefore visibility in the region of interest.

CONTRAST

Improving the contrast of the image can increase the detectability of objects.

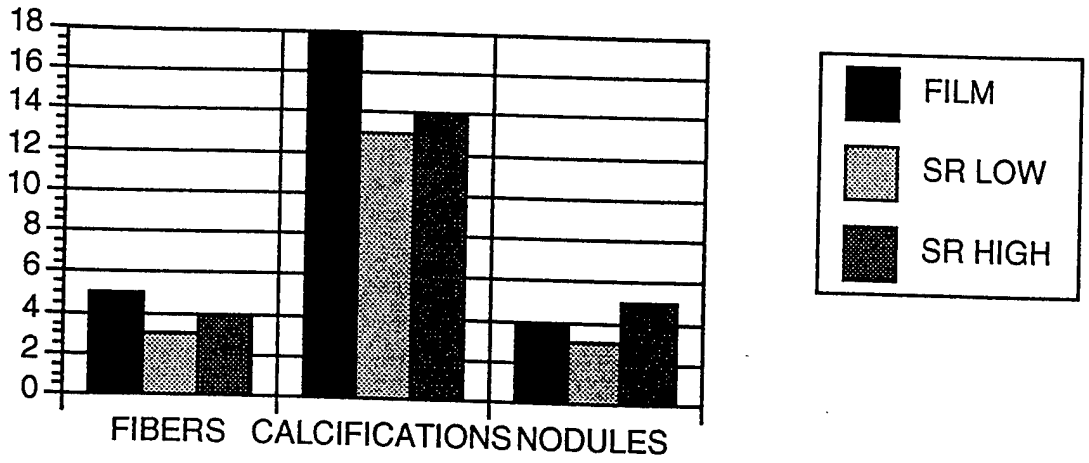

chart 5: This chart of objects detected on the RMI phantom demonstrates that the change from SR low contrast to SR high contrast increases the detectabililty of objects. High contrast makes the detection of masses to be greater than that of screen film mammography.

THE CENTER OF ROTATION

The contrast curve is rotated to increase the contrast. The center point for rotation is important in determining the contrast effect seen. If one wants to accentuate a calcium object against a background of higher optical density, the maximum separation will occur by placing the rotation center just above the OD of the calcium object. For any specific degree of contrast, this will allow the maximal visualization of the calcium, while minimizing the loss of information elsewhere in the image by creating too much contrast. The reason this occurs is that the system has limited ability to reflect low image optical densities and that for effective OD less than 0.3, further decreases have essentially no effect.

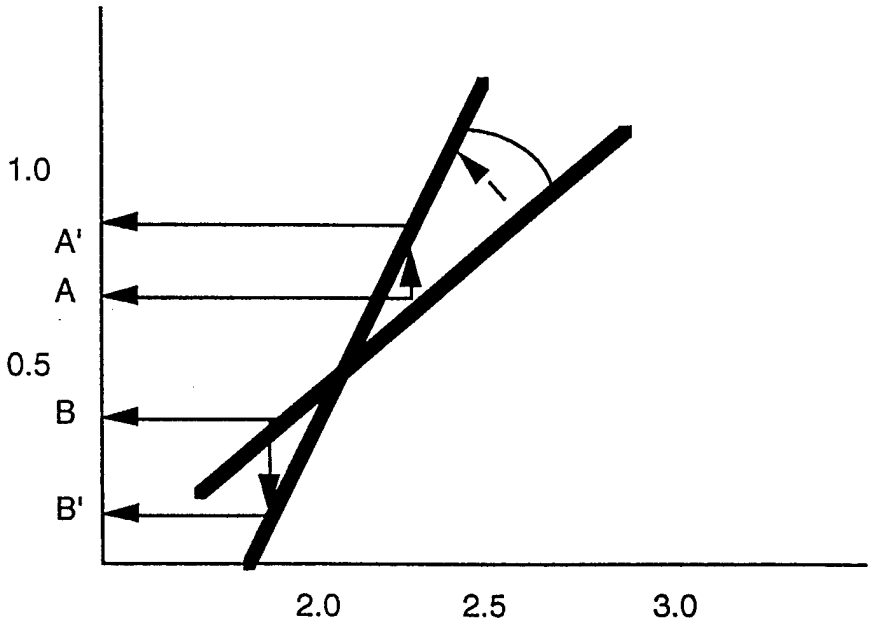

Thus if one increases the slope of the contrast curve and the center of rotation lies between the two objects to be separated, then the difference between the two points (the separation between A and B compared to A' and B') is increased.

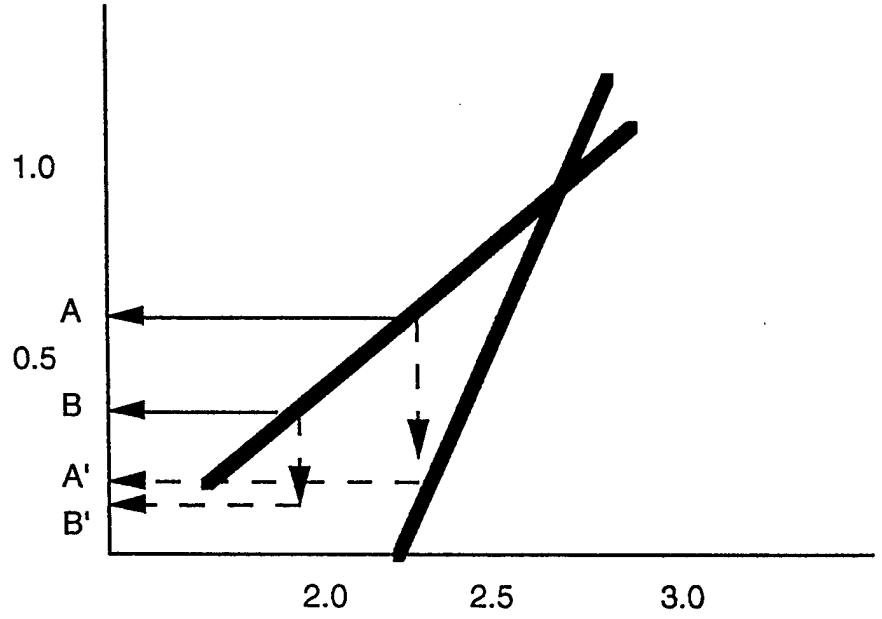

If one places the center of rotation of the contrast curve on either side of both regions one is attempting to separate, and then increases the contrast, then the two points will lie closer together, i.e. have less contrast (change from A to B to the space between A' and B'). This is because the OD of the less dense object cannot decrease much below its initial level.

SPATIAL FREQUENCY

All images can be separated into mathematical formulae that represent the frequencies present in an image. These mathematical formulae can be used to reconstruct the image as it was. One can also use image processing to change the emphasis of different spatial frequencies in an image. One can choose ranges of frequencies to emphasize or de-emphasize. This processing can make information more visible or can conceal information.

Kernel size:

One common method for changing the emphasis given different spatial frequencies in an image is to do a convolution where the information is multiplied by a group of numbers that are selected to affect certain spatial frequencies. The kernel size refers to the size of the group of numbers used as the multiplier. In general, the smaller the kernel, the greater the emphasis given to smaller objects, the larger the kernel, the greater the emphasis given to larger objects.

The use of small kernels emphasizes sharp margins and can be called edge enhancement. The use of large kernels de-emphasizes sharp margins and can be called smoothing or noise reduction.

Using small kernels emphasizes the visibility of noise in an image. Use of large kernels decreases the sharp edges that aid in the detection of micro calcifications.

The effect of changes in kernel size and spatial frequency emphasis:

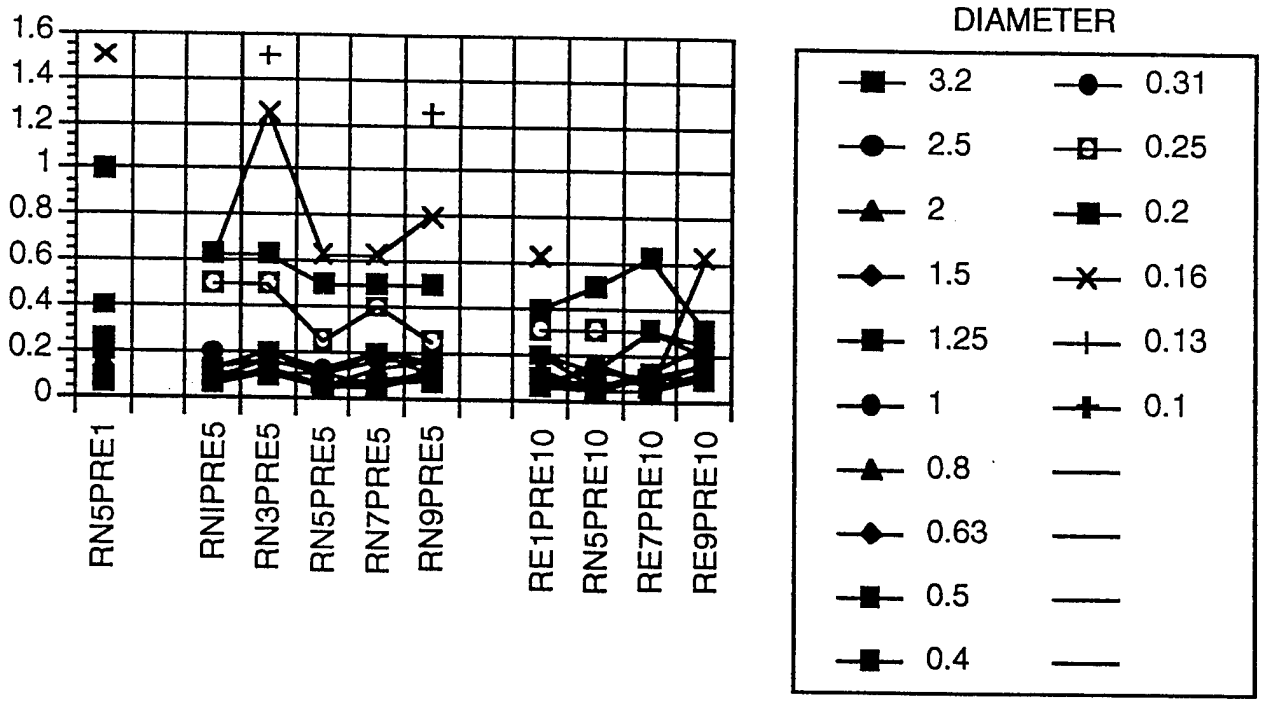

CHART 6: The effect of different degrees of emphasis (RE =1,5,10) for selected kernel sizes (RN = 1,3,5,7,9). Increasing the emphasis results in thinner objects being seen at all sizes. At the smallest kernel size (RN = 9), the high emphasis image increased the visible noise and the smallest objects were not visible in the noise.

On the CIRS phantom, increasing the emphasis (RE) increased the visibility of small masses (Chart 7A), but did not affect the detection of calcifications or fibers (Chart 7B)

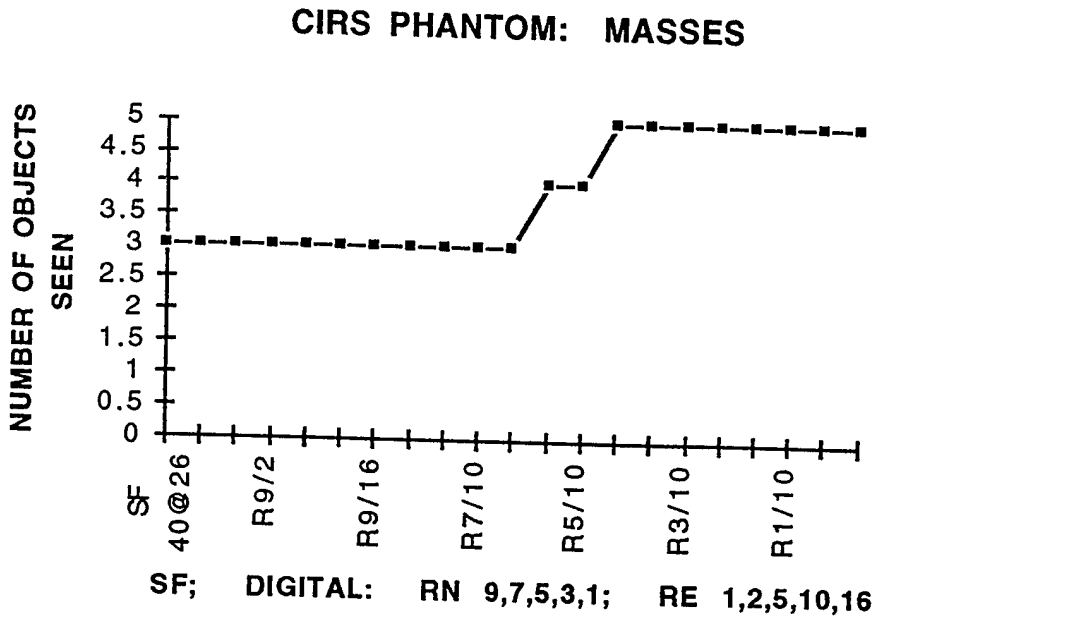

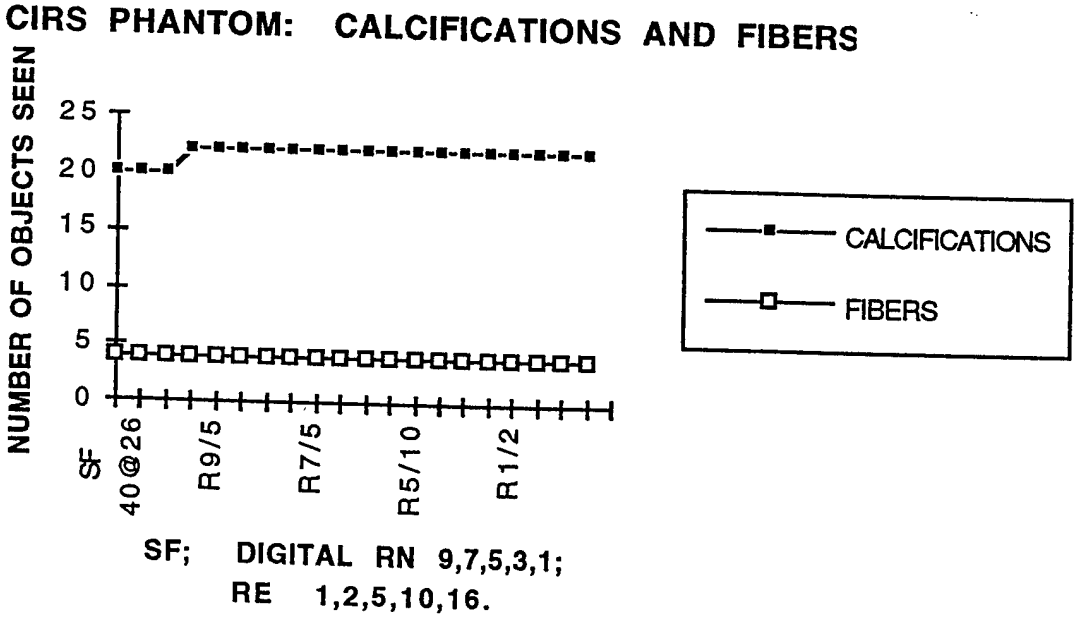

Chart 7: On the CIRS phantom, the detection of masses increases with increased spatial frequency filtering emphasis. The detection of calcifications and fibers did not changes. A. Masses. B. Calcifications and fibers.

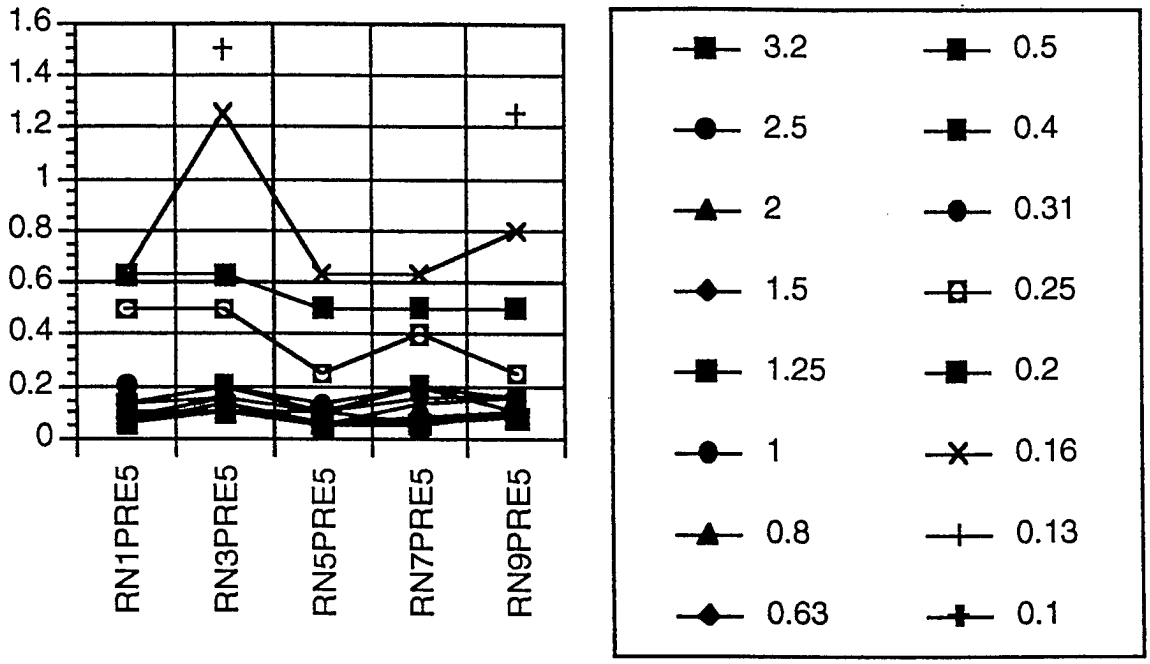

Chart 8: Effect on detectability of small objects with changes in kernel size (CDMAM, using different kernel sizes). There is some improvement in the detection of small objets (0.13 mm in diameter) with kernel size RN(compared to RN 1,3,5, and 7. There is no effect on larger objects.

SUMMARY

Image processing of digital breast images can have a marked effect on the appearance of the resulting image and the detectability of objects in it. Tests such as those described above will be used to test potential algorithms for appropriate final image diagnostic quality.

ACKNOWLEDGEMENT:

This research was supported in part by U.S. Army Medical Research Grant DAMD 17-93-J-3008. The content of this report does not necessarily reflect the position or policy of the U.S.Government and no official endorsement should be inferred.

IMAGE PROCESSING IN DIGITAL MAMMOGRAPHY: THE OPTIMUM IMAGE FOR EACH WOMAN'S BREASTS

Matthew Freedman, Dorothy Steller Artz, Seong Ki Mun

The goal of image processing in digital mammography is to improve for the human observer the visibility of the signs of breast cancer and to decrease the visibility of structures and noise that may either mimic the signs of cancer or interfere with the visibility of the signs of cancer. All radiographic images of the breast contain normal structures including glandular tissue, fibrous tissue, vessels, and skin pores that under certain circumstances can mimic the signs of cancer or hide the signs of cancer. In addition, all breast radiographs contain system induced noise of several types and this noise can both resemble the signs of breast cancer and obscure them. Image processing can enhance the visibility of disease or conceal it. Breasts can be glandular, fatty, heterogeneously dense or homogeneously dense. The optimum image processing will differ for these different patterns of breast composition and for individual variation within these patterns.

Radiologists look for five common signs of abnormalities that may be caused by cancer lesions: groups of microcalcifications, a focal radiodensity, a mass, architectural distortion of the normal breast fibers, and a change in appearance between two studies. In some cases the cancer is visible, in other cases the findings are related to the cancer, but do not themselves represent the cancer.

Image processing consists of a series of tools that alter the original image data set resulting in a new image data set that can be then displayed or have additional processing done. Image processing can be done in the analog or digital environments. I will mainly discuss the digital environment, but because most display devices for mammography are analog in nature, I will be discussing the interplay of digital image processing with analog display.

Image processing can be applied to analog mammography, digitized film mammography and digital acquisition mammography. My examples and illustrations will be based on data sets from digital acquisition mammography. The techniques shown can be applied to digitized film mammography, but the effects will not be quite the same. Some of the digital techniques shown have analog counterparts, but they will not be discussed.

The Influence of the Analog Display Device on Image Processing

With one specific exception, the display of digital mammograms is done on analog devices: usually as laser exposed film and less often on the cathode ray tubes (CRTs) of workstations. Both of these display devices have inherently non-linear responses to the input information. In both cases the response is S shaped, similar to the familiar H and D or characteristic film curve.

Imaging Science and Information Systems
Department of Radiology
Georgetown University Medical Center
Washington, D.C., U.S.A. 20007

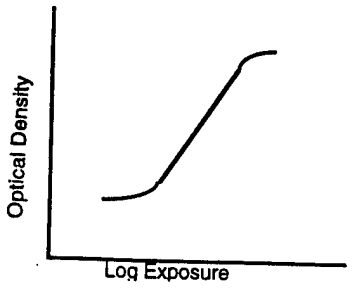

This curve shows the relationship of exposure to optical density when applied to film display media and pixel value to luminance when applied to CRTs. The curve is S shaped because of the inherent limitation of the response of these systems and low and high input values. The central portion shows the steepest gradient and corresponds to the region of highest contrast. The curve's upper portion is the shoulder and represents a region of progressively decreasing contrast as the optical density approaches its maximal value or the luminance approaches its minimal value. The curve's lower portion represents the toe and is a region of progressively decreasing contrast as the optical density decreases towards its minimal value or the luminance value approaches its maximal level.

The data sets resulting from image processing interact with the response curves of the display devices affecting the contrast in different portions of the final image. What this means is that in a region of the image where the pixel values are low, the contrast effect of the image processing will be less than in a region where the pixel values correspond to the mid portion of the display response curve. Since, in general, one desires the signs of cancer to have maximum contrast, one must compensate for the non-linear display response by shifting the look up table of the region of interest into a higher contrast region of the display device.

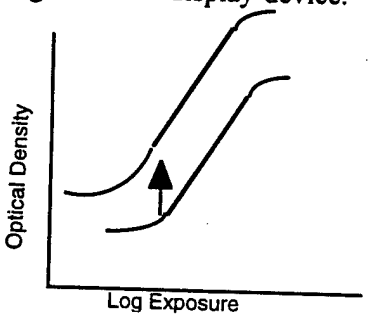

Alternatively, one can exaggerate the contrast scale in those regions of the image that would be mapped to the toe or shoulder of the display device by changing the look up table.

On a mammogram, microcalcifications can appear as white dots surrounded by white glandular tissue or white dots surrounded by darker fatty tissue. White dots against the white glandular background will be of lower contrast than those projected on fatty tissue. If, in addition, this region is mapped to a portion of the display response curve that is a low contrast region, that low contrast image effect will further decrease the contrast of the microcalcifications. Simply by remapping that portion of the image to a region of steeper gradient of the response curve will result in improved contrast and conspicuity of the calcifications.

Microcalcifications surrounded by fat are inherently of high object contrast, but if one projects them in a region of the response curve near its shoulder, their contrast will also be decreased and the calcifications will become harder to see. Bird (Radiology 1992; 184:613-617), who routinely slightly overexposes his images to better see calcifications within the whiter region of glandular tissue, then has images that are overexposed in the fatty breast regions and it is there that his group tends to miss cancers.

Methods for Projecting Important Image Regions into High Contrast Image Display Response Regions

Object conspicuity will be enhanced if it is projected in a high contrast region of the display. There are five potential methods of achieving this.

1. Use a contrast scale that is optimum for the range of pixel values of the imaged breast. One can, using image processing, vary the degree of contrast to be optimum for each breast. The fatty breast has a lower range of object radiodensity and thus one could use a higher display contrast (F) and yet maintain the whole image data visible within the range for the display device. For a dense breast, one would use a flatter contrast scale (D). One could have the machine automatically choose the correct slope of the look-up table to achieve the desired response. The problem with this is that with the current S-shaped look-up tables, the images of dense breasts printed with a wide contrast scale look washed out and microcalcifications become difficult to see because of the overall low contrast image that has resulted.

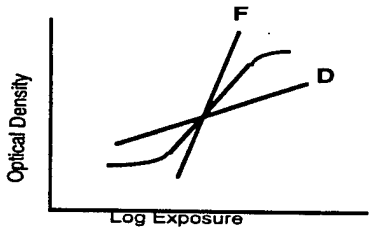

2. Produce two images from each digital data set, one darker than average and one lighter than average so that all parts of the image are visible. This would increase radiologist's time for interpretation.

3. Use a workstation and vary the window level to produce two or more high contrast images that cover the entire range of tissue densities in the image.

4. Use an image specific contrast linearized double or variable gradient look up table. The development of a perceptually linearized contrast curve for microcalcifications may be helpful. Currently, the American College of Radiology and the National Electrical Manufacturers Association (ACR-NEMA) are working on a set of radiology imaging standards called DICOM. As part of this they are working towards a perceptually linearized display protocol. A double gradient curve is an attempt to get a perceptually linearized contrast curve across an image of the breast. If we look at an image of a dense breast, there are regions in the image that are close to white where microcalcifications would be of low contrast with adjacent tissue and regions of fatty tissue where microcalcifications would be of high contrast. If one attempts to increase the contrast in the regions of low inherent contrast to match the inherent contrast in the fatty regions, the fatty regions of the breast would become too dark. The concept of the double gradient curve is to have an optimal steeper gradient for the region of low inherent contrast and a less steep gradient slope in the region of higher inherent contrast so that one has an image at least partially contrast optimized across its whole useful range of tissue densities.

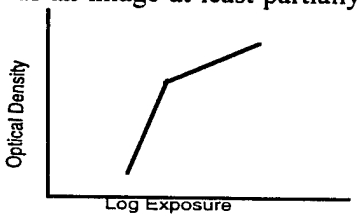

This type of curve has been made for some mammographic film. One should be able to devise a better linearized contrast to optical density curve electronically than that accomplished by film chemistry. This could be eventually optimized by using segmentation techniques to look at the pixel values in regions of glandular tissue.

5. Use low resolution histogram equalization to balance the tissue densities. Using image processing methods it is possible to decompose the digital image set into components with different spatial frequencies. There are at least three different decompositions that can be used to create daughter images with low and high spatial frequency. One can use convolutional methods to produce a low resolution mask, wavelet transforms, and Fourier transforms. Much of the structural information needed for mammographic interpretation lies in the high frequency space. Microcalcifications are high frequency structures, fibers distorted by architectural distortion are high frequency, the edges of masses are high frequency and the stellate boundaries of masses are high frequency. If one separates an image by spatial frequency, one can do separate processes on the low and high frequency components. If one's goal is to reduce the range of optical densities in an image, this processing can be done on the low resolution image leaving the high frequency information intact. If one has chosen the proper parameters, one can be left with an image that has increased the conspicuity of microcalcification. One can decrease the white glandular density improving the visibility of microcalcifications.

One can also use this to improve the visualization from the most radiodense portion of the breast to the skin line while still preserving important visualization of breast structures.

Methods for Enhancing Low Contrast Images of Radiodense Breasts

The opposite spectrum from the breast with a wide range of radiodensities is the radiodense breast with very low contrast between adjacent structures. Such breasts create their own problems in contrast optimization. These images tend to be of fairly uniform density in regions of fibroglandular tissue, but still show the full range of higher optical densities when the region near the skin line is included. In some ways they are like the fatty breast where there are large regions of uniform density; but unlike the fatty breast, the region close to the skin line is quite different than the central portion of the breast. In the homogeneous radiodense breast, there are large areas of low contrast dense tissue compared to small areas of high optical density. If one could increase the contrast in the fairly uniform regions of low optical density radiodense tissues, one might be able to start to detect structure that is otherwise not visible. What is needed is the ability to stretch the histogram in such regions so that it is mapped over a wider range of final image densities than its proportional contribution to the total image would normally warrant. Thus the situation is similar to that of the dual characteristic curve, but because the local range of densities is less, one can get into the problem of the original image data not having enough bits of gray depth. This results in a contoured image when this region is stretched. A digital mammogram obtained with storage phosphor technology is now limited to 10 bits. These bits are evenly spread over the total optical density range of the image. Thus if one works to expand a small region of the pixel value spectrum to a much wider optical density range, the image will separate into bands of equal density, each separate from the others with an appearance of banding.

Two approaches suggest themselves: 1. Acquire the digital data with greater bits of gray scale or 2. Interpolate between gray scale levels when increasing contrast to create a smoother image appearance. We are describing a perceptually smoothed image.

Spatial Frequency Enhancement in Digital Breast Images

The edges of microcalcifications, the edges of masses and the edges of breast fibers are high frequency structures. The use of edge enhancement can accentuate such structures. It is important, however, to match the frequencies enhanced to the structure to be visualized. If one is using a convolutional method of edge enhancement and chooses the wrong kernel size, one can obscure the structures one wishes to see. Thus very small calcifications can become harder to see as the kernel size is enhanced or the intensity of enhancement is increased. Thus one faces a tradeoff: increasing the edge enhancement degree will make it easier to see architectural distortion and larger microcalcifications, but will make it harder to see the very small microcalcifications.

In our clinical cases, we have found contrast enhancement of greater value in detecting small calcifications and have found that edge enhancement decreases microcalcification visibility if it is too

great in amount. We cannot determine how much of this effect is due to the actual effect of the edge sharpening and how much is due to the accentuation of noise.

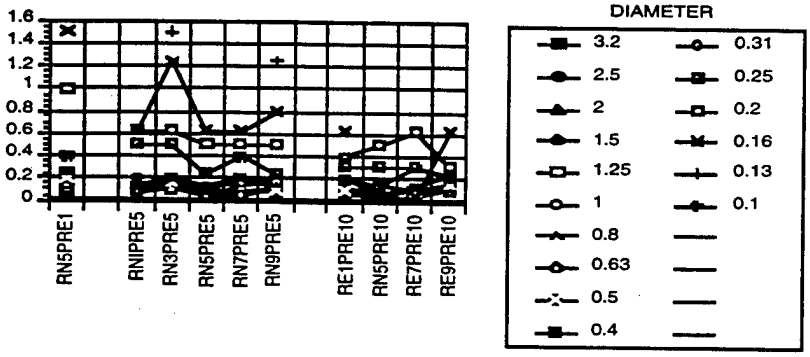

This chart shows the effect of different degrees of emphasis (RE =1,5,10) for selected kernel sizes (RN = 1,3,5,7,9). Increasing the emphasis results in thinner objects being seen at all sizes. At the smallest kernel size (RN = 9), the high emphasis image increased the visible noise and the smallest objects were not visible in the noise.

Image Noise in Digital Mammograms

The current group of digital mammography systems under development all appear to be quantum limited. Thus quantum noise is a component of the images in all of these systems when used at clinical exposures similar to those used for screen film mammography. Noise reduction strategies therefore become a potentially important tool in achieving optimum image quality. The noise in images will be greater in regions of more radiodense breast tissue. Thus in the regions where microcalcifications would already be of lower contrast, the noise can simulate them and make the calcifications harder to see. One could decrease the noise by using higher exposures, an approach that is not acceptable in the USA or develop more radiosensitive x-ray detectors; experimental work on this is underway. Alternatively, one can use image processing to decrease noise visibility. At least three strategies can be used to mask the noise: one can blur the image in regions of low exposure, one can apply edge enhancement asymmetrically to affect mainly higher exposure portions of the image, or one can use statistical noise reduction.

Image Blurring

Image blurring can be used to obscure the visibility of quantum noise. Such blurring occurs by averaging in part adjacent pixels. If used in regions where microcalcifications are, it can blur the edges of the microcalcifications as well. It produces a more pleasing image, but can hide the signs of disease.

Statistical Noise Reduction

Detecting Calcium in Regions of Quantum Mottle by Degree of Deviation of Pixel Value from the Mean

Statistical noise reduction is a complex process that we are currently exploring with the Space Telescope Science Institute. Quantum mottle has statistical characteristics that can be characterized mathematically. When one is seeking clinical microcalcifications, one is looking for five or more microcalcifications within a one centimeter radius. If one looks at an image composed of 100 micron pixels and wants to find a threshold for random noise pixel intensity such that one will identify less than 5 randomly intense pixels within 1 cm, one then looks to find only those pixels that are more than 3.8 standard deviations (SD) from the mean. At 3.8 SD, one should find no more than 4 pixels within a 1 cm radius that exceed that pixel intensity. One can use this method to smooth the image by reducing all regional fluctuation less than 3.8 SD to the mean value.

If one measures the absorption of calcium for 100 and 200 micron calcified objects, one can calculate the absorption of the calcium compared to the noise level in the image. If the noise is kept low enough, then the major structures still visible after this statistical analysis should consist of the microcalcifications and no more than 4 random hits due to fluctuation in pixel intensity.

Statistical Evaluation of Multiple Adjacent Pixels

Certain CADx algorithms use the simplifying rule of assuming that almost all calcifications will occupy four or more adjacent pixels. Most quantum mottle will affect individual pixels and to have multiple adjacent pixels all deviated in the same direction from the mean will be less frequent. These programs require that at least four pixels vary in the same direction by a certain amount from the mean value in order for the suspect region to be considered to be a likely calcification detection. One searches for four or more adjacent pixels of greater than a threshold value and then can reduce the other values towards the mean.

Hiding of tissue structure that could be confused with disease

Image processing can also be used to simplify images. It is possible to flatten the background structure of an image leaving the specific structures of interest easier to detect. Currently, we can do this by separating the complete breast image into high and low frequency images and then flattening the contrast scale in the low frequency image so that the structures reflected in it disappear or almost disappear. The size of the structures that are concealed is related to the pixel size and kernel size.

Dual Energy Strategies

The relative absorption of calcium, water, and fat become similar at higher x-ray beam energies and differ more at lower energies. If one can obtain two images at different energies, one can mathematically enhance the differences between the images. Two strategies can be used: energy subtraction in which one attempts to have one structure, for example, the water density material of the breast, disappear leaving a calcium only image, or additively, to enhance the visibility of calcium within the overall breast pattern. By using an appropriate filter layer between two image receptors, one can create the two different energy images with a single exposure.

Stereo Reconstruction

If one takes two images of the same breast in approximately the same orientation and directs one image only to the right eye and the other only to the left eye, two different phenomena can occur as the brain attempts to interpret the images. If they are identical, they look like one planar image. If they are slightly different in angulation, the brain can create a stereo image that appears to have depth. If such a stereo image is created and there is an object in one image that is not seen in the other, the brain will call attention to that different object by either making it appear flat instead of three dimensional like, or potentially projecting it in front of the total image. The extent to which this method could be used in increasing the conspicuity of changes in mammograms is uncertain.

Summary

Image processing can enhance an image making it easier to identify the signs of cancer or can obscure the signs of cancer. Careful tests of the effects of image processing should be completed first in geometric test objects before they are tried in digital data sets from patients. The major goal of image processing is to optimize the contrast of the signs of cancer; a secondary goal is to decrease the visibility of breast structure and image noise that can interfere with the visibility of cancer. This article discusses aspects of contrast enhancement related to both the digital data set and the interaction of that data set with the image display device, the use of image separation into high and low frequency images and the use of edge enhancement in the detection of the signs of breast cancer.

DISPLAY CHARACTERISTICS AND TRANSFORMATION IN FILM AND CRT MONITOR

Shih-Chung B. Lo, Denis Stewart, Matthew Freedman, and Seong K. Mun

Radiology Department, Georgetown University Medical Center,

Washington, D.C. 20007 U.S.A.

ABSTRACT

Hurter and Driffield first used the H&D curves in 1890 to show the density response of film to various exposures under experimental conditions [1] using photographic techniques. Our experiment was designed to reproduce these curves using standard radiographic techniques but also to compare them with curves produced using luminance values obtained from CRT images of the same image after laser film digitization. Theoretically, one should be able to receive the optical density (OD) measurement directly obtained from a densitometer based on the light transmission and the OD calculated from transmittance values obtained by a luminance probe with and without an object. This was proven in our base-line study. In the process of this experiment, we discovered that standard H&D curves could be reproduced almost exactly using values of luminance and the equation for optical density. Since it is almost impossible to use a densitometer to measure the OD of an area on CRT image, the OD conversion through digital to CRT display must rely on the luminance probe measurement. We found this alternative method was reliable and useful to translate the gray scale between various display media. These results, though not totally unexpected, provided us with the basic differences between conventional film and digitized film images, and opened up the possibility of "enhancing" the CRT displays in order to offer comparable diagnostic value to conventional film images.

1. INTRODUCTION

Accuracy of interpretation of medical images is necessary if the medical image is to be used for clinical care. When a radiologist views a conventional radiograph, for example, of the chest or of a bone, the radiologist can promptly determine whether the film quality is such that the image is interpretable. Criteria that are used include the absence of motion, proper positioning, appropriate image contrast, appropriate resolution, and absence of artifacts sufficient to interfere with diagnostic accuracy.

We have evaluated many input and output (front-end) devices used as a PACS peripheries. This included laser film scanners and a computed radiography for plain image input and laser film printer [2] and high definition TV monitors for display [3]. In this paper, we have extended our experience and look into practical physical issues and some clinical evaluation. We have evaluated (a) H&D curve responses (or it's equivalence) among different image media and a possible analytical transformation between them. (b) possible protocols to address the issue during the image, and (c) the advantage and disadvantage of using a specific electronic device in the PACS verse film and light-box system. Based on the initial observations that the main problems with the few images that we viewed occurred in areas that were of low or high optical density on the original film, initial work has focused on calculating the equivalent of the H&D characteristic curve for images projected on a CRT monitor. The H&D curve of monitor response using window width and level demonstrated a marked distortion of the curve which would help to explain the loss of diagnostic information at high optical density regions on the original film. However, the transformation seems make the CRT gray distribution performing close to the film, with limit degree of in our experiment.

0-8186-2195-8/91 $1.00 © 1991 IEEE

2. MATERIALS AND METHODS

The first phase of the experiment consisted of H&D curve response using films of two latitudes (Fuji HR-G) at an x-ray voltage setting at 90 KVp. (we found that no significant difference between 90 and 129 KVp). Films were placed immediately below the step wedge and the radiation source was set at a constant height of 37" above the film screens. With KVp setting constant, mAS settings were manipulated in order to explore the full range of optical density for both types of film.

Standard film-screen images were obtained of the step-wedge at a given x-ray voltage and various mAS settings and subsequent exposure readings were obtained for each wedge block. The Keithley Dosimeter (Model: 35055) was used to record all of the exposure values at all of the settings previously used. Optical density values were obtained using the densitometer (X-Rite 301 Densitometer). It is important that one should not use the H&D measurements in this paper as the bench marks for those films used in our experiment, since the experiment was not in an ideal situation where considerable x-ray scattering was not involved. However, this does not diminish the value of this experiment, because our purpose was to use this curve as a baseline study and to try to link it with the curve, described below, obtained using photometer probe (Tektronix J16 Digital Photometer with J6523 1° Narrow Angle Luminance Probe).

During the luminance readings, individual objects on the film were isolated from possible outside light scatter by using a dark template held against the film in a dark room setting. The photometer and narrow angle probe were used to obtain luminance values of the image blocks on a standard radiographic view box with the distance between probe and light source remaining constant (24") and with the incoming light value obtained after each reading. Luminance values were obtained from the film image blocks - "light out" (L(out)), and the "light in" (L(in)) value was obtained without film on the box. Equivalent optical density (EOD) values were then calculated using the equation below:

$$EOD = \log(L(in) / L(out)) \qquad \ldots(1)$$

The second phase of the experiment included (a) film digitization using a Dupont laser scanner [2], (b) digitized image display on a Tektronix CRT, (c) recording each luminance value from various exposure blocks (d) calculating EOD (see eq. 1), and (e) plotting curve with EOD verse the relative exposure to mimic the H&D curve. Note that the window widths and levels were set at 2048. Once the images were brought up on the CRT, the luminance values were recorded at each area of the step wedge using the Tektronix Photometer just as the luminance values were obtained from the film using the same photometer. This was done for all films previously acquired. Luminance values were obtained from the digitized image blocks ("light out") and the "light in" value was obtained at window width and level settings of 0 and 0 (white screen). Equivalent optical density values were then calculated also using equation (1).

The third phase of the experiment was designed as an attempt to shift our CRT-obtained curve such that it would more closely approximate the film-derived images. This was done by (a) changing the window widths and levels and (b) gray scale transformation in a systematic fashion and recording the luminance values at these new settings. We have changed level/window setting from 2048/2048 to 3076/2048 and 2048/4096 which tried to make the H&D curve of CRT act as the H&D curve of film in the high OD region. Level/window of 2048/4-96 is generally considered relevant by some radiologists in our department for portable chest film reading on the CRT. The gray scale transformation was made with the same attempt.

3. RESULTS

The H&D curve of open box in Fig. 1 corresponds to the data obtained using the

densitometer and the conventional film. Note that the slope of the middle portion (between toe and shoulder portions) corresponds to a latitude ("exposure range over which appropriate optical densities are produced") of between (-3.8) and (-2.6), roughly. The curve with the "diamonds" in Fig. 1. represents the response of the calculated or "equivalent" optical density from the luminance probe measurements. Notice the similarities in latitude, slope, and shape of these two curves obtained from the film using the densitometer (OD/film) and the photometer (EOD/film).

Figure 1. H&D Curves of Film and CRT Display

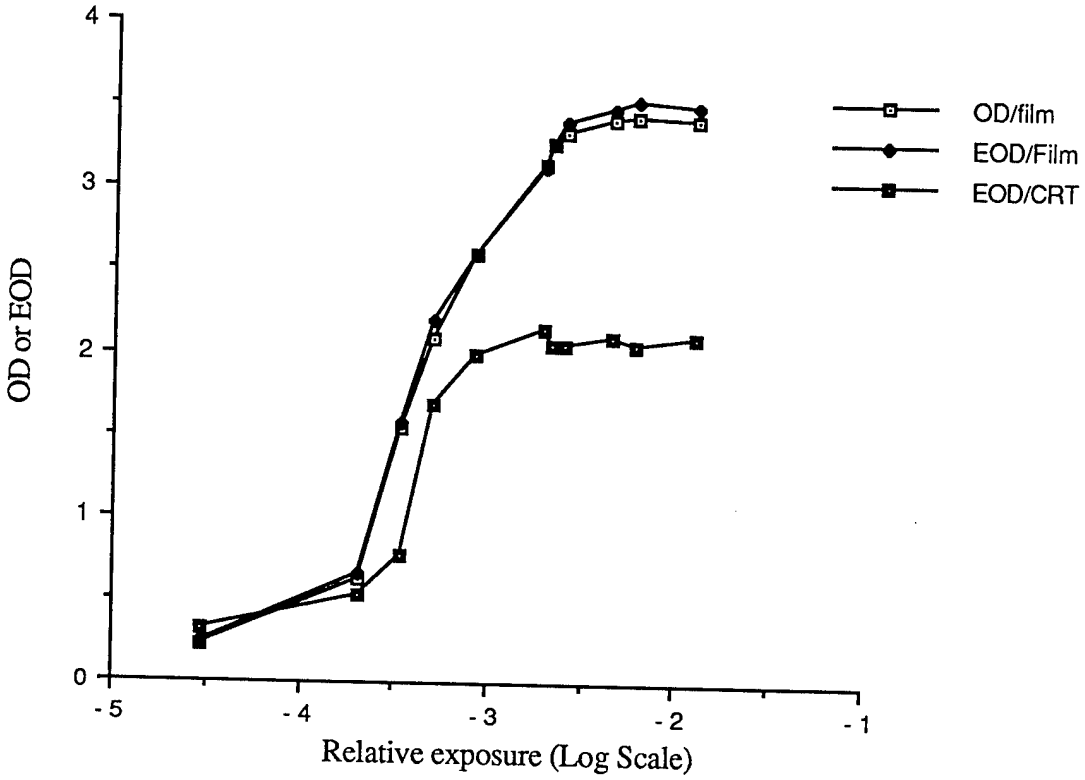

The curve with the closed boxes represents data obtained from the CRT (window width and levels of 2048) using the photometer. Notice that the latitude and shape of this curve are markedly different from those of the other two curves on this graph.

Fig. 2 represents a comparison of the H&D curves obtained from the CRT at several different window width and level settings which is one of the standard methods to enhance contrast in digital radiography. Note that the curve with the open boxes is identical to the one in Fig. 1 for EOD/film and the curve with closed diamonds, labeled with EOD/CRT in Fig. 1, is identical to L2048/W2048 in Fig. 2. Those two curves are shown to contrast the curves obtained from window level/width settings of 3072/2048 and 2048/4096, labeled with closed boxes and open diamonds, respectively. With higher level setting (L3072/W2048 vs. L2048/W2048), almost all of the image blocks became darker and the EOD measures shifted to higher optical density. The curve, however, was distorted in the low exposure region. With higher width settings (L2048/W4096 vs. L2048/W2048), low exposure areas with EOD less than 2.0 were not affected by the operation of higher width. However, the high optical density region, corresponding to relative exposures higher than -2.7, shifted to higher EODs.

Figure 2. H&D Curves at Various Window Widths and Levels on a CRT

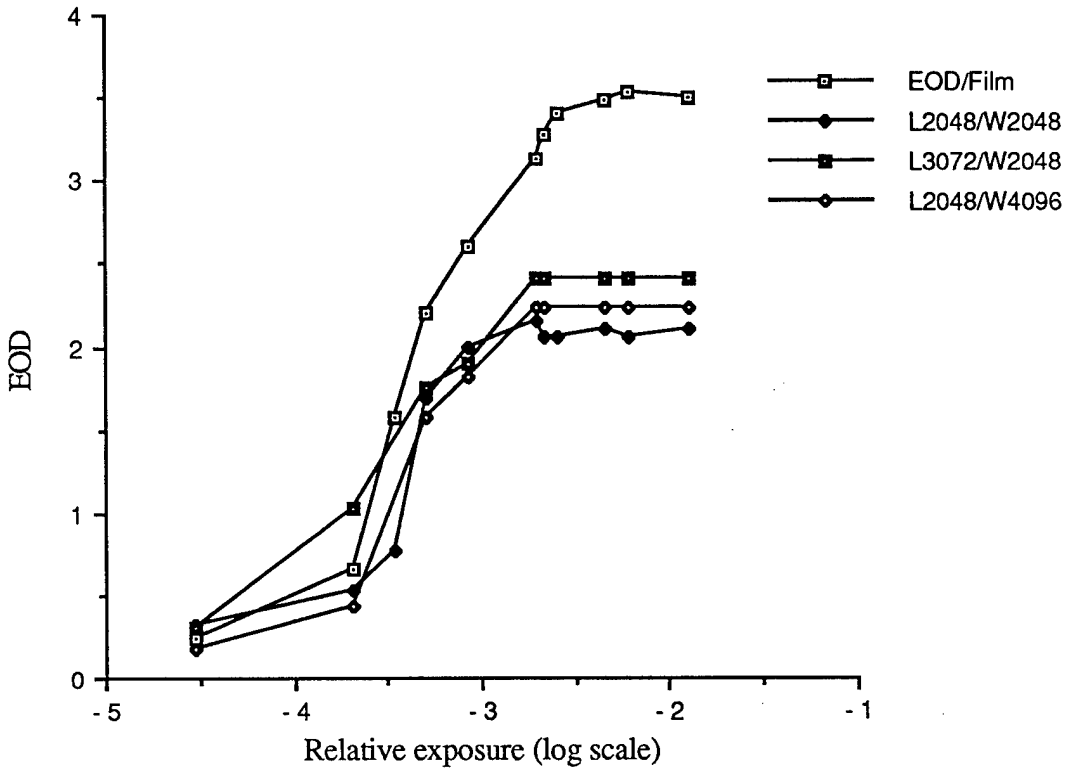

Fig 3. shows the results obtained from CRT by remapping the digital value using a gray level transformation. The curves labeled with open boxes and closed diamonds are identical to the ones in Fig. 1 for EOD/film and EOD/CRT (with L2048/L2048), respectively. The closed boxes shown in Fig.3 is the H&D curve response after a transform. It is seen that the curve was lifted for the relative exposure region higher than -3.4 and this curve is closer to the curve obtained from film. However, beyond the relative exposure of -3.0, the EODs saturated at 2.8. This is due to the fact that the minimum luminance increment is 0.11 fL in the CRT [3].

4. CONCLUSIONS AND DISCUSSION

The gray measurements of a film are conventionally made by a densitometer. The electronic image display on CRT for a radiography is not new, however, the gray characteristics on the CRT are somewhat different from those of film. The important point upon analysis of Fig. 1 is that standard H&D curves determined with a densitometer can be reproduced nearly exactly using a luminance meter with narrow angled probe (OD/film and EOD/film) This fact enabled us to use this same luminance meter to determine H&D curves from the CRT, and subsequently compare the gray scale characteristics in physical measurement.

The difference in the dark region was due to the luminance scattering from the local area of the block to the probe. In an ideal system, the EOD measure is log(Li/Lo). With local scattering, the equivalent optical density is given by

$$EOD = \log((Li(1+Si)/Lo(1+So)) \quad \ldots(2)$$

Figure 3. H&D Curves on Film, CRT, and Transfomed Gray Tone on CRT

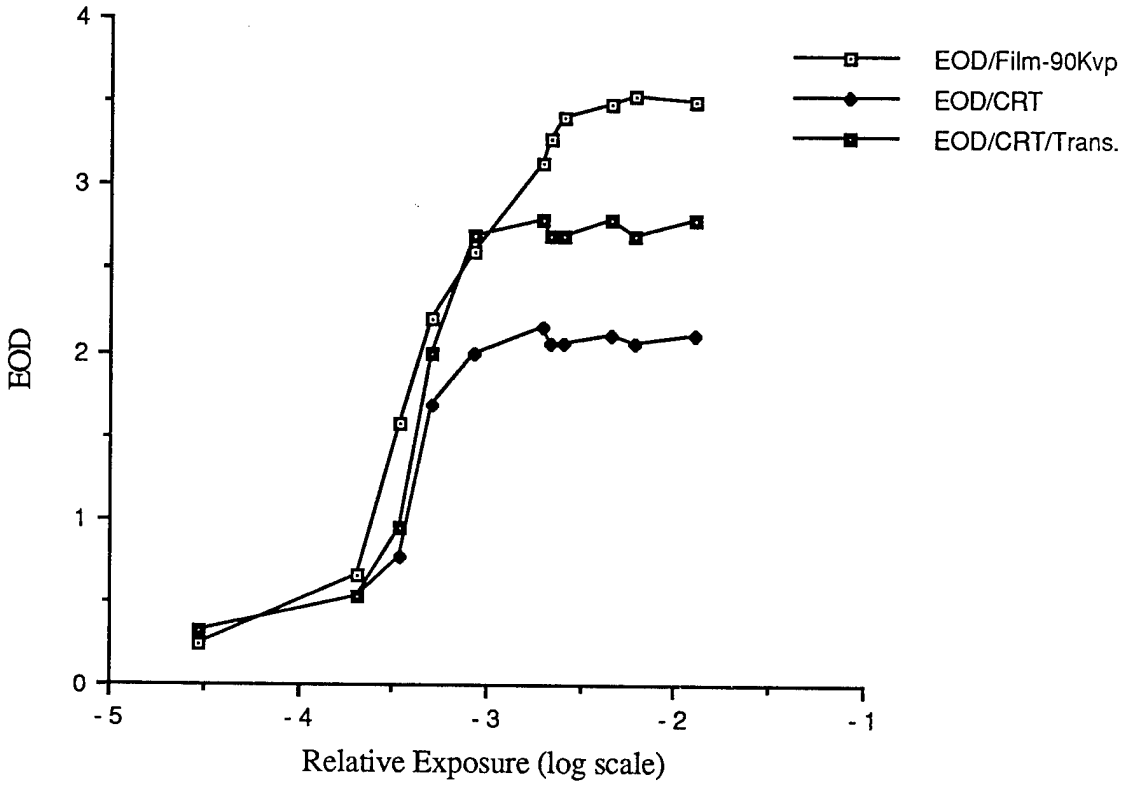

where L is the primary luminance, S is the scattering factor, i and o standard for "light-in" and "light-out" measure in the experiment, respectively. In the bright blocks, the scattering factor So is close to the scattering factor Si from light in situation. Therefore, no significant difference was found in the low and medium exposure region. This is not the case for the dark blocks. With dark blocks, the So is much smaller or insensitive to the probe that makes Si greater than So. This derivation clarifies the EOD is higher than OD in the dark optical density region in Fig. 1, since $(1+S1)/(1+So)$ is greater than 1 which implies $\log(Li(1+Si)/Lo(1+So) > \log(Li/Lo)$. Theoretically, the latter equals to OD measure. Since the EOD measure only slightly overdetermines the value of the optical density for a dark region, it does not affect the purpose of this project where the comparable H&D curves in both film and CRT are concerned.

The second important point in this experiment is that we have quantitatively demonstrated a major difference between the curves of film based and CRT based radiography. The CRT curve shows a markedly reduced latitude as well as shape in comparison to the film based curves. This difference implies that there is only appropriate contrast for visual discrimination over a small range of exposure compared to the film curve, and thus limits the gray range on the CRT at a given window/level setting used. It must be mentioned that the CRT curve only exists below optical densities of 2.0. In the third phase of the experiment, window/level setting slightly improve the maximum OD to 2.3 with some distortion of the curve shape. However, with a proper gray level transformation, the curve moves to a maximum OD at 2.8 without distortion of the curve shape. The reason for the maximum OD 2.8 is that the physical limitation of the minimum luminance increment is 0.11 fL for the CRT as indicated in reference [3].

Despite the low OD range of a CRT at a given time, the capability of using an almost infinitiely dynamic range of digital gray levels is the the advantage of the CRT display. Since OD

range is not the main factor for visual discrimination of two subtle contrast areas, this capability has made the CRT potentially useful in the low contrast area where dynamic gray range is needed to adjust the contrast in a distinguishable region [4].

The shape of standard (i.e., film based) H&D curves typically depends on several factors. Among these are the quality of the x-ray beam and film developing techniques such as time, temperature, and solutions [5]. The CRT curve appears to have a steeper slope than the other curves, but the reasons for this are not readily apparent.

5. REFERENCES

1. Hendee, W, *Medical Radiation Physics*. 2nd Ed. 1979, Year Book Medical Publishers Inc.
2. Lo, S-CB, Taira, RK, Mankovich, NJ, Hunag, HK, and Takeuchi, H, "Performance Characteristics of a Laser Scanner and Laser Printer System for Radiological Imaging." Compu. Radiol. Vol. 10, No. 5, 1986, pp. 227-237.
3. Lo, S-CB, Gaskill, JW, Mun, SK, and Krasner, B., "Contrast Information of Digital Imaging in Laser Film Digitizer and Display Monitor", J. Digital Imaging. Vol. 3, No. 2, 1990, pp. 119-123.
4. Freedman, M, "Chest Radiographic Image Quality: PACS and CR", Presented at The First PACS-RIS School, Washington D.C. March 28-30, 1991.
5. Sprawls, P, *Physical Principles of Medical Imaging*. Aspen Publishers, Rockville, MD. 1987, pp. 224-229.

AD_____

GRANT NO: DAMD17-93-J-3008

TITLE: CLINICAL OPTIMIZATION OF CURRENT DIGITAL MAMMOGRAPHY SYSTEMS (BREAST CANCER)

PRINCIPAL INVESTIGATOR: Matthew T. Freedman, M.D.

CONTRACTING ORGANIZATION: Georgetown University
37th & O Streets, NW
Washington, DC 20057

REPORT DATE: January 20, 1994

TYPE OF REPORT: Annual Report

PREPARED FOR: U.S. Army Medical Research, Development, Acquisition, and Logistics Command (Provisional), Fort Detrick
Frederick, Maryland 21702-5012

REPORT DOCUMENTATION PAGE

Form Approved
OMB No. 0704-0188

1. AGENCY USE ONLY (Leave blank)	2. REPORT DATE	3. REPORT TYPE AND DATES COVERED
	20 January 1994	Annual Report (12/15/92 - 12/14/93)

4. TITLE AND SUBTITLE
Clinical Optimization of Current Digital Mammography Systems (Breast Cancer)

5. FUNDING NUMBERS
Grant No.
DAMD17-93-J-3008

6. AUTHOR(S)
Matthew T. Freedman, M.D., M.B.A.

7. PERFORMING ORGANIZATION NAME(S) AND ADDRESS(ES)
Georgetown University
37th & O Streets, N.W.
Washington, D.C. 20057

8. PERFORMING ORGANIZATION REPORT NUMBER

9. SPONSORING/MONITORING AGENCY NAME(S) AND ADDRESS(ES)
U.S. Army Medical Research, Development, Acquisition, and Logistics Command (Provisional)
Fort Detrick
Frederick, MD 21702-5012

10. SPONSORING/MONITORING AGENCY REPORT NUMBER

11. SUPPLEMENTARY NOTES

12a. DISTRIBUTION/AVAILABILITY STATEMENT
Approved for public release;
distribution unlimited

12b. DISTRIBUTION CODE

13. ABSTRACT *(Maximum 200 words)*

Based on the work we have done this year, we believe that digital mammography using an existing commercial storage phosphor device combined with appropriate image processing does equal in phantoms the resolution of conventional screen film systems at an equivalent patient dose and can exceed the object detectability of conventional screen film systems when a higher patient dose is used.

During the optimization techniques, it also became apparant those some of the problems previously reported were secondary to static electrical charges and dust. We found it essential to be unusually careful in controlling dust to avoid calcium like artifacts. The preliminary studies suggest that the use of a 35 micron film digitizer coupled with appropriate image processing may allow the replacement of direct geometric magnification with electronic magnification. With electronic magnification, the conventional screen film image is digitized at 35 microns. A small section of this is then displayed as an enlarged image. With appropriate image processing, it is possible to see calcifications and details in shapes of calcifications that cannot be seen either directly or with a magnifying glass on the original image. Our experiments suggest that film digitization with very small pixel sizes may prove to be a viable method for digital mammography. We will be continuing our research with a 42 micron film digitizer when a machine arrives at our site early in 1994.

14. SUBJECT TERMS	15. NUMBER OF PAGES
Breast Cancer, Mammography, Digital, RAD VI	16. PRICE CODE

17. SECURITY CLASSIFICATION OF REPORT	18. SECURITY CLASSIFICATION OF THIS PAGE	19. SECURITY CLASSIFICATION OF ABSTRACT	20. LIMITATION OF ABSTRACT
Unclassified	Unclassified	Unclassified	Unlimited

FOREWORD

Opinions, interpretations, conclusions and recommendations are those of the author and are not necessarily endorsed by the US Army.

____ Where copyrighted material is quoted, permission has been obtained to use such material.

____ Where material from documents designated for limited distribution is quoted, permission has been obtained to use the material.

____ Citations of commercial organizations and trade names in this report do not constitute an official Department of Army endorsement or approval of the products or services of these organizations.

____ In conducting research using animals, the investigator(s) adhered to the "Guide for the Care and Use of Laboratory Animals," prepared by the Committee on Care and Use of Laboratory Animals of the Institute of Laboratory Resources, National Research Council (NIH Publication No. 86-23, Revised 1985).

____ For the protection of human subjects, the investigator(s) adhered to policies of applicable Federal Law 45 CFR 46.

____ In conducting research utilizing recombinant DNA technology, the investigator(s) adhered to current guidelines promulgated by the National Institutes of Health.

____ In the conduct of research utilizing recombinant DNA, the investigator(s) adhered to the NIH Guidelines for Research Involving Recombinant DNA Molecules.

____ In the conduct of research involving hazardous organisms, the investigator(s) adhered to the CDC-NIH Guide for Biosafety in Microbiological and Biomedical Laboratories.

1-26-94

PI - Signature Date

DIGITAL MAMMOGRAPHY
EXTENDING CURRENT TECHNOLOGIES:

REPORT ON FIRST YEAR OF PROJECTS

ENHANCEMENT OF CURRENT TECHNOLOGIES FOR DIGITAL MAMMOGRAPHY

1.0 INTRODUCTION:

The first year of the project was spent gathering preliminary data essential to understanding the requirements for digital mammography in two areas: image acquisition, and electronic image processing using two existing technologies, film scanner and storage phosphore plate system There are almost no publications in this field relevant to the specific work done in this project. There are related publications in chest imaging and these will be referred to as indicated.

Although digital mammography is in limited clinical use in Europe (1,2,3,4), it is still considered an experimental technique in the United States where it has been described as being promising, but not having sufficient resolution (4,5,6) or of insufficient resolution with the possibility of improved resolution far in the future (7). Based on our experiments in system optimization, we believe we understand the disagreement in opinions is likely due either to differences in exposure factors used or differences in the image processing parameters used by different centers. Unfortunately, the actual image processing parameters used by various authors and the actual exposures used are usually not mentioned in these articles, but as our work suggests, the appropriate setting of these factors is essential to high quality digital mammography.

Based on the work we have done this year, we believe that digital mammography using an existing commercial storage phosphor device combined with appropriate image processing does equal in phantoms the resolution of conventional screen film systems at an equivalent patient dose and can exceed the object detectability of conventional screen film systems when a higher patient dose is used. To achieve these results, however, it was necessary to use different image processing methods than those recommended by the manufacturer. These more optimal image processing methods were derived from optimization response surface experiments performed this year. The method used to arrive at the more optimal image processing settings was derived from the methods used for image optimization that we previously used with AGFA's CR system and Fuji CR's used for chest and bone images that we previously reported. (8,9)

During the optimization techniques, it also became apparent those some of the problems previously reported were secondary to static electrical charges and dust. We found it essential to be unusually careful in controlling dust to avoid calcium like artifacts.

The narrative summary that follows is based on individual experiments that are briefly described in the appendix. In this narrative, they are referred to by the number given them in the Appendix A.

2.0 THE ASSIGNED TASKS FOR THIS PROJECT ARE:

1. Evaluate the current status of existing digital mammography systems for direct digital mammography and film digitization.

2. Develop a strategy for the optimization of these existing systems including optimization of KVP and MAS.

3. Compare the accuracy of these existing systems to conventional screen film systems if the systems appear to be adequate replacements for existing screen film systems using ROC methodology

4. Provide recommendations about how these systems could be implemented to replace existing screen film mammography.

3.0 THE THREE COMPONENTS FOR SUCCESSFUL DIGITALMAMMOGRAPHY:

There are three components required for the successful development of a digital mammography system. These are the methods of image acquisition, the methods of image processing, and the methods for image display. This research deals primarily about the first two factors and image display is handled in a more comprehensive manner in a separate but related project The research from the first year has demonstrated the requirements for image acquisition and has demonstrated appropriate parameters for portions of the necessary image processing. Image display is also discussed.

This report will take each of the areas in turn, define initial state of knowledge, summarize the results of the research done by our team, and indicate the relevance of this work to the final project aims.

4.0 IMAGE ACQUISITION FOR DIGITAL MAMMOGRAPHY

4.1 Initial state of knowledge:

Relevant Prior Publications:

Publications on digital mammography implied that the development of a digital mammography system would require the development of new detectors because existing systems did not have adequate resolution. (4,5,6,7)

We could find no articles specifying the required resolution for digital mammography. There are a few articles describing that 100 micron pixel size appears not to be sufficient. One source (7) suggested specific resolutions were based on the assumption that it should equal the high contrast resolution of screen-film mammography: 20 line pairs per mm.

Oestmann (10) reporting work with a 5 lp/mm storage phosphor system reported that while a 5 lp/mm system was sufficient to detect all clusters of microcalcifications, that individual microcalcifications were less well seen at this resolution. He reports that he selected image processing settings that resulted in images "similar to those of conventional mammography." He used the same exposure as used for the conventional screen film images he obtained for comparison (30 KVP at 250 mAs). This is a higher KVP than would

normally be used for conventional mammography and would be expected to decrease the contrast of calcifications on the conventional images (our most common setting is 26 KVP).

Chan (11) reporting on the use of high quality film digitization at 100 micron pixel size found that digitized mammograms provided lower detectability of subtle microcalcifications than conventional screen film mammography. She found that unsharp masking improved the detectability of the calcifications, but that even with unsharp masking, the conventional screen film mammograms still had a higher detectability rate. She indicates that this is due to their being a higher false positive rate.

4.3 Exposure:

We assumed that any system developed would have to use the same or less exposure than conventional screen-film mammography.

4.4 Methods of obtaining a digital mammogram:

There are two methods of creating a digital mammogram: direct digital acquisition and digital transformation of an analog image. Direct digital mammography systems either existing or under development use storage phosphor plates, charged coupled devices (CCD), selenium plates or electron capture devices. Film digitization devices can be based on laser, monochromatic or diffuse light.

4.4.1 Direct Digital Mammography Devices:

A survey of existing direct digital mammography machines revealed that only Fuji Corporation had a working FDA approved system for digital mammography. We acquired such a system for testing in September, 1993. No other existing commercial machine was identified. Research devices are under development by Dr. Martin Yaffee in Toronto, by Lorad Corporation, 3M, and by Fischer Corporation in the U.S. and Fuji Corporation in Japan. In addition, several smaller companies are exploring various devices. These include Photometrics and Princeton Instruments. We are working with 3M and with Princeton Instruments on their machines and have had discussions with Photometrics, Lorad and others. These devices are not yet finished and were unavailable for testing. Images from some of these machines have been reviewed. Currently the Lorad images are the most promising, but we were unable to due a true assessment of the machine.

4.4.2 Film Digitization for Digital Mammography:

There are existing devices for film digitization based on laser or CCD technology using 100 to 200 micron pixel sizes available from multiple vendors including Lumisys, Vidor, Vision 10, and others. There are a few companies claiming 50 micron digitization capabilities, usually over a limited range of optical densities. We have been investigating the technology under development by DBA, Inc. This 42 micron pixel system has had construction delays and should be delivered to us in January, 1994, for intensive testing. Should film digitization prove to be an appropriate technology for further investigation, then the required pixel size for this technology could be determined. Tests to determine the preferred contrast characteristics for mammograms to be digitized will be determined once the machine is on site.

4.5 An Evaluation of the Resolution Requirements for Digital Mammography:

At the start of this project, we could find no information related to the pixel size that a digital mammography machine would have to have to equal the detectability of objects seen on screen-film mammography. The two articles mentioned above (Oestmann and Chan) suggested that 100 micron pixel size was insufficient. Screen-film mammography systems can have up to 20 line pairs per millimeter (lp/mm) of high contrast resolution. This would imply that one would need a system with 25 micron pixel size to equal the high contrast resolution of screen-film. The only contemplated systems that we are aware of that come close to this resolution are film scanners. If indeed this resolution was required, then all of the direct digital systems under development would end up being insufficient for digital mammography. Because of this we undertook both an experimental and theoretical approach to determine the effect of different pixel sizes on the detection of very small radiodense objects. The theory will be presented first followed by the experimental evidence that supports it. This will then be followed by a discussion of the implications of these findings for further research. (This material was presented at the Computer Assisted Radiology (CAR) Meeting in Berlin, June, 1994.)

4.5.1 Theoretical Approach to determining the pixel size needed to detect a small object of specified size:

Definitions:

A small object is an object close to the size of the pixel. They are assumed to be spherical and of calcium radiodensity.

Pixels are assumed to be square.

Voxels are rectangular solids that contain all the region from the x-ray tube to the region that project onto the pixel.

The detector is assumed to be a storage phosphor imaging plate with inherent light scattering potential.

The focal spot size is small, but finite; therefore an object being imaged casts a penumbra (or shadow).

4.5.1.1 FILLING THE PIXEL:

It order to obtain maximal information from a pixel, the process being evaluated should completely fill the pixel. Because microcalcifications are assumed to be spherical, the minimum detectable size is greater than the pixel diameter. In actual appearance, the microcalcifications are irregular, but closer in shape to a sphere than a cube. The diagram demonstrates the necessary size..

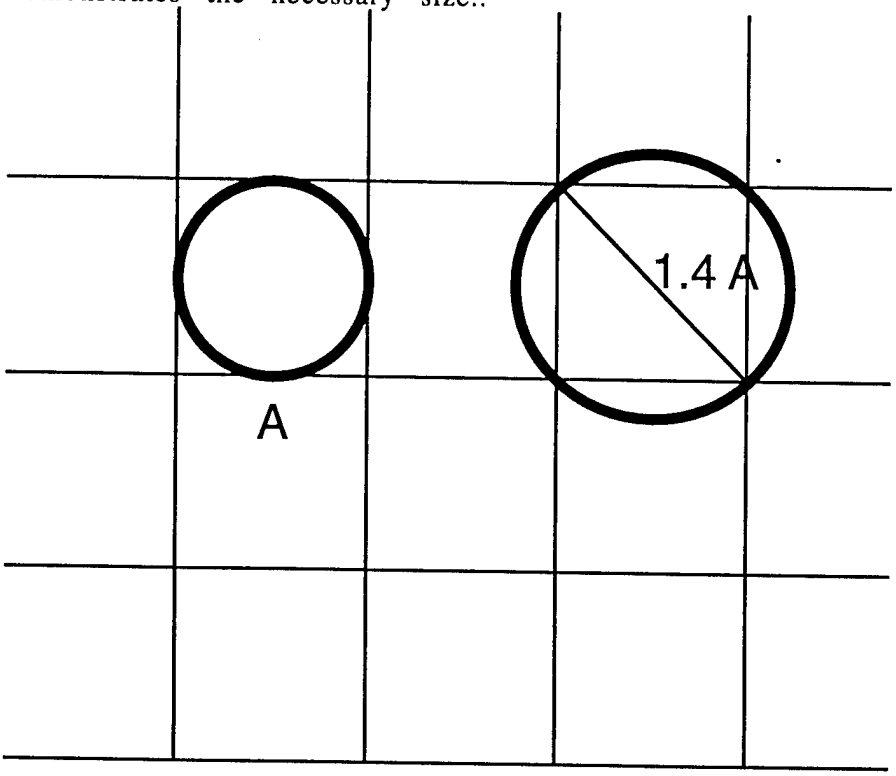

Figure 1: A sphere within a pixel has the same diameter as the pixel, but fills only 50% a cubic voxel of the same size. To fill a pixel of size A, need a sphere, if centered on pixel of size A, by Pythagorean Theorem: A $\sqrt{2}$.

4.5.1.2 EFFECT IF OBJECT IS NOT CENTERED TO PIXEL

If the spherical calcium object is not centered to the pixel, then the offset will result in less of the pixel being filled. If calcium is $\sqrt{2}$ A, minimum density will be 1/4 of that if pixel completely filled. (37% filled, but because of sphere only 1/4 of density) as shown in Figures 2 and 4.

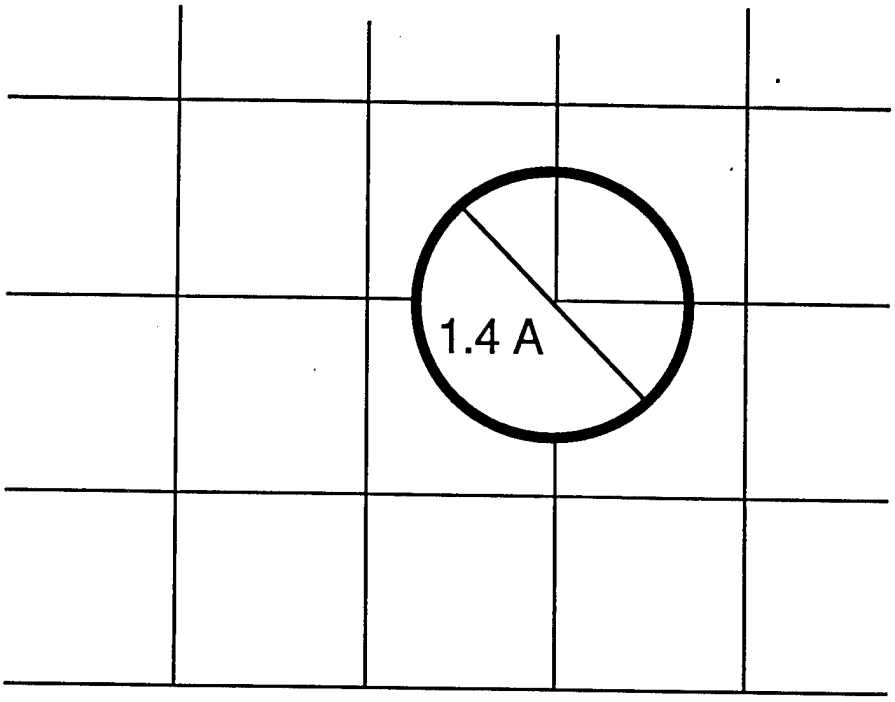

Figure 2: Drawing showing effect of maximal offset of $\sqrt{2}$ A sphere on area of pixel filled.

This positioning does not appear to be sufficient contrast to be detectable in experimental tests.

If offset maximal amount (oblique)
need 2A $\sqrt{2}$ to be certain that at least one pixel is completely filled.

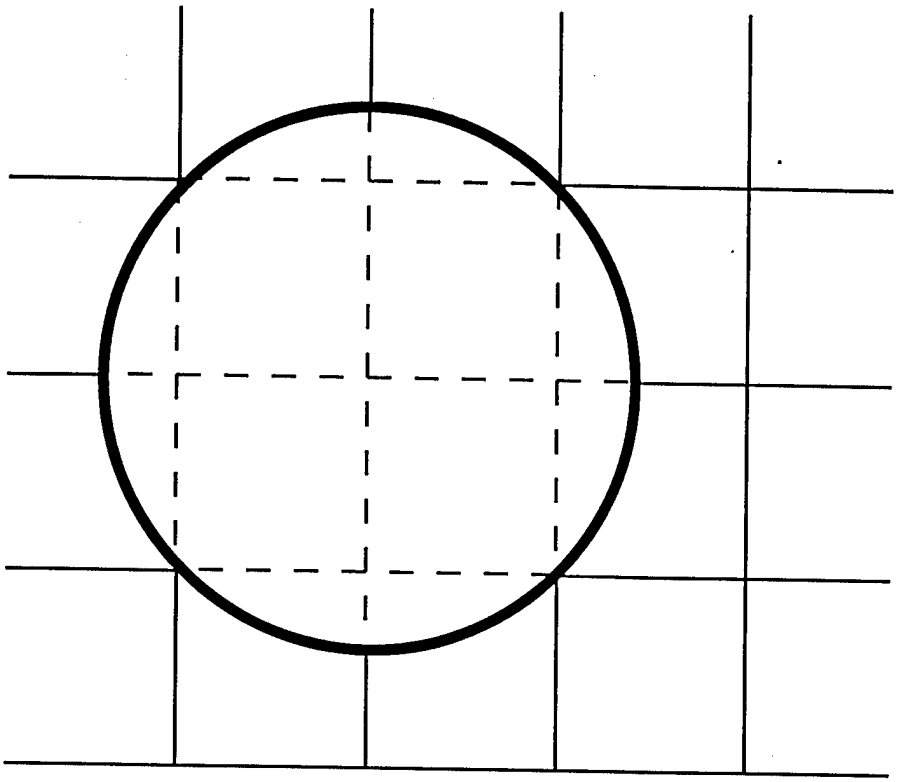

Figure 3: Drawing of sphere of diameter 2A $\sqrt{2}$ offset to corner of pixel.

Therefore in order to see a small calcific object with a detector with pixel size A, one needs a 2A $\sqrt{2}$ sized object. This hypothesis is supported by our experimental evidence.

Standard sized objects on mammographic phantoms are at 160, 240, and 320 microns. In order to see a

320 micron object need 114 micron pixel
240 micron object need 85 micron pixel
160 micron object need 57 micron pixel

On the phantom used for American College of Radiology certification, one needs to seen the 320 micron objects and some screen-film systems allow detection of 240 micron objects at least part of the time. Thus to equal screen-film one should be aiming either for a 114 micron or an 85 micron pixel size.

4.5.1.3. FILLING THE PIXEL: EXPERIMENTAL EVIDENCE

In the actual experiments (experiments listed in appendix as I-A), one does slightly better than this because the focal spot size in finite and therefore there is a penumbra around the small object enlarging its projected size. Thus, in tests, we can just faintly see the 160 micron object with 83 micron pixel. While this suggests that one may need only 2 A, rather than 2 A $\sqrt{2}$ to see object given contrast enhancement possible with image processing, actual measurements of the objects in the phantom indicate that as projected onto conventional screen film systems, that the objects and their penumbra are actually larger. This is shown in the following table:

MEASURED ALUMINUM SPECKS IN "ACR" PHANTOM

STANDARD	INSERT ONLY		COMPLETE	
	SF	SR	SF	SR
540:	650	650	700	700
400:	600	600	650	650
320:	350	450	400	450

In microns

SF = Screen Film Image
SR = Storage Phosphor Image

Differences due in part to magnification, Penumbra

MEASURED OBJECTS IN CIRS DETAIL PHANTOM

Calcium flecks in microns

Standard	Screen-Film SR		SR 1.5 X
390	700	700	1000+
270	500	500	800
230	400	400	600
200	300	350	500
160			300

Thus, these measurements suggest that the actual projected size of the 200 micron flecks seen on the CIRS phantom with a 100 micron pixel size are really 300 microns and the 160 micron aluminum hydroxide flecks seen on the RMI phantom with an 83 micron equivalent pixel are really probably about 200 microns supporting the theoretical model of a pixel of size A can detect a calcium object 2 A $\sqrt{2}$.

4.5.1.4 MEASURED SIZE OF CALCIFICATIONS IN BREAST BIOPSY SPECIMENS

Measurements using an 8 X magnifier and measuring reticle demonstrated that in 10 contact specimen biopsies radiographs (20 line pair system) that most of the calcifications that could be resolved as individual objects measured 300-600 microns. There were some 200 micron calcifications that could be individually identified, and then there were areas of calcification with particles that could not be resolved. Since this tested system has less noise, less scatter and less penumbra than any conventional screen film mammogram could have, we believe that the lower limit of size that we need to resolve for clinical purposes in 200 microns.

4.5.1.5 EFFECT OF NOT FILLING PIXEL

To better understand the implications of this model, it is helpful to understand the implications of failure of the projected object to completely fill the pixel. The effect is analogous to the partial volume effect seen with computed tomography. One sees decreased contrast.

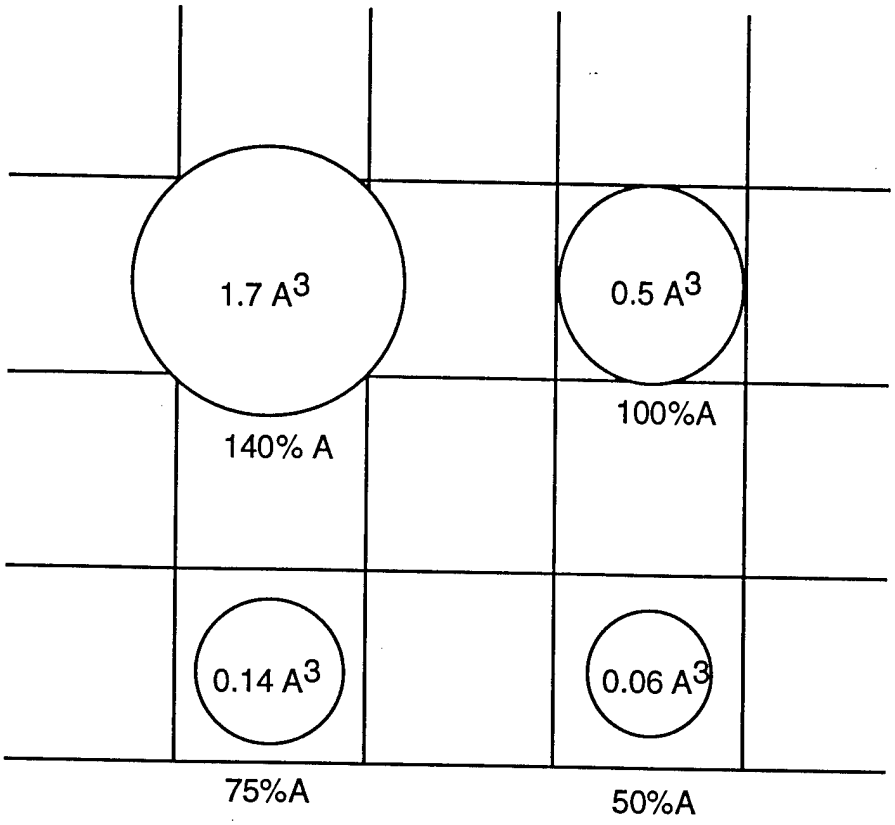

Figure 4: The volume of calcium projected in sphere of pixel size A with spheres of different sizes projected in center of pixel. (Based on solid geometry formulas.)

There is a rapid decrease in density when sphere is smaller than pixel size.

4.5.2 IMPLICATIONS OF THIS HYPOTHESIS:

4.5.2.1. The Direct Hit Phenomenon:

In this model we have assumed that the shadow from the calcium fleck will be maximally offset from the center of the pixel. In actual practice one would expect that intermittently, the shadow would fall directly on the center of a pixel and thus one could occasionally see a calcium object that is the size of the pixel (assuming that the calcium object and its penumbra completely fill the pixel. Calcium flecks intermediate in size between pixel size and 2 A $\sqrt{2}$ have an increasing chance of having their shadow projected directly over a pixel with the likelihood increasing as the size of the calcium fleck increases. The formula 2 A $\sqrt{2}$ is the size necessary to assure visualization.

4.5.2.2. The increased radiodensity phenomenon:

We have confirmed the model using calcium or aluminum hydroxide flecks in the phantom. Objects of increased radiodensity can be seen at smaller sizes. We found using the CDMAM phantom (Nuclear Associates) (experiments listed in appendix as IV-A-1)that an object that is visible at 320 micron diameter and thickness can also be seen with a 100 micron pixel. When the thickness is 1000 microns, its diameter need only be 130 microns. (if one offset an object A $\sqrt{2}$ times the pixel size by its maximal amount, it would fill 37% of the volume that would be filled if it were centered on the pixel. Thus the theory holds approximately.

The clinical applicability of this is that when there are malignancy associated calcifications, there are often many of them and they may be superimposed on each other, and thus visible at a smaller size. While this will help in many cancers, there are cancers with only a few calcifications. These will not have superimposed calcifications and will not demonstrate this phenomenon.

4.5.2.3. The signal to noise phenomenon:

This model is based on a receptor with a signal to noise ratio of the Fuji storage phosphor imaging plates and plate reader. The system in our experiments is noise limited. In our experiments, increasing the exposure to improve the signal to noise ratio improves the detectability of small objects. (experiments listed in appendix as IV-D) Therefore anything done to improve the signal to noise ratio will decrease the minimum size detectability: either better electronics or better receptors.

4.5.2.4 IMPLICATIONS FOR DIFFERENTIATING DUST PARTICLES FROM TRUE MICROCALCIFICATIONS

In our initial experiments we found that the digital system had many calcium fleck like artifacts. Because we believed these to be dust, we investigated the appearance of dust particles on storage phosphor systems. We found two effects: (1) dust reflected more light than is normally emitted by the phosphor screen, resulting in a high signal to noise ratio spot; (2) dust prevented the erasure of regions under dust particles resulting in a black spot on the subsequent image.

The high signal to noise ratio induced by the reflection of dust particles means that they can be seen at a smaller size than true areas of decreased light emission that result from the shadow cast by a true microcalcification. Thus it becomes possible to correctly differentiate some dust particles from true microcalcifications. Easily seen objects close to 1 pixel diameter is size are usually dust particles and should not be confused with microcalcifications.

Larger dust particles can be confused with microcalcifications and therefore one must keep the digital system unusually clean. Unlike dust in a screen-film system where the dust interferes with the exposure of the film and therefore creates an unusually bright, sharp edged defect, dust on a phosphor plate tends to result in an image that is not very different in brightness or edge characteristics from that of a true calcium particle.

4.5.2.5 IMPLICATIONS RELATED TO CHARACTERISTICS OF POTENTIAL DIRECT DIGITAL DETECTORS:

For systems with a signal to noise ratio at standard mammographic exposures similar to that of Fuji's storage phosphor imaging plates and plate reader lasers and electronics, one should consider 114 to 85 microns as the desired maximal pixel size.

One could expect to improve the detectability of small objects either by decreasing pixel size or improving signal to noise ratio.

One could decrease the effective pixel size either by developing a device with a smaller pixel or by using direct geometric magnification onto a receptor with a larger pixel size than optimally desired. (experiments listed in appendix as I-A,B,C,D) Advantages of using direct geometric magnification are that one may be able to use a receptor with higher radiation sensitivity than the high resolution systems provide, thus decreasing

patient dose. One could also use existing detectors without having to develop new detector systems. The disadvantages of using direct geometric magnification are that at least some current mammographic units do not have enough spread of the x-ray beam through the built in collimator to cover the whole breast in the magnification mode. Also the focal spot size of the x-ray tube would result in a larger penumbra around the actual object. There is also the potential for this system to exaggerate motion unsharpness by inadvertent patient motion.

One could improve signal to noise ratio either by having improved detectors or by accepting an increase in exposure. Our experiments demonstrate that an increased exposure does result in smaller objects being seen. (experiments listed in appendix as IV-A,D)

4.6 THE POTENTIAL FOR DECREASING EXPOSURE USING DIGITAL SYSTEMS:

In our tests, we found that the Fuji high resolution plates appeared to require the same exposure as our standard screen-film system for the demonstration of equal information. In the experiment (experiments listed in appendix as IV-A-1,2,3,4) that we did comparing the effect of decreased exposure on detectability of objects in the CDMAM phantom, we found at the lowest exposure level we tested, that the digital system performed better than the screen-film system, but we found in a small sample that only 1 of 20 of our cases had any region in the breast with such a low exposure and that these regions were clinically underexposed. Once we exceeded this minimal exposure, the screen film system performed better. This was an early experiment before we had reached our current knowledge of image processing, and will need to be reevaluated. Our preliminary data suggests however that there will be no potential decrease in exposure possible, unless one is willing to work with less information than screen film systems provide.

Other work in which we did direct geometric magnification onto a standard phosphor plate demonstrated that with appropriate image processing, that one could see more on magnification views with a lower exposure than on magnification views recorded on screen film systems. (experiments listed in appendix as I-B) This suggests that one should evaluate the value of doing geometric magnification views onto higher sensitivity, but lower resolution film than is used for standard mammography. Other work done elsewhere suggests that there may be value in using direct geometric magnification on all mammograms.

4.7 FILM DIGITIZATION:

Work done in our labs (experiments listed in appendix as II-A) indicated that film digitization at 170 microns was insufficient to allow detection of smaller microcalcifications. Work done by Chan (11) has indicated that 100 microns is either just sufficient or just insufficient for detection of microcalcifications.

We have done a limited amount of investigation of an experimental 35 micron film digitizer at the manufacturers office. Our experiments (experiments listed in appendix as II-B) with this device suggest that there may be some value to using film digitization for digital mammography. A version of this device will be placed at Georgetown shortly and next years report will detail our results more fully.

The preliminary studies suggest that the use of a 35 micron film digitizer coupled with appropriate image processing may allow the replacement of direct geometric magnification with electronic magnification. (12) With electronic magnification, the

conventional screen film image is digitized at 35 microns. A small section of this is then displayed as an enlarged image. With appropriate image processing, it is possible to see calcifications and details in shapes of calcifications that cannot be seen either directly or with a magnifying glass on the original image.

The benefit does not appear to come from the magnification, since the type of hand held magnifier commonly used by radiologists when they interpret screen film mammography is sufficient to detect 30+ line pairs per mm of high contrast detail. The benefit appears to result from the image processing that allows improvements in object contrast that occur from gray scale changes and edge enhancement. Our experiments suggest that film digitization with very small pixel sizes may prove to be a viable method for digital mammography.

We will be continuing our research with a 42 micron film digitizer when a machine arrives at our site early in 1994.

5.0 IMAGE PROCESSING:

Image processing is the second major component of digital mammography. Correct image processing enhances the ability to see abnormalities in digital images. Incorrect image processing can conceal information. there have been a few publications on optimizing image processing in chest images including several of our own, but we are not aware of publications on optimizing image processing in digital mammography. We presented our preliminary material at the annual Meeting of the Radiologic Society of North American in December 1994. (13) We will be presenting this material at the meeting of the Society of Photo-optical instrumentation Engineers (SPIE) in February, 1994 and this report will be published as part of their Proceedings. Apart from our own work in image processing in digital mammography and limited work done by Chan (11) on digitized film images, we are unaware of any reports of similar work.

5.1 The Types of Image Processing:

Image processing as currently available consists of three main potential changes in the image. These are changes in the look up table (LUT) to affect optical density and contrast, changes in spatial frequency to effect either edge enhancement or noise reduction, and methods for balancing the optical density in an image (often called histogram equalization) in order to better match the original information to the characteristics of the display device used. Each of these provides an important advantage to diagnosing breast cancer on digital mammography. Image processing can be used on any digital mammographic image, independent of the method used for acquiring the digital image. The techniques are the same for different digital detectors and for both direct digital and film digitization methods.

5.1.1 CHANGES IN LOOK UP TABLE:

Changes in the look up table change the way in which the acquired information which is related to the exposure received by the imaging plate is mapped to a specific optical density or luminance on the display device. This mapping is important because the original receptor may be linear or non linear in its response and all current display devices are non-linear, but differ in their non-linear response characteristics. If one considers only the display devices, for the moment, the response characteristics are characterized by a non-linear S-shaped curve. This curve, well described for film as the H and D or characteristic curve is also reflected in the pattern of display seen in the luminance values on monitors (14).

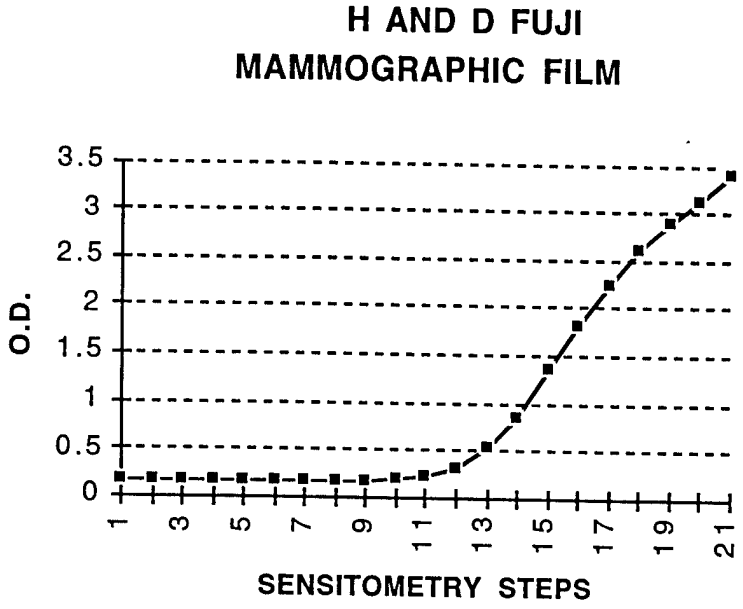

The characteristic curve is S-Shaped and is usually divided into three sections for discussion purposes: The toe, the shoulder and the central portion. The contrast in the toe (bottom) and shoulder (top) of the curve is less than that in the central portion of the curve. For digital mammography, the most important regions are the toe (the region of low exposure) and the central portion (where the highest contrast is). The dense breast is one in which there is a large amount of tissue that is close to the density of calcium. If this region of breast density is mapped into the toe region of the characteristic curve, then all structures in that region will be of lower contrast. If the calcifications are projected in a region of increased breast radiodensity, then they will be of low contrast compared to the background tissue and therefore more difficult to see. The application of changes in the LUT to change the final optical density and contrast are to change the optical density of the region where calcium could be partially obscured by shifting densities to the region above the toe of the characteristic curve and to increase the slope of the characteristic curve in regions of increased breast radiodensity.

In our evaluation of changes in the LUT (experiments listed in appendix as IV-A-1,2,3,4,B,C), we recorded the characteristic curve of the screen film system used for our current mammography, a second screen film system and then measured the optical density of mammograms in our collection at the sites where cancer had been found. In 1 of the 20 measured, the microcalcifications associated with the cancer were in a region where the optical density of the region of that breast was in the low contrast region of the toe of the characteristic curve. Thus a simple remapping of the optical density to a region above the toe of the characteristic curve would have improved the detectability of the calcifications in 5% of this small sample. A second experiment in which we changed the LUT of a digital image of the CDMAM phantom so that it was printed at different optical densities confirmed that at low OD, there was less detectability of objects, but that once one was above the toe of the characteristic curve, the detection rate did not change over a wide range of OD values.

Increasing the contrast in the steepest portion of the characteristic curve should also help in the detection of microcalcifications. Our preliminary tests suggest that there is

a limited range of this effect from a contrast value of roughly GA = 0.8 to GA = 2.5. Above and below this range, the detectability decreased. Within this range our preliminary results detected no change. Above GA = 2.5, the accentuation of noise limited the visibility of objects in the image of the phantom.

5.1.2 SPATIAL FREQUENCY CHANGES:

All images are composed of a combination of many spatial frequencies. High spatial frequencies correspond to sharp edges. Low spatial frequencies correspond to smooth edges. Several methods exist for altering the spatial frequency patterns within an image. Our work was done with a method called unsharp masking using a convolution kernel of various sizes. In this method, a kernel representing an array of numbers is multiplied by the pixel values in the image changing its final appearance. The method used was that of Fuji in which kernels of different sizes are named as settings of an RN factor and vary from 0 to 9. The emphasis given to this spatial frequency effect is named the RE factor and varies from 0 to 16. In addition there is an additional effect acting on the image only in regions of low optical density called the RT factor. The RT factor is used to decrease the visibility of noise at low exposure/low optical density regions of the image.

We tested various combinations of RN, RT, and RE settings in mammography phantoms. (experiments listed in appendix as IV-E) Our results indicate that the detection of microcalcifications is improved by small kernel sizes and by intermediate to high settings of frequency enhancement. Larger kernel sizes aided in the detection of small masses. None of the factors tested had much effect on the detection of fibers. Because the best detection of microcalcifications occurred with the smallest kernel size, it is possible that a still smaller kernel size could offer additional improvement. We found that certain of the settings, especially those with a larger kernel size or with a large amount of spatial frequency emphasis improved the detectability of objects in mammographic phantoms, but resulted in digitally obtained breast images that were sufficiently unusual in appearance that they would likely be rejected by radiologists. A setting that best demonstrated small masses could also obscure microcalcifications and visa versa. (experiments listed in appendix as IV-F)

Based on our preliminary data we now consider that settings of GA = 1.5, RN = 9, RE = 5 to be a partially optimized set of values for image processing of digital mammography.

The effect of this setting is shown in the two graphs below. In the first, the image processing setting recommended by Fuji for digital mammograms is used. For all small objects, the screen film system performs better. In the second graph, the change in image processing following our optimization procedure indicates that with proper image processing, screen film and digital mammography show equal detectability of objects on the CDMAM phantom.

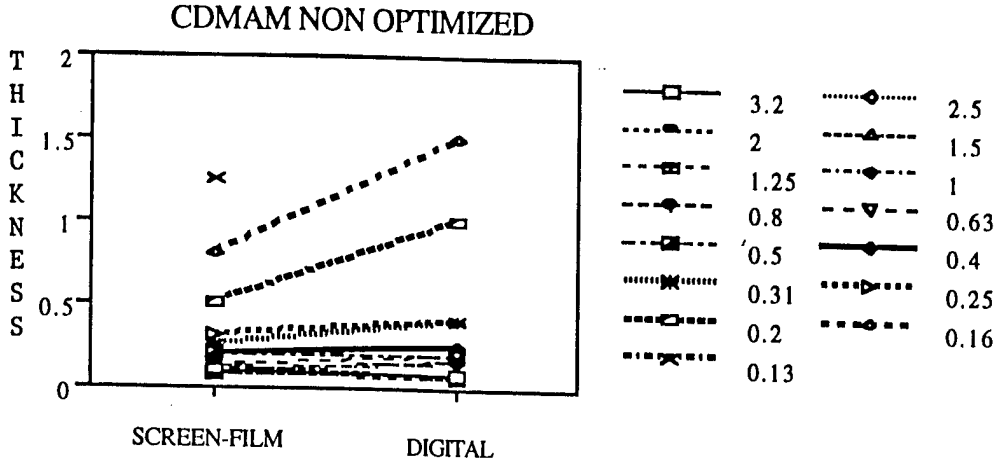

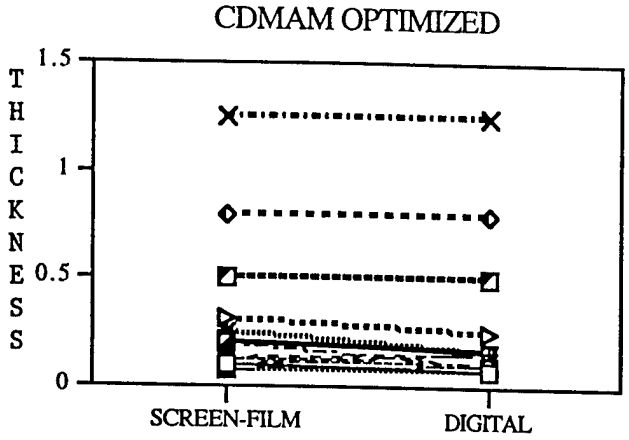

5.1.3 OPTICAL DENSITY ADJUSTMENT METHODS:

The range of radiodensities in the breast is wide and their distribution is unequal. On conventional screen film mammography it is difficult to have adequate contrast in the more radiodense regions of the breast and still have sufficient range of visible densities to adequately see the skin thickness. There are available methods for adjusting the range of optical densities within a final image that allow different optical density regions to have different LUT. These methods, sometimes called histogram equalization methods could be useful in the display of digital mammography. In late December, 1993, we had such an investigational device implemented on the Fuji system we use for digital mammography. We will be investigating the effect of this in 1994.

6.0 IMAGE DISPLAY

Image display is an essential part of digital mammography. Conventional screen film mammography allows the display of 20 lp/mm of high contrast information. At the lower contrast range in which mammography falls, however, it is somewhere between 2.5 to 5 lp/mm actual resolution. Conventional breast images are most often 8 x 10 inches, but in about 10% of cases, 10 x 12 images are produced.

There are two potential methods for the display of digital mammography: Display on workstations and display on laser prints. These two methods for display of

digital mammograms are limited in their capabilities and new methods are unlikely to emerge in the near future.

When one displays digital information, the display can be of different sizes. One therefore has to consider the number of pixels in the total display as well as their spacing. Using a larger monitor does not increase the number of pixels displayed, but may display them at a size that is easier to interpret due to the magnification resulting from the larger display. With laser camera prints, the limit is 300 dots per inch. The larger the film, the more pixels that can theoretically be displayed.

6.1 Pixel Size and Number Related Factors:

6.1.1 Display on a Workstation:

The highest pixel number available on workstation monitors is 2,048 x 2500 pixels. If one is projecting an image of the breast originally obtained on an 8 x 10 inch receptor, this implies that one would be limited to displaying 100 micron data if one wished to display the entire image at one time. As indicated above, this would result in an image that would approximately equal the image of screen film mammography.

If one captured the data at a smaller pixel size, one could not display the entire image at this higher pixel size, but would have to scan through the image region by region magnifying each section of the image to assure detection of microcalcifications.

6.1.2 Display on a Laser Print:

Laser print systems are currently limited to 300 dots per inch (DPI). If one is using 14 x 17 inch film, this is equivalent to approximately 4,000 x 5,000 pixels. Thus one could display a single breast at a size of 14 x 17 inches and thus display an image that used a 50 micron pixel on an originally sized 8 x 10 inch image. If one chose to display the image close to its original size of 8 x 10 inches, then one would be able to display the whole image with only 100 micron resolution.

6.2 The Effect of Image Display Size:

The effects of image display size are different for monitors and laser film prints.

6.2.1 Display on a workstation monitor:

Workstation monitors are limited to approximately 2000 x 2500 pixels. As one changes the size of the monitor, the number of pixels remains the same, but the size of each pixel in the display changes. When radiologists interpret screen film mammography, they usually use a magnifying lens to magnify the microcalcifications to make them more apparent. Typical magnification glasses used are 2 X or 3 X magnifiers. The use of such a magnifier allows as much as 30 line pairs of high contrast detail to be seen based on tests. Thus this use of a magnifier lens exceeds the high contrast resolution of screen film mammography. The best display size for digital mammograms is yet to be determined. Based on the measurements made with the hand magnifier, we will test monitors of different sizes in 1994 using

monitor displays of different sizes using image processing optimized images of breast phantoms. Our hypothesis is that displaying the image at 1.5 X normal size (12 x 15 inches) will likely provide full benefit, but we will also test larger sized monitors.

6.2.2 Display as a laser print:

Current laser print technology is limited to 300 dots per inch (dpi). According to our industrial sources higher resolution systems are not likely to be developed in the near future. There are at least two different methods of positioning information within each of the dots: the standard half-tone method and the Scitex patented method which divides each dot into multiple smaller dots for printing purposes. (15) The Scitex method currently only prints on paper, but appears to give a visually smoother image than halftone methods meaning that the edges of pixels are less apparent on image magnification. We are working with Scitex to test their system for the display of digital mammography.

With laser technology limited to 300 dpi, the choice of the desired resolution affects the final image display size. Currently, these have a maximal 4096 x 5000 in 14 x 17 inches. This means that each pixel in the final image is approximately 86 microns in size. If one starts with an 8 x 10 inch image of the breast and divides that image into 4000 x 5000 pixels, then each original pixel is 50 microns. Thus one can display a 50 micron image with slight magnification on a 14 x 17 laser print.

The effect of such a large image on the interpretive abilities of radiologists in not known to us. This would need to be tested.

7.0 COORDINATION OF RESEARCH WITH MILITARY MEDICAL CENTERS

Coordination of the research projects with radiologists at Madigan Army Medical Center (MAMC) and Brooke Army Medical Center (BAMC) has been underway since the award of the contract. Face to face discussions have been have been held with Col Sam Babu, M.D. and Major Donald Smith, M.D. at MAMC and with Col Anna Chacko, M.D., Major Michael Cawthon, M.D., and Major Robert Shah, M.D. at BAMC. Direct coordination of the projects will be with Majors Shah and Smith. Currently, these two have been kept informed of our progress in digital mammography and are collecting cases for film digitization for incorporation into the research project. Once the digital systems are ready for clinical tests, detailed planning sessions will be held with them regarding research design and the implementation of the ROC studies will be done jointly at MAMC, BAMC, and Georgetown.

Evidence of our ability to work in a collaborative relationship with the DoD is demonstrated in the attached bibliography (Appendix B) which lists recent joint publications of Georgetown and DoD physicians and scientists. I have underlined the names of the DoD participants. While the papers reported do not deal with mammography, but with other topics, we expect this pattern to continue as publications in the clinical aspects digital mammography occur.

8.0 SUMMARY:

During the first year of this research grant we have done a large number of small projects to define the essential parameters for digital mammography to be successful. We believe that our work to date has given us a much better understanding of the parameters necessary for proper image acquisition, image processing and display, and that this preliminary data will allow us to proceed rapidly with the remainder of the project.

This project was focused in defining the characteristics of existing digital mammographic systems and to test their applicability for digital mammography as a replacement for conventional mammography.

9.0 THE ASSIGNED TASKS FOR THIS PROJECT ARE:

1. *Evaluate the current status of existing digital mammography systems for direct digital mammography and film digitization.*

This is well underway with major factors defined.

2. *Develop a strategy for the optimization of these existing systems including optimization of KVP and MAS.*

The optimization method is underway and has demonstrated substantial improvement in image quality in digital mammography.

3. *Compare the accuracy of these existing systems to conventional screen film systems if the systems appear to be adequate replacements for existing screen film systems using ROC methodology.*

Using three mammographic phantoms initial comparisons have been performed. Clinical tests await further improvements in technology and will be conducted in 1995. Once the system is felt to be of sufficient quality, ROC studies will be performed. Radiologists from Georgetown, MAMC and BAMC will be involved in the ROC studies.

4. *Provide recommendations about how these systems could be implemented to replace existing screen film mammography:*

These recommendations will depend on further investigations. Data for the final implementation report are being gathered. Additional data is needed prior to recommending the best method for implementation. The results of all experiments will be incorporated into an implementation document that will be available at the conclusion of the contract.

BIBLIOGRAPHY:

1. Voegeli E. Special Investigation Comparing Digital with Film-screen Mammography. Digital Radiography Workshop: Quality Assurance and Radiation Protection. May 7-9, Mannheim. Schnetztor - Verlag; 1992: 90- 91.

2. Panizza P., Del Maschio A. Digital Luminescence Mammography. Digital Radiography Workshop: Quality Assurance and Radiation Protection. May 7-9, Mannheim. Schnetztor - Verlag; 1992:66-67.

3. Panizza P., Cattaneo M., Rodighiero M.G., et al. Course on Digital Radiology and PACS Technology - Clinical Application: Breast (L'Aquila) Scuola Superiore G. Reiss Romoli.1990; 2:43-62.

4. Statement of the Expert Group on "Perspectives of Digital Mammography." Digital Radiography Workshop: Quality Assurance and Radiation Protection. May 7-9, Mannheim. Schnetztor - Verlag; 1992: 102.

5. Oestmann J-W., Kopans D.N., Greene R.E. Digital Radiography in Breast Disease. Computed Digital Radiography in Clinical Practice. 1992: 139-146.

6. Shtern F. Digital Mammography and Related Technologies: A Perspective from the National Cancer Institute. Radiology 1992; 183:629-630.

7. *Digital Imaging in Diagnostic Radiology.* Eds. John D. Newell, Jr., M.D. and Charles A. Kelsey, Ph.D. Churchill Livingstone, New York. 1990: 66-70.

8. Freedman, M., Mun, SK, Pe, E, Lo S-C B, Nelson M: Image Optimization on the Fuji AC-1. SPIE: Medical Imaging (1993) Paper 1897-51.

9. Freedman M, Zuurbier RA, Pe, E, Jafroudi H, Mun, SK, Lo, S-CB: Image Processing of Musculoskeletal Images (abstract). Radiology (1993), 189 P: 381.

10. Oestmann, J.W., Kopans, D, Hall, D.A., et al. A Comparison of digitized storage phosphors and conventional mammography in the detection of malignant microcalcifications, Invest Radiol 1988; 23:725-728.

11. Chan, H-P., Vyborny, CJ, MacMahon, H., et al. Digital Mammography: ROC Studies of the Effects of Pixel Size and Unsharp mask filtering on the detection of subtle microcalcifications. Invest Radiol 1987; 22: 581-589.

12. Dawkins, T, Freedman M, Lo S-C B, Mun SK. 35 micron CCD Based Film Digitizer for Mammography. SPIE: Medical Imaging, February 1993, Paper 1897-53

13. Freedman M, Zuurbier RA, Pe, E, Jafroudi H, Mun, SK, Lo, S-CB: Image Processing in Digital Mammography (abstract). Radiology (1993), 189 P: 408.

14. Lo S-CB, Freedman M, Steward D, Mun SK: Contrast Characteristics on CRT Display Monitor. IMAC 91, Kyoto, Japan 1991, Proceedings pp 342-247.

15. Kirkhorn T, Kehler M, Nilsson J, et al. Demonstration of Digital Radiographs by Means of Ink Jet-Printed Paper Copies: Pilot Study. J Digital Imaging 1992; 5: 246-251

APPENDICES:

A. BRIEF SUMMARY OF EXPERIMENTS PERFORMED

B. LIST OF COLLABORATIVE ARTICLES WITH DOD PHYSICIANS AND SCIENTISTS

APPENDIX A: BRIEF SUMMARY OF EXPERIMENTS PERFORMED:

EXPERIMENTAL PHANTOMS USED:

1. RMI 156 PHANTOM: This phantom is used for certification procedures of the American College of Radiology. In contains fibers, aluminum oxide flecks and small masses.

2. The Nuclear Associates Round Phantom: This is an older mammography phantom containing microcalcification clusters and fibers of different widths.

3. The CIRS square detail phantom: This contains Aluminum oxide and calcium fleck clusters, small masses, and fibers.

4. The CIRS hemicircular phantom: This contains the same objects as #3, but can be used to test for different radiodensity breast composition (fatty vs water radiodensity)

5. The Nuclear Associates CDMAM Phantom: This consists of a series of electroplated gold disks of different diameters and thicknesses. This disks are placed in a non memorizable distribution of positions. This is a very sensitive contrast detail phantom, but its structure interacts with the Fuji RN-3 unsharp masking method producing distorted images.

THE EXPERIMENTS:

I. Experiments related to use of magnification onto 200 micron pixel (Fuji ST-3 imaging plates) and onto 170 micron pixels (AGFA experimental imaging plates:

A. Direct geometric magnification of RMI mammography phantom, Nuclear Associates Round phantom and CIRS phantoms.

Magnification factors: 1.5, 1.7, 2.0.

Image processing: Fuji standard and AGFA standard processing with optimization of image processing settings based on appearance of image on workstation monitor.

Findings: One can see most small objects if one uses pixel size approximately 1/2 of nominal size of object desired to be seen. It is possible with 2 x magnification and with proper image processing to see all objects on RMI phantom used for ACR certification at same exposure used for non-magnified image on screen film system. This system is limited to a 4 x 6 inch field of view, but can exceed visibility of screen film systems and exceed resolution requirements for ACR certification.

B. Effect of KVP changes in decreasing total exposure required to make an image. Demonstrated that by increasing exposure to 32 KVP that one could decrease exposure (in mR) to 1/3 that of standard screen film exposure and still show the same information in the Round phantom, which is one that contains calcium flecks. This effect could not be

reproduced in the RMI phantom possibly because the RMI phantom uses aluminum flecks rather than calcium flecks and the KVP affects the absorption of calcium and aluminum differently. The decreased exposure was probably related to the increased sensitivity of the Fuji ST-3 imaging plates.

Increasing the KVP to 36 resulted in images inferior to those of screen film since one could not correct for the contrast changes caused by the higher KVP by available image processing techniques.

Significance:

1. Using direct magnification onto a higher sensitivity receptor can improve detectability of objects compared to standard screen film mammography such that one can decrease required exposure.

2. Increasing KVP may provide a method of decreasing patient exposure using the image processing possible with digital information to restore the contrast lost with increased KVP.

3. Image processing can only correct part of the changes occurring with increased KVP. There is a limited range in which this correction is possible with existing image processing software.

C. Images made of breast biopsy specimens testing different methods of image processing:

Five breast biopsy specimens were radiographed using 1.7 X magnification onto a Fuji ST-3 imaging plate. These images were then subjected to a systematic pattern of image processing methods to look for enhancement of breast microcalcifications. Selected combinations of GA, GT, GS, GC, RN, and RE factors were tested to gather preliminary data for optimization of image processing for digital mammography.

Findings:

1. Exposure factors are important in that the settings that best demonstrate the calcifications also accentuate the appearance of noise: underexposed images can be "smoothed" using RT factors only with probable loss of information about microcalcifications.

2. Adjustment of the GS and GA factors to produce a pseudo threshold appearance for microcalcifications so that the calcifications are white against an almost black background were very attractive. This proved to be a clinically inapplicable method because it relied on there being a relatively homogeneous fatty background to the calcifications. In a breast with more tissue structure, this thresholding did not produce satisfactory images.

D. Magnification of specific lesions in women for clinical indications. The methods described above were used in two women in whom the greater visibility of microcalcifications possible on digital methods was considered to be clinically important. These were not research cases, but clinical cases. In one case the system demonstrated with greater certainty than screen film small microcalcifications in a lesion that on biopsy proved to be a fibroadenoma. The second case demonstrated that the calcifications were skin calcifications and did not require biopsy. In both cases, the calcifications were more

easily seen on the magnification digital views than on screen film magnification views due to the image processing that could be done.

II. EXPERIMENTS ON FILM DIGITIZATION OF MAMMOGRAMS:

A. Film digitization at 200 microns: 5 mammograms containing calcifications were digitized using a Dupont laser film digitizer. While the presence of calcifications in all five mammograms could be seen to be present, fewer calcifications could be seen and the detectability of shape was less on the digitized mammograms displayed on an ATT Comview workstation than on the original images.

B. Film digitization at 35 microns: Using a 35 micron prototype film digitizer in the offices of DBA Inc. a series of 10 mammograms containing calcifications were digitized. These were viewed on their workstation as magnified sections of images and were compared to direct geometric magnification mammograms of the same regions of microcalcification. We were able to demonstrate to those present that with electronic magnification that the calcifications could be seen on the workstation at least as well as on the geometric direct magnification views. Currently we have been unable to create adequate hard copies of these images to do a formal test of whether or not electronic magnification is a viable replacement for screen film direct geometrical magnification views. Since we currently call back approximately 1 of every 50 patients for direct geometric magnification views, we see the potential of this method for decreasing call backs and the patient anxiety associated with them as being important for further research. We should have this film digitizer on site early in 1994.

III. EXPERIMENTS IN IMAGE PROCESSING:

In September of 1993, we received the Fuji Mammography attachment for their storage phosphor imaging system. This is the only FDA approved digital mammography system.

A. We did tests of the system on the RMI, CIRS, and CDMAM Phantoms and found that using the system with the image processing parameters recommended by Fuji on all three phantoms that the images were inferior to conventional screen film systems. Our initial tests from the CDMAM phantom are shown in the following graph which demonstrates that for all smaller objects, the system either did not see the object or required that for a given diameter that the object be thicker.

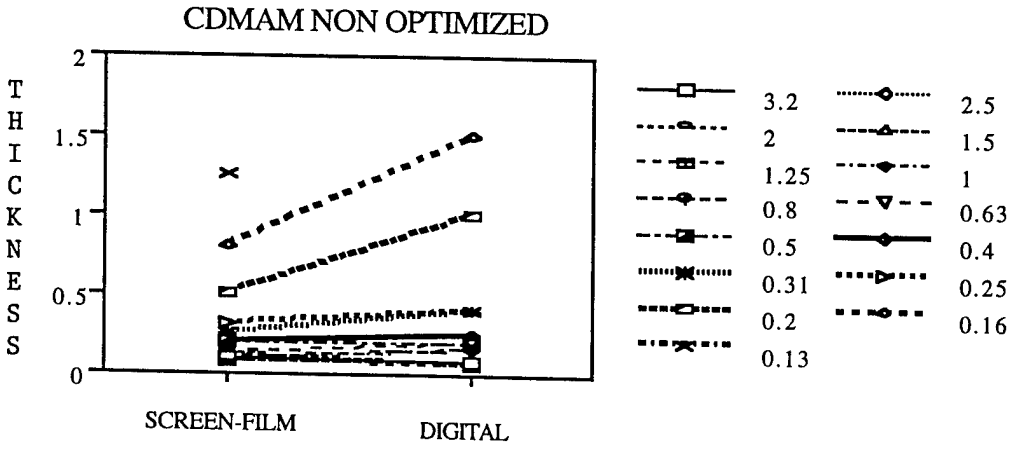

B. Tests of line pair high contrast resolution: Tests using a standard Nuclear Associates line pair phantom demonstrated that the system could only provide 4.5 lp/mm instead of the 5.0 lp/mm that it should meet according to specifications. Fuji was contacted and asked to make certain that the system was performing satisfactorily. After their check, optimization procedures for image processing were undertaken.

C. Tests after multiparameter optimization: Tests after the multiparameter optimization procedures (which are described below) show that for the CDMAM phantom, that following optimization, the system performed equivalently to screen film images.

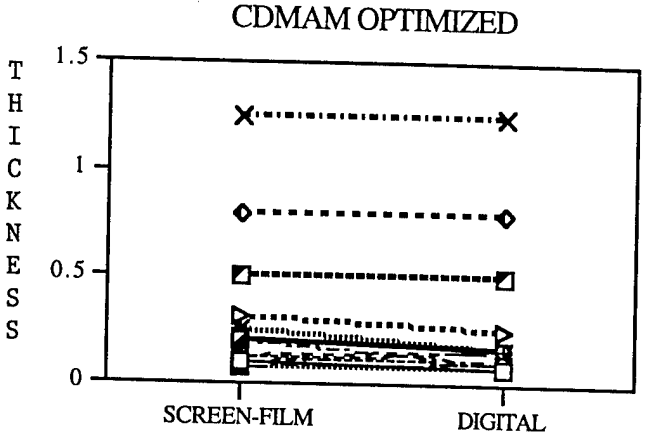

IV. Multiparameter optimization:

A. Exposure tests:

1. Images of the CDMAM phantom were obtained on screen film and Fuji HR-V imaging plates at 26 KVP at 4, 5, 6, 7, 8, 9, 10, 12, 16, 19, 20 MAS and were individually scored. These tests demonstrated that at 4 mAs, the digital system performed better than the screen film system. At all exposures 6 mAs or greater, the screen film system performed better. The screen film system appeared to reach a maximal value at 12 mAs, while the digital system continued to show slight improvement with each increase in exposure.

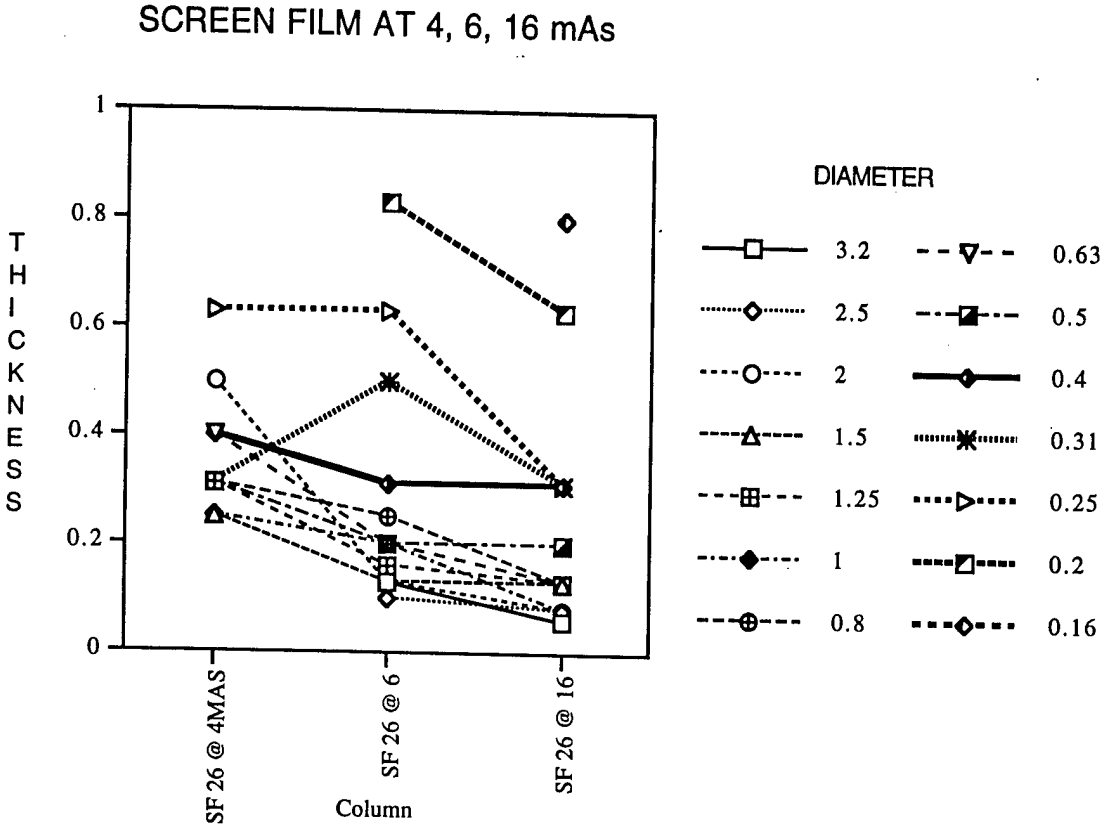

This chart demonstrates that with increasing exposures in the screen film system, the disks on the CDMAM phantom could be seen both thinner and with smaller diameters as exposure increased from 4 to 6 to 16 mAs.

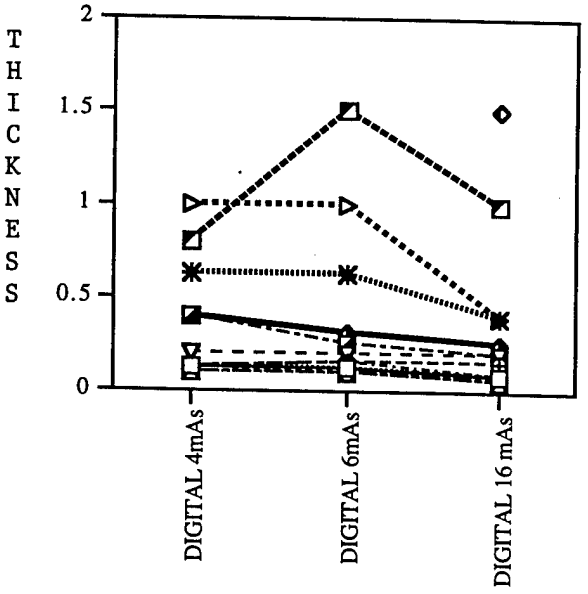

This chart shows for the digital system, that increased exposure between 4 to 6 mAs had little effect on detection. Increases to 16 mAs showed improved resolution with a smaller object seen and with thinner objects seen.

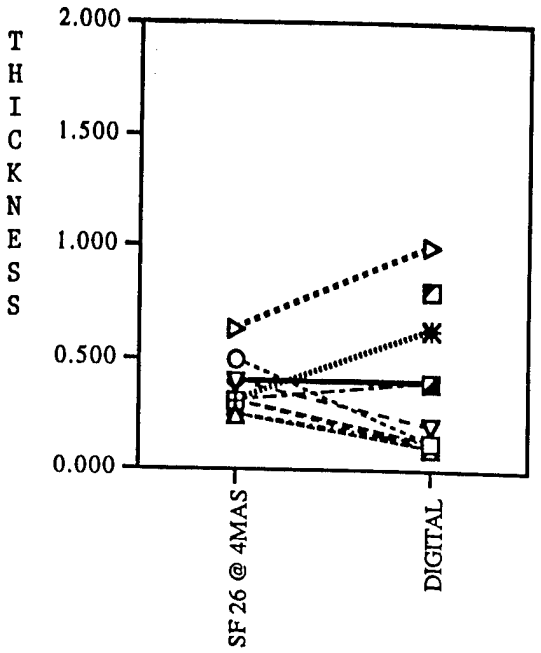

4

Chart: 4 mAs, screen film and digital. The screen film (SF) system performs better for some objects sizes and less well for others when compared to the digital system The digital system system shows one object (0.2 mm) that is smaller than those seen with the screen film system.

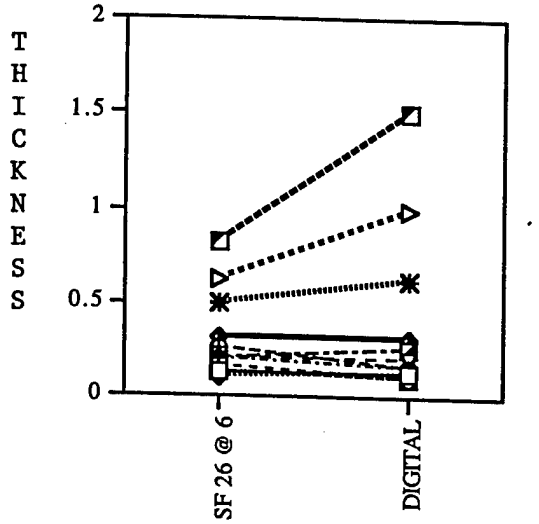

Chart: 6 mAs screen film and digital. At six mAs screen film (SF) shows thinner objects for each object diameter.

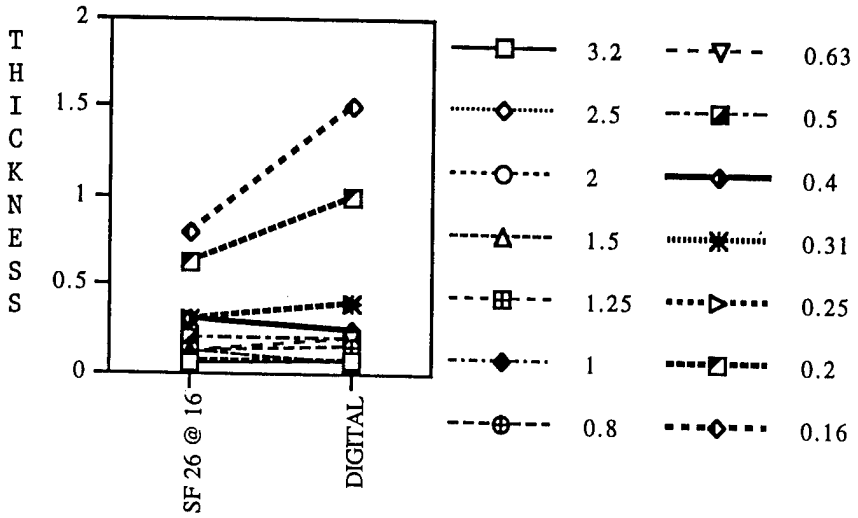

Chart: at 16 mAs, the screen film system shows thinner objects for all object sizes than does the digital system. At 16 mAs, both systems showed the 0.16 mm diameter object. This object could not be seen with 4 or 6 mAs.

These charts demonstrates that the digital system performs better for only the lowest exposure level with the image processing settings used. At higher exposures, the screen film system performed better. These results were obtained as part of the multiparameter optimization procedure and the image processing optimization method had not yet been applied to these images.

2. Measurement of number of mammograms that had exposure levels estimated to be less than 6 mAs. 20 mammograms with proven cancer were measured to determine the optical density of the image in the region of the cancer. The optical density of these images were compared to the optical density of the phantom images done on screen film to determine an estimate of the frequency with which the digital system might yield an advantage. Only one of the 20 cases had an optical density in this region.

3. Comparison of optical density on these 20 breast cancer cases to the characteristic curve of the screen film system used. This test demonstrated that the one case that fell within the range in where the digital system was better was in the optical density range of the toe of the characteristic contrast curve of the screen film system.

4. Measurements of the effect of optical density of the digital image on the demonstration of features. The digital system allows images to be printed on laser images at various optical densities. This demonstrated that images made in the estimated region of the toe of the laser film characteristic curve had a lower detectability of objects than those made in the steep portion of the curve. These values had to be estimated because of the non uniformity of the images secondary to the heel effect of the mammographic x-ray tube. Digital systems, based on their inherent image analysis methods, exaggerate the heel effect of x-ray tubes.

B. KVP effects: These had been previously studied using Fuji ST-3 imaging plates. Only 2 energies have been tested so far on the HR-V imaging plates: 26 and 36 KVP. On the CDMAM phantom, 26 KVP was better than 36 KVP. These tests were stopped because the dosimeter/KVP meter being used to check machine settings failed during the tests and

had to be returned to the factory for repair. These tests will be completed when the machine is returned.

C. Contrast effects: The effects of increasing contrast on the detectability of the objects in the RMI phantom was tested. Increasing the contrast of the digital image improves the detectability of objects.

D. Effect of Exposure: As shown in the attached graph, doubling the exposure from 20 to 40 mAs on the digital system improves the detectability of small objects on the RMI phantom. Doubling the mAs on the screen film system has no effect on detectability of objects. The various items under the digital category reflect different image processing settings of RN and RE.

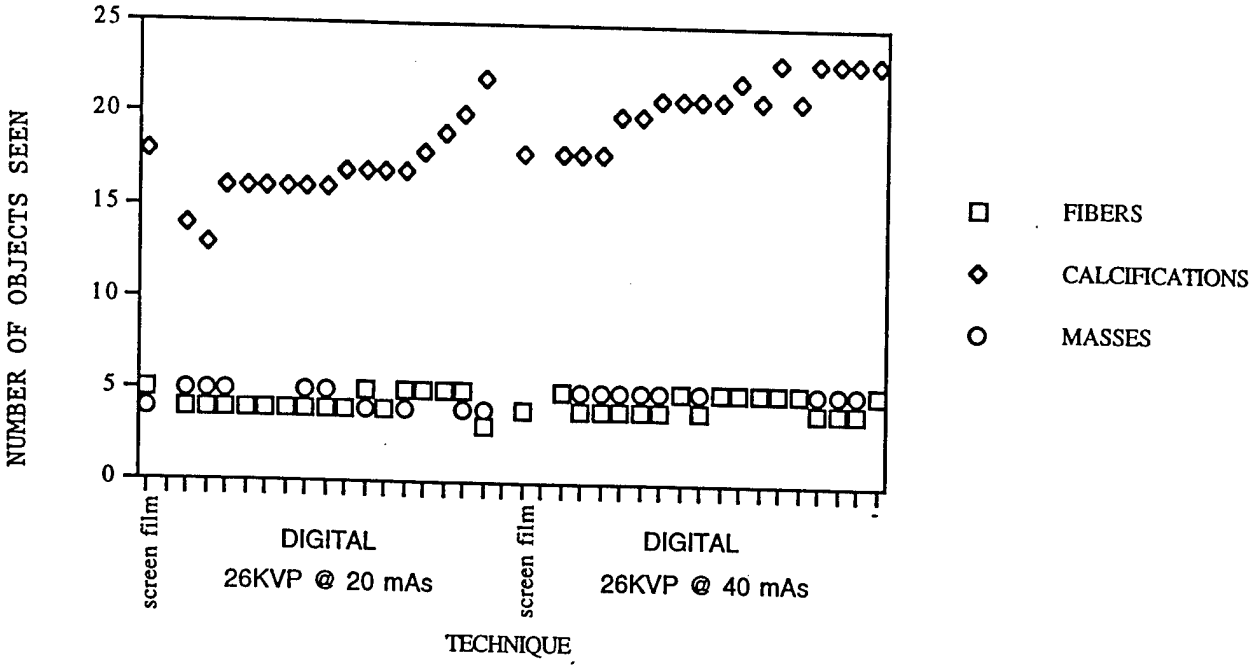

On this chart, the data of the digital sections is based on 16 different RN and RE combination. This chart demonstrates that for each exposure setting 26 KVP at 20 and at 40 mAs, that the screen film system equalled the results of digital for certain types of image processing, but that will other image processing, the visibility of microcalcifications was better with the digital system. The higher exposure with appropriate image processing, resulted in more microcalcifications being seen than were seen with screen film images. The higher exposure resulted in more calcifications being seen with the digital system for most image processing settings used.

E. Effect of spatial frequency filtering: There are two factors that affect spatial frequency filtering: the kernel size and the intensity of enhancement. Using the RMI, CIRS, and CDMAM phantoms, tests were performed using all possible combinations of Fuji RN factors of 1, 3, 5, 7, and 9 and RE factors 0, 2, 5, and 10 as well as selected RE factors of 1 and 16. Results in phantoms demonstrated that low RN combined with high RE improved the detectability of small nodules and that high RN combined with high RE increased the detectability of small calcifications or aluminum flecks. The high RN and RE combination also resulted in an increased visibility of noise which can simulate small calcium flecks.

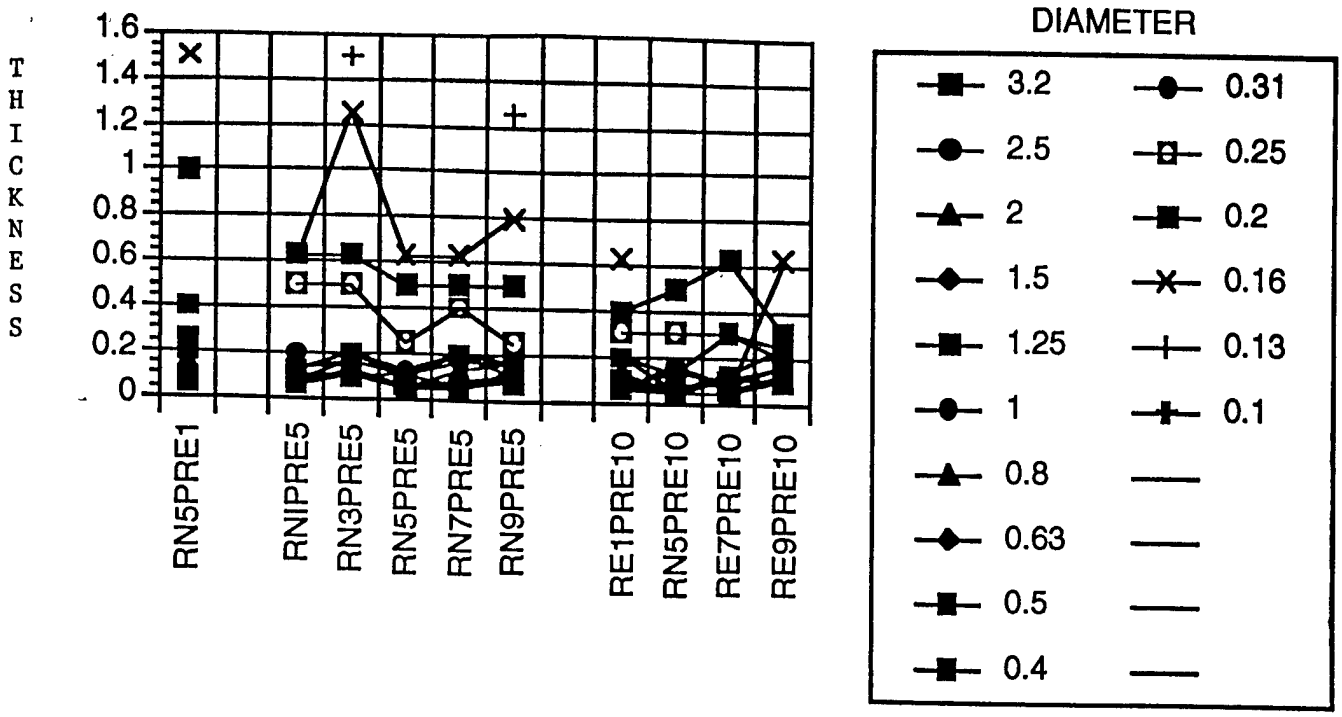

This graph demonstrates that with increasing spatial frequency filtering intensity (demonstrated as increased RE factors), objects could be detected at thinner diameters. However, at the highest intensity (RE = 10), the smallest objects (0.13 mm) could not be detected, most likely due to the exaggeration of noise which simulated small calcium like densities.

F. Tests of image processing on actual digital mammograms. Digital mammograms done for clinical indications have been stored in our system. The image processing factors that appeared potentially promising on tests on phantoms were then tested on the stored digital mammogram images from two women. These demonstrated that the low RN factors (the ones that increased the detectability of small masses) resulted in distorted images of the other aspects of breast anatomy and resulted in images that radiologists would likely consider unacceptable, especially if combined with higher RE factors. High RN combined with high RE settings resulted in images that appeared likely to be unacceptable as well. The optimal settings of RN 7 or 9 and RE 5, resulted in images that are likely to be considered clinically acceptable by radiologists and equal the diagnostic accuracy of screen film systems when tested on several available breast phantoms.

APPENDIX B: LIST OF COLLABORATIVE ARTICLES WITH DOD PHYSICIANS AND SCIENTISTS

In this list, the DoD physicians' and scientists' names have been underlined. While these articles are not related to digital mammography they are placed here to indicate to collaborative nature of our research in digital radiography.

PROCEEDINGS/TRANSACTIONS

1. Mun S K, Freedman M, Gelish A, DeTreville R, Sheehy M, Hanson M, Hill M, Zacharia E, Sullivan M, Sebera C W: Health Care Using High-Bandwidth Communication to Overcome Distance and Time Barriers for the Department of Defense. SPIE Conference, Enabling Technologies for High Bandwidth Applications, Boston, MA (September 10, 1992).

2. Leckie R G, Meyers C, Parker J, Smith D V, Freedman M, Sheehy M R, Cade L, Goeringer F: Evaluation of Traumatic Lateral Cervical Spine Computed Radiography Images: Quality Control Acceptability of Images for Clinical Diagnosis, Hardcopy versus High Resolution Monitors. SPIE: Medical Imaging (1993). Paper 1897-13.

3. Weiser J C, Leckie R G, Freedman M, Smith D V, Cawthon M A, Romlein J R, Willis C E: Significance of the Fuji AC 1 CR Algorithms on Hardcopy Images. SPIE: Medical Imaging (February 1993). Paper 1897-21.

4. Freedman M, Mun S K, Pe E, Weiser J C, Roblein J R, Lo S-C B, Nelson M: Quality Control of Storage Phosphor Imaging Devices. CAR 93, 7th International Symposium, Berlin (June 24-26, 1993); 456-460 pp.

5. Romlein J, Leckie R, Smith S, Quillin E, Freedman M: Evaluation of Specific PACS Equipment Components - Operational and Maintenance Experience. SPIE: Medical Imaging (February 1994). Paper 2164-19.

6. Leckie R, Ursone R, Willis C, Freedman M: A Basic Teaching Tool For Understanding the Fuji CR Algorithms. SPIE: Medical Imaging (February 1994). Paper 2165-76.

7. Leckie R, Ursone R, Weiser J C, Donnelly J, Norton G, Pe E, Freedman M: Visual comparison of CR Image Quality Based on Different Exposure Techniques. SPIE: Medical Imaging (February 1994). Paper 2165-77.

ABSTRACTS

1. Leckie R G, Freedman M, Weiser J, Willis C, Norton R T, Pe E: Comparison of Computed Radiography Image Quality Based on Different Exposure Techniques. Radiology (1993); 189P:215.

2. Leckie R G, Ursone R L, Freedman M, Donnelly J, Pe E, Norton G: Visual Comparison of Computed Radiographic Image Quality Based on Different Exposure Techniques (abstract). Radiology (1993); 189P:410.

3. Leckie R G, Freedman M, Willlis C, Weiser J C, Smith D V, Cawthon M A: Basic Clinical Principles of Computed Radiography for the Radiologist (abstract). Radiology (1993); 189P:415.

Preprint SPIE
Medical Imaging 95

Digital mammography: The effects of decreased exposure

Matthew Freedman MD MBA, Dot Steller RT(R), Hamid Jafroudi PhD, S.-C. Benedict Lo PhD, Rebecca A. Zuurbier MD, Raj Katial RT(R), Wendelin Hayes DO, Y. Chris Wu PhD, Jyh Shien Lin MS, Seong Ki Mun PhD

Division of Imaging Science and Information Systems and Division of Breast Imaging, Georgetown University School of Medicine, 3800 Reservoir Road NW, Washington, DC USA 20007

Keywords: Digital Mammography Exposure

ABSTRACT

It has been stated that digital mammography will reduce the exposure required for mammography. This poster explores the effects of decreased exposure on the information present in digital mammography. In general, the digital system performed better than screen film mammography with lower exposures. With the usual exposures used for screen film mammography, performance was equal. With high exposures sufficient to result in a dark film (OD 1.5), the digital system performed better than screen film with very small test objects.

Proposals have been made to decrease the tube loading required for slot scanning devices by increasing KVP. This would result in their being less object contrast due to the decreases in the absorption coefficient of calcium compared to water at higher KVP. This poster looks at the potential for correcting the loss in object contrast that would result from the use of high contrast look up tables. It was found that in the tested system, one could restore the information in one of the two test objects used (but not the other), but that the image processing methods used would result in an image that radiologists would probably find inadequate for interpretation.

METHODS

Tested System

Images for this series of experiments were obtained using a GE-CGR (Milwaukee, Wisconsin) 600 T dedicated mammography machine. The machine is in clinical use in an American College of Radiology approved facility and meets the quality standards for this approval. The images obtained at 28 KVP at varying mAs were obtained with a molybdenum target and filter. Those obtained at various KVPs were obtained with a molybdenum target and an aluminum filter. The mammographic screen film system used is Fuji (Tokyo) Kyokko UM Fine Screen with Fuji UM-MA-HC film. The digital system tested is the Fuji 9000 using high resolution imaging plates (HR-V).

Two test objects were used: the CIRS Detail (square) test object (Norfolk Virginia) and the CDMAM test object (Nuclear Associates, Carle Place, New York). The CDMAM test object was placed on top of four cm of acrylic.

Image Processing Optimization

Image processing methods are those included in the Fuji 9000 system. The optimized image processing settings for the detection of small objects were calculated through the application of the mathematical technique of multiple iterative response surfaces in geometric test objects.

Exposure reaching the Screen Film Cassette and Storage Phosphor Cassette

CIRS Detail Phantom

CIRS detail

KVP	mAs	mR pre grid	mR post grid	ODSF	KVP	mAs	mR pre grid	mR post grid	ODSF
28	6	15.7	6.57	0.16	22	5.9	2.2	0.83	0.4
28	12	31.6	13.22	0.18	28	3.8	5.9	2.47	1.22
28	20	42.3	17.70	0.21	36	6.9	28.7	13.23	1.5
28	25	53.0	22.18	0.25					
28	32	85.0	35.56	0.29					
28	40	106.6	44.60	0.42					
28	80	213.8	89.46	1.13					

CDMAM test object with 4 cm of added acrylic between test object and receptor

KVP	mAs	mR pre grid	mR post grid	ODSF	KVP	mAs	mR pre grid	mR post grid	ODSF
28	6	2	0.84	0.16	22	67.7	<1.0	<0.38	0.4
28	12	3.9	1.63	0.18	28	8.5	2.5	1.05	1.22
28	20	5.4	2.26	0.21	36	7.1	7.1	3.27	1.5
28	25	6.7	2.80	0.25					
28	32	10.9	4.56	0.29					
28	40	13.6	5.69	0.42					
28	80	27.3	11.42	1.13					

OD SF = optical density on screen film image. Pre-grid = exposure above grid. Post grid = exposure below grid corrected for changes in grid absorption with changes in KVP.

FINDINGS

THE EFFECT OF INCREASES IN KVP

When screen film mammography images and digital images obtained at different KVPs are compared, one can see that the higher KVP results in a decrease in the detection of small objects that cannot be retrieved with the image processing methods available to the authors except by the use of a very high contrast look up table (GA=9). This high contrast look up table results in images that are likely unacceptable for interpretation.

Findings in the CIRS Detail Test Object

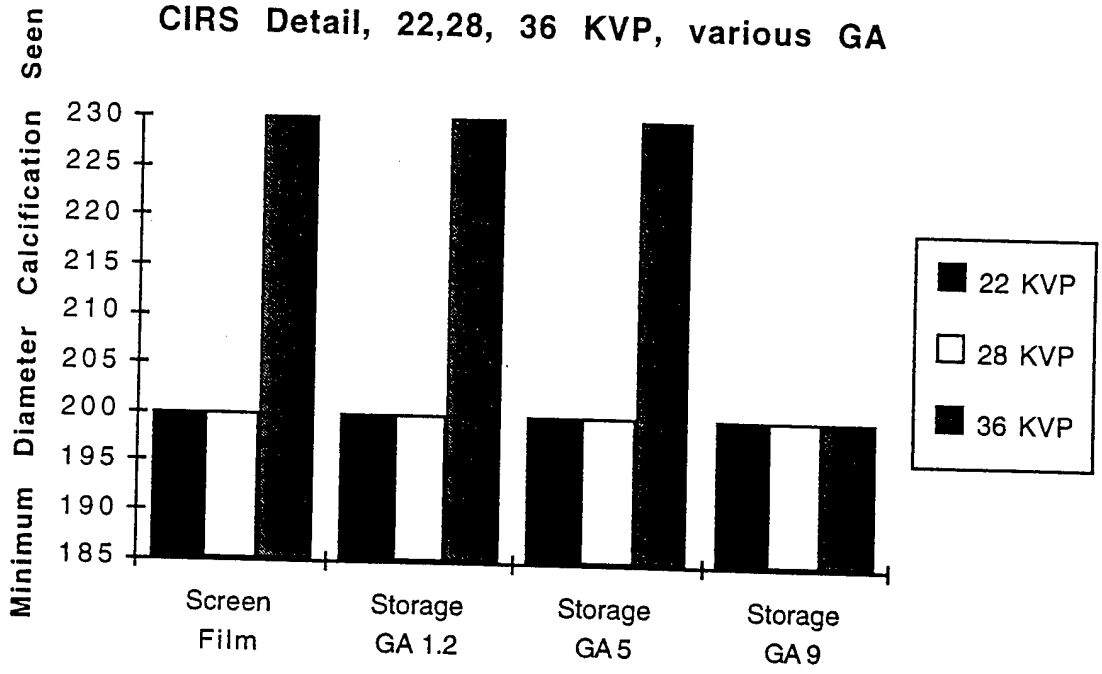

This chart shows the results for the CIRS Detail (square) test object. With this test object, no difference is seen between 22 and 28 KVP, with the smallest object measuring 200 microns. At 36 KVP, screen film, and storage phosphor processed with a GA of 1.2 and 5 did not allow retrieval of the smallest detail. At a GA of 9, at 36 KVP, the 200 micron objects could be seen, but this very high contrast image results in an unreadable appearance to the mammogram. This is because the range of optical densities in the original image exceeds the optimal range for this look up table resulting in images with regions that are maximally black or maximally white, resulting in loss of detail. In addition, the heel effect is exaggerated with these high contrast look up tables so that the entire breast cannot be visualized at the same time. (GA = gradient angle of the look up table. Storage = storage phosphor radiography.)

Findings in the CDMAM Test Object

The Nuclear Associates CDMAM test object also was used to compare screen film and storage phosphor radiographs at various KVPs.

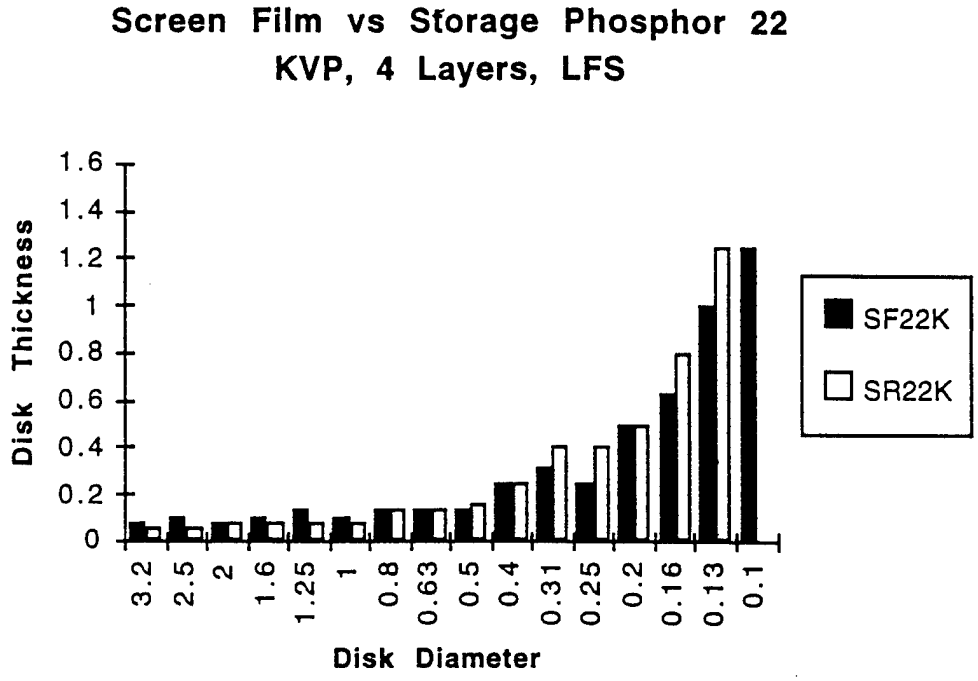

This chart demonstrates that at 22 KVP, the screen film system shows smaller objects and for the smaller objects shows them at lower contrast than the digital system. (SF= Screen Film. SR= Storage Phosphor Radiography. K = KVP)

Screen Film vs Storage Phosphor 28 KVP, 4 Layers, LFS

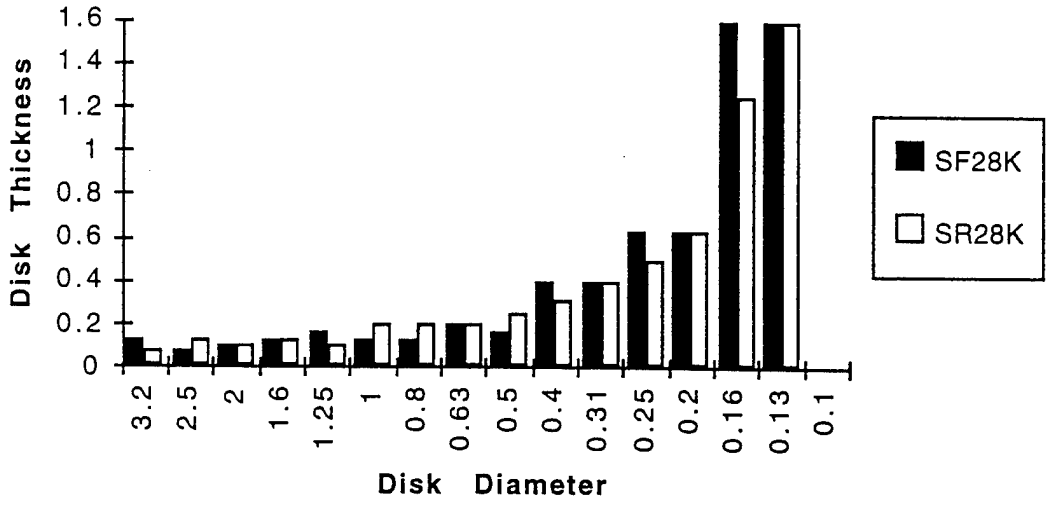

This chart shows that screen film and storage phosphor demonstrate the same size objects at approximately the same contrast levels when obtained at 28 KVP. (SF= Screen Film. SR= Storage Phosphor Radiography. K = KVP)

Screen Film vs Storage Phosphor 36 KVP, 4 Layers, LFS

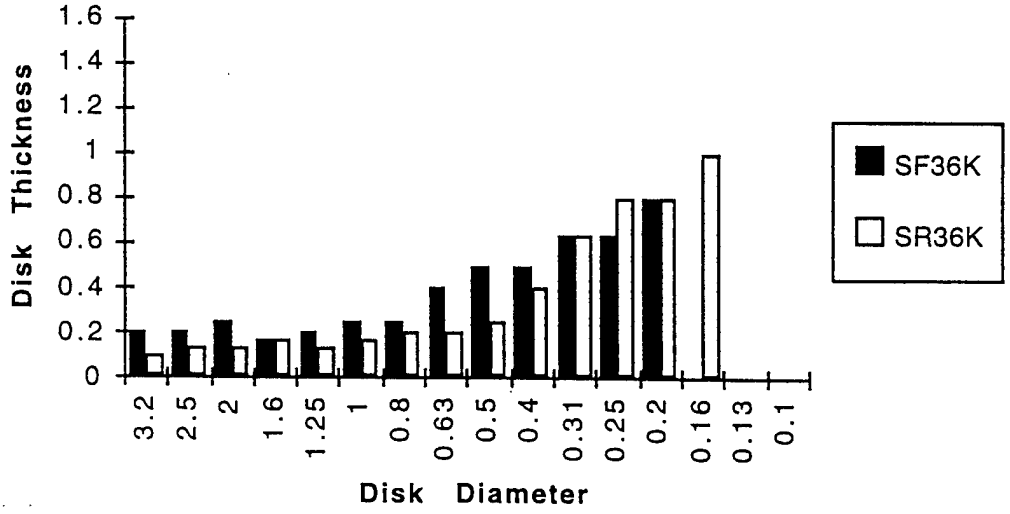

In this chart, the CDMAM phantom demonstrates smaller objects than screen film and shows them at lower contrast (thinner disk). (SF= Screen Film. SR= Storage Phosphor Radiography. K = KVP.)

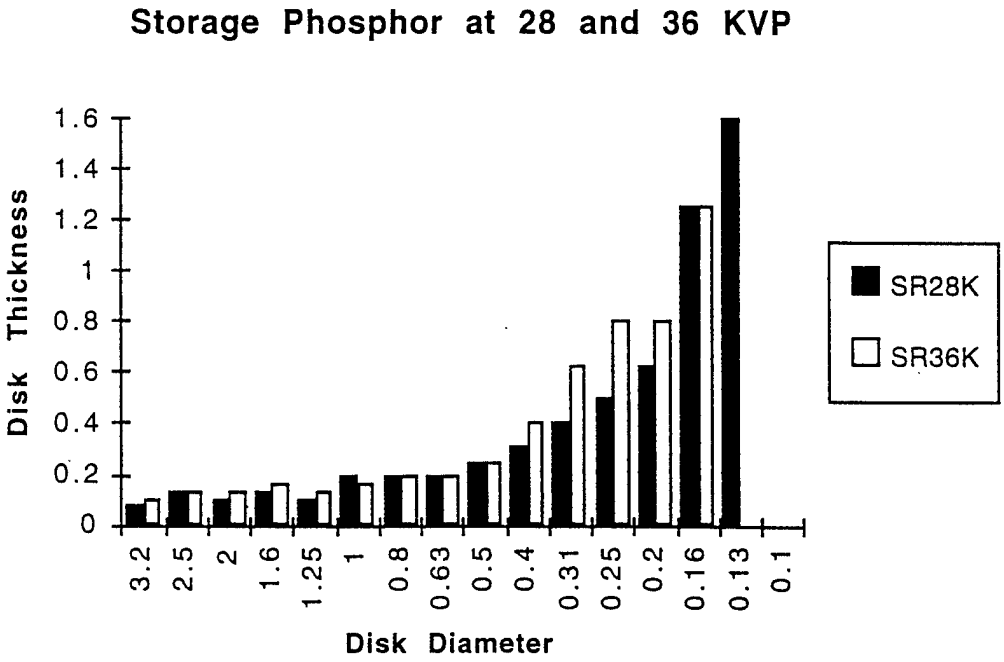

In this chart, one can see that storage phosphor (SR) at 28 KVP performs better than SR at 36 KVP. One can see the smallest (130 micron) object only at 28 KVP and for the other small objects, one sees them at lower contrast at 28 KVP. (SR= Storage Phosphor Radiography. K = KVP.)

Screen Film at 28 KVP vs Storage Phosphor at 36 KVP

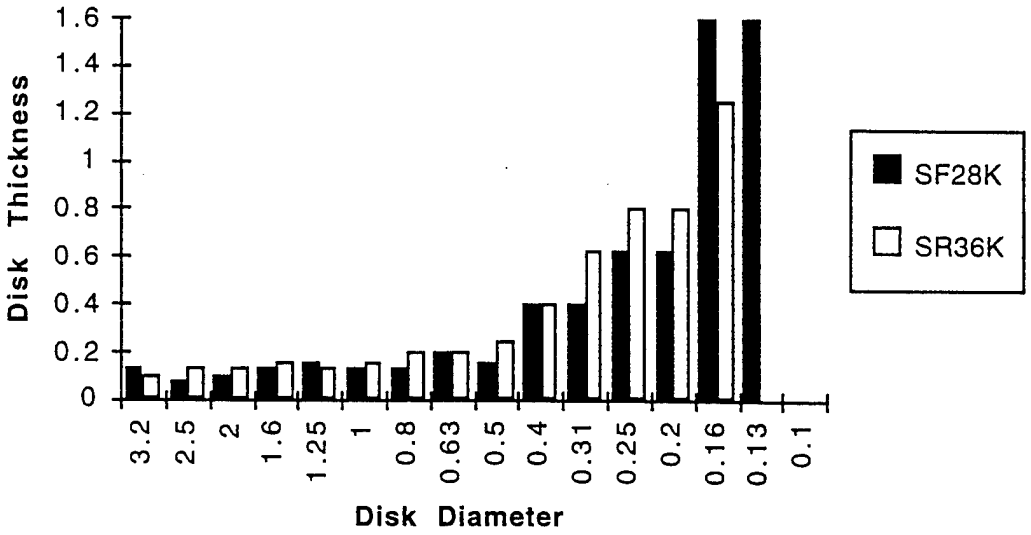

This chart demonstrates that one can see the 130 micron object at 28 KVP using screen film, but not with SR at 36 KVP. For most of the object in the lower third of the disk sizes shown, screen film detects them at slightly lower contrast than SR. (SF= Screen Film. SR= Storage Phosphor Radiography. K = KVP.)

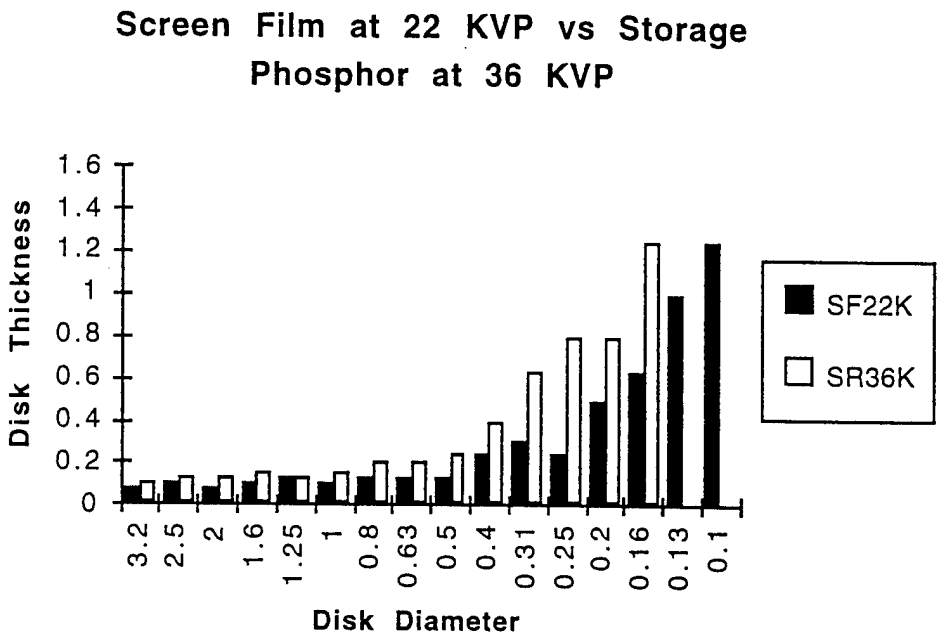

This chart demonstrates that screen film images at 22 KVP show the 100 and 130 micron objects which cannot be seen at 36 KVP with SR. Also for all of the other size objects, screen film allows their detection at lower contrast. The best screen film images were obtained at 22 KVP. (SF= Screen Film. SR= Storage Phosphor Radiography. K = KVP.)

Conclusion regarding KVP

Although SR with image processing allows more to be seen at 36 KVP when compared to screen film, it does not equal digital or screen film at 22 or 28 KVP. Screen film images at 22 KVP show the smallest objects in this test. Within this test system, with both the CIRS and CDMAM test objects, one could not reclaim the information regarding the smallest objects when 36 KVP was used; there was better conspicuity for most objects with both the screen film and digital images obtained at 22 or 28 KVP.

DIFFERENCES IN MAS AT 28 KVP

Tests demonstrated that the digital system performed better at low mAs and at the highest level of mAs. In the intermediate range of exposures, the systems performed equivalently.

Tests with the CIRS Detail Test Object

These charts demonstrate the findings as mAs is varied at 28 KVP.

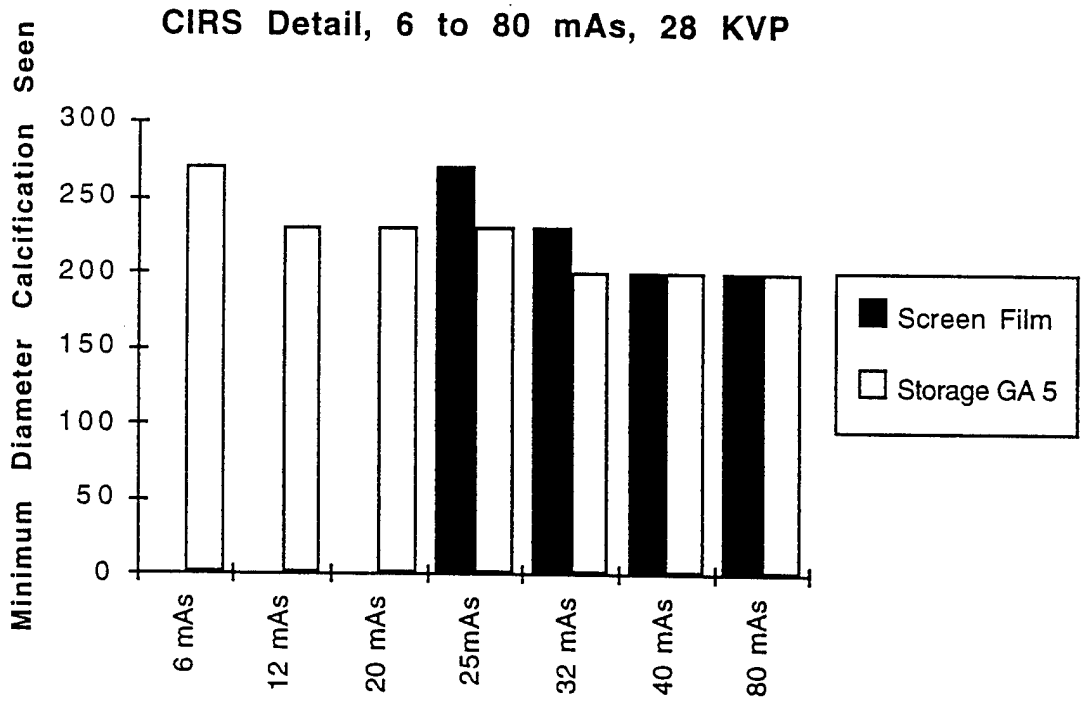

This chart demonstrates that at mAs less than 25, while the storage phosphor system could demonstrate objects, the screen film failed to demonstrate any of the objects. At 25 and 32 mAs, the storage phosphor demonstrated smaller objects than screen film. At 40, and 80 mAs, the two systems performed equivalently. (Storage = Storage Phosphor Radiography. GA = gradient angle of the look up table.)

Tests with the CDMAM Test Object

This test object shows similar results, with the digital system performing better at low mAs and the system performing equivalently at higher mAs.

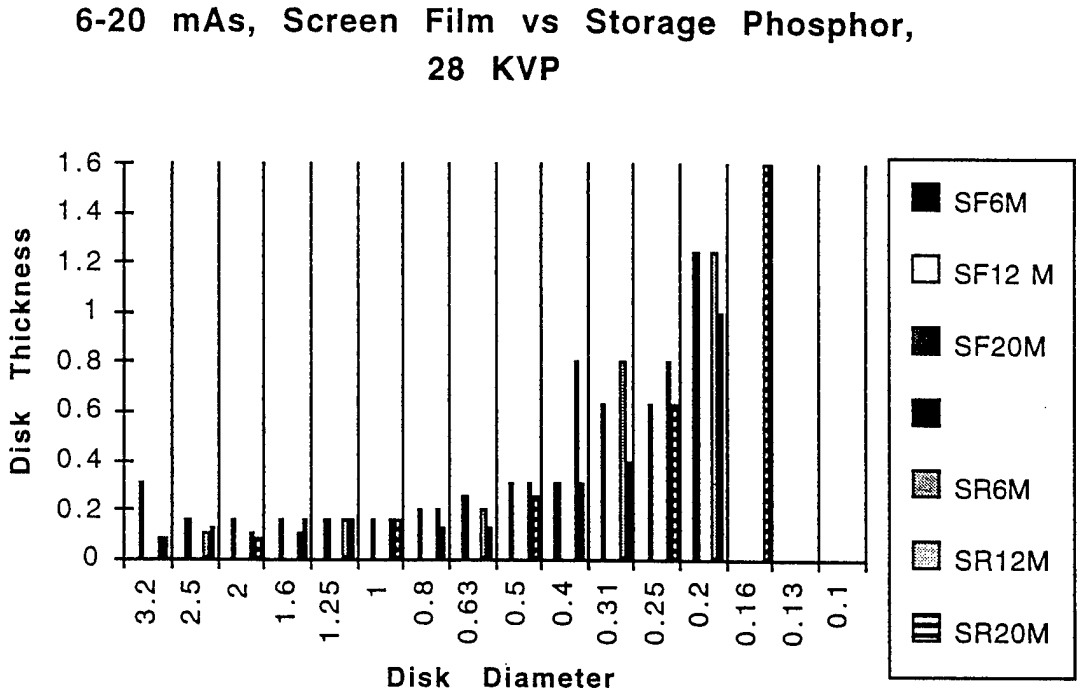

This chart demonstrates the effect seen as the mAs is increased from 6 to 20 mAs. Within each block, those values to the left are from screen film and those to the left are the digital values. Less is seen with the screen film than with the digital images in this group. (SF= Screen Film. SR= Storage Phosphor Radiography. M = mAs)

With higher mAs, the systems perform similarly:

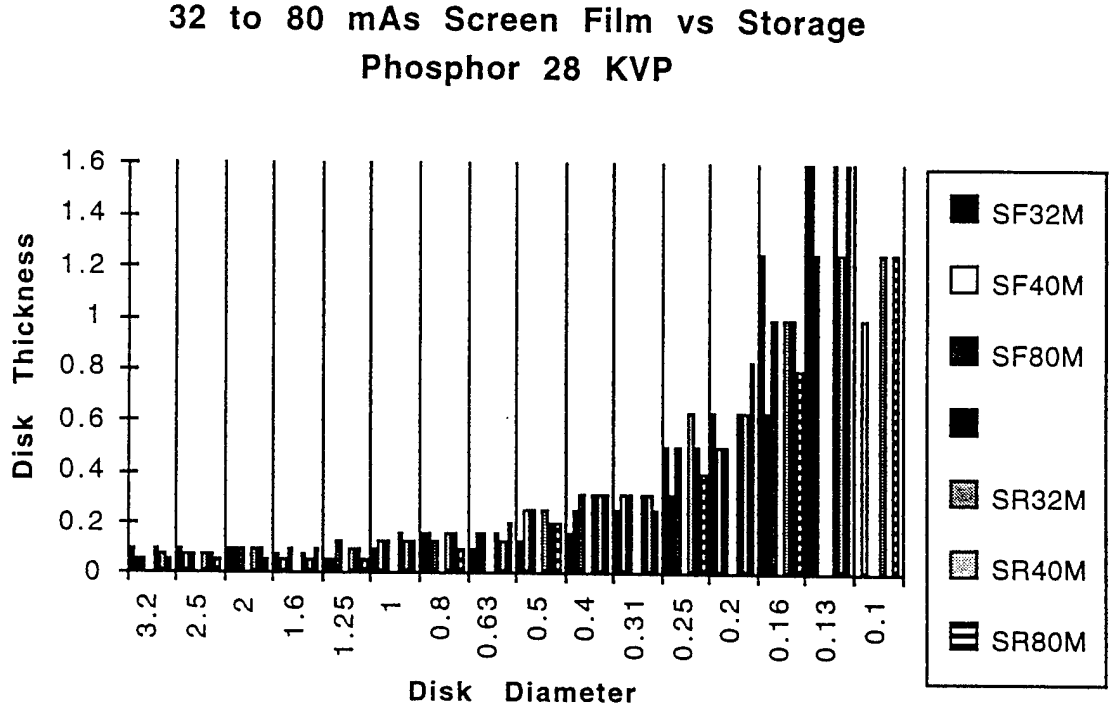

This chart demonstrates that the screen film and digital system are performing similarly with the larger test objects. With the smallest diameter objects, the screen film and digital systems allow their detection, but the screen film system allowed it to be seen at slightly lower contrast in this test. (SF= Screen Film. SR= Storage Phosphor Radiography. M = mAs)

Conclusion of Tests of Changes in mAs

In both test objects, the digital system performed better at lower mAs, and similarly at higher mAs.

CLINICAL IMPLICATIONS FOR DIGITAL MAMMOGRAPHY

Clinical implications of KVP findings:

Some digital mammography machines now under development use a higher KVP so that the heat loading on the x-ray tube will be less. The results of this study suggest that at least with the image processing available to us, one may not be able to recapture the contrast information which is detectable at a lower KVP. This is related to the decreasing absorption coefficient of calcium with a higher KVP.

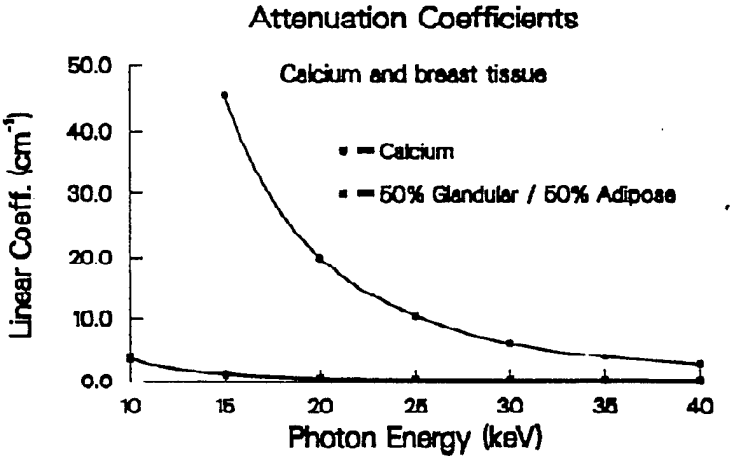

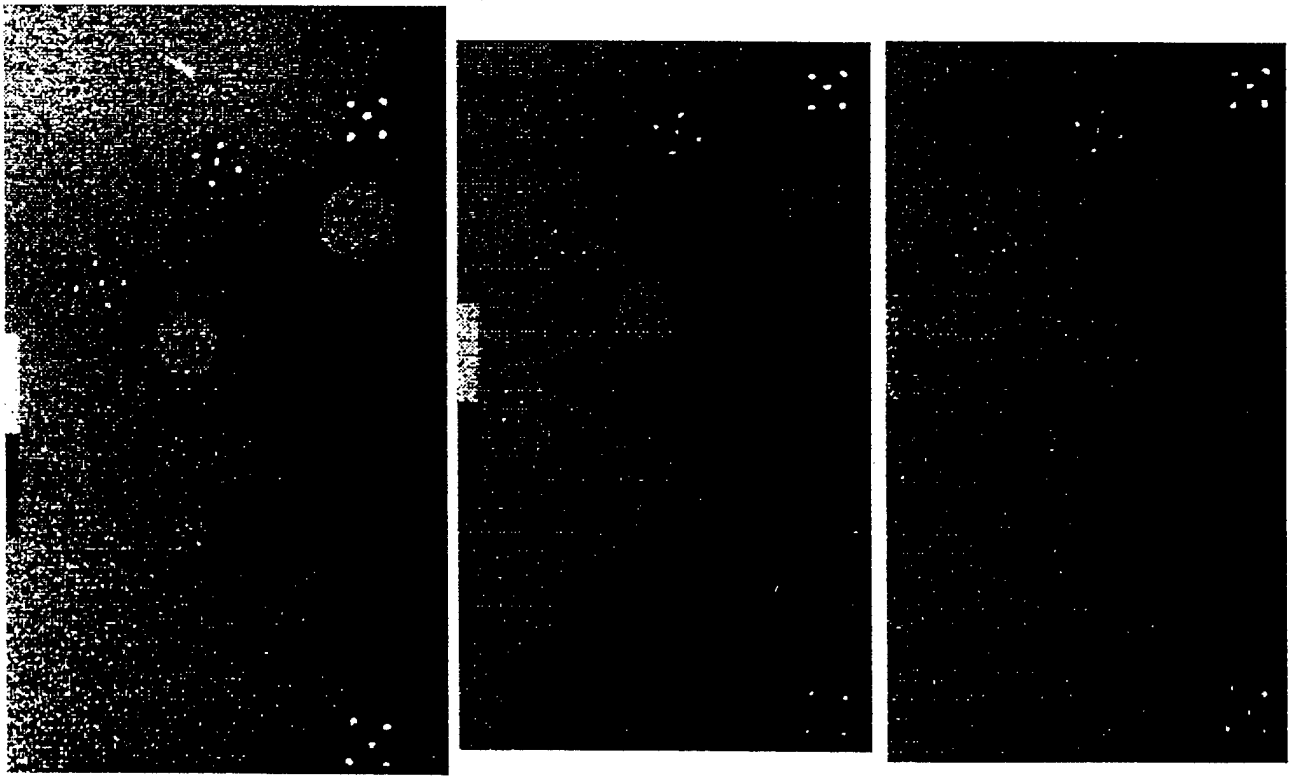

Storage phosphor 22 KVP Storage Phosphor 28 KV Storage Phosphor36 KVP

These three views of the CIRS detail test object demonstrate that increasing the KVP lowers contrast with storage phosphor systems and that this contrast information cannot be completely retrieved with image processing.

Using a high contrast look up table to at least partially restore contrast information would also increase the contrast and thereby the visibility of noise. While our tests show that one can use image processing to make the digital image better than the screen film image at 36 KVP, it did not equal the performance of either digital or screen film images at 22 and 28 KVP in the CDMAM test object.

Clinical Implications of the mAs Experiments

The breast shows a wide variation in radiodensity. Denser areas of the breast, if their exposure level falls into the critical range, will have better conspicuity of small objects with the digital system than with screen film. If one uses screen film images, sufficient exposure to demonstrate the smallest objects should be used. While digital systems provide more information at low exposures, a decrease in exposure in the test system we used could be achieved only if one were to accept less than the full information the system could provide.

CONCLUSIONS

The use of storage phosphor digital mammography in its current configuration will not allow the exposures for digital mammography to be decreased if one wishes to maintain full information. In the presence of underexposure (such as in a focally dense area of the breast or in generalized breast increased radiodensity), there is a point below which a digital system does contain more information than a screen film system.

With increases in KVP, one has less object contrast. With the system tested, one cannot recover the contrast information lost at 36 KVP by image processing and still maintain an image of the breast that would be considered readable by a radiologist.

Bibliography

Freedman M, Pe E, Zuurbier R, Katial R, Jafroudi H, Nelson M, Lo S-C B, Mun S K: Image Processing in Digital Mammography. SPIE: Medical Imaging, Vol. 2164 (1994); 537-554pp.

Freedman M, Mun S K, Pe E, Lo S-C B, Nelson M: Image Optimization on the Fuji AC-1. SPIE: Medical Imaging (1993). Vol 1897: 480-502.

SUPPORTED IN PART BY

1. U.S. Army Medical Research Grant DAMD 17-93-J-3008. The content of this report does not necessarily reflect the position or policy of the U.S. Government.

Single Image Hardcopy Display of Muskuloskeletal Digital Radiographs

Kevin Legendre, Dorothy Steller, Matthew Freedman, Seong K. Mun

Georgetown University Medical Center, Department of Radiology
Washington, D.C. 20007

ABSTRACT

Screen film radiography often fails to optimally display all regions of anatomy on muskuloskeletal exams due to the wide latitude of tissue densities present. Various techniques of image enhancement have been applied to such exams using computerized radiography but with limited success in improving visualization of structures whose final optical density lies at the extremes of the interpretable range of the film. An existing algorithm for compressing optical density extremes known as dynamic range compression has been used to increase the radiodensity of the retrocardiac region of the chest or to decrease the radiodensity of the edge of the breast in digital mammography. In the skeletal system, there are regions where a single image may contain both areas of decreased exposure that result in light images and areas of higher exposure that result in dark regions of the image. Faced with this problem, the senior author asked Fuji to formulate a modification of the DRC process that incorporates a combination of the curves used for chest and breast images. The newly designed algorithm can thus simultaneously lower the optical density of dark regions of the image and increase the optical density of the less exposed regions. The results of this modification of the DRC algorithm are presented in this paper.

Keywords: digital radiography, skeletal radiography, image enhancement, dynamic range compression

1. GENERAL CONSIDERATIONS

1.1 Muskuloskeletal anatomy

Skeletal radiographs typically image regions of anatomy containing a wide variety of tissue densities in the field of view. Difficulty is often encountered in simultaneously displaying bony structures of high density and the intermediate to low density structures of adjacent soft tissues, primarily muscle and fat. This problem is compounded by the fact that the region to be evaluated often presents a nonuniform shape and thickness, such as in dorsal plantar (DP) views of the feet. Regions of complex, overlapping bony structures also complicate exposure and visualization such as seen with lateral views of the carpal bones. Thus, compromises are often made by accepting that certain structures cannot be visualized on the same image with other structures that produce a significantly different optical density on film.

1.2 Screen-film radiography

Over the years, exposure techniques for muskuloskeletal imaging have been optimized through adjustments of kVp and mAs but adequate exposure of thicker and denser regions often results in overexposure of thinner, less dense areas such as soft tissues surrounding bony structures. Conversely, ideal exposure of soft tissue ultimately results in underexposure of many bony regions. With conventional screen-film systems, two separate films would be needed to optimally examine the extremes of the spectrum of tissue densities present. With screen film radiography, there is no option for image manipulation once the exposure is made to improve visualization of structures. This is where the promise of digital radiography comes into play.

1.3 Digital radiography

With the advent of computerized digital radiographic systems, the opportunity to "post-process" images for enhancement of various attributes has become a reality. Extensive investigations have already been done on varying factors analogous to the screen-film H&D curves such as the shape and slope of the curve the system

0-8194-1784-X/95/$6.00

employs to translate the amount of exposure on the storage phosphor plate to the final optical density represented on the output device, either a soft copy monitor image or a hardcopy film. These techniques fall under the realm of gradation processing. Even more involved methods have been developed to achieve edge enhancement or affect the spatial filtering of a portion or all of the image. These latter effects constitute frequency processing. These two concepts of image manipulation, gradation and frequency processing, have been developed to the point where highly diagnostic digital films have become a viable alternative to conventional screen-film studies. Yet, in regions of extreme variation in tissue density, the problem of optimally exposing the entire region of anatomy under investigation has persisted.

1.4 Dynamic range compression

In an effort to provide a wide diagnostic field on a single image, a new type of image processing algorithm has been developed. This algorithm, known as dynamic range compression (DRC), represents a new approach to image enhancement that is a distinctly separate entity from its cousins of gradation and frequency processing. The process is based in part on the principles of unsharp masking and can be mathematically demonstrated by Equation 1 and Equation 2 below.[1]

$$S_{DRC} = S_{ORIG} + f(S_{US}) \quad (1)$$

$$S_{US} = \Sigma S_{ORIG} / M^2 \quad (2)$$

First, a smoothed copy of the original image is generated using Equation 2 where M is the mask size, S_{ORIG} is the original image and S_{US} is the resultant smoothed image. This smoothing process is demonstrated graphically by comparing Figure 1A to Figure 2B below. Signal transformation processing is then applied to the smoothed image to raise the optical density (OD) of low density regions and simultaneously lower the OD of high density regions according to a pre-selected sigmoidal curve. The transformation process is shown by Figure 1C below. Original application of the DRC process used only simple curves to affect only either end of the density spectrum. At the request of the senior author, Fuji Film Co., Ltd. has developed a biphasic sigmoidal curve so that the lookup table values of the smoothed image component are affected at both density extremes.

Figure 1A

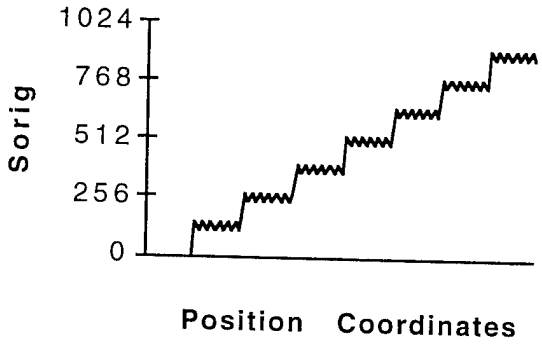

Figure 1B

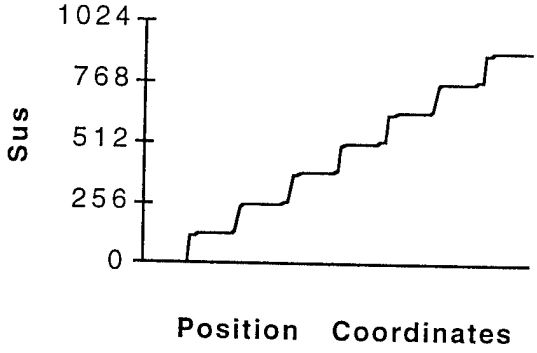

/$6.00

Figure 1C

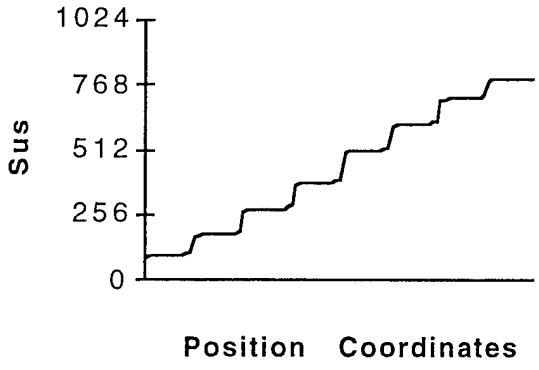

Figure 1 D

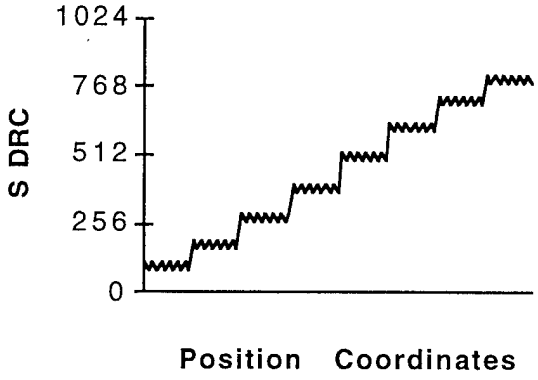

The intensity of the DRC effect, known as the DRE, can also be chosen independently ranging from a minimum of 0.0 (no effect) to a maximum of 2.0 (full effect).[2] As shown in Equation 1 above, the transformed smoothed image is then added back to the original image to a degree governed by the DRE selected. The final image signal is shown in Figure 1D. This process allows for the preservation of the spatially fine signal and fine detail present in the original image while compressing the lowest and highest density portions of the smoothed image to yield a resultant image (S_{DRC}) containing OD values more within the optimal interpretative range.

2. METHODOLOGY OF INVESTIGATING DRC IMAGING

2.1 The Fuji 9000 CR system

To investigate the effects of the DRC process, the Fuji 9000 CR system was used. In this system, cassettes loaded with a single Fuji ST-V storage phosphor imaging plate (Fuji Photo Film Co. Ltd., Tokyo, Japan) serve as the device for image capture. Following plate exposure, the technologist enters necessary data into the ID terminal (such as patient name) and chooses the type of exam (foot, wrist,etc.) which determines how the plate will be initially processed. At our institution, we have provided special menu options which allow the technologist to process the plate as a dual format image from a single exposure with standard processing for the left image and DRC processing for the right image. The shape of the sigmoidal curve and value of DRE have been pre-selected and assigned to the individual menu options. The plate is then fed to the image reader (FCR 9000 Image Reader CR-IR 317, Fuji Photo Film Co., Ltd., Tokyo, Japan) and preset gradation and frequency processing is automatically performed as determined by the initial menu option chosen. The images are then assessed on a high resolution CRT monitor where further gradation and frequency processing can be done if needed. Images are then printed using a twin format from a Fuji LP-414 laser printer (Fuji Photo Film Co. Ltd., Tokyo, Japan). The DRC process is applied to the 10 bit raw data obtained immediately after image reading and this data is subsequently clipped to 8 bits for storage on the CR system. Therfore one cannot currently choose to retrospectively apply the DRC process to an image but must instead select it at the ID terminal level prior to image reading. Further adjustments of gradation and frequency processing can still be applied to the 8 bit data if necessary.

2.2 Inital testing of the DRC effect

In inital testing of DRC processing, a fourteen level stepwedge was imaged with varying DRE values of 0.0, 0.1, 1.0 and 2.0 and twin format images were printed as above. The OD of each stepwedge level was then measured using a calibrated X-Rite densitometer (X-Rite Inc., Grandville, Michigan). These OD values were then plotted for each DRE value used with the results shown in Figure 2 below. When the DRE is set to 1.0 or 2.0 it can be seen that lower density regions (thicker stepwedge levels) were darkened (higher OD) and higher density regions (thinner levels) were lightened (lower OD) as predicted. These effects become more profound as the DRE is increased. The DRC process thus compresses the extreme OD values to closer within the interpretable range while preserving optimum midrange OD values along a straight line corresponding to a gamma of 1 for conventional film H&D curves.

Figure 2

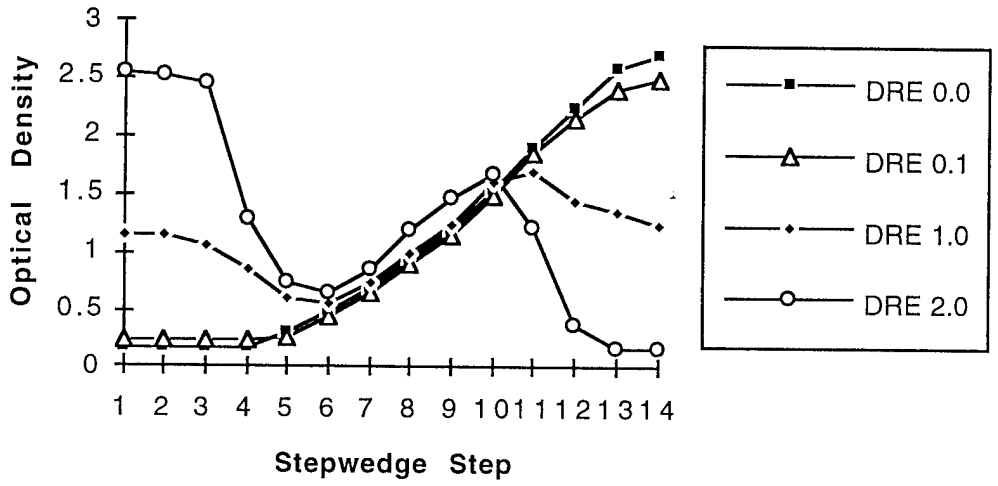

Figure 2: Optical density at various stepwedge levels for varying intensities of the DRC effect.

3. CLINICAL APPLICATION OF DRC TO MUSKULOSKELETAL IMAGES

3.1 Regions studied

The DRC process should be most useful in areas of widely varying tissue density and complex anatomy. For this reason, the process was studied by its application to the DP view of the foot and lateral view of the wrist. The foot is a roughly triangular structure that resembles the shape of the stepwedge used in initial testing and contains overlapping bony structures in the calcaneal region while the wrist presents multiple overlapping carpal bones on lateral exam.

3.2 Analysis by optical density readings

During the trial period of the study, 25 DP views of the foot and 16 lateral wrist exams were obtained, processed in dual fashion by both standard and DRC algorithms and then printed using the twin format discussed previously. The intensity of the DRC effect was applied using a DRE of 0.6 for the foot and 1.0 for the wrist images. Example images are shown in Image Pair 1 and Image Pair 2 below.

Image Pair 1

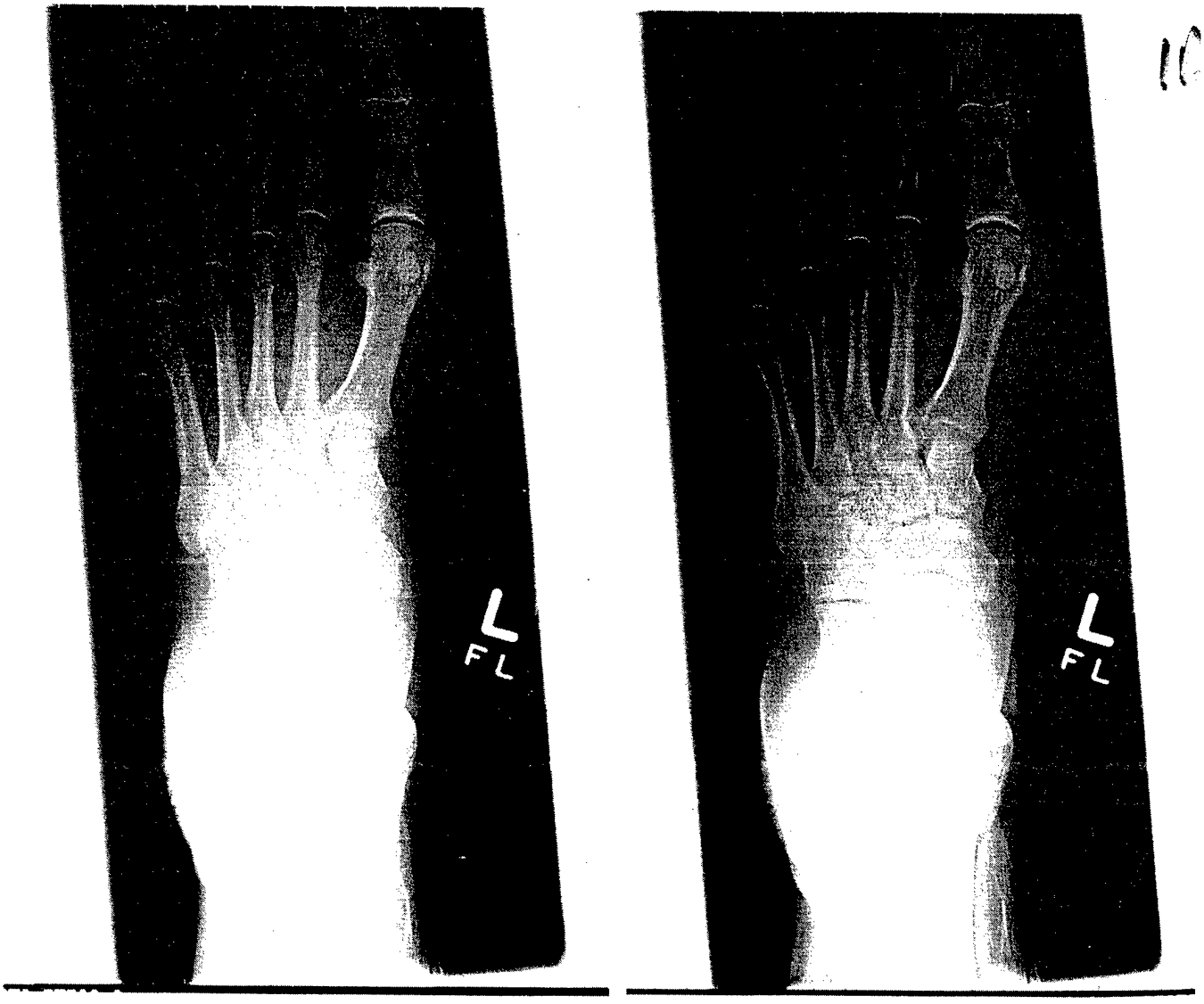

Standard processing

DRC processing

Image Pair 2

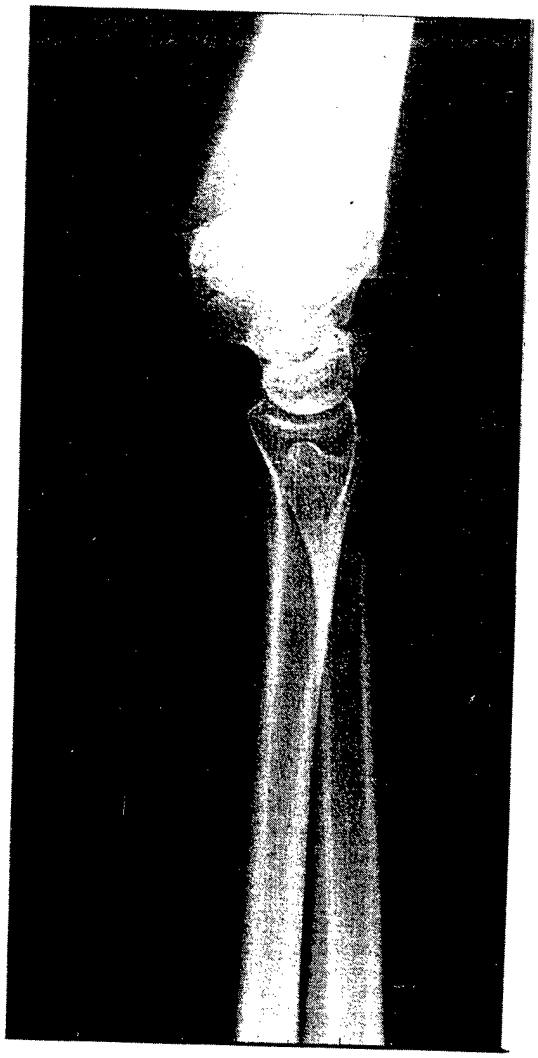

Standard processing

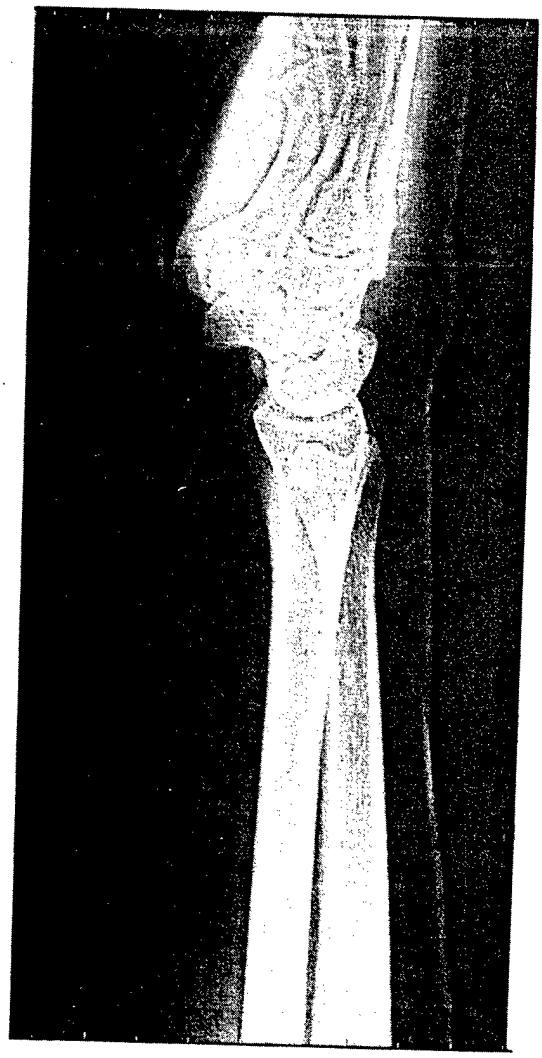

DRC processing

Optical density values were then recorded over selected regions of each image. In the foot, readings were taken over the proximal phalanx of the great toe, the navicular and the posterior calcaneus. In the wrist, readings were recorded from the lunate and soft tissues volar to the distal radius. Figure 3 displays the results of comparing the same anatomical regions of standard and DRC processed images for the foot and Figure 4 demonstrates recordings from the wrist exams. In both instances, the values of OD for DRC processed images lie closer to the midrange of the OD spectrum where optimal viewing conditions exist.

Figure 3

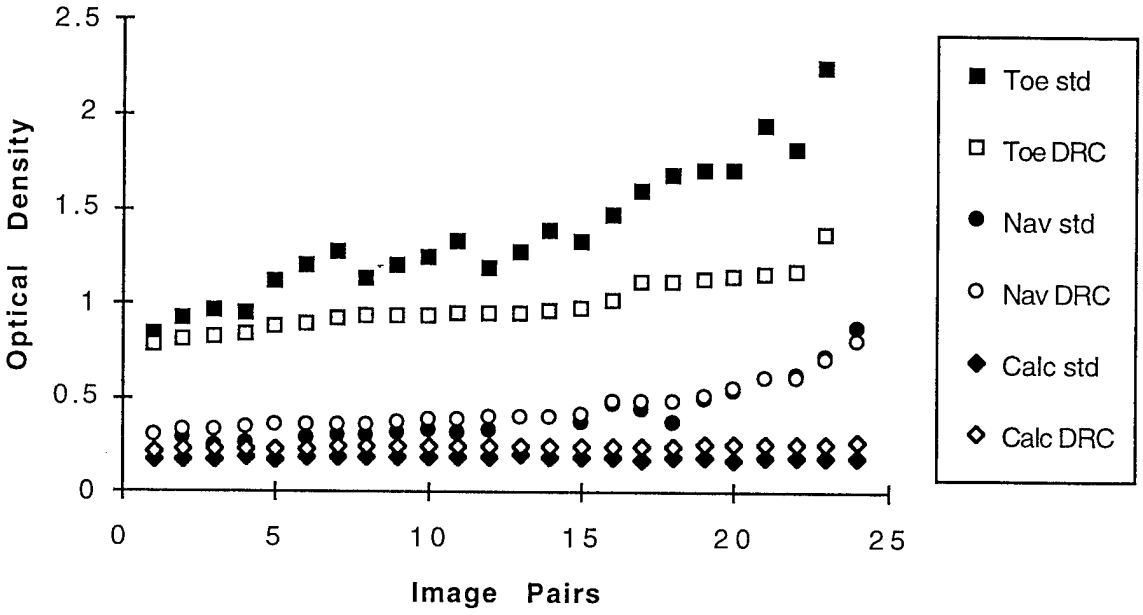

Figure 3: Optical density in regions of the great toe, navicular and calcaneus for standard versus DRC processing.

Figure 4

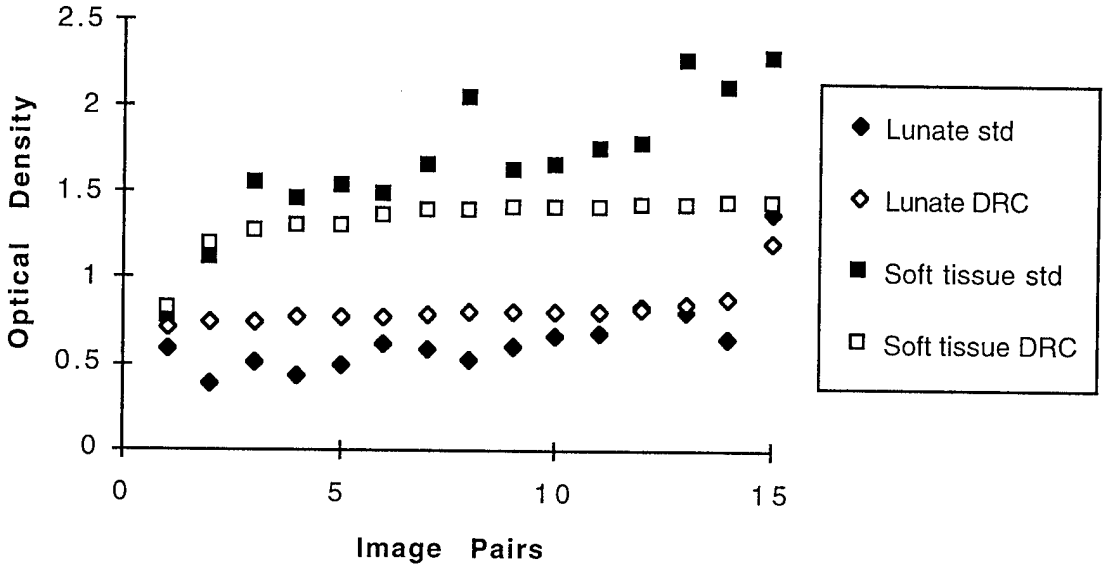

Figure 4: Optical density in regions of the lunate and soft tissues for standard versus DRC processing.

3.3 Radiographic assessment and comparison of image quality

The foot and wrist hardcopy image pairs were then reviewed independently by three radiologists who frequently read muskuloskeletal CR exams. Each image pair was assessed and compared with its twin with regard to the degree of various structures visualized on each image. Specifically, the soft tissues of the toes, the tarsal joint spaces and the bone texture of the phalanges and the talocalcaneal region were assessed in the foot. The wrist was evaluated for the soft tissues at the level of the radiocarpal joint, the visibility of the carpal joint spaces and carpal outlines and bone texture within the carpals themselves. Finally, overall interpretative quality for each image was assessed and compared. For each of the above image factors, the reviewer designated a preference for the standard image, the DRC image or no preference between the two. The results are shown in Table 1 below. For each criterion compared, DRC images were favored over the standard except in visualization of bony texture in the carpals of the wrist where the standard imaging was preferred in 31.2% (15/48) versus 20.8% (10/48) for DRC imaging. Visualization of bone texture in the phalanges of the toes showed no clear preference but in the talocalcaneal region DRC imaging was preferred in 92.0% (69/75) of cases. Similarly, the tarsal joints and carpal outlines were much better seen on DRC images as were the soft tissues of the toes. Of note, the soft tissues on DRC images were consistently well seen without the necessity of a bright light. Similar effects in the soft tissues of the wrist were present as well but less dramatic than in the feet. With regard to the overall image, there was a clear preference for DRC processing in the foot and to a lesser degree in the wrist.

TABLE 1

REGION EXAMINED	IMAGE PREFERRED (TOTAL OF 3 REVIEWERS)		
	Standard	DRC	No preference
FOOT			
Soft tissues of toes	10	52	13
Tarsal joints	10	35	30
Bone texture-phalanges	23	25	27
Bone texture-talus/calcaneus	4	69	2
Overall interpretative quality	3	50	22
WRIST			
Soft tissues	13	18	17
Carpal outlines/joint spaces	7	18	23
Bone texture-carpals	15	10	23
Overall interpretative quality	11	16	21

4. CONCLUSION

By evaluating images of the foot and wrist, it is clear that biphasic DRC processing represents a significant improvement over standard processing of CR images in displaying the full latitude of tissue densities present in a region of complex and widely varying anatomy. The process of dynamic range compression allows better visualization of overlapping bony structures that typically yield a low optical density region on film as well as demonstrating darker, high OD regions even without the use of a bright light. This latter benefit is especially apparent in anatomic regions of varying tissue thickness such as the feet. The key to the DRC process lies in compressing the optical density of tissue at the extreme limits of the interpretative range while still retaining sufficient image contrast to distinguish adjacent structures of similar density. That is, because of the biphasic shape of the lookup table, the same optical density on the film can represent different exposure levels. This technique therefore is most likely to be helpful for noncontiguous regions of similar optical density at final output. If contiguous, there would be insufficient image contrast to distinguish the adjacent structures by the interface between them. This anatomic constraint is met in foot and wrist radiographs. Additionally, regions represented by optical density extremes after DRC processing will tend to present somewhat lower contrast so it is desirable that such areas not be of vital clinical importance. Further investigation is still needed to assess the appropriate intensity of the effect to apply to various exams to optimize what could potentially represent a valuable step in the widespread acceptance and usage of digital radiographic examination of the muskuloskeletal system.

5. REFERENCES

1. M. Ishida, "Digital Image Processing," Miyanodai Technology Development Center, Fuji Photo Film Co., Ltd., Technical Review No. 1, 1993.

2. M. Kobayashi, "Image Optimization by Dynamic Range Control Processing," Symposium for Computer Assisted Radiology, 1993.

Digital Mammography: An evaluation of the Shape of Microcalcifications

Matthew Freedman, Dorothy Steller Artz, Hamid Jafroudi, Jacqueline Hogge,
Rebecca A. Zuurbier, Raj Katial, Curtis Green, Seong Ki Mun.

Division of Imaging Sciences and Information Systems, Department of Radiology
Georgetown University Medical Center, 3800 Reservoir Road, NW, Washington, DC 20007

Abstract

Microcalcifications can be identified on mammograms in approximately 50-55 % of breast cancer cases. Three factors affect the ability to use the presence of microcalcifications as a sign of cancer. They must be seen (conspicuity), their shape must be assessed (to differentiate benign and malignancy associated shapes) and they should be countable since the greater the number of clustered calcifications, the more likely they are malignancy associated. Concern has been expressed that digital systems with their inherently worse resolution would not allow adequate shape information to be captured. Using a 100 micron pixel size storage phosphor system we randomly selected 20 cases, 10 benign and 10 showing malignancy on biopsy and asked four radiologists to assess the calcifications present comparing the original screen film and the digital images and using the screen film biopsy specimen radiograph as ground truth. The preferences were mixed with some radiologists preferring screen film and others the digital images. Whatever their preferences, the radiologists were unable to use the shape criteria to distinguish benign and malignant cases in this case sample.

Key words: digital mammography microcalcification shape number conspicuity breast cancer

Introduction

Microcalcifications can be identified on mammograms in approximately 50-55 % of breast cancer cases. Three factors affect the ability to use the presence of microcalcifications as a sign of cancer. They must be seen (conspicuity), their shape must be assessed (to differentiate benign and malignancy associated shapes) and they should be countable since the greater the number of clustered calcifications, the more likely they are malignancy associated.

Certain physical properties of screen film mammography suggest that it should be better in evaluating the shape and number of calcifications: Screen film mammographic systems have higher inherent resolution than both 50 and 100 micron pixel digital systems. Screen film systems have resolution in the range of 17-20 line pairs per mm (lpm). 100 micron pixel systems have a theoretical 5 lpm and 50 micron systems a theoretical 10 lpm. The high resolution of film screen mammography is, however, at low contrast.

Certain physical properties of digital systems suggest that they should be better in providing improved conspicuity of microcalcifications: Digital systems provide the ability to enhance contrast. Digital systems have the propensity to enlarge structures to the size of the pixel which would result in some distortion of shape. The microcalcifications visible on screen film mammography are usually 250 microns in size or greater so that several pixels would be involved in the display of any visible microcalcification even if 100 micron pixel systems were used.

Display devices are currently not optimal for digital mammography and provide a confounding factor in evaluating the quality of current digital mammography: Printers for digital mammography are still not optimal. In the system we used scan lines are visible and interfere with the determination of shape. Soft copy display systems with adequate brightness are still limited to 2 x 2.5 K display (equivalent to a 100 micron pixel when displaying the whole breast) and optimal image processing parameters for display are not known..

One would therefore assume if one is interested in detecting microcalcifications (as is important in screening mammography) that one might find digital mammography better if indeed the conspicuity of microcalcifications is increased, but that screen film mammography would prove better in diagnostic mammography.

The subjective impression of this relationship, however, is not an absolute statement. If it is difficult to see microcalcifications when they are of low contrast, it is more difficult to determine their shape and to count the very small calcifications. The experiments reported here were performed to determine, with existing 100μ pixel equipment for digital mammography, what the balance is between this tradeoff: low contrast higher resolution of screen film mammography vs. higher contrast lower resolution of digital mammography.

Experimental methods

Equipment

Screen Film System: Fuji IM fine screens, Fuji IM mammographic film.

Digital System: Fuji HR-V imaging plates. Fuji 9000 image plate reader.

Image processing: individually optimized parameter settings, using Fuji standard image processing algorithm, .

Mammographic machine: GE/CGR 600T or 500T, using nominal 0.3 mm focal spot. Phototimed.

Printer: Fuji LP414 laser printer

Certification: Screen Film Mammographic facility is American College of Radiology certified.

Readers: Four Board Certified Diagnostic Radiologists each meeting American College of Radiology requirements as mammography interpreters. Three of the readers have experience with the appearance of digital mammography. One has previously seen only screen film mammography.

Clinical Cases: Random selection of 10 from 30 biopsy proven cancer cases. Random selection of 10 from 100 biopsy proven benign cases. Each case provided with screen film biopsy specimen radiograph. Each image masked so that only region of microcalcifications is shown. Each case was originally detected on screen film mammography and was considered suspicious for cancer following diagnostic evaluation which would have included magnification radiographs. The magnification radiographs were not provided to the radiologists.

Size of microcalcifications measured on cases used:

In each case the smallest and largest microcalcifications visible with the 2 X hand held magnifier were measured using an 8 X magnifier with a measuring reticle allowing measurements from 100μ-2500μ. If a smaller microcalcification could be seen only with the 8 x magnifier, it was not recorded.

Measurements on the biopsy specimens represent the range of microcalcifications visible with the 8 x magnifier. In 9 of the 20 cases, the specimen radiograph was obtained with magnification. Smaller calcifications could be detected in those cases that were magnified.

	Cancer				**Benign**			
Measurements in microns								
	Minimum size		Maximum size		Minimum size		Maximum size	
	AVE	range min	AVE	max range	AVE	range	AVE	range
SF	265	150-450	760	300-2500	265	200-400	1265	400-6000
CR	285	200-400	780	400-5000	285	250-400	1185	300-2500
Biop	156	50-300	783	250-2500	198	75-400	1635	200-6500

From this data one can see that the average size of the smallest microcalcifications in the benign and malignant cases were the same. There was one case of cancer with a 150 micron calcification visible on the screen film mammogram, otherwise the smallest calcifications visible on mammograms in both cancer and non-cancer cases measured 200μ.

On the CR and SF mammograms, at attempt was made to measure the same microcalcifications. The CR mammographic method slightly increases the measurable size of the microcalcifications. This may be an effect of the printer scan lines.

Case presentation: Each case was presented to the radiologists with the specimen radiograph, screen film and digital images. Left-right position of the screen film and digital images randomized. Original screen film mammogram provided. Hand held 2 power magnifier provided.

Questionnaire: Preference between screen film and digital for conspicuity of calcifications, shape of microcalcifications and number of microcalcifications. Is the level of suspicion from the screen film image low or high? From the digital image low or high? Based on all information, do you think the microcalcifications represent benign or malignant disease. Two of the radiologists said all cases were suspicious since all had gone to biopsy and refused to make these assessment in at least some of the cases.

Results

Conspicuity of microcalcifications

Radiologist	All			Cancer Cases			Benign		
	CR	SF	Equal	CR	SF	Equal	CR	SF	Equal
1	10	1	9	5	1	4	5	0	5
2	10	3	7	5	2	3	5	1	4
3	12	6	2	7	3	0	5	3	2
4	5	6	9	3	3	4	2	3	5
Sums	37	16	27	20	9	11	17	7	16

This shows a clear preference for the conspicuity of microcalcification on the digital images. Three of the four radiologists preferred it.

Shape of microcalcifications

Radiologist	All			Cancer Cases			Benign		
	CR	SF	Equal	CR	SF	Equal	CR	SF	Equal
1	8	2	10	4	2	4	4	0	6
2	0	12	8	0	6	4	0	6	4
3	4	5	11	2	3	5	2	2	6
4	0	7	13	0	3	7	0	4	6
Sums	12	26	42	6	14	20	6	12	22

This shows a mixed result of the interpreters of the shape of microcalcifications. Two favored screen film, one favor digital and one was balanced between the two methods.

Number of microcalcifications

Radiologist	All			Cancer Cases			Benign		
	CR	SF	Equal	CR	SF	Equal	CR	SF	Equal
1	6	2	12	3	2	5	3	0	7
2	5	12	3	3	6	1	2	6	2
3	7	7	6	3	4	3	4	4	2
4	3	7	6	0	7	3	2	4	4
Sums	21	28	27	9	19	12	11	14	15

This shows a mixed result of the interpreters of the number of microcalcifications. Two favored screen film, one favo digital and one was balanced between the two methods.

Screen film image
Suspicion of cancer

Radiologist	Cases with cancer			Benign Cases		
	Low	high	no response	Low	High	No response
1	4	6		5	5	
2	3	7		5	5	
3.	5	5		8	2	
4	0	5	5	0	7	3
Sums	12	23	5	13	19	3

This shows that the screen film images did not allow one to accurately choose between benign and malignant cases.

CR image
Suspicion of cancer

Radiologist	Cases with cancer			Benign Cases		
	Low	high	no response	Low	High	No response
1.	3	7		4	6	
2.	5	5		6	4	
3	4	6		8	2	
4	3	3	4	3	4	3
Sums	15	21	4	21	16	3

This shows that the digital images did not allow one to accurately choose between benign and malignant cases. The radiologists did slightly better in defining true negatives on the digital images in this small series, but this is more likely a random rather than a significant difference.

Final Conclusion
Malignant vs. Benign

Radiologist	Cancer Cases			Benign Cases		
	TP	FN	NR	TP	FN	NR
1.	7	3		5	5	
2.	7	3		5	5	
3	3	4	3	4	2	4
4			10		1	9
Sums	17	10	13	14	13	13

This shows that the radiologists could not distinguish between benign and malignant cases in this series.

Discussion

The preference opinions of the Radiologists do not allow clear summary conclusion. Three of the four radiologists prefer the conspicuity of microcalcifications on digital mammography. The fourth considered it equivalent. This may indicate the desirability of digital mammography in breast cancer screening.

Two of the four radiologists clearly consider that screen-film provides better information about shape and number of calcifications. One of the radiologists clearly preferred digital images for shape and number. The fourth radiologist considered screen film and digital images preferred in similar numbers of patients. These findings could mean that screen film is better for shape and counting of calcifications or that greater familiarity with digital images equalizes the preference between screen film and digital. It could also mean, that given a close call between two systems, the familiar appearance is preferred. All four of the radiologists considered the decision of preference in most of these cases difficult to determine.

The Radiologist who considered digital mammography better for delineation of shape and number of calcifications performed at the same level of accuracy for the classification into benign and malignant as two of other radiologists. The radiologist who clearly preferred the screen film images for all purposes felt that all the images were suspicious and refused to choose in most cases between benign and malignant. Thus preference for one system did not affect diagnostic accuracy of the radiologists.

There is the possibility that the case sample we used was too difficult for the test we wished to perform. Since all of these patients were considered sufficiently suspicious to go to biopsy, it may be that the inclusion of cases that were selected at the time of diagnostic mammography not to go to biopsy should have been included as well since the task of the radiologist is to determine whether or not biopsy is indicated. That task, however, is usually decided at the time of diagnostic mammography at which time magnification views are obtained. Such a dataset would, however, remain somewhat unproven since in situ carcinoma can remain quiescent for many years and thus there would always remain some uncertainty about the benign nature of those cases.

We know that there are limitations in the laser printing for digital mammograms at present. A better laser printer may result in slightly better digital images.

In this study, we used masking to identify the location of the microcalcifications. This was to be certain that the radiologists would be able to locate these sometimes very subtle findings. Because of the improved conspicuity found with the digital system, some of the cases might have been detected by the radiologists on the digital mammograms, but not on conventional mammograms. This would affect the clinical accuracy of the overall results.

The results of our ROC study which will use radiologists from outside the institution will be important in determining the clinical meaning of these differences. We intend to test additional patients who, at diagnostic mammography were classified as having benign disease. Most important will be the performance of a screening trial of this digital mammography system.

Summary

A series of 10 breast cancer cases and 10 benign biopsy proved cases were selected using randomization methods from a larger prospectively obtained series. Screen film and 100 micron pixel storage phosphor images were compared using the specimen radiograph as the representation of truth. Four radiologists were asked to indicate preferences. Excluding those cases for which the radiologists considered screen film and digital mammogram images equal, three of the four preferred digital mammography conspicuity, two of three preferred screen film for shape and number of microcalcifications, one preferred the digital image, and the fourth had almost equally divided preference between screen film and digital mammography for shape and number of microcalcifications. Whichever system the radiologists preferred, they failed to be able to distinguish benign and malignant cases in this randomly selected series. This suggests that the subtle differences the radiologists saw between these systems in the evaluation of shape and number may not be clinically significant.

The preference results are considered sufficiently close that an ROC study will be necessary to determine their clinical significance.

Bibliography

Brettle DS, Ward SC, Parkin GJS, et al. A clinical comparison between conventional and digital mammography utilizing computed radiography. British J of Radiology 1994; 67:464-468.

Egan RL, McSweeeney MB, Sewell CW. Intramammary calcifications without an associated mass in benign and malignant diseases. Radiology, 1980. 137:1-7.

Freedman M, Pe E, Nelson M, Lo S-C B, Mun S K: Digital Mammography: Demonstration of a Method of Achieving Adequate Resolution on a Storage Phosphor System. CAR 93, 7th International Symposium Berlin (June 24-26, 1993); 783pp.

Freedman M, Pe E, Zuurbier R, Katial R, Jafroudi H, Nelson M, Lo S-C B, Mun S K: Image Processing in Digital Mammography. SPIE: Medical Imaging, Vol. 2164 (1994); 537-554pp.

Freedman MT, Steller D, Jafroudi H, Lo SCB, Zuurbier RA,Katial R, Hayes W, Wu YC, Lin JS, Steinman R, Tohme WG, Mun SK. Digital Mammography: tradeoffs between 50- and 100-micron pixel size. SPIE Medical Imaging 1995. Paper 2432-09.

Millis RM, Davis R, Stacey AJ. The detection and significance of calcifications int he breast: a radiological and pathological study. British J of Radiology, 1976. 49:12-26

Oestmann JW, Kopans D, Hall DA, et al. A clinical comparison of digitized storage phosphors and conventional mammography in the detection of malignant microcalcifications. Invest Radiol 1988:725-728.

Powell RW, McSweeney MB, Wilson CE. X-ray calcifications as the only basis for breast biopsy. Annals Surgery 1983. 197:555-559.

Sickles EA. Further experience with microfocal spot magnification mammography in the assessment of clustered breast microcalcifications. Radiology 1980; 137:9-14.

Sickles EA. Microfocal spot magnification mammography using xeroradiographic and screen film recording systems. Radiology 1979; 131:599-607.

Acknowledgment

Supported in part by U.S. Army Medical Research Grant DAMD 17-93-J-3008. The content of this report does not necessarily reflect the position or policy of the U.S. Government and no official endorsement should be inferred.